

SLOVAK SOCIETY FOR GEOMETRY AND GRAPHICS

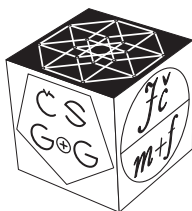
**32<sup>nd</sup> Symposium on  
Computer Geometry SCG'2023**



PROCEEDINGS OF THE  
**9<sup>TH</sup> SLOVAK-CZECH CONFERENCE ON  
GEOMETRY AND GRAPHICS 2023**

Kremnica

September 11–14, 2023



**43<sup>rd</sup> Conference on  
Geometry and Graphics**

CZECH SOCIETY FOR GEOMETRY AND GRAPHICS  
OF THE UNION OF CZECH MATHEMATICIANS AND PHYSICISTS

Language correction of the publication was not performed, language accuracy is the sole responsibility of the contributing authors.

Contributions included in the proceedings were selected by the scientific committee members based on reviews.

All rights reserved. No part of this work may be used or reproduced in any manner whatsoever or transmitted in any form or by any means, electronic or mechanical, including photocopy, recording, or any information storage and retrieval system, without written permission from the publisher and copyright owner.



Vydavatelský servis  
Republikánská 28, Plzeň

Proceedings of the 9<sup>th</sup> Slovak-Czech Conference on Geometry and Graphics 2023  
First edition

© Miroslav Lávička, Dagmar Szarková, Daniela Velichová, 2023

© Vydavatelský servis, 2023

ISBN 978-80-86843-82-7 (CD-ROM)

ISBN 978-80-86843-81-0 (online)

# 9<sup>th</sup> Slovak-Czech Conference on Geometry and Graphics 2023

**Organized by:**  
Slovak Society for Geometry and Graphics

## **Organizing Committee:**

Daniela **Velichová** – STU v Bratislave (coordination and programme)  
Daniela **Richtáriková** – STU v Bratislave (registration and administrative issues)  
Dagmar **Szarková** – SSGG, Bratislava (webpage and database)

## **Scientific Committee:**

Roman **Hašek** – Jihočeská univerzita v Českých Budějovicích (CZ)  
Pavel **Chalmovianský** – Univerzita Komenského v Bratislave (SK)  
Mária **Kmeťová** – Univerzita Konštantína Filozofa v Nitre (SK)  
Helena **Koncul** – Sveučilište u Zagrebu (HR)  
Miroslav **Lávička** – Západočeská univerzita v Plzni (CZ)  
Pavel **Pech** – Jihočeská univerzita v Českých Budějovicích (CZ)  
Monika **Sroka-Bizoň** – Politechnika Śląska, Gliwice (PL)  
Hellmuth **Stachel** – Technische Universität Wien (A)  
Daniela **Velichová** – Slovenská technická univerzita v Bratislave (SK)  
Gunter **Weiss** – Technische Universität Wien (A)





## Table of Contents

FOREWORDS. . . . .	9
PLENARY TALKS . . . . .	11
KRUPKA DEMETER	
<i>Variational forces: Remarks</i> . . . . .	13
KUŠAR DOMEN	
<i>Descriptive geometry in Slovenia, decline or opportunity.</i> . . . .	23
ŠÍR ZBYNĚK	
<i>Remarks on de Casteljau algorithm</i> . . . . .	35
CONTRIBUTED TALKS. . . . .	39
BEGANOVÁ JULIANA, VAJSÁBLOVÁ MARGITA	
<i>Dynamická učebnica deskriptívnej geometrie pre stavebné odbory</i> . . . . .	41
BOSÁKOVÁ ADRIANA	
<i>Contribution of a tangent of multiplicity one to the intersection multiplicity of two plane curves</i> . . . . .	49
BRAJERČÍK JÁN	
<i>Geometry of the Schwarzschild spacetimes</i> . . . . .	57
CIBULKA JAROSLAV	
<i>VTOL propeller development in start-up environment</i> . . . . .	63
ČAVARGA MARTIN	
<i>Mesh primitive counting formulas for subdivision surfaces.</i> . . . .	67
ČEČÁKOVÁ STANISLAVA, KOLÁŘOVÁ DANA	
<i>Sliceforms in the education of architecture students</i> . . . . .	77
DAS MANASWITA	
<i>On multicriteria triangulations</i> . . . . .	81
FERDIÁNOVÁ VĚRA, HOLEŠOVÁ MICHAELA	
<i>Examples of ovals in 19<sup>th</sup> century architecture in Ostrava.</i> . . . .	89
GUNČAGA JÁN, TKAČIK ŠTEFAN	
<i>Osobnosti slovenskej matematiky – inšpirácia a životné vzory pre budúce generácie</i> . . . . .	97

HLAVOVÁ MARTA	
<i>On the use of Bézier bicubic surface for shape reconstruction</i>	103
KOKTAVÁ MARIE, TKADLECOVÁ MIROSLAVA	
<i>The most famous illusions of Adalbert Ames Jr.</i>	109
KOLCUN ALEXEJ	
<i>Sú „prírodné fraktály“ naozaj fraktály?</i>	115
KORECOVÁ KRISTÍNA, CHALMOVIANSKÝ PAVEL	
<i>Triangulation of implicit surfaces with singularities</i>	119
KRÁLOVÁ ALICE	
<i>Parametrizace vybraných šroubových ploch a jejich zobrazení v programu Maple</i>	127
LINKEOVÁ IVANA, CIBULKA JAROSLAV	
<i>Parametric CAD model of axial blood pumps components</i>	133
MAKOVNÍK MARCEL	
<i>Subdivision and conchoids</i>	139
MOLNÁR EMIL	
<i>The Kárteszi points of a triangle, via three reflections theorem and geometric algebra</i>	145
MÜLLER JAKUB, LINKEOVÁ IVANA	
<i>Impact of surface continuity on 3D model</i>	147
ODEHNAL BORIS	
<i>Variations on Frégier's Theorem</i>	153
PABICH BRONISLAW	
<i>Printing as a supporting tool teaching mathematics through discovery</i>	159
PABICH BRONISLAW	
<i>The family of uniform polyhedra</i>	165
RÜCKSCHLOSSOVÁ TATIANA	
<i>Priamkové plochy – tlačené 3D modely vytvorené v prostredí Rhinoceros</i>	171
ŘADA JAKUB	
<i>Selected geometric constructions and proofs</i>	177

---

VORÁČOVÁ ŠÁRKA	
<i>Application of Euler path</i> . . . . .	185
VRŠEK JAN, LÁVIČKA MIROSLAV	
<i>Note on computation of symmetries of algebraic objects</i> . . .	191
WEISS GUNTER	
<i>3D-versions of theorems related to Miquel's Theorem</i> . . . .	195
ZAMBOJ MICHAL	
<i>Calculating on a parabola</i> . . . . .	203
LIST OF PARTICIPANTS . . . . .	211



## Forewords

The 9<sup>th</sup> SLOVAK-CZECH CONFERENCE ON GEOMETRY AND GRAPHICS was held on September 11–14, 2023 in Slovakia, in the old mining Slovak town Kremnica. This joint session of the 32<sup>nd</sup> SYMPOSIUM ON COMPUTER GEOMETRY SCG '2023 and the 43<sup>rd</sup> CONFERENCE ON GEOMETRY AND GRAPHICS was the next successful common event of two traditional conferences organized by national societies, the Slovak Society for Geometry and Graphics and the Czech Society for Geometry and Graphics.

About 47 conference participants from 7 countries – Slovakia, Czech Republic, Austria, Slovenia, Poland, Hungary and India, West Bengal – enjoyed rich programme with presentations related to a variety of geometry areas with three interesting invited plenary lectures. ZBYNĚK ŠÍR from the Faculty of Mathematics and Physics, Charles University in Prague, Czech Republic, presented lecture *Seven versions of de Casteljau algorithm*. He summarized the most important properties of de Casteljau algorithm, and demonstrated its utility on various interpretations and interesting examples. Invited lecture *Geometric modeling: Variational principle* presented by DEMETER KRUPKA from Lepage Research Institute in Prešov, Slovakia, introduced the current research in differential geometry, including applications of geometric methods in control of the motion of mechanical systems. Elementary ideas on the geometric control theory (geometric robotics) and introduction of mathematical modeling of processes and stability problems in physics and engineering using variational principles were also discussed. DOMEN KUŠAR from the Faculty of Architecture, Ljubljana University in Slovenia presented lecture entitled *Descriptive geometry in Slovenia, decline or opportunity*, an overview of the development of subject Descriptive geometry as part of curricula at educational institutions in Slovenia in the current digital age. Activities were mentioned leading to finding balance between the use of modern techniques and “classical” pedagogical approaches aiming to achieve the best possible knowledge and the greatest possible spatial abilities that future architects will need in their work.

Submitted 28 contributed talks from applied and pure geometry, graphics and education of geometry are published in this proceedings. These interesting contributions represent the variety of research carried currently in the field of geometry and prove the inspirational power of this scientific domain. High quality presentations delivered by experienced experts and initial scientific works of young scientists, who could benefit from the talks of their matured colleagues, proved to be a highly resilient mixture bringing new valuable ideas on both sides.

Conference was organized by the Slovak Society for Geometry and Graphics, residing at the Institute of Mathematics and Physics, Mechanical Engineering Faculty of the Slovak University of Technology in Bratislava, Slovakia, and it was held in hotel Golfer located over Kremnica town. Social programme included the visit to the old Mint factory in Kremnica, where coins have been struck uninterruptedly for almost seven hundred years. Participants could also visit City castle or Mining museum in the old gold mine Andrej's tunnel, and walk in the city historic centre. Conference dinner was a nice social event with musical piano accompaniment.

We would like to thank cordially to all conference participants for the great atmosphere of this event and its high scientific richness, which was achieved primarily thanks to your applied presentations that were all at a high level of professional and scientific quality.

It is our pleasure to invite you all to attend the next joint event, the 33<sup>rd</sup> SYMPOSIUM ON COMPUTER GEOMETRY SCG '2024 and the 44<sup>th</sup> CONFERENCE ON GEOMETRY AND GRAPHICS, which is going to be held in cooperation of representatives of both societies for geometry and graphics in September 2024 in Czech Republic, as the 10<sup>th</sup> CZECH-SLOVAK CONFERENCE ON GEOMETRY AND GRAPHICS.

We are proud to be keeping on the good tradition of our common meetings deeply rooted in the history.

Bratislava & Praha/Plzeň, November 25, 2023

Daniela Velichová  
*chair of SSG*

Miroslav Lávička, Zbyněk Šír  
*former, and new chair of CSGG*

## PLENARY TALKS





# Variational forces: Remarks

Demeter Krupka

*Lepage Research Institute*

*17 November St., 081 16 Prešov, Slovak Republic*

*email: demeter.krupka@lepageri.eu*

**Abstract.** This research-expository paper is devoted to variational modelling of mechanical forces, depending on velocities.

*Keywords:* Variational equation, Helmholtz conditions, Variational force

## 1 Introduction

This paper is based on several sources: lectures delivered by the author at the conferences *Geometric Mechanics and Control*, Beijing, BIT, *5th International Conference on Dynamics, Vibration and Control*, Shijiazhuang, China, July 2018, and the *23rd International Summer School on Global Analysis*, LRI, Brasov, Romania, August 2018; main source, however, is the paper D. Krupka, *Variational forces*, *Journal of Mathematical Sciences*, accepted by Yu. Sachkov, in print 2019 (delayed), where complete proofs can be found.

Recall that in classical mechanics a *Lagrange function*  $\mathcal{L} : I \times U \times \mathbf{R}^m \rightarrow \mathbf{R}$  of a mechanical system is usually defined to be the difference of *kinetic energy*  $\mathcal{T}$  and *potential energy*  $\mathcal{U}$ ,  $\mathcal{L} = \mathcal{T} - \mathcal{U}$ . While  $\mathcal{T}$  is in a sense a *universal function* of the form

$$\mathcal{T} = \frac{1}{2} g_{ij} \dot{x}^i \dot{x}^j,$$

where  $g_{ij}$  are the components of a metric tensor on the configuration space  $U$ , potential energy  $\mathcal{U}$  provides specific characteristic;  $\mathcal{U}$  does not depend on  $\dot{x}^i$ , and the first-order form  $\phi = \phi_i$ , where

$$\phi_i = -\frac{\partial \mathcal{U}}{\partial x^i},$$

is the *force*, associated with  $\mathcal{U}$ . The *Euler-Lagrange form* of  $\mathcal{L}$  is a family  $E(\mathcal{L}) = E_i(\mathcal{L})$ , whose components are the *Euler-Lagrange expressions*

$$E_i(\mathcal{L}) = -\frac{\partial \mathcal{L}}{\partial x^i} + \frac{d}{dt} \frac{\partial \mathcal{L}}{\partial \dot{x}^i} = -\frac{\partial \mathcal{T}}{\partial x^i} + \frac{d}{dt} \frac{\partial \mathcal{T}}{\partial \dot{x}^i} + \frac{\partial \mathcal{U}}{\partial x^i}.$$

The *Euler-Lagrange equations* are differential equations for curves  $t \rightarrow x^i(t)$ ,

$$-\frac{\partial \mathcal{T}}{\partial x^i} + \frac{d}{dt} \frac{\partial \mathcal{T}}{\partial \dot{x}^i} = -\frac{\partial \mathcal{U}}{\partial x^i}.$$

In this paper we study *variationally compatible extensions* of the concept of the *force*. The aim is to characterize a class of Lagrange functions  $\mathcal{L}$  admitting a decomposition  $\mathcal{L} = \mathcal{F} - \mathcal{U}$ , in which  $\mathcal{U}$  may depend on velocities  $\dot{x}^i$ .

The problem of variational compatibility of forces is not new; its elementary version was considered, probably for the first time, by Novotny [5]. Recent applications of the inverse variational problem to ordinary differential equations and geometric mechanics can be found in Voicu, Krupka [6] and Krupka, Urban and Volna [4]. Extensive, relatively complete literature on the inverse problem can be found in Krupka, Saunders [3] and Zenkov [7].

## 2 The Euler-Lagrange mapping

In this section we study the dependence of the Euler-Lagrange expressions  $E_i(\mathcal{L})$ , on the Lagrange functions  $\mathcal{L}$ . The family  $E(\mathcal{L}) = E_i(\mathcal{L})$  is called the *Euler-Lagrange form*. We wish to characterize the *kernel* and the *image* of the *Euler-Lagrange mapping*  $\mathcal{L} \rightarrow E(\mathcal{L})$ . The domain of definition of the Euler-Lagrange mapping is the vector space of  $C^2$ -functions on  $I \times U \times \mathbf{R}^m$  and its image space is the vector space of  $m$ -tuples of  $C^2$ -functions on  $I \times U \times \mathbf{R}^m \times \mathbf{R}^m$ ; this mapping is obviously linear.

A Lagrange function  $\mathcal{L}$  is said to be (variationally) *trivial*, if  $E_i(\mathcal{L}) = 0$  for all  $i$ .

**Theorem 1.** *A Lagrange function  $\mathcal{L} = \mathcal{L}(t, x^i, \dot{x}^i)$  is trivial if and only if there exists a function  $f = f(t, x^i)$  such that*

$$\mathcal{L} = \frac{df}{dt}.$$

Theorem 1 characterizes the *kernel* of the Euler-Lagrange mapping  $\mathcal{L} \rightarrow E(\mathcal{L})$ .

We shall now consider arbitrary systems  $\varepsilon = \varepsilon_i$  of sufficiently differentiable functions  $\varepsilon_i : I \times U \times \mathbf{R}^m \times \mathbf{R}^m \rightarrow \mathbf{R}$ , where  $i = 1, 2, \dots, m$ ; in agreement with the calculus of variations, differential geometry and mechanics the systems  $\varepsilon$  are called *source forms*.

A source form  $\varepsilon = \varepsilon_i$  is said to be *variational*, if there exists a function  $\mathcal{L} : I \times U \times \mathbf{R}^m \rightarrow \mathbf{R}$  such that

$$(2.1) \quad \varepsilon_i = -\frac{\partial \mathcal{L}}{\partial x^i} + \frac{d}{dt} \frac{\partial \mathcal{L}}{\partial \dot{x}^i}.$$

If  $\mathcal{L}$  exists, it is called a *Lagrange function for  $\varepsilon$* . Clearly, *variationality* of a source form  $\varepsilon$  means that  $\varepsilon$  belongs to the *image* of the Euler-Lagrange

mapping  $\mathcal{L} \rightarrow E(\mathcal{L})$  in the set of source forms or, in a different terminology, *integrability* of equation (2.1) with respect to the unknown function  $\mathcal{L}$ .

The following is a well-known *integrability condition* for the system (2.1).

**Theorem 2 (Helmholtz conditions).** *If a source form  $\varepsilon = \varepsilon_i$  is variational, then*

$$(2.2) \quad \frac{\partial \varepsilon_i}{\partial \dot{x}^j} - \frac{\partial \varepsilon_j}{\partial \dot{x}^i} = 0,$$

$$(2.3) \quad \frac{\partial \varepsilon_i}{\partial \dot{x}^j} + \frac{\partial \varepsilon_j}{\partial \dot{x}^i} - \frac{d}{dt} \left( \frac{\partial \varepsilon_i}{\partial \dot{x}^j} + \frac{\partial \varepsilon_j}{\partial \dot{x}^i} \right) = 0,$$

and

$$(2.4) \quad \frac{\partial \varepsilon_i}{\partial \dot{x}^j} - \frac{\partial \varepsilon_j}{\partial \dot{x}^i} - \frac{1}{2} \frac{d}{dt} \left( \frac{\partial \varepsilon_i}{\partial \dot{x}^j} - \frac{\partial \varepsilon_j}{\partial \dot{x}^i} \right) = 0.$$

**Theorem 3.** *Suppose that a source form  $\varepsilon = \varepsilon_i$  satisfies conditions (2.2), (2.3) and (2.4). Then there exist some functions  $f = f(t, x^k, \dot{x}^k)$ ,  $\eta_j = \eta_j(t, x^i)$  and  $h = h(t, x^i)$  such that  $\varepsilon_i$  are the Euler-Lagrange expressions of a Lagrange function given by*

$$(2.5) \quad \mathcal{L} = f - \eta_i \dot{x}^i - h.$$

In particular,  $\varepsilon$  is a variational source form.

**Remark 1.** Formula  $\mathcal{L} = f - \eta_i \dot{x}^i - h$  (2.5) defines a Lagrange function for the source form  $\varepsilon_i = P_i + Q_{ij} \dot{x}^j$ ; writing  $\varepsilon_i = P_i + Q_{ij} \dot{x}^j$  (2.2), then the functions  $f$  and  $\eta_j$  can be determined in explicitly as functions of  $P_i$  and  $Q_{ij}$ , and  $h$  remains arbitrary.

### 3 First order variational source forms

Consider a *first order* source form  $\varepsilon = \varepsilon_i$ , where

$$(3.1) \quad \varepsilon_i = \varepsilon_i(t, x^i, \dot{x}^i).$$

In this case Theorem 2 and Theorem 3 of Section 2 imply that the variability of  $\varepsilon$  is equivalent to the conditions

$$(3.2) \quad \frac{\partial \varepsilon_i}{\partial \dot{x}^j} + \frac{\partial \varepsilon_j}{\partial \dot{x}^i} = 0$$

and

$$(3.3) \quad \frac{\partial}{\partial \dot{x}^k} \left( \frac{\partial \varepsilon_i}{\partial \dot{x}^j} - \frac{\partial \varepsilon_j}{\partial \dot{x}^i} \right) = 0,$$

$$(3.4) \quad \frac{\partial \varepsilon_i}{\partial x^j} - \frac{\partial \varepsilon_j}{\partial x^i} - \frac{1}{2} \frac{\partial}{\partial t} \left( \frac{\partial \varepsilon_i}{\partial \dot{x}^j} - \frac{\partial \varepsilon_j}{\partial \dot{x}^i} \right) - \frac{1}{2} \frac{\partial}{\partial x^l} \left( \frac{\partial \varepsilon_i}{\partial \dot{x}^j} - \frac{\partial \varepsilon_j}{\partial \dot{x}^i} \right) \dot{x}^l = 0.$$

Note, however, that condition (3.3) follows from (3.2) and may be omitted.

The following two theorems provide a complete classification of variational first-order source forms.

**Theorem 4.** *Let  $\varepsilon = \varepsilon_i$  be a first-order source form. The following two conditions are equivalent:*

(a)  $\varepsilon$  is variational.

(b) *There exist a system of functions  $\eta = \eta_i$ ,  $\eta_i = \eta_i(t, x^j)$ , and a function  $h = h(t, x^j)$  such that*

$$(3.5) \quad \varepsilon_i = \frac{\partial h}{\partial x^i} - \frac{\partial \eta_i}{\partial t} + \left( \frac{\partial \eta_l}{\partial x^i} - \frac{\partial \eta_i}{\partial x^l} \right) \dot{x}^l.$$

**Theorem 5.** *If a first-order source form  $\varepsilon = \varepsilon_i$  is variational and is expressed by (3.5), then  $\varepsilon$  has a Lagrange function  $f = -\eta_i \dot{x}^i - h$ .*

## 4 Lagrange functions: Canonical decomposition

Now we discuss possible extensions of the basic classical mechanics formula  $\mathcal{L} = \mathcal{T} - \mathcal{U}$ , where  $\mathcal{T} = \mathcal{T}(\dot{x}^i)$  is the kinetic energy and  $\mathcal{U} = \mathcal{U}(x^i)$  is the potential energy, to the functions  $\mathcal{U}$ , which may depend both on positions  $x^i$  and velocities  $\dot{x}^i$ .

Let  $\mathcal{L} : U \times \mathbf{R}^m \rightarrow \mathbf{R}$  be any Lagrange function. Setting

$$\mathcal{T} = \frac{1}{2} \frac{\partial^2 \mathcal{L}}{\partial \dot{x}^i \partial \dot{x}^j} \dot{x}^i \dot{x}^j,$$

we get another Lagrange function  $\mathcal{T} : U \times \mathbf{R}^m \rightarrow \mathbf{R}$ , called the *kinetic energy*, associated with  $\mathcal{L}$ , and a decomposition  $\mathcal{L} = \mathcal{T} - \mathcal{U}$ , where  $\mathcal{U}$  is the *potential energy*, associated with  $\mathcal{L}$ . The Euler-Lagrange form of  $\mathcal{L}$  is

$$E_k(\mathcal{L}) = -\frac{\partial \mathcal{L}}{\partial x^k} + \frac{d}{dt} \frac{\partial \mathcal{L}}{\partial \dot{x}^k}.$$

**Lemma 1.** (a) *The Euler-Lagrange form of  $\mathcal{T}$  is expressed by*

$$\begin{aligned}
-\frac{\partial \mathcal{T}}{\partial \dot{x}^k} + \frac{d}{dt} \frac{\partial \mathcal{T}}{\partial \dot{x}^k} &= \frac{1}{2} \left( -\frac{\partial h_{ij}}{\partial x^k} + \frac{\partial h_{ik}}{\partial x^j} + \frac{\partial h_{jk}}{\partial x^i} \right) \dot{x}^i \dot{x}^j \\
&+ \frac{1}{2} \frac{\partial^2 h_{ij}}{\partial \dot{x}^i \partial \dot{x}^k} \dot{x}^i \dot{x}^j \dot{x}^l + \left( \frac{1}{2} \frac{\partial^2 h_{ij}}{\partial \dot{x}^k \partial \dot{x}^l} \dot{x}^i \dot{x}^j + \frac{\partial h_{ij}}{\partial \dot{x}^k} \dot{x}^j + h_{ik} \right) \dot{x}^l.
\end{aligned}$$

(b) The Euler-Lagrange form of  $\mathcal{U}$  is expressed as

$$\begin{aligned}
-\frac{\partial \mathcal{U}}{\partial x^k} + \frac{d}{dt} \frac{\partial \mathcal{U}}{\partial \dot{x}^k} &= \frac{1}{2} \left( -\frac{\partial h_{ij}}{\partial x^k} + \frac{\partial h_{ik}}{\partial x^j} + \frac{\partial h_{jk}}{\partial x^i} \right) \dot{x}^i \dot{x}^j \\
&+ \frac{1}{2} \frac{\partial^2 h_{ij}}{\partial \dot{x}^i \partial \dot{x}^k} \dot{x}^i \dot{x}^j \dot{x}^l + \left( \frac{1}{2} \frac{\partial^2 h_{ij}}{\partial \dot{x}^k \partial \dot{x}^l} \dot{x}^i \dot{x}^j + \frac{\partial h_{ij}}{\partial \dot{x}^k} \dot{x}^j \right) \dot{x}^l \\
&+ \frac{\partial \mathcal{L}}{\partial x^k} - \frac{\partial^2 \mathcal{L}}{\partial \dot{x}^l \partial \dot{x}^k} \dot{x}^l.
\end{aligned}$$

(c) The Euler-Lagrange form of  $\mathcal{U}$  is expressed as

$$\begin{aligned}
-\frac{\partial \mathcal{U}}{\partial x^k} + \frac{d}{dt} \frac{\partial \mathcal{U}}{\partial \dot{x}^k} &= \frac{1}{2} \left( -\frac{\partial h_{ij}}{\partial x^k} + \frac{\partial h_{ik}}{\partial x^j} + \frac{\partial h_{jk}}{\partial x^i} \right) \dot{x}^i \dot{x}^j \\
&+ \frac{1}{2} \frac{\partial^2 h_{ij}}{\partial \dot{x}^i \partial \dot{x}^k} \dot{x}^i \dot{x}^j \dot{x}^l + \left( \frac{1}{2} \frac{\partial^2 h_{ij}}{\partial \dot{x}^k \partial \dot{x}^l} \dot{x}^i \dot{x}^j + \frac{\partial h_{ij}}{\partial \dot{x}^k} \dot{x}^j \right) \dot{x}^l \\
&+ \frac{\partial \mathcal{L}}{\partial x^k} - \frac{\partial^2 \mathcal{L}}{\partial \dot{x}^l \partial \dot{x}^k} \dot{x}^l.
\end{aligned}$$

## 5 Variational forces

Now we study Lagrange functions  $\mathcal{L}: U \times \mathbf{R}^m \rightarrow \mathbf{R}$  satisfying the *metric homogeneity condition*

$$(5.1) \quad \frac{\partial^3 \mathcal{L}}{\partial \dot{x}^i \partial \dot{x}^j \partial \dot{x}^k} \dot{x}^k = 0.$$

Using the metric  $h_{ij}$  associated with  $\mathcal{L}$ , condition (5.1) can equivalently be expressed as

$$\frac{\partial h_{ij}}{\partial \dot{x}^k} \dot{x}^k = 0.$$

Its meaning is explained by the following theorem.

**Theorem 6.** *Let  $\mathcal{L}$  be a Lagrange function. The following two conditions are equivalent:*

- (a)  $\mathcal{L}$  satisfies the metric homogeneity condition.
- (b) The Euler-Lagrange form  $E(\mathcal{U})$  of potential energy  $\mathcal{U}$  is of order 1.

**Theorem 7.** *Let  $\mathcal{L}$  satisfy the metric homogeneity condition. Then*

$$\mathcal{U} = -h - \eta_i \dot{x}^i + \frac{df}{dt},$$

where

$$(5.2) \quad \begin{aligned} \eta_k &= -\frac{\partial^2 \mathcal{L}}{\partial \dot{x}^i \partial \dot{x}^k} \dot{x}^i + \frac{\partial \mathcal{L}}{\partial \dot{x}^k} + \frac{\partial f}{\partial x^k}, \\ h &= \frac{1}{2} \frac{\partial^2 \mathcal{L}}{\partial \dot{x}^j \partial \dot{x}^i} \dot{x}^j \dot{x}^i - \frac{\partial \mathcal{L}}{\partial \dot{x}^i} \dot{x}^i + \mathcal{L} \end{aligned}$$

for some function  $f=f(x^i)$ . The functions  $\eta_k$  and  $h$  do not depend on  $\dot{x}^i$ .

Our aim now will be to find explicit form of the Lagrange functions satisfying the metric homogeneity condition. Our partial results can be summarized as follows.

Given an arbitrary Lagrange function  $\mathcal{L}$ , we have the canonical decomposition  $\mathcal{L} = \mathcal{T} - \mathcal{U}$ , where

$$\mathcal{T} = \frac{1}{2} \frac{\partial^2 \mathcal{L}}{\partial \dot{x}^i \partial \dot{x}^j} \dot{x}^i \dot{x}^j.$$

Then the following conditions are equivalent:

- (a)  $\mathcal{L}$  satisfies the metric homogeneity condition.
- (b)  $E_i(\mathcal{U})$  do not depend on  $\ddot{x}^k$ , that is, for all  $i$  and  $j$ ,

$$\frac{\partial E_i(\mathcal{U})}{\partial \ddot{x}^j} = 0.$$

If these conditions are satisfied, then  $\mathcal{U}$  is of the form

$$\mathcal{U} = -h - \eta_i \dot{x}^i + \frac{df}{dt},$$

for some function  $f=f(x^i)$ , and

$$(5.3) \quad \begin{aligned} \eta_k &= -\frac{\partial^2 \mathcal{L}}{\partial \dot{x}^i \partial \dot{x}^k} \dot{x}^i + \frac{\partial \mathcal{L}}{\partial \dot{x}^k} + \frac{\partial f}{\partial x^k}, \\ h &= \frac{1}{2} \frac{\partial^2 \mathcal{L}}{\partial \dot{x}^i \partial \dot{x}^j} \dot{x}^i \dot{x}^j - \frac{\partial \mathcal{L}}{\partial \dot{x}^i} \dot{x}^i + \mathcal{L}. \end{aligned}$$

The functions  $h$  and  $\eta_i$  do not depend on  $\dot{x}^k$  and Euler-Lagrange expressions of  $\mathcal{U}$  are

$$(5.4) \quad E_k(\mathcal{U}) = \frac{\partial h}{\partial x^k} + \left( \frac{\partial \eta_l}{\partial x^k} - \frac{\partial \eta_k}{\partial x^l} \right) \dot{x}^l.$$

**Remark 2.** Equation (5.4) shows that for  $m = l$  (the case of mechanical systems with 1 degree of freedom) the Euler-Lagrange form  $E(\mathcal{U})$  cannot depend on  $\dot{x}$ .

It has already been noted in Section 4 that the kinetic energy part in the canonical decomposition of  $\mathcal{L}$  has some properties of the fundamental Finsler

functions in Finsler geometry. We shall now discuss these properties in more detail. We define a (possibly singular) *Finsler metric* as a system of real-valued functions  $g_{ij} = g_{ij}(x^k, \dot{x}^k)$  on  $U \times \mathbf{R}^m$ , satisfying the following conditions:

(a) The matrix  $g_{ij}$  is symmetric,

$$(5.5) \quad g_{ij} = g_{ji}.$$

(b) The derivatives satisfy

$$(5.6) \quad \frac{\partial g_{ij}}{\partial \dot{x}^k} = \frac{\partial g_{ik}}{\partial \dot{x}^j}, \quad \frac{\partial g_{ij}}{\partial \dot{x}^k} \dot{x}^k = 0.$$

**Theorem 8.** A Lagrange function  $\mathcal{L}: U \times \mathbf{R}^m \rightarrow \mathbf{R}$  satisfies the metric homogeneity condition if and only if

$$(5.7) \quad \mathcal{L} = \frac{1}{2} g_{ij} \dot{x}^i \dot{x}^j + h + \eta_i \dot{x}^i,$$

Where  $g_{ij}$  is a Finsler metric and  $h$  and  $\eta_i$  are some functions depending on  $x^i$  only.

**Theorem 9.** For every Finsler metric  $g_{ij}$  formula (5.7) defines a solution  $\mathcal{L}$  of equations (5.3).

**Remark 3.** Note that  $\eta_i$  can also be expressed as

$$\eta_k = -\frac{\partial}{\partial \dot{x}^k} \left( \frac{\partial \mathcal{L}}{\partial \dot{x}^j} \dot{x}^j \right) + 2 \frac{\partial \mathcal{L}}{\partial \dot{x}^k} = \frac{\partial}{\partial \dot{x}^k} \left( 2\mathcal{L} - \frac{\partial \mathcal{L}}{\partial \dot{x}^j} \dot{x}^j \right).$$

Integrating

$$2\mathcal{L} - \frac{\partial \mathcal{L}}{\partial \dot{x}^j} \dot{x}^j - \eta_j \dot{x}^j = \Psi,$$

where  $\Psi = \Psi(x^i)$  is an integration constant. Since

$$\begin{aligned} h &= \left( \frac{1}{2} \frac{\partial^2 \mathcal{L}}{\partial \dot{x}^i \partial \dot{x}^j} \dot{x}^j - \frac{\partial \mathcal{L}}{\partial \dot{x}^i} \right) \dot{x}^i + \mathcal{L} \\ &= \frac{1}{2} \left( \frac{\partial^2 \mathcal{L}}{\partial \dot{x}^i \partial \dot{x}^j} \dot{x}^j - \frac{\partial \mathcal{L}}{\partial \dot{x}^i} \right) \dot{x}^i - \frac{1}{2} \left( \frac{\partial \mathcal{L}}{\partial \dot{x}^i} \dot{x}^i - 2\mathcal{L} \right) \\ &= -\frac{1}{2} \eta_k \dot{x}^k - \frac{1}{2} (-\eta_j \dot{x}^j - \Psi) = \frac{1}{2} \Psi, \end{aligned}$$

we have

$$2\mathcal{L} - \frac{\partial \mathcal{L}}{\partial \dot{x}^j} \dot{x}^j = 2h + \eta_j \dot{x}^j.$$

Our main goal is in this section is to study variational properties of *first-order* source forms  $\phi_i: U \times \mathbf{R}^m \rightarrow \mathbf{R}^m$ ; we call these forms *forces*. A force  $\phi_i$  is said to be *variational*, if there exists a Lagrange function  $\mathcal{L}: U \times \mathbf{R}^m \rightarrow \mathbf{R}$  such that

$$(5.8) \quad \phi_i = E_i(\mathcal{L} - \mathcal{T}),$$

where  $\mathcal{T}$  is kinetic energy associated with  $\mathcal{L}$ , or, equivalently, if  $\phi_i = E_i(\mathcal{U})$ , where  $\mathcal{U}$  is potential energy associated with  $\mathcal{L}$ . Thus a variational force is exactly the Euler-Lagrange form of the potential energy  $\mathcal{U}$ . Allowing  $\mathcal{U}$  to depend on positions and velocities, then we also admit variational forces depending on  $x^l$  and  $\dot{x}^l$ .

The *inverse variational problem* for a force  $\phi_i$  consists of finding integrability conditions and solutions  $\mathcal{L} = \mathcal{L}(x^i, \dot{x}^i)$  of the system (5.8). We already know that the integrability condition is given by equations (3.2) and (3.4),

$$\begin{aligned} \frac{\partial \phi_i}{\partial \dot{x}^j} + \frac{\partial \phi_j}{\partial \dot{x}^i} &= 0, \\ \frac{\partial \phi_i}{\partial x^j} - \frac{\partial \phi_j}{\partial x^i} - \frac{1}{2} \frac{\partial}{\partial t} \left( \frac{\partial \phi_i}{\partial \dot{x}^j} - \frac{\partial \phi_j}{\partial \dot{x}^i} \right) - \frac{1}{2} \frac{\partial}{\partial x^l} \left( \frac{\partial \phi_i}{\partial \dot{x}^j} - \frac{\partial \phi_j}{\partial \dot{x}^i} \right) \dot{x}^l &= 0. \end{aligned}$$

The following two theorems give a more detailed information.

**Theorem 10.** The following two conditions are equivalent:

- (a)  $\phi_i$  is a variational force.
- (b) There exist functions  $P = P(x^i)$  and  $Q_k = Q_k(x^i)$  such that

$$\phi_k = \frac{\partial P}{\partial x^k} + \left( \frac{\partial Q_l}{\partial x^k} - \frac{\partial Q_k}{\partial x^l} \right) \dot{x}^l.$$

**Remark 4.** The class of variational forces admits a physical interpretation; it includes some *dissipative forces*, depending on velocities.

Theorem 10 should be completed by description of *all* Lagrange functions defining a fixed variational force  $\phi_i$ . The following is a solution of the *inverse variational problem* for forces, depending on positions and velocities.

**Theorem 11.** Let  $\phi_i$  be a variational force, let  $\mathcal{U}_0 = -P - Q_i \dot{x}^i$  be a Lagrange function for  $\phi_i$ . Then the following two conditions are equivalent:

- (a)  $\mathcal{L}$  satisfies  $\phi_i = E_i(\mathcal{L} - \mathcal{T})$ .
- (b)  $\mathcal{L}$  is of the form  $\mathcal{L} = \mathcal{T} - \mathcal{U}_0$ , where

$$\mathcal{T} = \frac{1}{2} g_{ij} \dot{x}^i \dot{x}^j$$

for some Finsler metric  $g_{ij}$ .

## 6 Newton's equations

As an example consider a source form  $\varepsilon = \varepsilon_i$ , where



$$\varepsilon_i = g_{ii}\ddot{x}^i - f_i,$$

and  $g_{il}$  and  $f_i$  are functions of  $t, x^i, \dot{x}^i$ .  $\varepsilon$  is called a *Newton's source form*.

**Lemma 2.** *The Newton's source form is variational if and only if*

$$g_{ij} - g_{ji} = 0,$$

$$\frac{\partial g_{ik}}{\partial \dot{x}^j} - \frac{\partial g_{jk}}{\partial \dot{x}^i} = 0,$$

$$\frac{1}{2} \left( \frac{\partial f_i}{\partial \dot{x}^j} + \frac{\partial f_j}{\partial \dot{x}^i} \right) + \frac{\partial g_{ij}}{\partial t} + \frac{\partial g_{ij}}{\partial x^l} \dot{x}^l = 0,$$

$$\frac{\partial g_{ii}}{\partial x^j} - \frac{\partial g_{jj}}{\partial x^i} + \frac{1}{2} \frac{\partial}{\partial \dot{x}^l} \left( \frac{\partial f_i}{\partial \dot{x}^j} - \frac{\partial f_j}{\partial \dot{x}^i} \right) = 0,$$

$$\frac{\partial f_i}{\partial x^j} - \frac{\partial f_j}{\partial x^i} + \frac{1}{2} \frac{\partial}{\partial t} \left( \frac{\partial f_i}{\partial \dot{x}^j} - \frac{\partial f_j}{\partial \dot{x}^i} \right) + \frac{1}{2} \frac{\partial}{\partial x^k} \left( \frac{\partial f_i}{\partial \dot{x}^j} - \frac{\partial f_j}{\partial \dot{x}^i} \right) \dot{x}^k = 0.$$

Now we easily find solutions  $\mathcal{L}$  of the inverse problem equations

$$g_{ii}\ddot{x}^i - f_i = -\frac{\partial \mathcal{L}}{\partial x^i} + \frac{d}{dt} \frac{\partial \mathcal{L}}{\partial \dot{x}^i}.$$

**Theorem 12.** *The Newton source form is variational if and only if*

$$\frac{\partial f_i}{\partial x^j} - \frac{\partial f_j}{\partial x^i} - \frac{1}{2} \frac{\partial}{\partial x^l} \left( \frac{\partial f_i}{\partial \dot{x}^j} - \frac{\partial f_j}{\partial \dot{x}^i} \right) \dot{x}^l = 0.$$

## Acknowledgments

The author thanks to Prof. Daniela Velichova for invitation to the *9th Slovak-Czech Conference on Geometry and Graphics*, Kremnica, Slovakia (September 2023), to deliver a talk *Geometric modelling: Variational principle*. He appreciates the support of the National Science Foundation of China (grant 11872107) and kind hospitality of Prof. Dohghua Shi during his stay in BIT, where essential part of the research on these topics was done. He is also thankful to Prof. Yong-Xin Guo for invitation to the *5th International Conference on Dynamics, Vibration and Control*, 2018, Shijiazhuang.

## References

- [1] D. Krupka, On the local structure of the Euler-Lagrange mapping of the calculus of variations, in: *Differential Geometry and its Applications*, O. Kowalski, Ed., Proc. Conf., Nove Mesto na Morave, Czechoslovakia, Sept. 1980; Charles University, Prague, 1982, 181-188; arXiv:math-ph/0203034

- 
- [2] D. Krupka, Variational forces, *Journal of Mathematical Sciences*, accepted by Yu. Sachkov, in print 2019 (delayed)
  - [3] D. Krupka, D. Saunders, Eds., *Handbook of Global Analysis*, Elsevier, 2008
  - [4] D. Krupka, Z. Urban, J. Volna, Variational submanifolds of Euclidean spaces, *Journal of Mathematical Physics* 59, 032903 (2018)
  - [5] J. Novotny, On the inverse variational problem in the classical mechanics, in: *Differential Geometry and its Applications*, O. Kowalski, Ed., Proc. Conf., N. Mesto na Morave, Czechoslovakia, Sept. 1980; Charles University, Prague, 1982, 189-195; arXiv:math-ph/0203034
  - [6] N. Voicu, D. Krupka, Canonical variational completion of differential equations, *J. Math. Phys.* 56 (4), 043507 (2015); doi:10.1063/1.4918789
  - [7] D.V. Zenkov, Ed., *The Inverse Problem of the Calculus of Variations*, Atlantis Studies in Variational Geometry, Atlantis, 2015; ISBN 978-94-6239-108-6

# Descriptive Geometry in Slovenia, decline or opportunity

Domen Kušar

*Fac. of Architecture, Univ. of Ljubljana  
Zoisova 12, 1000 Ljubljana, Slovenia  
email: domen.kusar@fa.uni-lj.si*

**Abstract.** Descriptive geometry is a science that has been indispensable in all areas of technical education for many years. In addition to the way of representing spatial elements and their relationships on a two-dimensional medium, it also developed a spatial representation. We have been following the downward trend of spatial ability among students of the Faculty of Architecture of the University of Ljubljana since 1999.

With the advent of computers, especially computer graphics, the attitude towards descriptive geometry also changed. Since computers took over the presentation of space, it was no longer necessary. Therefore, the number of hours was reduced, and in many faculties, it was simply abolished or combined with other similar subjects. In Slovenia, this happened at many technical faculties. Part of the blame is also on the side of educators who did not understand the situation and the role that descriptive geometry can play and adapted the material to current needs or even upgraded it.

At the Faculty of Architecture of the University of Ljubljana, beside classical knowledge we included into the course computer programs and new teaching methods. Flexibility helped us to carry out the subject remotely without major problems during Covid. With the project of pilot updating the course using information and communication technology, we wanted to bring the course even closer to students and make it accessible at any time. However, it turned out that digitization also has its limitations, as pedagogical work also requires a personal approach and communication between the pedagogue/assistant and students. This means finding a balance between the use of modern techniques and "classical" pedagogical approaches with the aim of achieving the best possible knowledge and the greatest possible spatial representation that future architects will need in their work.

*Keywords:* Descriptive geometry, teaching methods, Slovenia

## 1 Descriptive Geometry at the faculties in Slovenia

About 2 million people live in Slovenia. For them and others, there are six universities and 25 other higher education institutions offering education at various levels. The three largest universities are state-owned.

The largest and oldest is the University of Ljubljana. Its beginnings date back to the 17th century when a Jesuit college was founded. The first university was established in 1810 during the French occupation. After the end of the Illyrian provinces in 1813, it was abolished. Instead, the Imperial Lyceum was established as a higher education institution. The current University was created

after the collapse of Austria-Hungary in 1919. It included five faculties: law, philosophy, technical theology, and medicine. It is interesting that between 1919 and today, the university changed its name 7 times. Today, the University of Ljubljana consists of 23 faculties and 3 academies. Around 40,000 students study there annually.

Second in size and age is the University of Maribor. It was founded in 1975 although its beginnings date back to 1859 when the Higher Theological School was founded on the initiative of Bishop Anton Marin Slomšek. Today, 17 faculties are included in the University of Maribor most of which are based in Maribor but some are also in Kranj, Celje, Ljubljana, Velenje, Krško, and Brežice. The number of students at the University of Maribor is approximately 15,000.

University	Faculty	Study	Course	ECTS
University of Maribor	Faculty of Civil Engineering, Transportation Engineering and Architecture	Civil engineering	Geometric modeling & Descriptive geometry	4
		Transportation Engineering	Geometric modeling & Descriptive geometry	4
		Architecture	Drawing, visual expression	4
	Faculty of Mechanical Engineering	Mechanical engineering	Technical Documentation	4
University of Ljubljana	Biotechnical Faculty	Wood Science and Technology	Technical drawing and descriptive geometry	4
		Landscape Architecture	Descriptive Geometry	5
	Faculty of Mechanical Engineering	Mechanical engineering	Technical drawing and computer aided modelling of geometry	5
		Civil engineering	Engineering communication	3
	Faculty of Civil Engineering and geodesy	Construction management (BA)	Engineering communication	3
		Geotechnology and mining	Geometry in engineering I	5
	Faculty of natural science and Engineering	Geotechnology and mining	Geometry in engineering II	5
		Faculty of architecture	Single-Cycle Master Study Programme Architecture	Descriptive geometry
First-Cycle University Study Programme Urbanism	Descriptive geometry		3	

Table 1: Descriptive Geometry and subjects directly related to it at higher education institutions in Slovenia.

In addition to these two largest universities, there are four smaller ones and 25 other smaller higher education institutions in Slovenia. Descriptive geometry or the contents of this subject are present in various programs of various technical faculties of the two largest universities (table 1). The objects comprising these contents have different names:

- Descriptive Geometry (Faculty of Architecture, Biotechnical Faculty)
- Technical Drawing and Descriptive Geometry (Biotechnical Faculty)
- Technical Drawing and Computer Aided Modelling of Geometry (Faculty of Mechanical Engineering)
- Engineering Communication (Faculty of Civil Engineering and Geodesy)
- Geometry and Engineering (Faculty of Natural Science and Engineering)
- Technical Documentation (Faculty of Mechanical Engineering)
- Geometric Modelling and Descriptive Geometry (Faculty of Civil Engineering, Transportation Engineering and Architecture)

- Drawing, Visual Expression (Faculty of Civil Engineering, Transportation Engineering and Architecture)

In addition to the contents that are part of descriptive geometry, most subjects also offer knowledge in the field of drawing, production of technical documentation, and the use of computer programs (CAD) for modeling and presentation.

Interestingly, the Faculty of Mathematics does not directly offer the course described geometry nor can it be found at the Faculty of Education. The consequence of this is the fact that in previous primary education, fractals of descriptive geometry were present in only individual subjects of primary school, such as mathematics and technology. In high schools, descriptive geometry is taught as a subject only in certain courses of the high school of construction.

Perhaps the reason for such a situation lies in the fact that, according to one of the lecturers of descriptive geometry, mathematicians should show disinterest in descriptive geometry saying that it is no longer relevant and stop dealing with it. Since there were still demands for this knowledge at the technical faculties, it was passed down from professor to assistant and then on in the last decades. This is probably the reason why architects, builders, and mechanical engineers teach these subjects at universities. In addition to descriptive geometry, they are active in other scientific fields specific to individual faculties. This method also has a positive side because teachers know the field of education well and know more precisely which knowledge in the field of descriptive geometry will be useful to students after the end of their studies.

## **2 Descriptive Geometry at the Faculty of Architecture in Ljubljana**

Descriptive geometry has been part of the curriculum of the Faculty of Architecture since the faculty was established as the Department of Architecture within the Technical Faculty of the University of Ljubljana. It represented the only language for the presentation of three-dimensional objects (buildings) on a two-dimensional medium (paper). With this, it was also the basis of the language of communication between experts from different disciplines who participated in the construction. Therefore, it is understandable that the subject had a large number of hours. As construction became an increasingly complex task, which, with the development of technology, required the cooperation of several different experts, the architect's knowledge also had to increase. The development of computer graphics, on the other hand, brought innovations in the understanding and representation of space and the relationships within it, as well as communication between experts. With this, the importance of descriptive geometry as a means of presentation became smaller. As a result, fewer hours were devoted to the subject. If the total number of hours of lectures and exercises was 120 hours in the academic year 1991/92, it was 90 hours in 2019/20 and is 60 hours today.

Every year, between 200 and 300 students want to enroll at the Faculty of Architecture. Since we can only enroll 115, students have an entrance exam. It tests the ability of candidates to study architecture in the form of a drawing exam and an interview. Even though part of the entrance exam also included a spatial representation test, study candidates come to the Faculty of Architecture with virtually no prior knowledge. Therefore, we want to give the key content of the course for one semester. These are the following types of space presentation methods:

- Monge's method,
- axonometry,
- quoted projection, and
- central projection.

As part of this, we discuss the basics from the position of a point, a line, and a plane through the determination of lines and planes, some metric tasks (determining the correct size of angles and lengths), and cross-section and piercing. Shadows are a special chapter.

In addition, we begin to familiarize students with the AutoCAD program right from the start. Within the scope of the course, students must complete exercises that are divided into basic exercises which are drawn with a pencil or computer and submitted weekly and three complex exercises that are drawn with a computer. The exercises were submitted to the online classroom.

Students are motivated by three colloquiums. Together, these comprise all the material of the course, and, as long as they are evaluated positively, they can replace the exam.

An online classroom, which has over 200 units of different learning materials, serves to help students. It contains information and instructions for creating exercises, solved examples of tasks, summaries of lectures and exercises, study sheets, material for monitoring exercises, and more.

The presentation of material in lectures and exercises is classical with the use of a blackboard, chalk, ruler, and ruler. The good thing about this method is the development of the construction in slow steps. The downside is the limitation in terms of size, precision, obscuring the drawing with a body, padding, errors, and the like. For this reason, in lectures and exercises, we increasingly use PowerPoint presentations. The advantage of this method is especially accuracy and the possibility of repetition or later viewing.

### **3 Teaching method during the Pandemia**

If before 2020 working and learning at a distance was more a matter of individuals and rare events, the COVID-19 crisis plunged us into a new way of education. At the FA, this happened within a week because the management received information that such a situation would last for a long time and not just the initially promised 14 days. For this purpose, the decision was made to close the FA and to conduct all activities remotely. As professors, we found ourselves

in different ways. First of all, it was a question of which method of remote working to choose or which program to use. At first, we used different programs (CISCO WEBEX, MS TEAMS, and ZOOM). The programs are mostly similar but each has its specifics. The FA management decided to use the Zoom program and provided all employees with the appropriate licenses. The selected uniform program for all also enabled the mutual education of employees which facilitated the transition to a new way of working.

The leap to remote work was unproblematic for Descriptive Geometry. The reason lies in the fact that the vast majority of the content we discussed has already been digitized as presentations in PowerPoint, worksheets, solved tasks, etc.

The lectures were thus held online with presentations in PowerPoint. It was similar to the exercises with the assistant preparing worksheets in advance that the students could print or draw and use in the exercises. Pictures of home exercises were uploaded to the online classroom where they were evaluated and corrected.

The rich material of the online classroom was also already there. However, it was necessary to supplement it with an explanation of each task. During the year, more than 200 units of teaching material were available in the online classroom. Certain contents were also added to the library. At the same time, it should be emphasized that the FA immediately started scanning key textbooks, books, and other literature from the faculty library. Thus, students could access study material and literature online.

A special challenge was conducting remote colloquiums. Different questions have arisen: how to distribute tasks, ensure equal opportunities for everyone, supervise independent work and return solved tasks. Here, we proceeded by publishing in advance the data (coordinates of points) that were included in the colloquium. At the beginning of the colloquium, the students were given the task text. They were monitored utilizing the included cameras. For someone to quickly draw a solution, scan/picture it, and send it to someone else to redraw it turned out to be impossible in the given time. It showed that no copying was taking place. The main difference was that we let them use literature and notes at home. Therefore, the tasks were more complex.

Considering the different ways of presenting the material and making exercises for conducting colloquiums and exams, we were interested in the advantages and disadvantages of individual systems or what would be worthwhile to use in the future as well.

The mass media, at least in Slovenia, constantly told us about the severe consequences that the pandemic would cause in the educational process, especially about the great drop in knowledge. My personal experience with my four children was the opposite because I did not feel that the level of knowledge would drop significantly. In addition, they had more time because there were no more trips to school and back, and the lessons also turned out to be normal a lot of time for nothing. With all that in mind, we were wondering how about

descriptive geometry. Will the level of knowledge drop or not? What will be the grades for exercises and colloquiums?

We conducted the research for the period 2014/15 to 2021/22. All students taking the descriptive geometry course were included in the research.

The evaluation of the exercises of both the first and second semesters showed results that were slightly better than in previous years. There are probably several reasons for this:

- Due to remote learning, students had more time because they did not have to travel to Ljubljana. A large part of the students did not live in Ljubljana and had to commute to Ljubljana every day. According to students who depend on public transport, they can spend up to 3 hours a day driving.

- Remote consultations require monitoring what is happening because even a short absence can mean that you have to wait again for your turn. In addition, individual consultations in the lecture hall reach a significantly smaller number of students than remotely.

The results of the colloquia show an interesting picture. The grades of the first colloquium were a little worse but then a little better. The results of the last – the 6th colloquium were worse. Since the tasks in individual colloquiums are similar, it is difficult to say why this happened. Possible reasons are the lack of time in certain terms (work on other subjects).

More interesting is the comparison of the year 2018/19 as the last "normal" and the summer semester 2021/22 where the first semester was remote and the second was live. Here, we indulged in a risky experiment. We gave the 2021/22 generation the same tasks as the 2018/19 year. We assumed that the intergenerational connection of the current generations was bad and that was why the students did not have the tasks of the previous colloquiums. Based on the results, we can confirm this. The results of the 4th and the 5th colloquia this year were far worse than those of two years ago. This is partly due to the "new" method of live performance which is the same as in 2018/19 since the use of literature is not allowed when solving tasks on the FA. It took the students practically the whole semester to reach the average (6 colloquiums). The bad results of the 4th and the 5th colloquium could be attributed to a different method of solving than they were used to in the first semester.

Working remotely has both positive and negative aspects. For remote work, the subject must be more organized and structured. The online classroom must also be better organized. On the other hand, this method requires fewer resources from the students since they do not have to go to college and stay in Ljubljana and it allows more time for other things. Therefore, it is not surprising that at the end of the year, more than half of the students preferred distance learning. Of course, they mostly missed social contacts.

Based on this, we decided to keep some of the good practices of remote work and upgrade them. We included the subject as a pilot project of updating subjects using Information and Communication Technology for teaching purposes, which



was led by the Centre for the Use of ICT in the Pedagogical Process of the University of Ljubljana.

#### 4 Pilot project of using information communication technology at subject Descriptive Geometry

In the academic year 2022/23, the FA started with a renewed study program. This also changed the content of the course Descriptive Geometry.

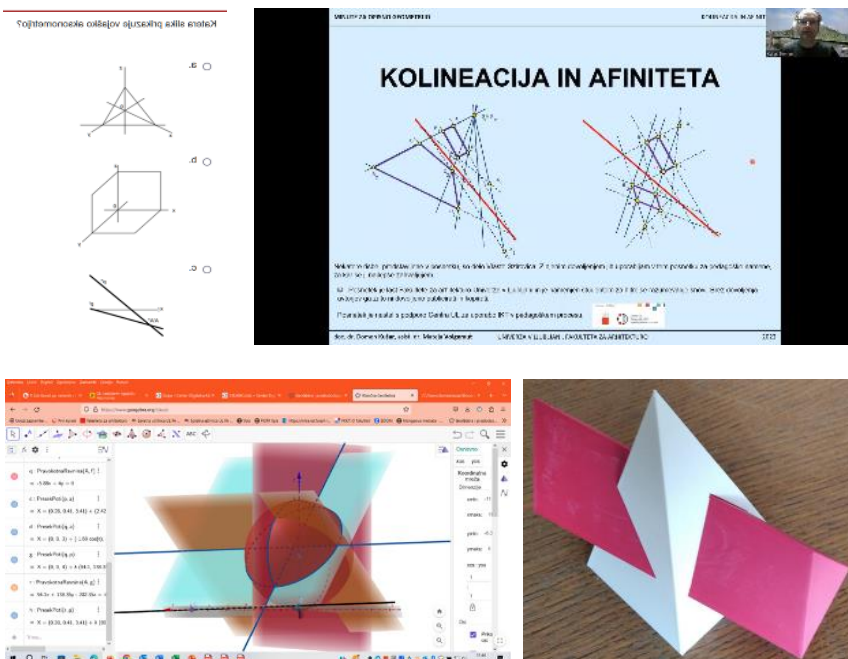


Fig. 1: Some improvements of the subject made within the Pilot Project (quiz, video, use of the GeoGebra program, and 3D printing)

To maintain an appropriate level for the subject, we connected with the colleagues of the Digital University, and based on our experience and the experience of our colleagues from abroad, we designed the renovation and upgrade of the subject. We prepared a different set of study materials available in the online classroom. This included: examples of solved exercises, digitization of the textbook, quizzes, short videos, and presentations of various procedures in PowerPoint. As part of the course, we empowered students to use the AutoCAD program and tried to inspire them to use the GEOGEBRA program. The latter enables good visualization of the relationships between the elements in the room. For this purpose, simulations of some exercises were made. The exercises that the students created individually in the AutoCAD program were submitted to the

online classroom where they also received feedback. We also introduced them to 3D printing and printed the best exercises on a 3D printer (Fig. 1).

Students who regularly attended lectures and exercises praised the material available to them. Even better results would be achieved if students took more time to use all these options. Unfortunately, around the New Year, we noticed general fatigue among students. This may be the result of the large volume of assignments at the end of the semester in other courses because the FA has the largest workload for students at the end of the semester. In the future, we plan to add new shorter videos and integrate 3D printing more into the study process.

## 5 Spatial ability and Descriptive Geometry

An integral part of human ability is spatial intelligence, which includes spatial perception (Gilford, 1996, Mohrer 2008, McGee, 1979). Human abilities consist of linguistic, mathematical, kinesthetic, natural science, musical, and spatial intelligence. We know many components of spatial perception. Spatial perception covers a wide range of skills. It can be improved with experience and practice. It is well known that all engineers need good spatial perception, and so do architects. There are also studies examining the correlation between spatial perception and academic success. It is known that spatial skills and knowledge of mathematics are significantly related at all levels of students' education. Teaching descriptive geometry can improve students' spatial perception to some extent (Ilić, M., Kosić – Jeremić, S., Stavrić, M. (2020). According to experts, the right half of the brain participates in the perception of space (Soros, 2010) because it has been known for many years that the right hemisphere is larger in men and develops earlier than in women (de Lacoste, Hovarth, Woodwart, 1991). This is probably also the reason that confirms the differences between the sexes in the results of spatial representation tests. The difference is most evident in mental rotation tasks, less in orientation, and none in visualization (Linn, Peterson, 1986). Most experts agree that differences do not become apparent until late puberty and that growing up has a major influence on the development of this ability (Nyborg, 1983). The development of the study of spatial representation also required the development of measurement instruments. The first well-known test was developed in 1931 as the Mental Cutting Test (hereafter MCT), and in 1971 Shepard and Metzler developed the rotation test (MRT) (Fig. 2) (Gorska 2005). Both tests are generally applicable even though they are quite specialized in certain areas. MRT is more specialized for spatial perceptions of rotation and mirroring while MCT is for plane-object relationships. DAT (Differential Aptitude Test, developed in 1990) and TPS (Spatial Imagination Test, developed in 2003) aim to cover the comprehensive evaluation of spatial perception. All tests are subject to development and improvement. Suzuki and Shiina [1999] transformed and refined the MRT and standardized the difficulty of each case.

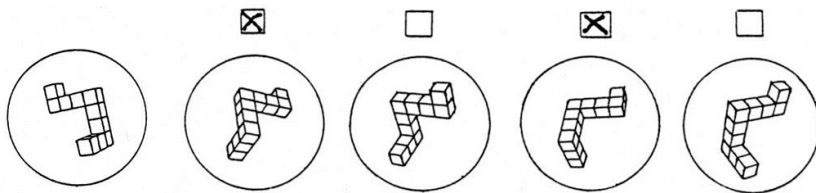
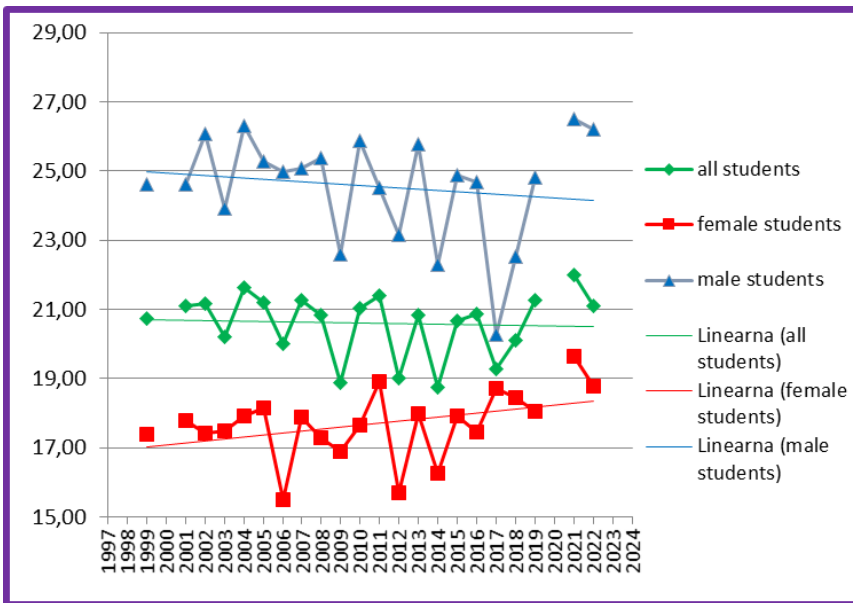


Fig. 2: Sample Mental Rotating Test Task.

When it comes to spatial representation research, it is usually a one-time event that tries to cover a certain population in a certain and geographically limited area. The results of the tests are mostly similar and show the difference between the sexes and progress after the year of study (Leopold et al. 2001, Takeyama et al. 1999). The reasons for such a situation lie in a large number of factors that influence the development of the spatial perception of generations. At the same time, for a realistic comparison, it is necessary to have the same testing conditions, which means that various testing improvements are questionable in this case, regardless of the advantages they otherwise bring. Therefore, we set the conditions for the test at the Faculty of Architecture of the University of Ljubljana (hereafter FA) in 1999 and have always adhered to them since then. This allowed us to compare generations realistically. The long-term analysis is also important regarding the opinion that the level of knowledge of mathematics and technology among new students is declining across Europe. Is this decline also followed by a decline in the level of spatial representation? Reasons for supporting the thesis would probably be found in the environment where we live. New information technology has also brought new patterns of youth behavior. Traditional games for children and adolescents are becoming less and less popular because they are being replaced by digital and virtual games. The result of traditional spatial games was the development of the spatial representation that these games contained. It is difficult to say what the consequences of this exchange are because, on the other hand, information technology makes it easier to perceive space and the relationships within it. Therefore, results that would show long-term trends in this area are even more important (Kušar, 2014).

Every year at the beginning of the academic year, at the Faculty of Architecture of the University of Ljubljana, we conduct a spatial representation test. Testing is carried out at the beginning of the academic year. First-year students participate in this. We have been carrying out this testing since 1999. For this purpose, we use the MRT (mental rotating test). Regardless of the possibilities that information technology offers us, the method of implementation remains the same every year. This ensures adequate conditions for the evaluation and comparison of results. So far, a total of 3,370 students have taken the test. Solved poles are evaluated according to the criteria given in the instructions for solving. We do this even though a different way of assessment might have given

better results – In terms of the normal distribution of results (Bolcskei et al., 2013) that can be expected for this area and the new digital version of MRT (Kušar, D., Volgemut, M., Pletenac, L. (2018)). A comparison of the results shows fluctuations in the spatial representation of the entire population (Graph 1). There is a downward trend in spatial perception. This is more pronounced in the male population while in the female population, there is even a trend of increasing the level of spatial representation. The gender gap shows up throughout the years of testing. A comparison with the results of work on FA showed interesting facts. The correlation between colloquium results and tests of spatial representation is small. This can be partly attributed to the fact that the MRT covers the area of mental rotation but the others do not or are significantly worse. This is also confirmed by comparing the results of exercises where the skill of spatial rotation is required. There, students who have excelled at the MRT also do better in school exercises.



Graph 1: Average of MRT results and trend lines.

## 6 Conclusion

The classical importance of descriptive geometry as a way of communication between experts of different disciplines in the form of representing 3D objects on a 2D medium (plan) is decreasing in Slovenia. The result of this process is first seen in reducing the number of hours or, in some cases, even canceling the course. On the one hand, new content has been added to the descriptive geometry

subject, mostly related to the production of technical documentation and/or geometric modeling using computer programs and 3D printing. In Slovenia, this is also related to the fact that the majority of professors who teach descriptive geometry are no longer mathematicians by education. Instead, they are civil and mechanical engineers and architects. This is probably because descriptive geometry is no longer appreciated by mathematicians. On the other hand, however, technical fields still need it.

In Slovenia, this is also related to the fact that the majority of professors who teach descriptive geometry are no longer mathematicians by education. Instead, they are mechanical engineers and architects. This is probably because descriptive geometry is no longer appreciated by mathematicians. On the other hand, however, technical fields still need it. Since it is known that work in the descriptive geometry course improves spatial representation, the abolition of these contents also manifests itself as a drop in the level of spatial representation. This is also related to changes in society which is comparable to the results of some research outside of Slovenia. A good spatial representation is absolutely necessary in most technical and natural science fields. Since descriptive geometry is usually a demanding subject for students, we wanted to bring it closer to them as part of the Pilot Project. To this end, we have updated the learning material with quizzes, videos, problem-solving examples, 3D printing, and the like. At the same time, we wanted to equip students with additional knowledge of using some computer programs. Surveys completed by students at the end of the year show the correctness of the decision.

## Acknowledgements

The author has been supported by the Faculty of Architecture, University of Ljubljana.

## References

- [1] A. Bolcskei et al.: *New ideas in scoring the Mental rotating test*. Ybl Journal of built environment, Vol. 1 Issue 1: 59-69, 2013
- [2] M. de Lacoste, D. Horvath, D. Woodward (1991): *Possible sex differences in the developing human fetal brain*.  
<http://www.ncbi.nlm.nih.gov/pubmed/1779024>
- [3] J. P. Gilford (1996). *Personality*. New York: McGraw-Hill
- [4] R. Gorska (2005): *Modern Research on Spatial Abilities – An Overview and New Results*. 11th Scientific and professional Colloquium of CSCGCG: Abstracts, Varaždinske toplice, Croatia
- [5] M. Ilić, S. Kosić-Jeremić, M. Stavrić (2020): *Descriptive Geometry and Spatial Ability-Correlation and Mutual Impact at Engineering Students*. Tehnički vjesnik, 27(6), 2001-2007

- [6] D. Kušar, M. Volgemut (2014): *Thirteen years of MRT, results, options and dilemmas*. 16th International Conference on Geometry and Graphics: Proceedings, Innsbruck, Austria, pp. 1248-1256
- [7] D. Kušar, M. Volgemut, L. Pletenac (2018): *Digitizing spatial visualization tests*. In: Cocchiarella, C. (eds.). Proceedings of the 18th International Conference on Geometry and Graphics: 40th anniversary, Milan, Italy, August 3-7, 2018. Milano: International Society for Geometry and Graphics, pp. 1631-1642
- [8] C. Leopold, R. Gorska, S. Sorby (2001): *International Experiences in Developing the spatial visualisation abilities of engineering students*. Journal for geometry and Graphics, Vol. 5, Nr.1: 81-93, 2001
- [9] M.C. Linn, A.C. Petersen (1986): *A meta-analysis of gender differences in spatial ability: Implications for mathematics and science achievement*. In J. S. Hyde & M. C. Linn (Eds.), *The psychology of gender: Advances through meta-analysis*. Baltimore: Johns Hopkins University Press
- [10] M.G. McGee (1979): *Human Spatial Abilities: Psychometric studies and environmental, genetic, hormonal and neurological influences*. Psychological Bulletin, 86(5), pp. 899-918
- [11] J. Mohler (2008): *A review of spatial ability research*. Engineering Design Graphics Journal, vol 72, no 2, 2008
- [12] H. Nyborg (1983): *Spatial ability in men and women: Review and new theory*. Advances in Behaviour Research and Therapy, 5(2), 89-140, 1983
- [13] K. Shiina, K. Suzuki (1999): *Design of modified mental rotation test and its error analysis*. Journal for Geometry and Graphics, Vol. 3, Nr. 2: 211-219, 1999.
- [14] C. Soros (2010): *Measurement of development of spatial ability of Hungarian engineering students – questions and results*. 2nd Croatian Conference on geometry and Graphics: Abstracts, Šibenik, Croatia
- [15] K. Takeyama, R. Maeguchi, K. Chibana, K. Yoshida: *Evaluation of Objective test using a pair of irthographic projections for descriptive geometry education*. Journal for Geometry and Graphics, Vol. 3, Nr.1: 99-111, 1999

# Remarks on de Casteljau algorithm

Zbyněk Šír

*Faculty of mathematics and physics UK  
Sokolovská 83, Prague 130 00, Czech Republic  
email: zbynek.sir@mff.cuni.cz*

**Abstract.** In memory of Paul de Casteljau (1930-2022) we will present several remarks on his famous algorithm. First, we will outline the original affine version. Then we will analyze the projective version (Farin 1983) and will present two interpretations within the classical projective geometry. We will also study alternative versions of the rational algorithm based on the factorization of the curve denominator (Šír and Jüttler 2015). Finally, we will show the generalizations of the de Casteljau algorithm to the case complex curves.

*Keywords:* Bézier curve, de Casteljau algorithm, subdivision, knot insertion, bipolar coordinates

## 1 Affine de Casteljau algorithm

The affine version of the algorithm was first published in [1]. In this version the recursion given as

$$\begin{aligned} \mathbf{P}_j^0 &:= \mathbf{P}_j \\ \mathbf{P}_j^k &:= (1-t)\mathbf{P}_j^{k-1} + t\mathbf{P}_{j+1}^{k-1} = \begin{pmatrix} \mathbf{P}_j^{k-1} & \mathbf{P}_{j+1}^{k-1} \end{pmatrix} \begin{pmatrix} 1-t \\ t \end{pmatrix}, \end{aligned}$$

see Figure 1, provides Bézier curves

$$\mathbf{P}_0^n = \sum_{j=0}^n B_j^n(t) \mathbf{P}_j^0 = \sum_{j=0}^n \binom{n}{j} t^j (1-t)^{(n-j)} \mathbf{P}_j^0.$$

Many properties follows directly from the definition such as the affine covariance, tangent property, subdivision property, convex hull property or the numerical stability.

## 2 Rational de Casteljau algorithm

The rational version of the algorithm, see [2], involves real weights  $w_i$  and their recursion in the following way:

$$\mathbf{P}_j^k := \frac{(1-t)w_j^{k-1}}{(1-t)w_j^{k-1} + tw_{j+1}^{k-1}} \mathbf{P}_{j-1}^{k-1} + \underbrace{\frac{tw_{j+1}^{k-1}}{(1-t)w_j^{k-1} + tw_{j+1}^{k-1}}}_{w_j^k :=} \mathbf{P}_{j+1}^{k-1} \quad (1)$$

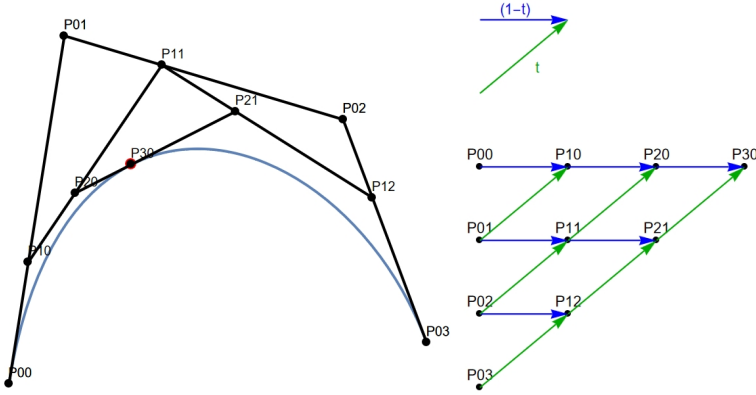


Fig. 1: Affine algorithm (left) and its computational structure (right).

and provides the rational Bézier curve

$$\mathbf{P}_0^n = \frac{\sum_{j=0}^n B_j^n(t) w_j^0 \mathbf{P}_j^0}{\sum_{j=0}^n B_j^n(t) w_j^0}. \quad (2)$$

Note that, while the expression  $(1-t) \mathbf{P}_j^{k-1} + t \mathbf{P}_{j+1}^{k-1}$  is the only affine parameterization of the segment  $\mathbf{P}_j^{k-1} \mathbf{P}_{j+1}^{k-1}$  over  $t \in [0, 1]$ , (1) provides infinitely many such rational parameterizations, depending on the weights.

The most elegant projectively covariant geometric interpretation of the rational algorithm uses so called Farin points defined for each computational level

$$\mathbf{f}_j^k := \frac{w_j^k \mathbf{P}_j^k + w_{j+1}^k \mathbf{P}_{j+1}^k}{w_j^k + w_{j+1}^k}.$$

The position of the new control point is the given by prescribing the the cross-ratio

$$(\mathbf{P}_j^k, \mathbf{P}_{j+1}^k, \mathbf{f}_j^k, \mathbf{P}_j^{k+1}) = \frac{1-t}{t},$$

see Figure 2.

### 3 Alternative rational algorithms

In [5] some alternative algorithms for rational curves were presented. They are based on the factorization of the denominator of (2)

$$\sum_{j=0}^n B_j^n(t) w_j^0 = \prod_{k=1}^n ((1-t)u^k + t v^k)$$



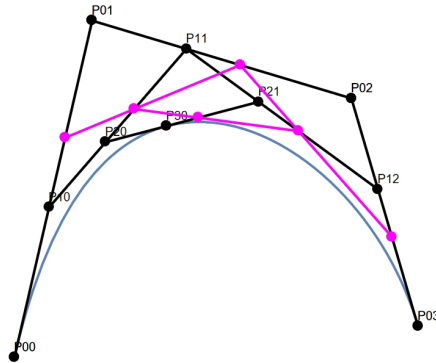


Fig. 2: Rational algorithm with the Farin points (magenta).

and use the recursion

$$\mathbf{P}_j^k = \frac{(1-t)u^k}{(1-t)u^k + tv^k} \mathbf{P}_{j-1}^{k-1} + \frac{tv^k}{(1-t)u^k + tv^k} \mathbf{P}_j^{k-1}.$$

For a curve of degree  $n$  there are up to  $n!$  possible orderings of the factors and thus  $n!$  possible algorithms, see Figure 3. While the alternative algorithms do not

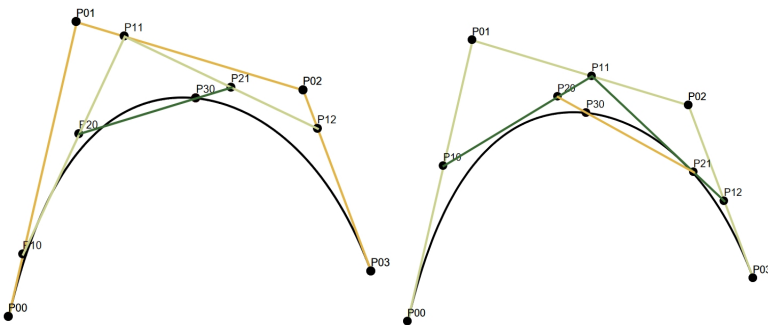


Fig. 3: Two of the six possible alternative algorithms.

anymore possess the tangent and subdivision properties, they present a computational advantage due to constant division ration for each level of the algorithm.

## 4 Rational algorithm for complex curves

Quite remarkably, the rational de Casteljau algorithm (1) can be considered also over the complex numbers, [4]. In this case the underlying geometry is that of Möbius geometry and bipolar coordinates, see [3] for details. All linear segments are replaced by circular segments producing a rather impressive geometrical configuration, see Figure 4.

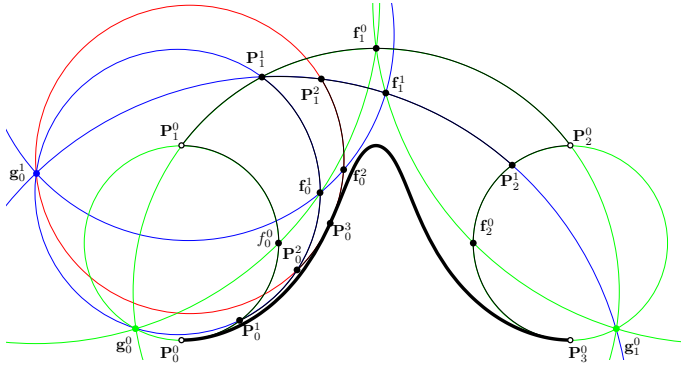


Fig. 4: Complex algorithm with the Farin points  $f_i^j$ .

## 5 Conclusion

We have seen several interesting version of the famous de Casteljau algorithm. Among others variants let us mention several algorithms for surfaces, be Boor algorithm for B-spline curves or algorithms for trigonometric splines. Even after more then 60 years de Casteljau algorithm still stimulate new research ideas.

## References

- [1] de Casteljau, P.: Outillage methodes calcul, Enveloppe Soleau 40.040, Institute National de la Propriété Industrielle, Paris, 1959.
- [2] Farin, G.: Algorithms for rational Bézier curves. *Computer-Aided Design* 15, 73-77, 1983.
- [3] Jüttler, B.; Schicho, J. and Šír, Z.: Apollonian de Casteljau-type algorithms for complex rational Bézier curves. *Computer Aided Geometric Design*, 107: 102254, 2023.
- [4] Sánchez-Reyes, J.: Complex rational Bézier curves. *Computer Aided Geometric Design* 26, 865-876, 2009.
- [5] Šír, Z., Jüttler, B.: On de Casteljau-type algorithms for rational Bézier curves. *Journal of Computational and Applied Mathematics* 288, 244-250, 2015.

## CONTRIBUTED TALKS



# Dynamická učebnica deskriptívnej geometrie pre stavebné odbory

## Dynamic university textbook of descriptive geometry for construction study programs

**Juliana Beganová, Margita Vajsablová**

*Katedra matematiky a deskriptívnej geometrie*

*Stavebná fakulta STU v Bratislave,*

*Radlinského 11, 810 05 Bratislava*

*Slovenská republika*

*email: juliana.beganova@stuba.sk*

*margita.vajsablova@stuba.sk*

**Abstract.** The digital form of study materials gives students a more effective way to learn geometric terms and constructions. The university textbook Descriptive geometry construction study programs was published by a collective of authors in 2022 in electronic form and is suitable for students of study programs focused on civil engineering, architecture, landscape planning, geodesy and cartography. In the paper, we will show the use of various forms of dynamic presentations of geometrical content, which include theory and visualization of concepts and constructions using 2D images, anaglyph images, animations and videos, taking into account the type of software environments and tools used. This approach greatly supports students' understanding and their spatial imagination.

*Keywords:* university textbook, AutoCAD, GeoGebra, anaglyph image, video

*Kľúčové slová:* vysokoškolská učebnica, AutoCAD, GeoGebra, anaglyf, video

## 1 Dynamická učebnica deskriptívnej geometrie

Modernizácia učebných materiálov a ich elektronická forma s interaktívnymi a dynamickými prvkami je významným faktorom efektívnej výučby geometrie na technických vysokých školách. Vo výučbe na technických odboroch sa ukázalo efektívne využiť elektronických dynamických učebníc publikovaných autormi zo Stavebnej fakulty [2], [3], [4], [5] a Strojníckej fakulty STU [6].

Vysokoškolská učebnica Deskriptívna geometria pre stavebné odbory [1] bola publikovaná kolektívom autoriek z Katedry matematiky a deskriptívnej geometrie na Stavebnej fakulte STU v Bratislave v roku 2022 ako jeden z výstupov projektu KEGA 008STU-4/2020. Učebnica je určená pre študentov na bakalárskom stupni študijných programov zameraných na staviteľstvo, architektúru, krajinné plánovanie, geodéziu a kartografiu. Učebnica pokrýva učivo prednášok a cvičení predmetov Deskriptívna geometria na Stavebnej fakulte, Deskriptívna geometria a matematické zručnosti I na Fakulte

architektúry a dizajnu a Deskriptívna geometria na Ústave manažmentu STU v Bratislave.

Kapitoly učebnice sú vo forme dynamických prezentácií jednotlivých tém v prostredí softvéru PowerPoint, pričom geometrické pojmy a princípy konštrukcií sú vizualizované stereoskopickými obrázkami a videami, čo vo veľkej miere podporí pochopenie a priestorovú predstavivosť študentov. Obrázky, ktoré slúžia ako podklady pre vyhotovenie animácií a videí boli vytvorené v prostredí AutoCADu a GeoGebry. Animácie textov a obrázkov majú logickú nadväznosť a umožňujú študentom plnohodnotné pochopenie problematiky aj v samostatnom štúdiu.

Takmer 700 strán učebnice je členených do 12 kapitol, ktoré sú delené na podkapitoly tvoriace samostatné prezentácie. Prezentácie obsahujú teóriu, ale aj široké spektrum riešených konštrukčných úloh a príkladov. V obsahu jednotlivých kapitol je daný dôraz na vedomosti potrebné v príprave inžiniera a aplikácii zobrazení a zobrazovacích metód v práci s objektami stavebnej praxe.

## **2 Proces tvorby dynamických prvkov učebných materiálov s geometrickým obsahom**

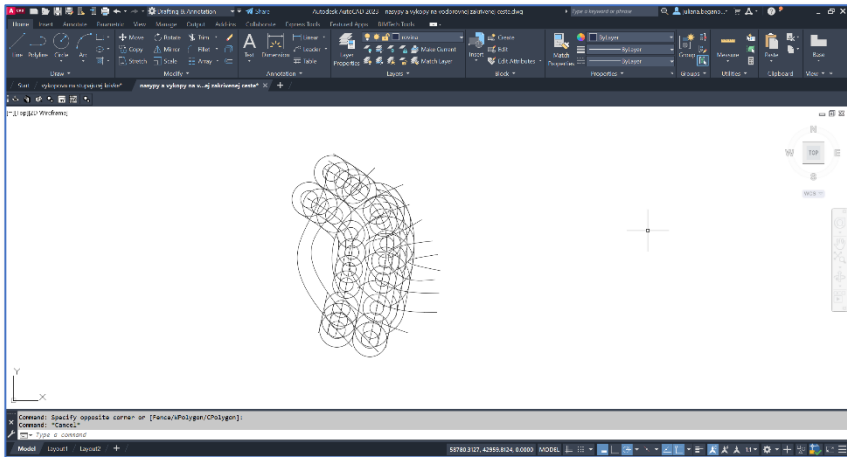
V tvorbe vysokoškolskej učebnice Deskriptívna geometria pre stavebné odbory boli použité viaceré softvéry a programovacie prostredia.

Webová stránka s interaktívnym obsahom bola vytvorená pomocou Microsoft Visual Studio Code. Kapitoly učebnice sú vo forme PowerPoint prezentácií, ktoré okrem textovej zložky obsahujú množstvo obrázkov a videí. Presnosť grafického vyjadrenia geometrických objektov a grafických podkladov pre konštrukčné úlohy bola zabezpečená ich tvorbou v softvéri AutoCAD.

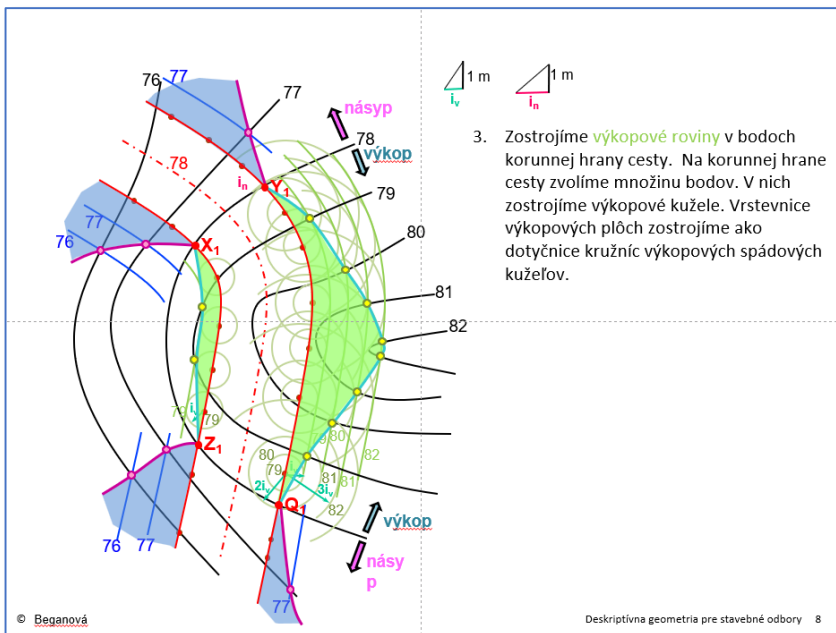
Nástrojmi softvéru GeoGebra boli vyhotovené 3D objekty a anaglyfy, a tiež 2D a 3D objekty a ich animácie. Nasnímanie videí z animácií spustených v GeoGebre bolo realizované pomocou softvéru oCam a následne boli videá úpravené a strihané pomocou Video Editoru. Na ilustráciu geometrických pojmov a ich aplikácií v stavebníctve a architektúre boli použité fotografie, a tiež ilustrácie obrázkami vytvorenými v prostredí Wolfram Mathematica.

### **2.1 Podklady pre konštrukčné úlohy vytvorené v AutoCADe**

Geometrické objekty boli nakreslené a úlohy boli vyriešené v programe AutoCAD, ktorý sa využíva na presné kreslenie, a to bez textového označenia, bez nastavení farby, hrúbky a iných vlastností (Obr. 1). Následne boli exportované ako Windows Metafile a vložené do PowerPointu, kde boli doplnené o formáty, animácie a texty, ktoré popisujú obrázok aj celý postup konštrukcie (Obr. 2). Animácie geometrických objektov (bodov, priamok, kružníc, kriviek a pod.) sú synchronne ladené so súvisiacou teóriou.



Obr. 1: Ukážka obrázku nakresleného v prostredí AutoCADu

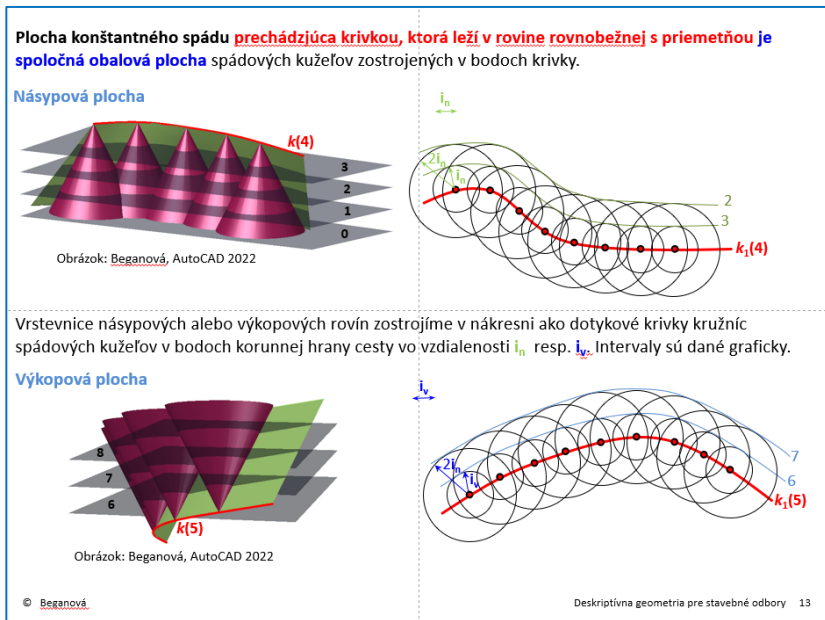


Obr. 2: Ukážka obrázku s doplnenými formátmi a popismi na snímke v PowerPoint prezentácii

## 2.2 Zobrazenie objektov v 3D priestore vytvorených v AutoCADE a v GeoGebre

Pre lepšiu priestorovú predstavivosť boli v AutoCADE a v GeoGebre zobrazené 3D modely objektov, ktoré boli použité v prezentáciách učiva v PowerPointe.

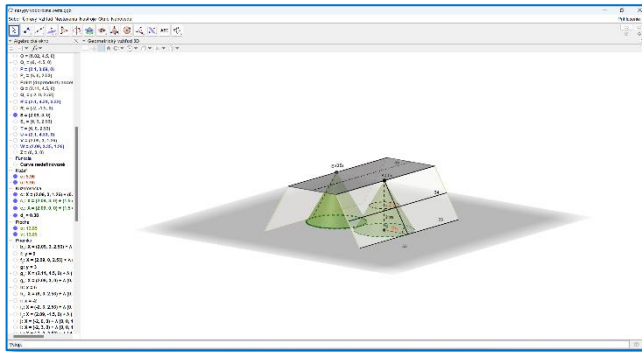
Na Obr. 3 je ukážka 3D modelu plôch konštantného spádu ako obálky kužeľových plôch vytvoreného v AutoCADE a aplikovaného na snímke v PowerPointe, a to s výkladom učiva o projektovaní násypových a výkopových plôch pozdĺž korunných hrán cesty v tvare kriviek ležiacich vo vodorovných rovinách.



Obr. 3: Stránka v PowerPoint prezentácii s 3D modelmi vytvorenými v softvéri AutoCAD

Na Obr. 4 je ukážka 3D modelu rovin daného spádu ako obálky kužeľových plôch vytvorený v GeoGebre a na Obr. 5 je tento model aplikovaný na snímke v PowerPointe s výkladom učiva o projektovaní násypových a výkopových rovin pozdĺž vodorovných priamych korunných hrán cesty, príp. pozdĺž hrán vodorovnej plošiny.





Obr. 4: 3D model nakreslený v softvéri GeoGebra

Napríklad, nech sa cestné teleso nachádza vo výške 35 m a vodorovná rovina s ktorou ho potrebujeme prepojiť násypmi vo výške 33 m. Korunnou hranou cesty zostrojíme rovinu konštantného spádu so spádom  $s_n = 1$  v mierke 1 : 100.

Zvolíme ľubovoľný bod **A** korunnej hrany cesty. Bodom **A** zostrojíme spádový kužeľ. Jeho výška bude 2 m, stred podstavnej kružnice bude ležať v rovine s kótu 33. Polomer kružnice bude  $r = 2i_n$ .

Vypočítame  $i_n = \frac{1}{1} = \frac{1}{1} = 1$

Hľadaná plocha konštantného spádu je dotyková rovina spádového kužeľa v bode **A** prechádzajúca korunnou hranou cesty.

**Postup:**

1. Násypové roviny zobrazíme pomocou hlavných priamok rovnobežných s korunnou hranou cesty vo vzdialenosti  $i_n$ .
2. Hlavná priamka s kótu 33 je priesečnica násypovej roviny s terénom.

**Poznámka:** Ak je topografická plocha daná vrstevnicovým plánom, zostrojíme priesečnicu násypovej roviny s terénom.

Obrázok: Beganová, GeoGebra 2022

© Beganová

Deskriptívna geometria pre stavebné odbory 15

Obr. 5: 3D model použitý na snímke v PowerPointe

## 2.3 Využitie softvéru GeoGebra a ďalších softvérov pri tvorbe videí


Niektoré témy a postupy konštrukcií v deskriptívnej geometrii sú náročné na priestorovú predstavivosť a nie vždy je možné zabezpečiť 3D model. Veľkou pomôckou sa ukázali videá, ktoré prezentujú celý objekt zo všetkých strán alebo zobrazia celý postup, napr. otáčanie roviny v stredovom premietaní. Na Obr. 6 je ukážka strany učebnice, kde je vložené video zobrazujúce strechu so zakázaným odkvapom. Strecha je vyriešená v kótovanom premietaní a priložené video zobrazuje 3D model tejto strechy otáčajúci sa, a teda poskytujúci pohľad

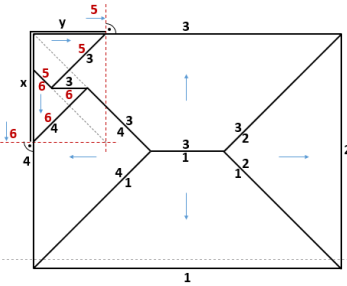
na riešenie zo všetkých strán. 3D model bol nakreslený v softvéri GeoGebra a v GeoGebre bol tiež vytvorený spôsob animácie tohto objektu. Následne bola animácia v GeoGebre spustená a nasnímaná pomocou oCam. Video vytvorené v prostredí oCam bolo upravené pomocou Video Editor a vložené na snímku v PowerPointe. Na každej strane učebnice obsahujúcej video je žltá značka, pri ktorej je popísaný postup opakovaného spustenia videa.

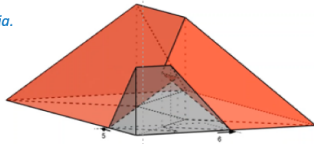
**Riešenie prípadu a)  $y < x < 2y$**

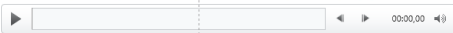
1. Označíme voľné odkvapky a vyriešime časť strechy bez zakázaných odkvapov.
2. Krajnými bodmi zakázaného odkvapu vedieme roviny 5 a 6.
3. Zostrojíme priesečnice 35 a 46.
4. Nárožie 34 bude ukončené v prieniku s úžľabím 35 alebo 46 podľa toho, ktoré ho ukončí skôr. Je to úžľabie 46.
5. Z priesečníka 34 a 46 vychádza hrebeň 36, ktorý je ukončený v prieniku s úžľabím 35.
6. Z priesečníka hrán 35 a 36 vychádza hrana 56.
7. Vyznačíme smer stekania vody v rovinách 5 a 6.

*Pre spustenie videa prejdite myšou na video-obrázok a kliknite na zobrazenú možnosť prehrávania.*







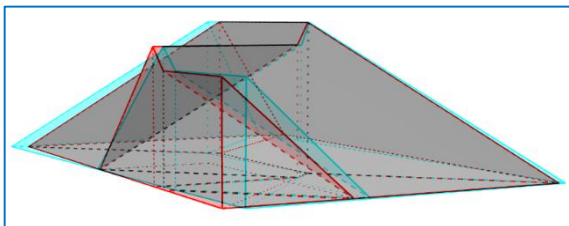


Beganová, Valášková

Obr. 6: Ukážka snímky v PowerPoint prezentácii s vloženým videom

## 2.4 Využitie softvéru GeoGebra pri tvorbe anaglyfov

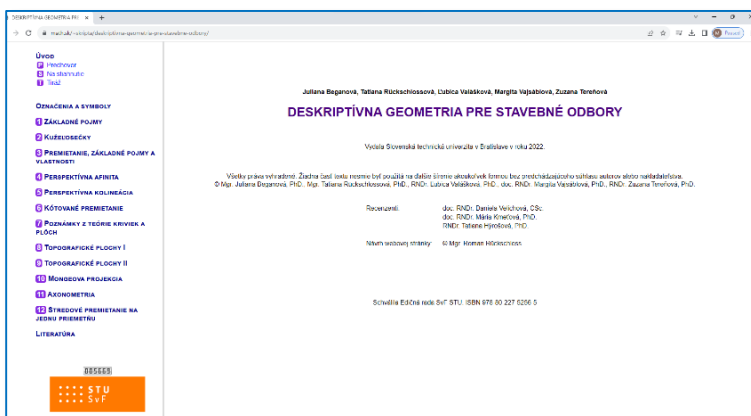
Ako ďalší spôsob názorného zobrazenia geometrických 3D objektov sú v učebnici zakomponované anaglyfy. Z 3D modelov, ktoré boli nakreslené v softvéri GeoGebra sú vytvorené anaglyfy a tie sú zobrazené na snímkach v Powerpointe. Pre ich použitie sú potrebné 3D okuliare. Na Obr. 7 je anaglyf modelu riešenia návrhu strechy pomocou rovín s rovnakým spádom vytvorený v softvéri GeoGebra.



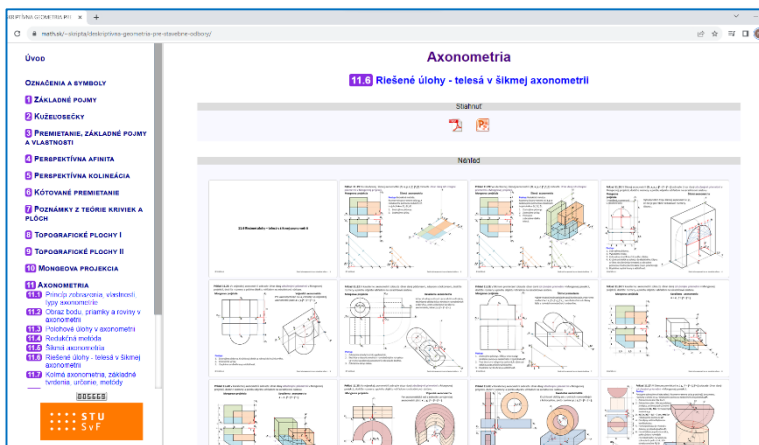
Obr. 7: Anaglyf vytvorený v softvéri GeoGebra

## 2.5 Interaktívny obsah na webovej stránke vytvorenej v Microsoft Visual Studio Code

Učebnica Deskriptívna geometria pre stavebné odbory [1] je dostupná na stránke [www.math.sk](http://www.math.sk) v časti Výuka v predmete Deskriptívna geometria alebo na stránke [www.svf.stuba.sk](http://www.svf.stuba.sk) v časti Dokumenty/Edičná činnosť/Skriptá. Obsah učebnice bol upravený a vložený na stránku vytvorenú pomocou Microsoft Visual Studio Code. Architektúra webovej stránky obsahuje interaktívny výber jednotlivých kapitol a ich podkapitol. Každú podkapitolu je možné otvárať a stiahnuť v dvoch formátoch, a to ako pdf súbor pre potreby tlače a ppsx súbor s prezentáciou vytvorenou v PowerPoint vhodnou na štúdium a výučbu, nakoľko zahŕňa animácie a všetky dynamické prvky kapitol učebnice.



Obr. 8: Úvodná stránka učebnice s interaktívnym obsahom vľavo



Obr. 9: Stránka učebnice Deskriptívna geometria pre stavebné odbory

Na Obr. 8 je úvodná stránka učebnice s interaktívnym obsahom vľavo a na Obr. 9 je stránka s otvorenou podkapitolou 11.6, kedy sa zobrazuje aj jej prehľad snímok. Na hornej časti sú ikony s výberom formátov súborov pdf a ppsx.

### 3 Záver

V tomto článku sme chceli ukázať využitie kombinácie softvérov, a to AutoCADu a Geogebra, podporujúcich presné vykreslenie 2D a 3D objektov, tvorbu anaglyfov a videí (GeoGebra, oCam, Video Editor). Zároveň sme ukázali efektívne zakomponovanie týchto výstupov do PowerPoint prezentácií tvorených kapitoly učebnice Deskriptívna geometria pre stavebné odbory.

### PodĎakovanie

Tento článok vznikol za podpory projektu VEGA 1/0468/20.

### Literatúra

- [1] J. Beganová, T. Rückschlossová, L. Valášková, M. Vajsáblová, Z. Tereňová: *Deskriptívna geometria pre stavebné odbory*, STU v Bratislave, 2022, ISBN 978-80-227-5256-5. Dostupné online: DESKRIPTÍVNA GEOMETRIA PRE STAVEBNÉ ODBORY (math.sk)
- [2] K. Mészárosová, Z. Tereňová: *Deskriptívna geometria I: Stredové premietanie a lineárna perspektíva*. Spektrum STU, Bratislava, 2019. Dostupné online: <https://www.vydavatelstvo.stuba.sk/online-knihy/deskriptivna-geometria-1>
- [3] K. Mészárosová, T. Rückschlossová, Z. Tereňová: *Deskriptívna geometria II: Prvá časť - Rotačné a skrutkové plochy*. Nakladateľstvo STU, Bratislava, 2014. Dostupné online: <https://www.math.sk/skriptaDG2/1/>
- [4] K. Mészárosová, T. Rückschlossová, Z. Tereňová: *Deskriptívna geometria II: Druhá časť – Priamkové, translačné, klinové a kanálové plochy*. SPEKTRUM STU, Bratislava, 2018. Dostupné online: <https://www.math.sk/skriptaDG2/2/>
- [5] M. Vajsáblová: *Metódy zobrazovania*. Vydavateľstvo STU, Bratislava, 2011. Dostupné online: [http://www.svf.stuba.sk/docs//dokumenty/skripta/metody\\_zobrazovania/index.html](http://www.svf.stuba.sk/docs//dokumenty/skripta/metody_zobrazovania/index.html)
- [6] D. Velichová: *3D Geometria*. Bratislava: Spektrum STU, 2021. 458 s. Dostupné online: <http://www.evilm.stuba.sk/~velichova/Geometria/3DGEOM/3DGeometria.html>
- [7] Softvéry: PowerPoint 2013, GeoGebra softvér 5.0, AutoCAD 2022, AutoCAD 2023, oCam. Ink, Video Editor 2022, WOLFRAM Mathematica 12.1.1.0. Copyright 1988-2020 Wolfram Research, Inc.

# Contribution of a tangent of multiplicity one to the intersection multiplicity of two plane curves

Adriana Bosáková

*Faculty of Mathematics, Physics and Informatics,  
Comenius University in Bratislava  
Mlynská dolina, 842 48, Bratislava, Slovak Republic  
email: adriana.bosakova@fmph.uniba.sk*

**Abstract.** Intersection multiplicity of two plane curves  $F$  and  $G$  at some point  $P$  has a well-known property of  $I_P(F, G) \geq mn$ , where  $m$  and  $n$  are the multiplicities of the point  $P$  on the curves  $F$  and  $G$  respectively. To each common tangent of  $F$  and  $G$  at  $P$  can be assigned a nonnegative integer, a number equal to its contribution to the intersection multiplicity. This can be done via local investigation methods. The sum of these contribution numbers of all common tangents is equal to the remainder  $R = I_P(F, G) - mn$ . We investigate the values of this contribution number for common tangents of the multiplicity 1.

*Keywords:* algebraic geometry, intersection multiplicity, tangent, curve

## 1 Introduction

Intersection multiplicity is an important notion in algebraic geometry. It is a number which reflects the complexity of an intersection of two plane curves. Our goal is to contribute to the research of the connection of the local geometric and algebraic properties of the curves with the multiplicity of their intersection.

Let  $F \in k[x, y]$  be a polynomial over some algebraically closed field  $k$ . For  $F = \sum c_{i,j}x^i y^j$  ( $c_{i,j} \in k$ ), we define the *order of the polynomial*  $F$  ( $\text{ord}(F)$ ) and the *degree of the polynomial*  $F$  ( $\text{deg}(F)$ ) as

$$\begin{aligned}\text{ord}(F) &= \min\{i + j \mid c_{i,j} \neq 0\}, \\ \text{deg}(F) &= \max\{i + j \mid c_{i,j} \neq 0\}.\end{aligned}\tag{1}$$

Polynomial  $F$  is called *homogeneous*, if  $\text{ord}(F) = \text{deg}(F)$ . For a non-constant polynomial  $F$ , we define an *affine algebraic curve* (*curve*) as a subset of the affine plane  $\mathbb{A}^2(k)$ , the set

$$\{P \in \mathbb{A}^2(k) \mid F(P) = 0\}.\tag{2}$$

We shall use the same capital letter  $F$  both for the polynomial and the curve it defines. If  $\text{deg}(F) = 1$ , the curve corresponding to  $F$  is called a line.

We are interested in the local algebraic and geometric properties of an intersection of two such curves. In this article, by local we shall always mean in the Euclidean topology. Therefore, we focus on the situation in a small neighbourhood of the origin, the point  $O = (0, 0)$ . If we need to investigate a situation in some other point  $P \neq (0, 0)$ , we simply apply a change of coordinates, which maps the point  $P$  onto  $O$  and proceed analogously.

## 2 Local properties of plane curves

Let  $\text{ord}(F) = m$ . Then the polynomial  $F$  can be written as

$$F = F_m + F_{m+1} + \cdots + F_{m+M},$$

where  $F_i \in k[x, y]$  is either a homogeneous polynomial of the degree  $i$  or a zero polynomial and  $F_m \neq 0$ . We define the *multiplicity of the origin on the curve  $F$*  as the number  $m_O(F) = m$ . Since the field  $k$  is algebraically closed, the polynomial  $F_m$  can be written as a product of  $m$  (not necessary different) linear polynomials. These define  $m$  lines, called *the tangents* of  $F$  at the origin. If  $F_i = \prod T_i^{e_i}$ , where  $e_i \in \mathbb{N}$  and  $T_i$  define pairwise distinct lines, we call the number  $e_i$  the *multiplicity of the tangent  $T_i$* .

In a small neighbourhood of the origin, the curve  $F$  can be decomposed into a finite set of branches  $b_1, \dots, b_r$ . Each branch  $b_i$  is defined by a parametrization  $b_i(t) = (t^{c_i}, \beta_i(t))$  for some  $c_i \in \mathbb{N}$  and a (possibly infinite) power series  $\beta_i(t)$ . Each branch has a uniquely defined tangent and a multiplicity  $m_i$ , where  $m_O(F) = m = \sum_{i=1}^r m_i$ . Proper proofs of the properties above and more about branches can be found in [2], [3] or [1].

**Example 2.1.** Let  $F$  be a curve defined by the polynomial

$$F = x^4 y^2 - x^2 y^4 + x^5 y^4 + y^7 - x^8. \quad (3)$$

Then  $m_O(F) = 6$ , and the tangents of  $F$  at this point are  $T_1 = x$  (with the multiplicity 2),  $T_2 = y$  (with the mult. 2),  $T_3 = y - x$  (with the mult. 1) and  $T_4 = y + x$  (with the mult. 1). The curve  $F$  decomposes at the origin into five branches,  $b_1, \dots, b_5$ . Their parametrizations, multiplicities and tangents are listed below.

branch	mult.	tangent
$b_1(t) = (t^3, t^2 - \frac{1}{3}t^4 + \cdots)$	$m_1 = 2$	$x = 0$
$b_2(t) = (t, -t + \frac{1}{2}t^2 + \cdots)$	$m_2 = 1$	$y + x = 0$
$b_3(t) = (t, t + \frac{1}{2}t^2 + \cdots)$	$m_3 = 1$	$y - x = 0$
$b_4(t) = (t, t^2 + \frac{1}{2}t^4 + \cdots)$	$m_4 = 1$	$y = 0$
$b_5(t) = (t, -t^2 + \frac{1}{2}t^4 + \cdots)$	$m_5 = 1$	$y = 0$

The branches of the curve  $F$  are illustrated on Figure 2.1.

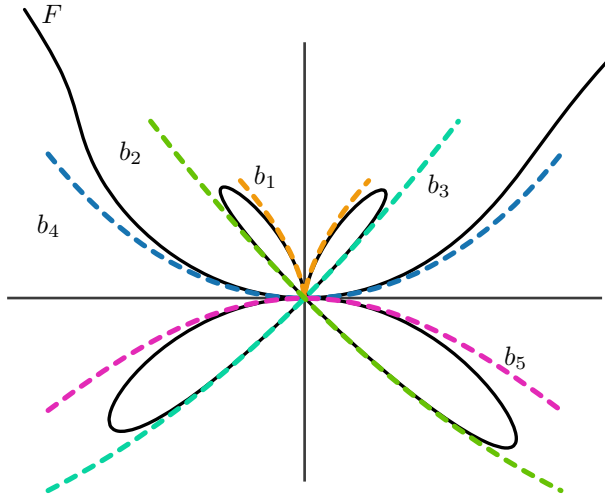


Fig. 1: The curve  $F$  and its five branches in a small neighbourhood of the origin.

Following lemma describes how the branches look like in a case of a tangent of the multiplicity 1. It is later used in the proof of our main result, Theorem 4.1.

**Lemma 2.2.** Let  $F$  be a curve defined by the polynomial

$$F = \sum_{\substack{i \in \{0, \dots, M\} \\ j \in \{0, \dots, M'\}}} f_{i,j} x^{m+i-j} y^j. \quad (4)$$

Let  $y = 0$  be a tangent of  $F$  at the origin of the multiplicity 1. Then there is exactly one branch of  $F$  at the origin with the tangent  $y$  and it can be parametrized by

$$b(t) = (t, t^{h+1} (-f_{0,h} - V(H)t^H + (\text{terms of higher degree}))), \quad (5)$$

where  $h \in \mathbb{N}$  is the smallest number such that  $f_{h,0}$  is nonzero. The function  $V(H)$  is defined as follows. For  $H \geq h$ , there is exactly one pair of integers  $e, i \in \mathbb{N}$ , such that  $H = eh + i$ , where  $i < h$ . Then

$$V(H) = V(e, i) = \sum_{j=0}^{e+1} (-f_{h,0})^{e+1-j} f_{jh+i, e+1-j} \quad (6)$$

*Proof.* We omit the proof of this lemma. It can be proven by a direct (and a rather lengthy) calculation of the Puiseux expansion.  $\square$

### 3 Intersection multiplicity of two plane curves

Let  $F$  and  $G$  be two curves which intersect at the origin. We define their *intersection multiplicity* at this point as

$$I_O(F, G) = \dim k[x, y]/(F, G) \quad (7)$$

where by  $\dim$  we mean the dimension of  $k[x, y]/(F, G)$  as a vector space. More about the intersection multiplicity can be found in numerous books about algebraic geometry, for example [5], [4] or [3].

Let  $m_O(F) = m$  and  $m_O(G) = n$ . Their intersection multiplicity at the origin has a well known property  $I_O(F, G) \geq mn$ . By adding a remainder  $R$ , we can change this inequality to the equality

$$I_O(F, G) = mn + R. \quad (8)$$

**Example 3.1.** Let  $F$  and  $G$  be two curves (illustrated in Figure 3.1) defined by the polynomials

$$\begin{aligned} F &= x^2 - y^5, \\ G &= x^3 - y^4. \end{aligned} \quad (9)$$

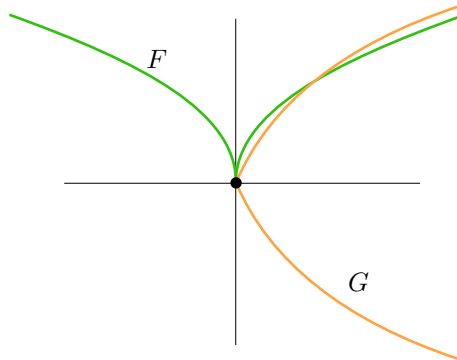


Fig. 2: Intersection of the curves  $F$  and  $G$ .

Then  $m = m_O(F) = 2$ , and  $n = m_O(G) = 3$ . They intersect at the origin with the multiplicity  $I_O(F, G) = 8$ . Therefore the remainder for this example is equal to

$$R = I_O(F, G) - mn = 8 - 2 \cdot 3 = 2. \quad (10)$$



For each common tangent  $T$  of  $F$  and  $G$  at  $O$  we can describe how much it contributes to the remainder  $R$  in the following way. Let  $F$  decompose into  $r$  branches at the origin, the branches  $b_1, \dots, b_r$ . Then

$$I_O(F, G) = \sum_{i=1}^r I_O(b_i, G), \tag{11}$$

where  $I_O(b_i, G) = \text{ord} G(b_i(t))$ . Let  $m_i$  denote the multiplicity of the point  $O$  on the branch  $b_i$ . Then  $m = m_O(F) = \sum_{i=1}^r m_i$ .

Let  $b_{t_1}, \dots, b_{t_s}$  be the set of all branches of  $F$  with the tangent  $T$ . Then the *contribution of a tangent to the intersection multiplicity* is the number  $C_T$ , such that

$$\sum_{j=1}^s I_O(b_{t_j}, G) = (m_{t_1} + \dots + m_{t_s})n + C_T. \tag{12}$$

Therefore, if  $\tau$  is a set of all common tangents of  $F$  and  $G$  at  $O$ , we have the property

$$I_O(F, G) = \sum_{i=1}^r I_O(b_i, G) = mn + \sum_{T \in \tau} C_T \tag{13}$$

Different approaches for the algebraic and geometric description of the remainder  $R$  can be found in [8] and [7].

### 4 Contribution of a tangent of multiplicity 1

Let  $F$  and  $G$  be two plane curves, let the point  $O$  be of the multiplicity  $m$  and  $n$  on the curves  $F$  and  $G$  respectively. Then  $F$  and  $G$  can be defined by the polynomials

$$F = \sum_{\substack{i \in \{0, \dots, M\} \\ j \in \{0, \dots, M'\}}} f_{i,j} x^{m+i-j} y^j, \quad G = \sum_{\substack{i \in \{0, \dots, N\} \\ j \in \{0, \dots, N'\}}} g_{i,j} x^{n+i-j} y^j. \tag{14}$$

for some  $f_{i,j}, g_{i,j} \in k$  and  $M, M', N, N' \in \mathbb{N}_0$ .

Let the line  $y = 0$  be a common tangent of  $F$  and  $G$ . Then  $f_{0,0} = g_{0,0} = 0$ . Let the tangent  $y = 0$  be of the multiplicity 1 on the curve  $F$ . Then  $f_{0,1} \neq 0$ . We denote  $Q = \frac{-f_{1,0}}{f_{0,1}}$ .

**Theorem 4.1.** Let  $F$  and  $G$  be curves defined as above. Let  $C_y$  be the contribution of the tangent  $y$  to their intersection multiplicity at  $O$ . Then

- $C_y \geq 2$  if, and only if,

$$f_{0,1}(g_{0,1}Q + g_{1,0}) = g_{0,1}(f_{0,1}Q + f_{1,0}), \tag{15}$$

- $C_y \geq 3$  if, and only if,

$$f_{0,1} (g_{0,2}Q^2 + g_{1,1}Q + g_{2,0}) = g_{0,1} (f_{0,2}Q^2 + f_{1,1}Q + f_{2,0}), \quad (16)$$

- $C_y \geq 4$  if, and only if,

$$\begin{aligned} & f_{0,1} (g_{0,3}Q^3 + g_{1,2}Q^2 + g_{2,1}Q + g_{3,0}) - f_{1,1} (g_{2,0} + g_{0,2}) = \\ & = g_{0,1} (f_{0,3}Q^3 + f_{1,2}Q^2 + f_{2,1}Q + f_{3,0}) - g_{1,1} (f_{2,0} + f_{0,2}). \end{aligned} \quad (17)$$

*Proof.* This can be proven by direct calculation. Since the multiplicity of the tangent  $y$  on the curve  $F$  at the origin is 1, there is exactly one branch  $b$  of the curve  $F$  with this tangent and it can be parametrized by

$$b(t) = (t, t^{h+1} (-f_{0,h} - V(H)t^H + (\text{terms of higher degree}))), \quad (18)$$

where  $h$  is the smallest number such that  $f_{h,0}$  is nonzero, as defined in Lemma 2.2.

The intersection multiplicity of  $G$  and  $b$  at  $O$  is equal to the order of the polynomial  $G(b(t))$  and has the property

$$I_O(b, G) = 1n + C_y. \quad (19)$$

We show the proof for the case  $C_y \geq 2$ . Let the multiplicity of the tangent  $y$  on the curve  $G$  be  $s$ . Then  $g_{0,0} = \dots = g_{0,s-1} = 0$ ,  $g_{0,s} \neq 0$  and

$$\begin{aligned} G(b(t)) &= \sum_{\substack{i \in \{0, \dots, N\} \\ j \in \{0, \dots, N'\}}} g_{i,j} t^{n+i-j} t^{j(h+1)} (-f_{0,h} - V(H)t^H + (\dots))^j = \\ &= t^{n+hs} \left( g_{0,s} \left( \frac{-f_{h,0}}{f_{0,1}} \right)^s \right) + t^{n+1} (g_{1,0}) \\ &\quad + (\text{terms of degree } \geq n+2). \end{aligned}$$

We need to find the conditions under which the order of the polynomial  $G(b(t))$  is  $n+1$ . One of the following two cases happen.

1. Let  $h = s = 1$ . Then

$$\begin{aligned} G(b(t)) &= t^{n+1 \cdot 1} \left( g_{0,1} \left( \frac{-f_{1,0}}{f_{0,1}} \right)^1 \right) + t^{n+1} (g_{1,0}) + (\dots) = \\ &= t^{n+1} \left( g_{0,1} \frac{-f_{1,0}}{f_{0,1}} + g_{1,0} \right) + (\dots), \end{aligned} \quad (20)$$

therefore the order of the polynomial  $G(b(t))$  is  $n+1$  if, and only if  $g_{0,1} \frac{-f_{1,0}}{f_{0,1}} + g_{1,0} \neq 0$ .

2. Let  $h > 1$  (hence  $f_{0,1} = 0$ ), or  $s > 1$  (hence  $g_{0,1} = 0$ ). Then  $n + hs > n + 1$  and the order of the polynomial  $G(b(t))$  is  $n + 1$  if, and only if  $g_{1,0} \neq 0$ .

Both these cases can be described by a single common condition,  $\text{ord}(G(t)) = n + 1$  if, and only if

$$g_{1,0}f_{0,1} \neq g_{0,1}f_{1,0}, \quad (21)$$

otherwise, it is greater. In other words  $C_y = I_O(b, G) - n \geq 2$  if, and only if,

$$g_{1,0}f_{0,1} = g_{0,1}f_{1,0}. \quad (22)$$

This is equivalent to our desired condition,

$$\begin{aligned} f_{0,1}g_{0,1} \frac{-f_{1,0}}{f_{0,1}} + g_{1,0}f_{0,1} &= f_{0,1}g_{0,1} \frac{-f_{1,0}}{f_{0,1}} + g_{0,1}f_{1,0}, \\ f_{0,1} \left( g_{0,1} \frac{-f_{1,0}}{f_{0,1}} + g_{1,0} \right) &= g_{0,1} \left( f_{0,1} \frac{-f_{1,0}}{f_{0,1}} + f_{1,0} \right), \\ f_{0,1} (g_{0,1}Q + g_{1,0}) &= g_{0,1} (f_{0,1}Q + f_{1,0}). \end{aligned} \quad (23)$$

Analogous process can be repeated for the proof of the cases of  $C_y \geq 3$  and  $C_y \geq 4$ .  $\square$

**Remark 4.2.** Currently we do not have an equivalent result for  $C_y \geq 5$  and higher. However, the results of Theorem 4.1 show a certain pattern in the conditions. This suggests what the conditions for the general case of  $C_y \geq z$  ( $z \in \mathbb{N}$ ) could look like.

## 5 Conclusion

Contribution of an tangent to the intersection multiplicity ( $C_t$ ) is a geometrical property of an intersection connected to the intersection multiplicity. In this article, we are focused on the simplest case, where the multiplicity of a given tangent is 1. We have calculated necessary and sufficient conditions for small values of the number  $C_t$  in this case.

## Acknowledgements

The author has been supported by VEGA 1/0596/21.

## References

- [1] Bohumil Bydžovský: *Úvod do algebraické geometrie*, Jednota československých matematiků a fysiků, 1948.
- [2] William Fulton: *Algebraic Curves: An Introduction to Algebraic Geometry*, <http://www.math.lsa.umich.edu/~wfulton/>.
- [3] Egbert Brieskorn, Horst Knörrer: *Plane Algebraic Curves*, Birkhäuser Basel, 1986.

- [4] Ernst Kunz: *Introduction to Plane Algebraic Curves*, Birkhäuser Basel, 200.
- [5] Daniel Perrin: *Algebraic Geometry, An Introduction*, Springer-Verlag London, 2008.
- [6] David Eisenbud, Joe Harris: *The Geometry of Schemes*, Springer-Verlag New York, 2000.
- [7] Maťašovský, Alexander: *Lokálna Bézoutova veta* 2014, PhD thesis, Univerzita Komenského
- [8] Eduard Bođa, Peter Schenzel *Local Bezout estimates and multiplicities of parameter and primary ideals* Journal of Algebra, vol. 488, p. 42-65, 2017

# Geometry of the Schwarzschild spacetimes

Ján Brajerčík

*Department of Physics, Mathematics and Technologies  
Faculty of Humanities and Natural Sciences, University of Prešov  
Ul. 17. novembra 1, 080 01 Prešov, Slovak Republic  
email: jan.brajercik@unipo.sk*

**Abstract.** In a broader sense, a Schwarzschild spacetime is a smooth manifold, endowed with an action of the special orthogonal group  $SO(3)$  and a Schwarzschild metric, an  $SO(3)$ -invariant metric field, satisfying the Einstein equations. Explicit formulas of all Schwarzschild metrics on 4-dimensional manifold  $\mathbf{R} \times (\mathbf{R}^3 \setminus \{(0, 0, 0)\})$  are introduced, using spherical charts. Existence of a Schwarzschild metric on different manifolds is also discussed.

*Keywords:* Schwarzschild metric, spacetime, special orthogonal group, Einstein equations.

## 1 Introduction

This contribution concerns mathematical foundations of the *general relativity theory* published by Albert Einstein in 1915 [1]. The theory provides a unified description of gravity as a geometric property of four-dimensional spacetime. Relation between the curvature of spacetime and the matter of spacetime is given by the *Einstein field equations*. In generally, these equations represent a system of second order partial differential equations for metric fields. Its exact solution for a case of a single spherical non-rotating mass was found by Karl Schwarzschild in 1915 [5]. The solution is well-known as *Schwarzschild metric* and is formulated in adapted coordinates on the subset  $\mathbf{R} \times (\mathbf{R}^3 \setminus \{(0, 0, 0)\})$  of  $\mathbf{R}^4$  where the mass is placed in its origin. This space with the Schwarzschild metric represents one of the basic models of the general relativity called *Schwarzschild spacetime*.

In this contribution we revise the process of finding the solution of the corresponding Einstein equations on the manifold  $\mathbf{R} \times (\mathbf{R}^3 \setminus \{(0, 0, 0)\})$  by geometric approach. The resulting family of Schwarzschild metrics is parametrized by a function and two real parameters, the integration constants. For any Schwarzschild metric, one of the parameters determines a submanifold, where the metric is not defined, the Schwarzschild sphere. In particular, the family admits a global metric whose Schwarzschild sphere is empty.

By the winding mapping of the real line  $\mathbf{R}$  onto the circle  $S^1$ , these results are transferred to the manifold  $S^1 \times (\mathbf{R}^3 \setminus \{(0, 0, 0)\})$  which topologically differs from  $\mathbf{R} \times (\mathbf{R}^3 \setminus \{(0, 0, 0)\})$ .

All our assertions are derived independently of the signature of the Schwarzschild metric; the signature can be chosen as an independent axiom.

## 2 The special orthogonal group and the rotations

Let us consider  $\mathbf{R}^3$  as a real Euclidean vector space of dimension 3 endowed with the canonical (Euclidean) scalar product. A square matrix  $A$  of dimension 3 with real entries

$$A = \begin{pmatrix} a_{11} & a_{12} & a_{13} \\ a_{21} & a_{22} & a_{23} \\ a_{31} & a_{32} & a_{33} \end{pmatrix}$$

is said to be *orthogonal*, if its row vectors  $(a_{11}, a_{12}, a_{13})$ ,  $(a_{21}, a_{22}, a_{23})$ ,  $(a_{31}, a_{32}, a_{33})$  constitute an orthonormal basis of  $\mathbf{R}^3$ . The set of orthogonal matrices is denoted by  $O(3)$ . The matrix multiplication defines on the set  $O(3)$  a group structure. Its subgroup consisting of all orthogonal matrices with determinant 1 is called the *special orthogonal group* and is denoted  $SO(3)$ . With a smooth structure  $SO(3)$  is also a Lie group.

The group  $SO(3)$  is related with the rotations of  $\mathbf{R}^3$ . Equations of counter-clockwise rotations of  $\mathbf{R}^3$  around the  $x$ -axis, the  $y$ -axis and the  $z$ -axis in the canonical oriented frame in  $\mathbf{R}^3$  are

$$\begin{aligned} \bar{x} &= x, & \bar{y} &= y \cos \beta_1 - z \sin \beta_1, & \bar{z} &= y \sin \beta_1 + z \cos \beta_1, \\ \bar{x} &= x \cos \beta_2 + z \sin \beta_2, & \bar{y} &= y, & \bar{z} &= -x \sin \beta_2 + z \cos \beta_2, \\ \bar{x} &= x \cos \beta_3 - y \sin \beta_3, & \bar{y} &= x \sin \beta_3 + y \cos \beta_3, & \bar{z} &= z, \end{aligned}$$

respectively, where  $\beta_1$ ,  $\beta_2$  and  $\beta_3$  are the corresponding rotation parameters (angles). We call these transformations of  $\mathbf{R}^3$  *elementary rotations*. By *rotation of  $\mathbf{R}^3$*  we mean any composition of elementary rotation around the  $x$ -axis, the  $y$ -axis and the  $z$ -axis. Each rotation  $\rho$  of  $\mathbf{R}^3$  is uniquely determined by its matrix  $B$  given by  $\rho(x, y, z) = B \cdot (x, y, z)$  for all  $(x, y, z) \in \mathbf{R}^3$ .

**Lemma 1.** A matrix of dimension 3 is special orthogonal if and only if it is a matrix of some rotation of  $\mathbf{R}^3$ .

## 3 Spherical atlas

Let us denote by  $U, \bar{U}, V$  open subsets of  $\mathbf{R}^3$  determined as

$$\begin{aligned} U &= \mathbf{R}^3 \setminus \{(x, y, z) \in \mathbf{R}^3 \mid x \geq 0, y = 0\}, \\ \bar{U} &= \mathbf{R}^3 \setminus \{(x, y, z) \in \mathbf{R}^3 \mid x \leq 0, z = 0\}, \\ V &= (0, \infty) \times (0, 2\pi) \times (0, \pi), \end{aligned}$$

and by  $\Lambda : V \ni (r, \varphi, \vartheta) \rightarrow (x, y, z) \in U$  the mapping, defined by the equations

$$x = r \cos \varphi \sin \vartheta, \quad y = r \sin \varphi \sin \vartheta, \quad z = r \cos \vartheta.$$

Analogously, denote by  $\bar{\Lambda} : V \ni (\bar{r}, \bar{\varphi}, \bar{\vartheta}) \rightarrow (x, y, z) \in \bar{U}$  the mapping, defined by equations

$$x = -\bar{r} \cos \bar{\varphi} \sin \bar{\vartheta}, \quad y = -\bar{r} \cos \bar{\vartheta}, \quad z = -\bar{r} \sin \bar{\varphi} \sin \bar{\vartheta},$$

Both  $\Lambda$  and  $\bar{\Lambda}$  are invertible. Denoting  $\Psi = \Lambda^{-1}$ , and  $\bar{\Psi} = \bar{\Lambda}^{-1}$  we have

**Lemma 2.** The charts  $(U, \Psi)$ ,  $(\bar{U}, \bar{\Psi})$  constitute a smooth atlas on  $\mathbf{R}^3 \setminus \{(0, 0, 0)\}$ .

Now consider  $X = \mathbf{R} \times \mathbf{R}^3 \setminus \{(0, 0, 0)\}$  with the atlas formed by two charts  $(\mathbf{R} \times U, \Phi)$ ,  $(\mathbf{R} \times \bar{U}, \bar{\Phi})$ , where  $\Phi = (t, \Psi) = (t, r, \varphi, \vartheta)$ ,  $\bar{\Phi} = (t, \bar{\Psi}) = (t, \bar{r}, \bar{\varphi}, \bar{\vartheta})$ , and  $t$  is the canonical coordinate on  $\mathbf{R}$ .

In this paper, we call this atlas the *spherical atlas* on  $X$ ; the charts  $(\mathbf{R} \times U, \Phi)$ ,  $(\mathbf{R} \times \bar{U}, \bar{\Phi})$  are called *first* and *second spherical charts* on  $X$ .

## 4 Invariant metric

A *metric* of  $X$  is everywhere non-degenerate and symmetric  $(0, 2)$ -tensor field on  $X$ . A  $(0, 2)$ -tensor field  $g$  on  $X$  is said to be *invariant* with respect to a diffeomorphism  $\alpha : X \rightarrow X$ , if its pullback  $\alpha^*g$  satisfies

$$\alpha^*g = g.$$

In the first spherical chart on  $X$ , a  $(0, 2)$ -tensor field  $g$  has an expression

$$\begin{aligned} g = & g_{tt}dt \otimes dt + g_{tr}dt \otimes dr + g_{t\varphi}dt \otimes d\varphi + g_{t\vartheta}dt \otimes d\vartheta \\ & + g_{rt}dr \otimes dt + g_{rr}dr \otimes dr + g_{r\varphi}dr \otimes d\varphi + g_{r\vartheta}dr \otimes d\vartheta \\ & + g_{\varphi t}d\varphi \otimes dt + g_{\varphi r}d\varphi \otimes dr + g_{\varphi\varphi}d\varphi \otimes d\varphi + g_{\varphi\vartheta}d\varphi \otimes d\vartheta \\ & + g_{\vartheta t}d\vartheta \otimes dt + g_{\vartheta r}d\vartheta \otimes dr + g_{\vartheta\varphi}d\vartheta \otimes d\varphi + g_{\vartheta\vartheta}d\vartheta \otimes d\vartheta. \end{aligned}$$

Our aim is to determine  $(0, 2)$ -tensor fields  $g$  on  $X$  invariant with respect to the following transformations of  $X$ :

*action of SO(3)*

$$\text{SO}(3) \times X \ni (A, (t, x, y, z)) \mapsto (t, A \cdot (x, y, z)) \in X,$$

*time translations*

$$\mathbf{R} \times X \ni (\varepsilon, (t, x, y, z)) \rightarrow \tau_\varepsilon(t, x, y, z) = (t + \varepsilon, x, y, z) \in X,$$

*time reflection*

$$X \ni (t, x, y, z) \rightarrow \sigma(t, x, y, z) = (-t, x, y, z) \in X.$$

**Theorem 1.** Each  $(0, 2)$ -tensor field  $g$  on  $X$  invariant with respect to the action of  $\text{SO}(3)$ , to the time translations, and to the time reflection, is in the first spherical chart expressed by

$$g_{\mathbf{R} \times U} = J(r)dt \otimes dt + P(r)dr \otimes dr + Q(r)(\sin^2 \vartheta d\varphi \otimes d\varphi + d\vartheta \otimes d\vartheta),$$

where  $J$ ,  $P$ , and  $Q$  are arbitrary functions of  $r$  on  $\mathbf{R} \times U$ .

Analogous result can be obtained for invariant  $(0, 2)$ -tensor field  $g_{\mathbf{R} \times \bar{U}}$  in the second spherical chart. Taking  $g_{\mathbf{R} \times U}$  and  $g_{\mathbf{R} \times \bar{U}}$  such that the corresponding components coincide on the intersection of domains we get invariant  $(0, 2)$ -tensor field  $g$  globally defined on  $X$  (see [4] for details).

## 5 Einstein equations

In this section our aim is to find all invariant metrics on  $X$  satisfying the Einstein equations. First we recall the basic notation and concepts to this purpose. If we have a metric  $g$  on  $X$ , i.e. symmetric, regular  $(0, 2)$ -tensor field  $g$  on  $X$ , its chart expression using coordinates  $(x^i)$  is

$$g = g_{ij} dx^i \otimes dx^j.$$

The symmetry requirement is in this chart expression represented by the condition  $g_{ij} = g_{ji}$  for all  $i, j$ ; regularity means that  $\det(g_{ij}) \neq 0$  everywhere. The functions

$$\Gamma_{ij}^k = \frac{1}{2} g^{kl} \left( \frac{\partial g_{il}}{\partial x^j} + \frac{\partial g_{jl}}{\partial x^i} - \frac{\partial g_{ij}}{\partial x^l} \right),$$

where  $g^{kl}$  are functions defined by  $g_{jk} g^{kl} = \delta_j^l$ , are the *Christoffel symbols*, the components of the *Levi-Civita connection associated with the metric  $g$* , in a chart  $(U, \varphi)$ . The *curvature tensor* of the Levi-Civita connection is a  $(1, 3)$ -tensor field on  $X$ , expressed by

$$R_{kij}^l \frac{\partial}{\partial x^l} \otimes dx^k \otimes dx^i \otimes dx^j,$$

where

$$R_{kij}^l = \frac{\partial \Gamma_{jk}^l}{\partial x^i} - \frac{\partial \Gamma_{ik}^l}{\partial x^j} + \Gamma_{im}^l \Gamma_{jk}^m - \Gamma_{jm}^l \Gamma_{ik}^m.$$

The *Ricci tensor* is a  $(0, 2)$ -tensor field on  $X$ , expressed by

$$R_{ij} dx^i \otimes dx^j,$$

where the components  $R_{ij}$  is defined by a  $(1, 3)$ -contraction of the curvature tensor,

$$R_{ij} = R_{ijk}^k.$$

Contracting the  $(1, 1)$ -tensor field  $R_j^i = g^{im} R_{mj}$  we obtain a function  $R$  on  $X$ , the *scalar curvature* of  $g$ , or the *Ricci scalar*. In coordinates,

$$R = g^{ij} R_{ij}.$$

*Extremals* of the Hilbert variational functional, in which the scalar curvature stands for the Lagrangian, are determined by the *Einstein equations*,

$$R_{ij} - \frac{1}{2} R g_{ij} = 0. \tag{1}$$



We consider invariant metric  $g$  on  $X$ , in first spherical chart determined by Theorem 1. Due to the regularity condition, smooth functions  $J, P, Q$  are non-zero at every point of their domain. Just three of the Einstein equations (1) are non-trivial and independent. Due to the functions  $J, P, Q$  depend on  $r$  only we get the system of three ordinary differential equations

$$\begin{aligned} \frac{P'}{P} \frac{Q'}{Q} + \frac{1}{2} \left( \frac{Q'}{Q} \right)^2 - 2 \frac{Q''}{Q} + 2 \frac{P}{Q} &= 0, \\ \frac{J'}{J} \frac{Q'}{Q} + \frac{1}{2} \left( \frac{Q'}{Q} \right)^2 - 2 \frac{P}{Q} &= 0, \quad (2) \\ \frac{J'}{J} \frac{Q'}{Q} + 2 \frac{Q''}{Q} + 2 \frac{J''}{J} - \frac{P'}{P} \frac{Q'}{Q} - \frac{J' P'}{J P} - \left( \frac{J'}{J} \right)^2 - \left( \frac{Q'}{Q} \right)^2 &= 0, \end{aligned}$$

where  $'$  denotes the derivative with respect to  $r$ . Supposing  $Q(r) > 0$  on its domain, the structure of the equations (2) allows us to denote  $q(r) = \sqrt{Q(r)}$  where  $q(r)$  can be viewed as a smooth function depending on  $r$ , and the coordinates  $(t, r, \varphi, \vartheta)$ , on  $\mathbf{R} \times U$ , can be replaced by  $(t, q, \varphi, \vartheta)$ . If  $Q(r) < 0$ , for all  $r$ , then we denote  $q(r) = \sqrt{-Q(r)}$ , and proceed as above. Setting

$$j(q) = J(r), \quad p(q) = P(r) \left( \frac{dr}{dq} \right)^2,$$

a metric  $g$  can be rewritten in the form

$$g = j(q)dt \otimes dt + p(q)dq \otimes dq + q^2(\sin^2 \vartheta d\varphi \otimes d\varphi + d\vartheta \otimes d\vartheta),$$

and the system (2) turns to easily solvable system

$$\begin{aligned} \frac{j}{qp} \left( \frac{p'}{p} - \frac{1}{q}(1-p) \right) &= 0, \\ -\frac{1}{q} \left( \frac{j'}{j} + \frac{1}{q}(1-p) \right) &= 0, \quad (3) \\ -\frac{1}{4} \frac{q^2}{p} \left( \frac{2}{q} \left( \frac{j'}{j} - \frac{p'}{p} \right) + 2 \frac{j''}{j} - \frac{j' p'}{j p} - \frac{(j')^2}{j^2} \right) &= 0. \end{aligned}$$

**Theorem 2.** (*Schwarzschild solution*) For any constants  $C, C', C' \neq 0$ , formula

$$g = C' \left( 1 - \frac{C}{q} \right) dt \otimes dt + \left( 1 - \frac{C}{q} \right)^{-1} dq \otimes dq + q^2(\sin^2 \vartheta d\varphi \otimes d\varphi + d\vartheta \otimes d\vartheta)$$

defines a solution of the Einstein equations (3). The domain of definition of this solution is an open set of  $\mathbf{R} \times U$  defined by  $q \neq C$ .

Again, analogous result can be obtained in the second spherical chart. Taking values of  $q, C, C'$  coinciding at the intersection of the chart domains we get the solution defined globally on  $\mathbf{R} \times (\mathbf{R}^3 \setminus \{(0, 0, 0)\})$  (for  $C \leq 0$ ), or on open subset of  $\mathbf{R} \times (\mathbf{R}^3 \setminus \{(0, 0, 0)\})$  given by equation  $q \neq C$  ( $C > 0$ ). For any fixed  $q$ , the Theorem 2 defines a metric  $g$  on  $\mathbf{R} \times (\mathbf{R}^3 \setminus \{(0, 0, 0)\})$ . We get a family parametrized by the constants  $C$  and  $C'$ . Any element of this family is a *Schwarzschild metric*. The manifold  $\mathbf{R} \times (\mathbf{R}^3 \setminus \{(0, 0, 0)\})$  endowed with a Schwarzschild metric  $g$ , is a *Schwarzschild spacetime*.

## 6 Schwarzschild solution on $S^1 \times (\mathbf{R}^3 \setminus \{(0, 0, 0)\})$

Let us consider the canonical product manifold structure on the topological space  $S^1 \times (\mathbf{R}^3 \setminus \{(0, 0, 0)\})$ , and a *winding mapping*  $\kappa_0$  from  $\mathbf{R}$  to  $S^1$ . This mapping induces a surjection

$$\kappa : \mathbf{R} \times (\mathbf{R}^3 \setminus \{(0, 0, 0)\}) \rightarrow S^1 \times (\mathbf{R}^3 \setminus \{(0, 0, 0)\})$$

by  $\kappa(t, x, y, z) = (\kappa_0(t), x, y, z)$ . Our objective is to introduce an analogue a Schwarzschild metric for the manifold  $S^1 \times (\mathbf{R}^3 \setminus \{(0, 0, 0)\})$  which topologically differs from the manifold  $\mathbf{R} \times \mathbf{R}^3 \setminus \{(0, 0, 0)\}$ .

**Theorem 3.** Let  $g$  be a Schwarzschild metric on  $\mathbf{R} \times \mathbf{R}^3 \setminus \{(0, 0, 0)\}$ . The metric  $h$  on  $S^1 \times (\mathbf{R}^3 \setminus \{(0, 0, 0)\})$  such that

$$g = \kappa^* h$$

is a globally well defined solution of the Einstein equations.

## Acknowledgements

The author would like to thank Professor Demeter Krupka for the suggestion to deal with this problem and his cooperation during its solution.

## References

- [1] A. Einstein: *Die Feldgleichungen der Gravitation*, Sitzungsberichte der Königlich Preussischen Akademie der Wissenschaften zu Berlin. 1915, 844–847
- [2] F. De Felice, C.J.S. Clarke: *Relativity on Curved Manifolds*, Cambridge Monographs on Mathematical Physics, Cambridge. 1990
- [3] S.W. Hawking, G.F.R. Ellis: *The Large Scale Structure of Space-Time*, Cambridge University Press, Cambridge. 1973
- [4] D. Krupka, J. Brajerčík: *Schwarzschild Spacetimes: Topology*, Axioms. 2022, 11, 693
- [5] K. Schwarzschild: *Über das Gravitationsfeld eines Massenpunktes nach der Einsteinschen Theorie*, Sitzungsberichte der Königlich Preussischen Akademie der Wissenschaften zu Berlin. 1916, 189–196

# VTOL propeller development in start-up environment

Jaroslav Cibulka

*Dept. of technical mathematics, Fac. of Mechanical Eng., Czech Technical University in Prague  
Technická 4, Praha 6 – Dejvice, 160 00, Czech Republic  
email: jaroslav.cibulka@fs.cvut.cz*

**Abstract.** City air mobility transport with vertical take-off and landing capabilities challenges engineers across development spectra. Fast prototyping of parametric propeller geometry will be introduced as well as start-up approach to new geometry requirements. Capabilities and deficiencies of open propeller geometry software will be compared to classical licensed software approach. SLA 3D printer used as a suitable tool for basic geometry evaluation and aero-acoustic testing will be described.

*Keywords:* VTOL, propulsion unit, propeller, blade, parametric CAD model.

## 1 Introduction

There are 3 main propulsion systems used for VTOL. First one and the easiest to design is *separate propeller units* for horizontal and vertical flight. This system allows effective design of each horizontal and vertical propellers however creates higher drag forces during horizontal flight and adds weight of non-used system. This problem can be solved by second type which is *tilting rotor system*. Here transition phase of flight is carried by rotating rotors. The problem of this system is need of compromise on propeller design for both vertical and horizontal flight propeller efficiency and technical complexity of rotating rotor system. The last system is *ducted fan configuration* where turbofan stator and rotor systems are located inside wings ducts for vertical flight with benefits of higher ground effect and other physical phenomena. Ducted fan approach provides better aero-acoustic optimization possibilities also allowing rotation of whole unit during transition phase.

## 2 Propeller design approach

Procedure of every propeller design starts with analytical computation of propeller design parameters based on aircraft performance demands [1]. From propeller diameter, propeller revolutions per minute, desired power and air conditions (pressure and density), main propeller design parameters (angle of attack, angle of incidence, chord length, twist/lean/sweep angles) are computed.

These parameters give complete description of propeller design which can then be constructed by one of following approaches. [2]

## 2.1 Design engineer with commercial CAD software

This approach means construction of whole propeller by design engineer, starting with propeller profile construction (usually from NACA library), manual positioning of profiles along stacking line and final surface creation with desired surface continuity. Problems of this approach are time consumption, cost (engineer with commercial CAD software such as CATIA) and complicated possibilities of geometry optimization and modification.

## 2.2 Parametric CAD of propulsion unit

Parametric CAD tools for propeller/blade design are the best option for fast prototyping. *Qprop* for propeller and *Xrotor* for blade design opensource tools, constantly being developed on MIT, give complete independent control of parametric design together with low-fidelity aero-acoustic analyses. After mastering non-intuitive environment, user is able to generate, quickly analyze and optimize propulsion unit geometry. [3]

## 2.3 Parametric CAD of aircraft

Another parametric CAD tool for description of whole aircraft is than implemented into design procedure to give geometry control of the whole aircraft. NASA OpenVSP is a simple .exe opensource software allowing user to create and parametrically describe simplified geometry of whole aircraft with all avionic systems (wings, flaps, propulsion units, landing gear). This geometry is than used for advanced high-fidelity aero-acoustic analyses to give complete mathematical model of aircraft behavior. [4]

## 2.4 In-house parametrical geometry software

For the final stages of blade/propeller design, to capture all details and prepare geometry built specifically for specific aircraft, python/c++ in-house software are used. The main benefit of this step is high quality CAD generation with easy and fast possibility of very fine parameter optimization.

## 3 SLA 3D printer – fast prototyping tool

Stereolithography (SLA) 3D printing is the most common resin 3D printing process that has become vastly popular for its ability to produce high-accuracy, isotropic, and watertight prototypes and end-use parts in a range of advanced materials with fine features and smooth surface finish.

Most common desktop SLA 3D printer works on a simple principle of submerging horizontal plate into vane with transparent bottom. LCD UV display

than lights on printed area. By repeating process of lifting, submerging and printing each layer, the desired resin object is printed.

The process of preparation consists of several steps. Firstly watertight geometry needs to be transformed into mesh *.stl* format. Then in slicing software the model is pre-processed by setting up internal (honeycomb, triangular etc.) and external (supports) structures. Display and layer parameters are also set in slicing software.

Final 3D print can be postprocessed directly in post-processing machine or by cleaning in alcohol and hardening in UV oven.

Accuracy of average desktop SLA printer is the accuracy of LCD display (full-HD, 4K) in horizontal plane and 0.01mm in vertical plane.

## References

- [1] T. Theodorsen. „Theory of Propellers”. McGraw-Hill, New York, 1948.
- [2] A. M. Stoll and E. V. Stilson and J. Bevirt and P. P. Pei, “Conceptual Design of the Joby S2 Electric VTOL PAV“, 14th AIAA Aviation Technology, Integration, and Operations Conference, doi:10.2514/6.2014-2407.
- [3] M. Drela, „QPROP Formulation”, MIT Aero & Astro June 2006.
- [4] R. A. McDonald and J. R. Gloudemans, “Open Vehicle Sketch Pad: An Open Source Parametric Geometry and Analysis Tool for Conceptual Aircraft Design”, AIAA 2022-0004, AIAA SCITECH 2022 Forum, January 2022.
- [5] J. Cibulka, 3D Modelling of Compressor Blades, Prague 2020 master thesis, CTU in Prague, supervisor doc. Ing. Ivana Linkeová, Ph.D.



# Mesh primitive counting formulas for subdivision surfaces

Martin Čavarga

*Department of Algebra and Geometry, Comenius University Bratislava  
Mlynská dolina 5692, 841 04, Bratislava, Slovak Republic  
email: martin.cavarga@fmph.uniba.sk*

**Abstract.** Subdivision surfaces are commonly used to simulate additional detail for mesh objects on the scene. For certain problems, such as Lagrangian shrink-wrapping, determining the number of vertices of the subdivision surface is crucial for estimating vertex density. Furthermore, gauging the number of mesh primitives relative to the subdivision level becomes useful for memory preallocation during the surface creation process. We propose a general method for estimating these values using solutions to simple systems recurrence equations.

*Keywords:* Subdivision, mesh, level-of-detail, recurrence.

## 1 Introduction

Subdivision surfaces, created by refining a base cage surface, are used in geometric design [7] and real-time rendering [8]. This paper presents counting formulas for estimating mesh primitive (vertices, edges, faces) counts based on the connectivity of the base mesh and the recursive properties of subdivision (see Fig. 1 (a)). These formulas help in computing vertex density [6] and in efficient memory allocation for subdivision surface construction.

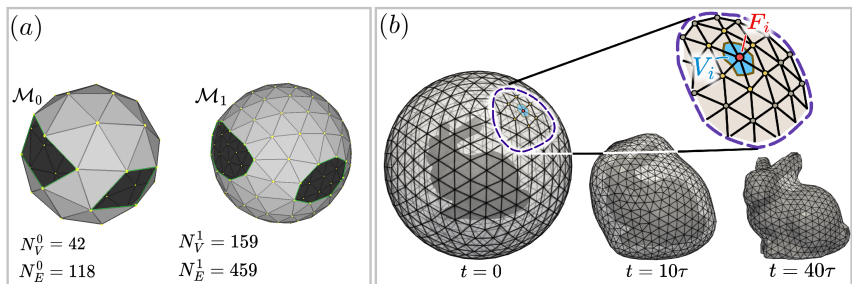


Fig. 1: (a) The amount of mesh vertices  $N_V^s$  and edges  $N_E^s$  with respect to subdivision level  $s = 0, 1, \dots$  depends on the initial connectivity  $\mathcal{M}_0$ . (b) Three snapshots of the evolution of an icosphere with subdivision level  $s = 3$  under an advection-diffusion shrink-wrapping model introduced in [6]. The detail shows a chosen mesh vertex  $F_i$  (red) with its corresponding barycentric Laplacian co-volume  $V_i$  (blue).

## 2 Motivation

According to Section 2.4 of [6] a semi-implicit formulation of a parabolic advection-diffusion evolution applied to manifold mesh surfaces, requires us to ensure that the time step size  $\tau > 0$  is close to the value of mean area  $\mu(V)$  of a barycentric Laplacian co-volume  $V$  surrounding each mesh vertex (see Fig. 1). The most straightforward approach is to compute a 2-dimensional scaling factor

$$\phi = \sqrt{\frac{\tau}{\mu_r(V)}}, \quad \text{where } \mu_r(V) = \frac{4\pi r^2}{N_V^s}. \quad (1)$$

This assumes a spherical evolving surface with uniform vertex distribution. To achieve stability and return to the original scale, the mesh is scaled using  $\phi$  and then reverted with  $1/\phi$ .

For a surface formed by  $s > 0$  subdivision steps, a counting formula evaluates  $N_V^s$  from the recursive nature of the subdivision operation. A typical example of such surface is an *icosphere* which is a form of *spherical geodesic grid* used as a discrete computational domain for applications such as climate modeling [13] and global data visualization [16]. Starting from initial vertex count of an icosahedron  $N_V^0 = 12$  we have

$$N_V^1 = 42, \quad N_V^2 = 162, \quad N_V^3 = 642, \quad N_V^4 = 2562, \quad N_V^5 = 10242, \dots$$

Other, more general surfaces with different initial valences for each vertex, would need individual evaluation, which is clearly impractical.

## 3 Related work

In acoustic simulations Alarcão et al. [2] subdivided an icosahedron's radiation pattern for ray direction determination, with formulas for counting vertices and faces:

$$N_V^s = 5 \left( 2^{2s} - 2^s + 2 \sum_{m=1}^{2^s} m \right) + 2, \quad N_F^s = 20 \cdot 4^s. \quad (2)$$

[12] discusses the OLAM geodesic grid construction, beginning with an icosahedron inscribed in the earth. Each triangle subdivides into  $N^2$  smaller triangles, introducing  $30(N^2 - 1)$  new edges and  $10(N^2 - 1)$  vertices. This approach differs from the icosahedron counting formula (2) as it does not consider recursion and solely focuses on 4:1 triangle subdivisions.

Both techniques, however, only handle a single type of triangular base surface under a 4:1 triangle subdivision.



## 4 Manifold mesh subdivision theory

Polygonal meshes are perhaps the most widely adopted representation in the realm of 3D data storage and display. We evaluated the formal definitions of meshes in the prominent literature from the field, such as Botsch et al. [3], and Hoppe et al. [10], and formulated the following definition:

**Definition 4.1.** Let  $\mathcal{K}$  be an abstract simplicial complex containing at most 2-simplices (triangles). Let  $V = \{\mathbf{v}_1, \dots, \mathbf{v}_{N_V}\} \subset \mathbb{E}^3$  a finite set of points referred to as the *vertex set*. Then  $(\mathcal{K}, V)$  is called a *triangle mesh*. A *polygon* is a union of 2-simplices (triangles) each of which is edge-adjacent to another triangle<sup>1</sup>. Let  $\mathcal{M} \supseteq \mathcal{K}$  possibly contain polygons in addition to triangles in  $\mathcal{K}$ . Pair  $(\mathcal{M}, V)$  is then called a *polygonal mesh*.

A pure point-set surface image  $\overline{\mathcal{M}} \subset \mathbb{E}^3$  of the mesh is known as the *geometric realization* of  $(\mathcal{M}, V)$ . This notion is explained in more detail in Section 2 of [10].

Meshes approximating smooth surfaces require distinguishing between general simplicial realizations and those approximating smooth surfaces. Hence, we distinguish between manifold and non-manifold meshes.

**Definition 4.2.** Let  $X$  be a topological 2-manifold, and  $F : X \rightarrow \mathbb{E}^3$  its immersion. A polygonal mesh  $(\mathcal{M}, V)$  is then said to be a *manifold mesh* if  $\overline{\mathcal{M}} = F[X]$ . If the geometric realization  $\overline{\mathcal{M}}$  does not have a boundary  $\partial\overline{\mathcal{M}}$ , we say that  $(\mathcal{M}, V)$  is *watertight*.

A 2-manifold mesh is sometimes referred to as a *surface mesh* for which there exists an efficient data structure [15] which uses ordered 1-simplices - *half-edges* (see Fig.2).

Now define a map  $\mathcal{M} \rightarrow \mathcal{M}^*$  referred to as a *tessellation-changing operation* on  $\mathcal{M}$ , such that  $\mathcal{M}^* \cap \mathcal{M} \neq \emptyset$  where  $\mathcal{M}^*$  is also an extension of the resulting simplicial complex  $\mathcal{K}^*$  containing modified polygons forming a polygonal mesh  $(\mathcal{M}^*, V^*)$ . An example of such operation is evidently subdivision:

**Definition 4.3.** Let  $T = \{i_0, i_1, i_2\} \in \mathcal{M}$  be a triangle in a surface mesh  $\mathcal{M}$ . A tessellation-changing operation  $\Sigma : \mathcal{M} \rightarrow \mathcal{M}^*$  which introduces new 0-simplices (vertices)  $\{i_{01}^*\}$ ,  $\{i_{12}^*\}$ , and  $\{i_{20}^*\}$  per each edge

<sup>1</sup>For example, triangles  $T_0 = \{i, j, k\}$  and  $T_1 = \{j, i, l\}$  are *edge-adjacent* sharing edge  $\{i, j\} \in \mathcal{K}$ .

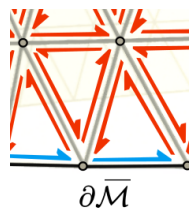


Fig. 2: Each triangle has 3 half-edges, and each interior edge has two opposing half-edges, and there is a single half-edge for each boundary edge.

$\{i_0, i_1\}, \{i_1, i_2\}, \{i_2, i_0\} \in \mathcal{M}$ , and replaces  $T$  with four triangles:

$$\begin{aligned} T_0 &= \{i_0, i_{01}^*, i_{20}^*\}, & T_1 &= \{i_{20}^*, i_{01}^*, i_{12}^*\}, \\ T_2 &= \{i_{01}^*, i_1, i_{12}^*\}, & T_3 &= \{i_{20}^*, i_{12}^*, i_2\}, \end{aligned} \quad (3)$$

is called a 4:1 *triangle subdivision* on  $\mathcal{M}$ . If the change in connectivity information (for triangles and edges) also propagates to all three possible edge-neighboring triangles  $T^{(01)}$ ,  $T^{(12)}$ , and  $T^{(20)}$  of  $T$ , we say that  $\Sigma$  is *compatible with*  $T^{(01)}$ ,  $T^{(12)}$ , or  $T^{(20)}$ . If  $\Sigma$  is targeting all triangles of  $\mathcal{M}$ , and compatible with respect to all neighbors of all triangles, we say that  $\Sigma$  is *globally-compatible*.

A subdivision of  $T$  compatible with respect to  $T^{(e)}$ ,  $e \in \{01, 12, 20\}$  provided that no neighbors of  $T^{(e)}$  are also subdivided yields two edge-adjacent triangles  $T^{(e)} \mapsto T_0^{(e)}, T_1^{(e)}$  sharing vertex  $\{i_e^*\} \in \mathcal{M}^*$ . For the purposes of this paper, however, we only consider globally-compatible subdivisions, that is: if  $T$  subdivides into  $T_0, T_1, T_2$ , and  $T_3$ , so do its edge neighbors  $T^{(e)}$ ,  $e \in \{01, 12, 20\}$  if they exist.

An *approximating*<sup>2</sup> variant of such subdivision is a scheme proposed by Loop [11]. An interpolating variant would be, for example, a simple spherical projection scheme

$$\mathbf{v}_e^* \leftarrow \text{proj}_{\mathbb{S}^2}(\mathbf{v}_e^*) = \mathbf{v}_e^* / \|\mathbf{v}_e^*\|. \quad (4)$$

for constructing an icosphere.

This is, of course, not the only way to subdivide triangle faces in  $\mathcal{M}$ . If we also add an interior vertex  $\{i_{012}^*\} = \{i^*\} \in \mathcal{M}^*$  subdividing  $T$  into three quadrilaterals

$$Q_0 = \{i_0, i_{01}^*, i^*, i_{20}^*\}, \quad Q_1 = \{i_{01}^*, i_1, i_{12}^*, i^*\}, \quad Q_2 = \{i^*, i_{12}^*, i_2, i_{20}^*\}, \quad (5)$$

we formulate the *combinatorial Catmull-Clark subdivision* variant for triangles with its approximating scheme described in [4] and [5]. This scheme can be extended to subdivide an arbitrary mesh ( $m \geq 3$ )-gon with the resulting quads  $Q_0, \dots, Q_{m-1}$  sharing the inserted interior vertex  $\{i^*\}$ . For example, if  $m = 4$ , we get

$$\{i_0, i_{01}^*, i^*, i_{30}^*\}, \quad \{i_{01}^*, i_1, i_{12}^*, i^*\}, \quad \{i^*, i_{12}^*, i_2, i_{13}^*\}, \quad \{i_{30}^*, i^*, i_{13}^*, i_3\}. \quad (6)$$

The subdivision operation can, of course, be repeated  $s > 0$  times

where we write  $\Sigma^s = \overbrace{\Sigma \circ \dots \circ \Sigma}^{s\text{-times}}$ . Infinite application of subdivision then leads to a *limit surface*.

<sup>2</sup>Such that  $(\{i\}, \mathbf{v}_i) \neq \Sigma(\{i\}, \mathbf{v}_i)$  because of the movement of positions  $\mathbf{v}_i$  of the original vertices  $\{i\} \in \mathcal{M}$  under  $\Sigma$ .

## 5 Counting formulas

Recall that in Section 2, we wanted to evaluate the number of mesh vertices  $N_V$  as a function of the subdivision level. This number is closely related to both the count of edges  $N_E$  and faces  $N_F$  through the *Euler polyhedron formula* [9]. In this section, we utilize all the tools at our disposal to prove such "counting formulas" for different types of subdivision.

**Theorem 5.1.** *Let  $\mathcal{M}_s = \Sigma^s(\mathcal{M})$ ,  $s \in \mathbb{N}_0^+$  be a watertight triangle surface mesh, and let  $\Sigma : \mathcal{M}_{s-1} \mapsto \mathcal{M}_s$ ,  $s > 0$  be a globally-compatible  $4 : 1$  subdivision inserting a single vertex for each edge  $e \in \mathcal{M}_s$ . Let  $N_V^s$ ,  $N_E^s$ , and  $N_F^s$  denote the number of vertices, edges, and faces of  $\mathcal{M}_s$  respectively. Then given starting counts  $N_V^0, N_E^0$ , and  $N_F^0$  we have:*

$$N_E^s = 4^s N_E^0, \quad N_F^s = 4^s N_F^0, \quad (7)$$

$$N_V^s = \frac{1}{3} (N_E^0 (4^s - 1) + 3N_V^0). \quad (8)$$

*Proof.* First, we consider that  $\Sigma$  subdivides each face into 4 faces, that is  $N_F^s = 4N_F^{s-1}$  which yields  $N_F^s = 4^s N_F^0$  for any  $s \in \mathbb{N}$ . However, since we insert a new vertex for each existing edge, the number of added vertices in step  $s$  will be equal to edge count  $N_E^{s-1}$ . This gives rise to a system of recurrence equations:

$$\begin{aligned} N_V^s &= N_V^{s-1} + N_E^{s-1}, \\ N_E^s &= 4N_E^{s-1}. \end{aligned} \quad (9)$$

Before solving this system, we need to verify that under  $\Sigma$  the number of edges in  $\mathcal{M}_{s-1}$  increases to 4 times the count in previous step (the second equation for  $N_E$ ).

Since for a triangle mesh without boundary, the total number of half-edges is:

$$N_H = 2N_E = 3N_F, \quad (10)$$

and subdivision from Definition 4.3 updates the number of edge by doubling the amount of existing edges, and adding 3 new interior edges per each triangle, we have

$$N_E^s = 2N_E^{s-1} + 3N_F^{s-1} = 4N_E^{s-1},$$

using (10).

After solving (9) using the  $s$ -th power of the matrix of the system, we get  $N_E^s = 4^s N_E^0$  and (8).  $\square$

The fact that the proof of the above theorem depends only on identity (10) yields:

**Corollary 5.1.** *The statement of Theorem 5.1 is independent from the genus of the surface mesh.*

Introducing boundary violates identity (10) which must be replaced by

$$N_H = 2N_{IE} + N_{BE} = 3N_F, \quad (11)$$

where  $N_E = N_{IE} + N_{BE}$  with interior and boundary edge counts  $N_{IE}$ ,  $N_{BE}$  respectively.

**Theorem 5.2.** *Let  $\mathcal{M}_s = \Sigma^s(\mathcal{M})$ ,  $s \in \mathbb{N}_0^+$  be a possibly non-watertight triangle surface mesh, and let  $\Sigma : \mathcal{M}_{s-1} \mapsto \mathcal{M}_s$ ,  $s > 0$  be a globally-compatible 4 : 1 subdivision inserting a single vertex for each edge  $e \in \mathcal{M}_s$ . Let  $N_V^s$  denote the number of vertices,  $N_{IE}^s$  the number of interior edges, and  $N_{BE}^s$  the number of boundary edges of  $\mathcal{M}_s$ . Then:*

$$\begin{aligned} N_V^s &= \frac{1}{6}(4^s - 4 + 3 \times 2^s)N_{BE}^0 + \frac{1}{3}(4^s - 1)N_{IE}^0 + N_V^0, \\ N_{IE}^s &= 2^{s-1}((2^s - 1)N_{BE}^0 + 2^{s+1}N_{IE}^0), \\ N_{BE}^s &= 2^s N_{BE}^0. \end{aligned} \quad (12)$$

*Proof.* Recurrence relation (9) needs to be adjusted, so that it handles edge vertex insertion differently for interior, and for boundary edges.  $\Sigma$  applied to boundary edges simply doubles their amount  $N_{BE}^s$ . For counting interior edges  $N_{IE}^s$  requires us to use the generic identity  $N_E^s = 2N_E^{s-1} + 3N_F^{s-1}$  combined with (11) which yields the second equation in:

$$\begin{aligned} N_V^s &= N_V^{s-1} + N_{IE}^{s-1} + N_{BE}^{s-1}, \\ N_{IE}^s &= 4N_{IE}^{s-1} + N_{BE}^{s-1}, \\ N_{BE}^s &= 2N_{BE}^{s-1}. \end{aligned} \quad (13)$$

(12) is then the solution of system (13).  $\square$

**Theorem 5.3.** *Let  $\mathcal{M}_s = \Sigma^s(\mathcal{M})$ ,  $s \in \mathbb{N}_0^+$  be a watertight quad surface mesh, and let  $\Sigma : \mathcal{M}_{s-1} \mapsto \mathcal{M}_s$ ,  $s > 0$  be a globally-compatible 4 : 1 subdivision inserting a single vertex for each edge  $e \in \mathcal{M}_s$ , and a vertex*

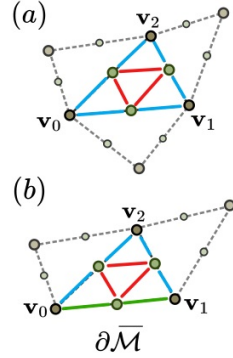


Fig. 3: (a) subdividing interior (Theorem 5.1) (b) and boundary triangles (Theorem 5.2).

for each face  $Q \in \mathcal{M}_s$ , according to connectivity scheme (6). Then

$$\begin{aligned} N_E^s &= 2^s(N_E^0 + 2(2^s - 1)), \\ N_F^s &= 4^s N_F^0, \\ N_V^s &= (2^s - 1)^2 N_F^0 + (2^s - 1)N_E^0 + N_V^0. \end{aligned} \quad (14)$$

*Proof.* Similarly to the derivation of previous recurrence formulas, we conclude that the amount of pre-existing edges doubles during subdivision, and we add four additional interior edges connecting from the newly inserted edge vertices  $\{i_e^*\}, e \in \{01, 12, 23, 30\}$  to the new interior vertex  $\{i^*\}$ . Analogously, the newly inserted vertices  $\{i_{01}^*\}, \{i_{12}^*\}, \{i_{23}^*\}, \{i_{30}^*\}$ , and  $\{i^*\}$  contribute to the updated vertex count:

$$\begin{aligned} N_V^s &= N_V^{s-1} + N_E^{s-1} + N_F^{s-1}, \\ N_E^s &= 2N_E^{s-1} + 4N_F^{s-1}, \\ N_F^s &= 4N_F^{s-1}. \end{aligned} \quad (15)$$

Solving (15) then yields (14).  $\square$

## 6 Tests and performance improvement

We tested the simplest triangle case in Theorem 5.1 for an icosphere, and additional watertight input meshes. We also verified the validity of counting formulas (8) for tori with higher genus (see Fig. 4 (b)). An icosphere with two holes (see Fig. 1 (a) and Fig. 4 (a)) was used to verify Theorem 5.2. Moreover, the utility of theorems in Section 5 was tested via time measurement speedup for Loop subdivision on dataset in 4 (c) while using preallocated memory with the a priori known mesh vertex, edge, and face counts (see Table 1).

Armadillo	Blub	Bunny	Max Planck	3Holes	Rocker Arm
0.85%	3.61%	2.08%	2.08%	2.06%	2.08%

Table 1: Speedup percentages for various test meshes.

$s$	1	2	3	4	5	6
Speedup [%]	-94.43	-31.23	-7.23	9.13	15.15	12.83

Table 2: Recursive vs preallocated icosphere construction speedup with respect to subdivision level  $s$ .

Evidently, the computation of new vertex positions in Loop subdivision [11] limits the potential gain from preallocation. For this reason we

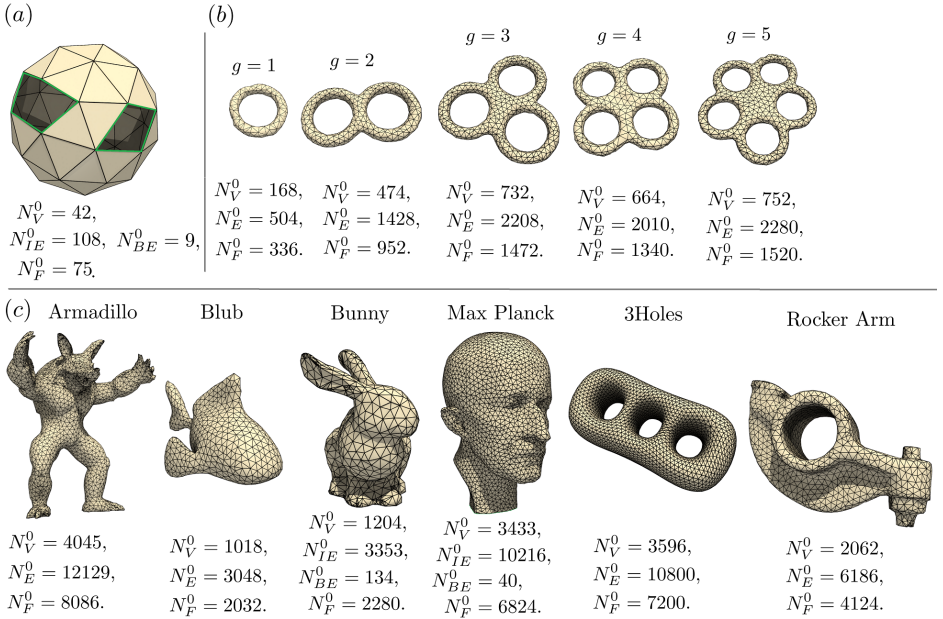


Fig. 4: Three different tests carried out on mesh datasets: (a) icosphere with boundary, (b) testing counting formulas for arbitrary genus, and measuring preallocation performance on standard datasets (c).

performed another set of tests for an icosphere subdivision scheme (4). We tried to mitigate the expensive vertex position computation by performing simple barycentric interpolation within base triangles of an icosahedron followed by more complex connectivity construction. As can be seen in Table 2, we sacrifice a lot of computation time to the construction of connectivity up to subdivision level  $s = 3$  after which we start to save as much as 15 % of the time.

Note that for the test mesh collection (c), we performed *isotropic remeshing* [1] to obtain better vertex distribution. This step was done in Mesh-Lab™ by the Visual Computing Lab team from ISTI, Pisa, and the final 3D visualizations were rendered in ParaView™ by the Kitware team.

## 7 Conclusion

Originating from the motivation for vertex counting formula, specifically for 4:1 subdivision aimed at stabilizing the semi-implicit formulation of Lagrangian evolution (refer to Section 2), this paper derives and justifies the utility of counting formulas for mesh vertices, edges, and faces under

recursive face subdivision operations (see Section 4). Theorems in Section 5 formulate the "counting formulas" for triangle 4:1 subdivision for meshes with arbitrary genus, and extend the statement even for meshes with boundary loops (Theorem 5.2), and for Catmull-Clark scheme on quad meshes (Theorem 5.3).

We validate the theoretical results with tests in Section 6 including the measurement for performance improvement under memory preallocation which yields up to 3.6% speedup for Loop subdivision and 15% acceleration in parametric icosphere construction.

## 8 Acknowledgments

The credit for test meshes goes to the Stanford 3D Model Repository (Armadillo, Bunny), Keenan Crane (Blub), Leif Kobbelt and the team at RWTH Aachen (Max Planck), to INRIA (Rocker Arm), and to the Libgl team (3Holes). Additionally, considerable gratitude goes to the development team of the PMP library led by Daniel Seiger and Mario Botsch.

Special thanks goes to doc. RNDr. Zbyněk Šír, PhD. for providing his installation of Wolfram Mathematica™ for obtaining solution (14) of system (15) moments before the presentation of this paper.

## References

- [1] Alliez, Pierre, Eric Colin De Verdiere, Olivier Devillers, and Martin Isenburg. Isotropic surface remeshing. *Shape Modeling International.*, pp. 49-58. IEEE, 2003.
- [2] Alarcão, Diogo, J. Luis Bento Coelho, Roberto Tenenbaum: On the Use of Hybrid Methods for Fast Acoustical Simulations in Enclosures, *Proceedings of Forum Acusticum '02*, 2002.
- [3] Botsch, Mario, Leif Kobbelt, Mark Pauly, Pierre Alliez, and Bruno Lévy. *Polygon Mesh Processing*, CRC press, 2010.
- [4] Doo, D. and Sabin, M. Behaviour of recursive division surfaces near extraordinary points, *Computer-Aided Design*, vol 10 (6), p. 356-360, 1978.
- [5] Catmull, Edwin, and Clark, James. Recursively generated B-spline surfaces on arbitrary topological meshes, *Seminal graphics: pioneering efforts that shaped the field*, p. 183-188, 1998.
- [6] Čavarga, Martin: Advection-Driven Shrink-Wrapping of Triangulated Surfaces, *Proceedings of the 26th Central European Seminar on Computer Graphics : CESC G 2022*, pp. 95-104, 2022.
- [7] DeRose, Tony and Kass, Michael and Truong, Tien: Subdivision Surfaces in Character Animation, *Proceedings of the 25th annual conference on Computer graphics and interactive techniques*, pp 85-94, 1988.

- [8] Dupuy, Jonathan and Deliot, Thomas: Bisection Based Triangulation of Catmull Clark Subdivision, *SIGGRAPH '22 Advances in Real-Time Rendering*, 2022.
- [9] Henle, Michael. *A combinatorial introduction to topology*. Dover Publications. ch. 5, s. 26, 1994.
- [10] Hoppe, H., DeRose, T., Duchamp, T., McDonald, J., & Stuetzle, W.: Mesh optimization, *Proceedings of the 20th annual conference on Computer graphics and interactive techniques*, pp 19-26, 1993.
- [11] Loop, Charles. *Smooth subdivision surfaces based on triangles*, 1989.
- [12] Osthoff, Carla, Roberto P. Souto, Fabrício Vilasbôas, Pablo Grunmann, Pedro L. Silva Dias: Improving Atmospheric Model Performance on a Multi-Core Cluster System, *Atmospheric Model Applications*, ch 1, pp 1-26, 2012.
- [13] Randall, David A., Todd D. Ringler, Ross P. Heikes, Phil Jones, and John Baumgardner. Climate modeling with spherical geodesic grids. *Computing in Science & Engineering* 4, no. 5: pp. 32-41, 2002.
- [14] Sieger, Daniel and Botsch, Mario. *The Polygon Mesh Processing Library* <http://www.pmp-library.org>, 2019.
- [15] Sieger, D., and Botsch, M. Design, implementation, and evaluation of the surface mesh data structure, *Proceedings of the 20th International Meshing Roundtable*, pp. 533–550, 2012.
- [16] Xie, Jinrong, Hongfeng Yu, and Kwan-Liu Ma. Visualizing large 3D geodesic grid data with massively distributed GPUs. *2014 IEEE 4th Symposium on Large Data Analysis and Visualization (LDAV)*, pp. 3-10. IEEE, 2014.



# Sliceforms in the education of architecture students

**Stanislava Čecháková, Dana Kolářová**

*Dept. of load-bearing structures, Fac. of Architecture,  
Czech Technical University  
Thákurova 9, 166 34 Prague 6, Czech Republic  
email: cecaksta@fa.cvut.cz, kolarova@fa.cvut.cz*

**Abstract.** The article is focused on the use of Sliceforms in the education of architecture students at CTU. It shows not only historical models created via this method, but also the work of current students who used the latest technologies for their creation (CAD modelling, GeoGebra, laser cutting, 3D printing). Sliceforms are useful in improving cross-subject relationships, most notably showing a close relationship between mathematics and descriptive geometry.

*Keywords:* Sliceforms, models of surfaces, geometry

## 1 Introduction

Sliceform models are models of surfaces, solids or other objects, which are designed by slicing them at regular distances in two directions. Although these models have a long history, their potential is still growing. The term ‘Sliceforms’ was coined by Gerald Jenkins, the publisher of the first book written by John Sharp about these types of models.

## 2 Historical background

The first models of this type, called moving models, were created towards the end of the 19th century. In 1874 Alexander von Brill (1842-1935) proposed a series of paper models of second order surfaces. These models were inspired by a model of an elliptic paraboloid made from circles which was created by the German-educated mathematician Olaus Henrici (1840-1918). Alexander Brill apparently first simply displayed these, but by 1888 his brother, the publisher Ludwig Brill, was selling them as ‘Carton Models’.

In the nineteenth century mathematical models were made for teaching and understanding geometry. Currently, these historical models can be seen in several places around the world, such as the British Museum of Science in London or the Smithsonian National Museum of American History in Washington.

John Sharp, a chemist by education, played a fundamental role in reviving this method nowadays. He was a strong supporter of both artists and mathematicians who wanted to join forces in creating, investigating, and disseminating ideas connecting the two practices. His colourblindness implies the importance of shape, forms and illusions.

At the Czech Polytechnic in Prague (nowadays CTU) this idea was used in the year 1876 to make models of translation surfaces and models of paraboloids. The reference is published in the book KKK ([1] p.441). Presently, RNDr. Marie Kupčáková is credited for the rediscovery of this method in the Czech republic [2].



Fig. 1: Torus – Villarceau circles (foto J.Ryszawy)

## 2.1 Sliceforms at the Faculty of Architecture in Prague

Architecture students in their first year of their studies within the subject of descriptive geometry create models of geometric objects. This year they were tasked to do it using Sliceforms technology. They used the latest technologies for their creation (CAD modelling, GeoGebra, laser cutting, 3D printing).



Fig. 2: Slice form model of the building of the Faculty of Architecture CTU (foto J. Ryszawy)

Sliceforms are useful for improving cross-subject relationships, most notably showing a close relationship between mathematics and descriptive geometry.

Photos of other models are published here:

<https://media.cvut.cz/cs/foto/20230517-slice-forms-fa>

## 2.2 Recommended Model Realization

We prepared instructions on how to create a sliceform model and published them on the web site of subject descriptive geometry at FA CTU. The following example shows a circular conoid. GeoGebra modelling was used.

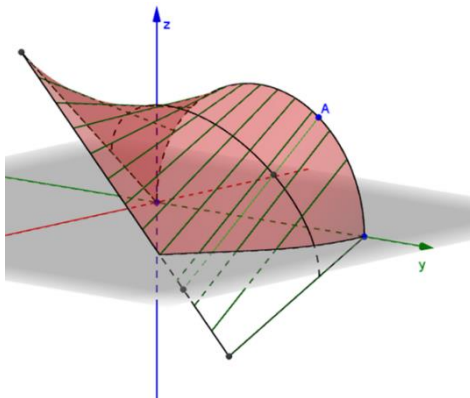


Fig. 3: Model of circular conoid made by GeoGebra (Čečáková)

The location of the conoid in the coordinate system is very important. Parametric representation was used:

Directrix is a semi-circle

$$k(t) = [0; 6 + 6 \cos t; 6 \sin t], \quad t \in \langle 0; \pi \rangle$$

Directrix line

$$r(u) = [9; 8 - 8u; 8u], \quad u \in \mathbb{R}$$

Directrix plane

$$\vartheta(x, z): y = 0.$$

Surface  $p(t, s) = [9s; 6 + 6\cos t; 6\sin t + s(2 - 6\cos t - 6\sin t)], \quad t \in \langle 0; \pi \rangle, s \in \langle 0; 1 \rangle$ .

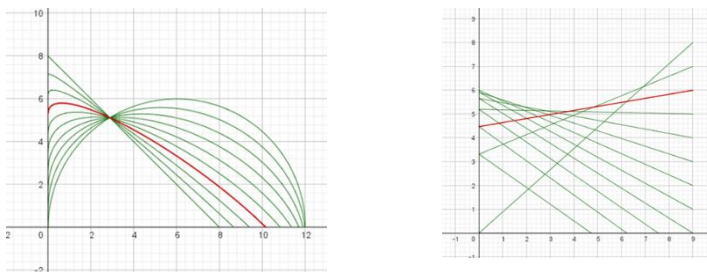


Fig. 4: Slices of conoid in two directions

### 3 Conclusion

Modelling is an important component in the education of architectural students. The Sliceforms method combines a mathematical background with a creative approach in modelling. By simply connecting these approaches, we show students the meaning behind theoretical subjects. Geometry is represented here on the boundary between science and art. Finally, we would like to quote from John Sharpe's book: "Geometry is a part of mathematics that does not belong to mathematicians. It plays a role in all cultures in defining aesthetics from patterns through architecture to other aspects of day to day design."

### Acknowledgements

This work has been supported by grant of FA CTU no. 15122/105/1052305E012.

### References

- [1] KADEŘÁVEK, František, KLÍMA, Josef, KOUNOVSKÝ, Josef, 1932. *Deskriptivní geometrie*. V Praze: Jednota čsl. matematiků a fyziků. Knihovna spisů matematických a fyzikálních.
- [2] KUPČÁKOVÁ, Marie, 2023. *Tvořivá geometrie: 7*. 1. Hradec Králové: Libor Dvořák. ISBN 978-80-907970-2-4.
- [3] LU, Yongquan, DEMAINE, Eric D., 2015. *A Pattern Tracing System for Generating Paper Sliceform Artwork* [online]. Phoenix, Arizona: Tessellations Publishing [cit. 2023-08-24]. ISBN 978-1-938664-15-1. ISSN 1099-6702. Available at: <http://archive.bridgesmathart.org/2015/bridges2015-367.html>
- [4] SHARP, John, 2022. *Surfaces: explorations with sliceforms*. 2. St Albans: Tarquin Publications. ISBN 1-85853-201-9.
- [5] SHARP, John, 2004. *Sliceforms: Mathematical models from paper sections*. 2. Stradbroke Norfolk England: Tarquin Publications. ISBN .1899618066
- [6] SHARP, John, 1998. Sliceform Sculptures-a Bridge between Art and Mathematics. In: *Bridges: Mathematical Connections in Art, Music, and Science: Conference Proceedings* [online]. 1. Southwestern College, Winfield, Kansas: Bridges Conference, s. 275-276 [cit. 2023-08-16]. ISBN 0-9665201-0-6. ISSN 1099-6702. Available at: <http://archive.bridgesmathart.org/1998/bridges1998-275.html>

# On multicriteria triangulations

Manaswita Das

*Dept. of Algebra & Geometry, Fac. of Mathematics Physics & Informatics, Comenius University Mlynska Dolina 6284, 84248 Bratislava, Slovak Republic  
email: Manaswita.das@fmph.uniba.sk*

**Abstract.** We survey the research of ‘Multicriteria Optimized Triangulation’. This approach extends the classical Delaunay triangulation by incorporating optimization objectives such as edge lengths, angles, and even user-defined constraints. Multiple authors preferred stochastic methods mainly containing genetic optimization and edge flip. This approach proves useful in various applications, where different factors need to be considered simultaneously for constructing accurate and adaptable geometric structures. Hence we will search for the explorations done and results achieved in successive experiments afterwards, and discuss the classification of edge-based criteria.

*Keywords:* Optimal triangulation, genetic optimization, Delaunay triangulation, minimum weight triangulation.

## 1 Introduction

Triangulating a planar point set  $S$  of  $n > 2$  points,  $n \in \mathbb{N}$ , is a fundamental task with applications across diverse fields, including computer graphics, computer vision, and robotics. We distinguish optimal and locally optimal triangulations.

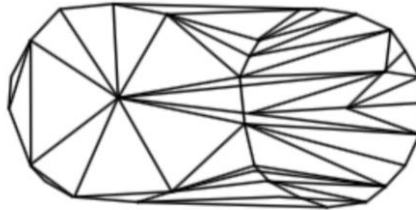


Fig. 1: Two criteria triangulating 39 points [33].

An **optimal triangulation**, denoted as  $OT(S)$ , is one that, with respect to specific criteria, outperforms all other possible triangulations of the given point set  $S$ . **Locally optimal triangulation**, referred to as  $LOT(S)$ , means that every convex quadrilateral formed by two adjacent triangles shares an edge that aligns with the given criterion.  $LOT(S)$  is, e.g., the **Greedy**,  $GT(S)$  [16].

Achieving local optimality is often made possible through the ingenious use of the local **edge-flip procedure** [35]. Any initial triangulation can be flipped into the **Delaunay Triangulation (DT)** within a  $O(n^2)$  number of steps [22]. One can find the notation and terminology of the field in [38], [1] or [3] (in Slovak).

Often, two primary criteria come into play; the first minimizes the total length of edges, *Minimum Weight Triangulation (MWT)* [16], while the second maximizes the smallest angle, *DT* [6]. They may have flipping distance zero, see Fig. 2a, in an almost minimal example not containing the *Travelling Salesman Cycle (TSC)* [7]. Moreover,  $T(S_7)$  is Hamiltonian triangulated [5], since the triangles can be connectively stripified.

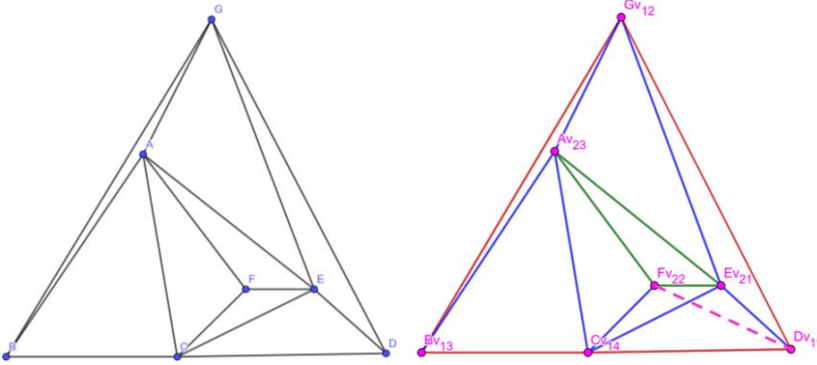


Fig. 2a: Graph  $T(S_7)$  for dataset  $S = \{ A (4,6), B (0,0), C(5,0), D (11.1,0.1), E (9,2), F (7,2), G (6,10) \}$  [7] ; 2b:  $T(S_7)$  including the flipped edge with universal notation and colour encoding and the Dash-ed edge converts *DT* into *MCT* and enables the *TSC* as a subgraph [5].

Apart from the metric or angular criteria of *MWT* and *DT*, there exist a user-defined criteria of selective edge insertion, i.e., *Constrained Delaunay Triangulation (CDT)* [4]. If the constraints depend on the characteristics and attributes of the input-data points, then the triangulation is termed as *Data Dependent Triangulation (DDT)* [17].

If we require the *TSC* in  $T(S_7)$ , the removal of CE and insertion of edge DF, see Fig. 2b, has to be done. This single flip leads to the inclusion of the path ABCFDEGA, which is the *TSC* for  $T(S_7)$ . The modified  $T(S_7)$  is thus either *CDT* or (*flipped*) multicriteria [5]. The solution, shown in Fig. 1, was achieved by genetic algorithm using flipping procedure [33]. In the following, we survey the published results and discuss the classification of criteria.

## 2 Multicriteria Optimized Triangulation (MCT)

The approach of applying multiple triangulation criteria to achieve a single, optimized triangulated version was termed as '*Multicriteria Optimized Triangulation*' [33]. *Genetic Optimization (GO)* has been used to provide the approximate solution of triangulation of a set of points,  $S$ , in the Euclidean plane, employing biological terminology, referring to the set as 'a population,' a potential solution as 'an individual,' the binary operation as 'a crossover, named 'De Wall', and the unary operation as 'a mutation'. It has been performed for

100 or 200 generations and a well-designed fitness function is used in two versions.

$$eval_1(T(S)) = \sum_{i=1}^m w_i f_i,$$

$$eval_2(T(S)) = \prod_{i=1}^m f_i,$$

where  $T(S)$  is a triangulation;  $m$  is the total number of triangulation criteria;  $w_i$ ,  $i = 1, 2, \dots, m$  are weight coefficients. Here  $w_i \in \langle 0; 1 \rangle$ ,  $\sum w_i = 1$ ; and  $f_i$ ,  $i = 1, 2, \dots, m$  are functions for particular criteria. The overall computational time complexity of the procedure was  $O(n^2)$ , due to the crossover operation. The underlying operation is edge flip. Though *DT* and *MWT* provides the base for formulating triangulation, the versatile *GO* encompasses several other criteria, e.g., *Maximum Height*, *Minmax Length*, *Minmax Aspect Ratio*, *Minmax Angle*, *Minimization of Maximum Angle Sum* and *Maximization of Sum of Minimum Angles*, *Maximizing the Minimum Radius* and *Minimizing the Maximum Radius and Minimum Sum of Radius Triangulation*. A slight difference in the preferred criteria can bring prominent changes in a triangulation, see Fig. 1. The left side is representing the max edge length triangulation and the right side is incorporating *DT*. The number of successful cases is directly proportional to the probability of crossover, which is inversely proportional to the computational time.

*MCT* was mentioned as an useful approximation method in the survey of triangulations [29], [31] and in the survey of probabilistic methods of triangulation [30] and the author included *MCT* as a tool to obtain specific triangulations as a part of Computational Geometry Education [27], [28]. *MCT*, as a type of triangulation, was referred for yielding applications of computational geometry [2], [26]. The author contributed a discussion on multiple edge-based criteria and a valuable bibliography comprising 60 items in [32]. In [21], the authors presented a comprehensive dataset of astronomical data for 88 star constellations and assessed edge quality. Notably, only 7 star constellations contained subjective edges that did not adhere to Delaunay criterion, which is potentially attainable through combining several criteria and constructing *MCT*.

Dorzan et al. proposed *Ant Colony Optimization (ACO)* metaheuristics to find the *MWT* [9-11], [13], [15], [23]. *ACO* is a metaheuristic that employs a colony of artificial ants to solve challenging discrete optimization problems. These algorithms construct solutions incrementally by adding specific components to an evolving solution, utilizing both pheromone trails and heuristic information to guide their actions, instead of using genetic information, like [33]. Pheromone values stored in variables influence their probabilistic decisions when navigating a graph. They explained an *ACO* algorithm comprising two specific components; ‘Initialization’, which sets algorithm parameters, and ‘BuildSolution’, which extends a partial solution by adding feasible components from current neighbors. The authors designed an

instance generator and the *ACO-MWT* algorithm was implemented in C with twelve parameter settings and for each setting, 30 runs were performed. They considered the computation as “parametrically expensive”. In a series of papers published from 2010 onwards, they conducted experiments using the *ACO* algorithm on previously used instances and compared its performance to the *Simulated Annealing (SA)*, which involved five different parameter settings [12], [14]. This made the *SA* a relatively more cost-effective option in terms of parameter tuning. Though *GO* appears to be qualitatively superior and also mentioned as an evolutionary algorithm for *MCT* in [47], the complexity has been increased in the case of Re-triangulation of *Standard Tessellation Language (STL)* meshes in [44].

In 2009 and consecutive years, Feciskanin R. discussed the generation of *Triangular Irregular Networks (TINs)* for modeling georelief surfaces from irregularly distributed input points using *Lawson’s General Optimization Algorithm (LOP)* [18-20], whether *SA* has been used for *DDT* construction as a part of texture reconstruction in [42]. It explores two types of triangulation criteria: shape-dependent and data-dependent and in 2016, Rodriguez N. & Silvera R. proposed a *Higher Order Delaunay Triangulation (HODT)*, satisfying both the data dependent criterion and good triangle shape, to build the *TIN*, using similar process of *LOP* [39].

The authors of three research papers [36], [45], [46] refer to [33] in the context of parallel computing. The two short papers in Chinese aim to use stochastic optimization for *MWT*. The immune algorithm is inspired by the immunologic defense metaphor.

In 2002, Hlavaty T. and Skala V. outlined a deterministic procedure that employed a brute force approach to generate triangulations based on specific criteria [24]. In the same year, Skvortsov explored various applications and constructions of *DT* in the field of geoinformatics. The study highlighted Multicriteria Triangulation as an approximate algorithm for *DT* [41]. Karbowski K. incorporated *MCT* into a chapter discussing point cloud filtration and triangulation in a mechanical engineering monograph [25].

For the educational purposes, we are building a triangulation, named *Dash*, providing the *Distance Matrix* and *Edge-Crossing Matrix* for optimizing the qualitative and demanded edge insertion and flipping procedure for estimating subgraphs of triangles like *Euclidean Minimum Spanning Tree (EMST)*, eventually to verify the *TSPLIB* dataset and the experiments are in the pre-processing stage. *Dash* is a deterministic method that involves three stages: *I.* Forming outer and inner convex hull with the extreme and internal points respectively, i.e., the *Nested Convex Hull (NCH)* [38], *II.* Performing *DT* in the *NCH*, and *III.* Flipping of Edges. The color encoding and universal notation has been proposed to reduce visual complexity, see Fig. 2b. The time complexity for computing the first two stages has an upper bound  $O(n \log n)$ .

The *Distance Matrix* of *Dash* is organized with vertices as indices, where values above the diagonal indicate edge lengths, and values below represent the



sequence of the three stages. However, *Ludo* is a stochastic procedure that incorporates random edge insertion and flipping. The *Edge-Crossing Matrix* representation provides essential information: *I*. Whether the edges intersect or remain unconnected, and *II*. If connected, the angle between them [5]. We surveyed the above papers in the context of investigating the usage of *MCT*.

### 3 Discussing Single Criteria Edge-Based Classification

There are multiple criteria to obtain the triangulation, out of which *DT* and *MWT* satisfy the two most prominent criteria of maximization of minimum angle and minimization of the weight, respectively. Though the former one has the optimal time complexity of  $\Theta(n \log n)$ , the later one is NP-hard [37]. The time complexity for getting a triangulation combining two specific criteria incorporated with angle and height is  $O(n \log n)$  or  $O(n^2)$  (worst case scenario for the crossover operation in most of the cases) [33]. The criteria of generation of triangulation incorporating predefined edges, i.e., *CDT* is an appropriate way of getting the demanded triangulated version and it can be achievable in  $O(n \log n)$  time [4]. This is a user-defined criteria and another similar criterion is *DDT*, whose complexity is dependent on the characteristics and attributes of the vertices [17]. The *Minmax Angle* and *Maxmin Height Triangulation* can be computed in  $O(n^2 \log n)$  and the *Minmax Height Triangulation* can be computed in  $O(n^2)$  time [40]. Achieving the inclusion of *TSC*, i.e., *Minimum Hamiltonian Cycle (MHC)* goes beyond a specific optimal triangulation with singular criteria. In Fig. 2b, it becomes evident that when Delaunay criterion is coupled with flipping, it results in the incorporation of the subgraph *MHC*. In  $T(S_7)$ , employing Delaunay Triangulation within the *NCH* significantly reduces time complexity at a specific level. This is because it provides the necessary edges, thus eliminating the need for flipping. Consequently, the number of edges that can be flipped is reduced to just three, which greatly simplifies the computational process. Hence, criteria based on subgraph inclusion in triangulation hold promise for a substantial reduction in time complexity.

### 4 Conclusion

In [21], the authors observed that 7 edges of star constellations were not satisfying the Delaunay criterion, which can be probably obtained further through *MCT*, hence one promising avenue is the continued collection and exploration of *MCT*. Delaunay triangulations are fundamental in computational geometry and characterizing and analyzing specific subgraphs [43] within *DT* is very crucial. We arrived at constrained edge insertion criteria, leading to containing a prominent subgraph *MHC* and *EMST* [5]. Hence, there is a significant potential for synergy between multicriteria triangulations and subgraph analysis. Combining these approaches, such as using alpha shapes to describe complex data in geographic regions can yield valuable insights.

## References

- [1] AURENHAMMER, F., KLEIN, R., Der-Tsai LEE. 2013. *Voronoi diagrams and Delaunay Triangulations*. Singapore: World Scientific.
- [2] ČERVEŇANSKÝ, M. et al. Parallel GPU-based data-dependent triangulations. *Computers & Graphics*, 2010, 34.2: 125-135.
- [3] CHALMOVIANSKÝ, P. et al. 2001. *Zložitosť geometrických algoritmov*. Bratislava: FMFI UK.
- [4] CHEW, PL. 1989. Constrained DT. *Algorithmica* **4**, 97–108.
- [5] DAS, M., ČAVARGA, M., FERKO, A. 2023. On Planar Hamiltonian Triangulation (Not) Containing the Minimum Hamiltonian Cycle (TSP); Utilizing Deterministic, Stochastic, and Natural Approach. Extended abstract. *SVK 2023 Proceedings*. [online] Bratislava: FMFI UK.
- [6] DELAUNAY, B. 1934. Sur la sphere vide. *Bulletin of Academy of Sciences of the USSR*, pp.793-800, 1934.
- [7] DILLEN COURT, MB. 1987. Traveling Salesman Cycles are not Always Subgraphs of Delaunay Triangulations or of Minimum Weight Triangulations. *Information Processing Letters*, 1987, 24, 339–342. [https://doi.org/10.1016/0020-0190\(87\)90160-8](https://doi.org/10.1016/0020-0190(87)90160-8).
- [8] DORZÁN, M. G. et al. Approximated algorithms for the minimum dilation triangulation problem. *Journal of Heuristics*, 2014, 20: 189-209.
- [9] DORZÁN, M. G. et al. Approximations on minimum weight triangulations and minimum weight pseudo-triangulations using ant colony optimization metaheuristic. *Fund. Inf.*, 2012, 119.1: 1-27.
- [10] DORZÁN, M. G. et al. Globally optimal triangulations of minimum weight using Ant Colony Optimization metaheuristic. *Journal of Computer Science & Technology*, 2010, 10.
- [11] DORZÁN, M. G. et al. Metaheuristic approaches for MWT and MWPT Problems. In: *XVII Cong. Arg. de Ciencias de la Computación*. 2011.
- [12] DORZÁN, M. G. et al. Simulated annealing aplicado a triangulaciones y pseudotriangulaciones de peso M. In: *XVI Congreso Argentino de Ciencias de la Computación*. 2010.
- [13] DORZÁN, M. G. et al. Soluciones aproximadas para el problema de Triangulación de Peso Mínimo utilizando ACO. In: *XV Congreso Argentino de Ciencias de la Computación*. 2009.
- [14] DORZÁN, M. G. et al. Triangulaciones y pseudotriangulaciones de peso mínimo: resolución aproximada con simulated annealing. *VII Jornadas de Matemática Discreta y Algoritmica*. Espana, 2010.
- [15] DORZÁN, M. G. et al. Using ACO metaheuristic for MWT problem. In: 2011. *30th International Conference of the Chilean Computer Science Society*. IEEE, 2011. p. 228-237.
- [16] DÜPPE, R.D, GOTTSCHALK, H. H. 1970. Automatische Interpolation von Isolinien bei willkuerlich verteilten Stutzpunkten. pp. 423-426. *Allgemeine Vermessungsberichten* 77, 129 (10), 1970.

- [17] DYN, N., LEVIN, D., RIPPA, S. 1990. Data Dependent Triangulations for Piecewise Linear Interpolation, *IMA Journal of Numerical Analysis*, Volume 10, Issue 1, January 1990, Pages 137–154.
- [18] FECISKANIN, R. Optimization of triangular irregular networks for modeling of geometrical structure of georelief. In: *Int. Cart. Conf.* 2007.
- [19] FECISKANIN, R. Problémy modelov georeliéfu tvorených tvarovo optimalizovanými nepravidelnými trojuholníkovými sieťami. *Kartografické listy*, 2010, 18: 49-56.
- [20] FECISKANIN, R. *Optimalizácia nepravidelných trojuholníkových sietí pre modelovanie georeliéfu*. 2009. PhD Thesis. Masarykova univerzita, Přírodovědecká fakulta.
- [21] FERKO, A., MORAVČÍK, J., KOLINGEROVÁ, I. Souhvězdí jako podgrafy triangulací. *PMFA*, 2016, 61.1: 14-20.
- [22] FORTUNE, S. 1993. A Note of Delaunay Flips. pp. 723-726. *Pattern Recognition Letters*. Vol. 14 No. 9 North-Holland 1993.
- [23] HERNÁNDEZ et al. Using ACO metaheuristic for MWT problem 2011. In: 2011, *International Conference on Services Computing*, IEEE, july, 4-9, 2011, Washington, DC, USA. ISBN 978-0-7695-4462-5.
- [24] HLAVATÝ, T.; SKALA, V. Generátor trojúhelníkových sítí zadaných vlastností brutální silou. TR DCSE/TR-2002-09. 2002. Pilsen: WBU.
- [25] KARBOWSKI, K. *Podstawy rekonstrukcji elementów maszyn i innych obiektów w procesach wytwarzania*. Krakow: PK, 2008. *Kartografické listy*, 2010, 18: 49-56.
- [26] KNAUF, J. F., KRÜGER, B., MECKE, K. Entropy of unimodular lattice triangulations. *Europhysics Letters*, 2015, 109.4: 40011.
- [27] KOLINGEROVÁ, I. Computational geometry education for computer graphics students. In: *Computer Graphics Forum*. Oxford, UK: Blackwell Publishing Ltd, 2008. p. 1531-1538.
- [28] KOLINGEROVÁ, I. et al. 2018. Neighbourhood graphs and locally minimal triangulations. *Transactions on Computational Science* 31. Berlin, Heidelberg: Springer, 2018. pp. 115-127 ((Lecture Notes in Computer Science, ISSN 0302-9743; 10990)).
- [29] KOLINGEROVÁ, I. On triangulations. In: *International Conference on Computational Science and Its Applications*. Berlin, Heidelberg: Springer Berlin Heidelberg, 2004. p. 544-553.
- [30] KOLINGEROVÁ, I. Probabilistic methods for triangulated models. In: *8th Int. Conference on Computer Graphics and Artificial Intelligence 3IA*. 2005. p. 93-106.
- [31] KOLINGEROVÁ, I. Simulated Annealing and Genetic Algorithms in Quest of Optimal Triangulations. *Generalized Voronoi Diagram: A Geometry-Based Approach to Comp. Int.*, 2009, 247-266.
- [32] KOLINGEROVÁ, I. Triangulace s hranovými kritérii - Šípkové Růženky právem ne neprávem zapomenuté? *Pokroky matematiky, fyziky a astronomie*, 2020, 65.4: 223-233.

- [33] KOLINGEROVÁ, I., FERKO, A. 2001. Multicriteria-optimized triangulations. *The Visual Computer* 17 (6), 380-395.
- [34] KRÜGER, B. *Simulating triangulations: Graphs, manifolds and (quantum) spacetime*. 2016. PhD. Thesis. Erlangen: Friedrich-Alexander-Universität Erlangen-Nürnberg (FAU), 2016.
- [35] LAWSON, C.L.: Software for C1 Surface Interpolation. *Mathematical Software III*, Academic Press, New York (1977),161-194.
- [36] MORÓN, Célio E.; RIBEIRO, José RP; DA SILVA, Nilton C. A teaching environment for the development of parallel real-time programs. In: *FIE'98. 28th Annual Frontiers in Education Conference. Moving from 'Teacher-Centered' to 'Learner-Centered' Education. Conf. Proceedings (Cat. No. 98CH36214)*. IEEE, 1998. p. 903-908.
- [37] MULZER W., ROTE G. 2008. Minimum Weight Triangulation is NP-hard. *Journal of the ACM*, Volume 55, Issue 2, Article 11, pp 1-29.
- [38] PREPARATA, F.P, SHAMOS, M.I, 1985. *Computational Geometry, An Introduction*. Springer Verlag.
- [39] RODRÍGUEZ, N., SILVEIRA, R. I. Implementing data-dependent triangulations with higher order Delaunay triangulations. In: *Proceedings of the 24th ACM SIGSPATIAL Int. Conf. on Advances in Geographic Information Systems*. 2016. p. 1-10.
- [40] VASSILEV S.T., 2005. *Optimal Area Triangulation*. PhD. Thesis. Saskatoon: University of Saskatchewan.
- [41] SKVORTSOV, A. V. 2002. *Comprehensive research and development of effective computationally stable algorithms for computational geometry and their implementation in a geoinformation system*. PhD. Thesis in Russian. Tomsk: Tomskij gosudarstvennyj universitet.
- [42] TÓTH, Z. Towards an optimal texture reconstruction. *Proceedings of the 8th Central European Seminar on Computer Graphics*. Vienna: Institute of Computer Graphics and Algorithms, 2004. p. 23-30.
- [43] VELTKAMP, R.C. 1992. The  $\gamma$ -neighborhood graph. *Comput. Geom.* 1(4), 227–246 (1992).
- [44] WANG, Chung-Shing; CHANG, Teng-Ruey. Re-triangulation in STL meshes for rapid prototyping and manufacture. *The International Journal of Advanced Manufacturing Technology*, 2008, 37: 770-781.
- [45] YANG Jie and LI Dehua and JIN Lianghai and WANG Zuxi, 2007. A new immune algorithm for solving minimum weight triangulation (in Chinese). *Computer Engineering*. Vol. 33, No. 21: 189-191.
- [46] ZHANG Dongmei and JIANG Pengfei and HE Xingheng and YANG Jie. 2007. Research on parallel genetic algorithm for minimum weight triangulation based on PVM (in Chinese). *Computer Engineering and Applications*. Vol. 43, No. 2: 86-88.
- [47] ZHANG, Wen-Xiang, et al. Constrained remeshing using evolutionary vertex optimization. In: *Computer Graphics Forum*. 2022. p. 237-247.

# Examples of ovals in 19<sup>th</sup> century architecture in Ostrava

## Ukázky konstrukcí oválu v ostravské architektuře 19. století

Věra Ferdiánová, Michaela Holešová

*Dept. of mathematics, Faculty of Science, University of Ostrava  
30. dubna 22, 701 03 Ostrava, Czech Republic  
email: vera.ferdianova@osu.cz*

*Dept. of Structural Mechanics and Applied Mathematics, Faculty of Civil Engineering  
University of Žilina, Univerzitná 8215/1, 010 26 Žilina, Slovak Republic  
email: michaela.holesova@uniza.sk*

**Abstract.** The teaching of geometry, especially planimetry, in high schools focuses on basic constructions and the use of congruences and similarities in construction problems. In optional seminars or in technically oriented schools, construction techniques for conics are introduced, but the construction of ovals tends to be in the background. Students are usually not exposed to the problem until they are at university. This paper will illustrate various oval constructions on original technical documentation (blueprints) of buildings in 19<sup>th</sup> century Moravian Ostrava and introduce the issue closer to students.

Výuka geometrie, zejména planimetrie na středních školách je zaměřena na základní konstrukce a využití shodností a podobností v konstrukčních úlohách. V nepovinných volitelných seminářích nebo na technicky orientovaných školách se představují konstrukční techniky pro kuželosečky, ale konstrukce oválů bývá na pozadí. Studenti se s problematikou setkávají povětšinou až na vysoké škole. Příspěvek bude ilustrovat různé konstrukce oválů na původní technické dokumentaci budov v Moravské Ostravě 19. století a přiblížení této problematiky studentům

*Keywords:* Serlio's oval, arches, architecture Ostrava

*Klíčová slova:* Serliův ovál, oblouky, architektura Ostrava

### 1 Teaching ovals from the perspective of high school mathematics and engineering practice

The teaching of geometry in the Czech and Slovak Republics within the subject of mathematics is divided into planimetric and stereometric parts in secondary schools. Planimetry is mostly included in the second year of secondary schools, where mathematics is taught at the rate of 4h/t. According to the RVP, the main outcomes of this part are Fundamentals of Planimetry and Geometric Representation. Due to the time allocation, ovals are not included. Technically

oriented secondary schools of civil or mechanical engineering offer courses in descriptive geometry, where basic constructions of ovals can follow the teaching of constructions of conics. At the high school level, the teaching of conics constructions is incorporated into an elective seminar following the seminar on quotation and Monge. Due to the long-standing common teaching system, the situation in Slovakia is similar, so that the teaching of ovals is incorporated into the teaching of descriptive geometry at technical colleges or is mentioned in the teaching of curve geometry. The aim of our paper is also to point out and introduce basic constructions that are understandable by high school students or could be used in project activities that would be focused on the discovery of ovals within architectural elements of buildings or in construction. The pilot integration therefore took place in the Synthetic and Constructive Geometry lecture, which is attended by mathematics students at the OU. Therefore, we decided to rediscover the construction practices that were used by builders in their designs, and we prioritically focused on ovals, which are widespread in building practice and were already used in Baroque buildings [4].

## 1.1 The historical context of Ostrava

Ostrava is the third largest city in the Czech Republic and is located in the North Moravian region very close to the borders with Poland and Slovakia. Overall, it is mostly perceived as a city with heavy industry and automotive industry.

However, within the city there is an emphasis on the development and accessibility of services for the population and the improvement of their quality of life.

If we look back to the beginning of the 18th century, there was no indication that the small mining town would later become one of the important cities not only within the Habsburg monarchy, but especially later in the newly founded republic (more in [1]). Coal had already been discovered in the area in 1763 in the Burňa valley, where mining was expected to take a maximum of 10 to 20 years. As there was not such a great demand for this raw material, the development of mining was slow and the main boom did not come until the second half of the 19th century, when the industrial revolution in our territory began to gain momentum. This involved a sufficient amount of labour, and the first mines in the Ostrava region used miners from the surrounding area. In later years, a large migration from Halych began, from which only miners and then their families were the first to arrive. This also increased the demand for housing and buildings to provide for the basic needs of the population. Therefore, within Ostrava, quarters and colonies were built for the incoming population, as well as hospitals, schools, pubs and other cultural facilities. [2] Since the planning or architectural aspect of the individual buildings in the first half of the 19th century was under the Moravian Ostrava, it was only in later

times that the first architectural studios opened and independent architects and builders began to work in Ostrava, mostly from the Viennese schools, such as. František Fiala, Ottokar Böhm, Hans Ulrich, Alois Schön, Felix Neumann.[6][7] Today some of their buildings have been preserved and underline the Art Nouveau appearance of the historical centre of Ostrava, so they can be used for further research.

## 2 Oval and their construction

The oval from the point of view of mathematics can be understood in different Ways. Brun, in his work *Ueber Ovale und Eiflächen*, conceives of an oval as a finite plane closed curve having two and only two points in common with every line in its plane that passes through it. He then specifies other properties of the curve in question, that it has no nodal points, is convex, etc. Overall, this is a comprehensive work focusing on ovals using the knowledge of the time. [3]

In terms of engineering practice, it defines an oval using properties as a plane closed curve satisfying the following properties:

- They are differentiable (smooth-looking),
- simple (not self-intersecting), convex,
- their shape does not depart much from that of an ellipse,
- there is at least one axis of symmetry.

The word oval derived from the Latin word "ovus" for egg, because oval is a closed curve in a plane which "loosely" resembles the outline of an egg.

In technical practice, it is used quite a lot, mainly because it can approximate the elliptical shape appropriately and quite accurately, and thus not only architecturally interesting buildings could be created, but also their decoration and other structural elements.

Among the most famous ovals are the so-called Serlio's ovals, described by Sebastiano Serlio in *Il primo libro d'architettura* [5].

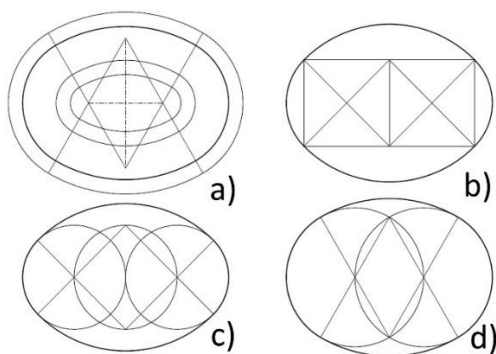


Fig. 1: The constructs of Serlio's ovals

Four types of Serlio's ovals are drawn in the figure, where in case a) the ratio of the length of the major and minor semi-axes is not constant, in case b) the ratio  $a/b = (\sqrt{2} + 1) / (2\sqrt{2} - 1)$  and the ratio of the radii of the defining circles is  $1/2$ . For case c) je  $a/b = \sqrt{2}$  and the ratio of the radii of the circles is  $\sqrt{2} - 1$ , for case d) is  $a/b = 3 / (4 - \sqrt{3})$  and the ratio of the radii of the defining circles is  $1/2$ . (Fig. 1)

### 3 Identification of ovals on specific buildings and their use in project-based learning

One way to incorporate the construction of ovals into the curriculum in high school is through project-based learning. After teaching conics and therefore the application of circles in practice, we would recommend supplying basic information about ovals and, for example, the reconstruction of objects, where students should decide whether a given structural element is an oval or a circle. A simple awareness of the basic property of a circle given by three points, for example, will show that a design feature involves the use of a circular arc (Fig. 2). When reconstructing, they can use a simple tool within GeoGebra and insert the chosen engineering feature as a background.

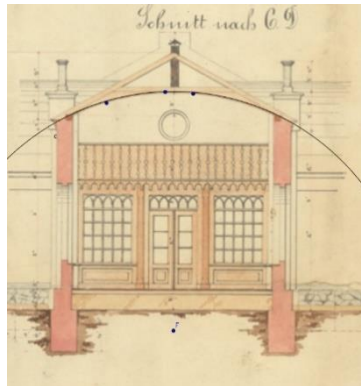


Fig. 2: Reconstruction of the circular arch in the technical drawing [8]

If this is not a use of circles, then by looking for constructions of ovals, students will become more in depth about the properties of circles and in fact the ellipse, which is a curve of non-constant curvature.

A nice example of the use of ovals is in 19th century Ostrava architecture, where in the original plans one can still see the individual insertions - the centres of the circles used to define the drawn oval. In order to strengthen the cross-curricular links, the students will also explore the historical context of the time in their home area. The technical documentation of the German House, which was built to the design of Felix Neuman and was a response by the German



population to the planned construction of a Czech house, was used as a demonstration.[1] The building still stands in front of today's Hotel Imperiale and contained a representation area and a hall, a restaurant with a capacity for 600 people. In the garden there was a music pavilion for 120 people. The opening ceremony took place in 1895. The Dutch Renaissance style, popular in Germany, was used with a red facade that attracted attention from afar. During World War II, the building was damaged during the bombing of Ostrava and it was subsequently decided to demolish it.[1][7]

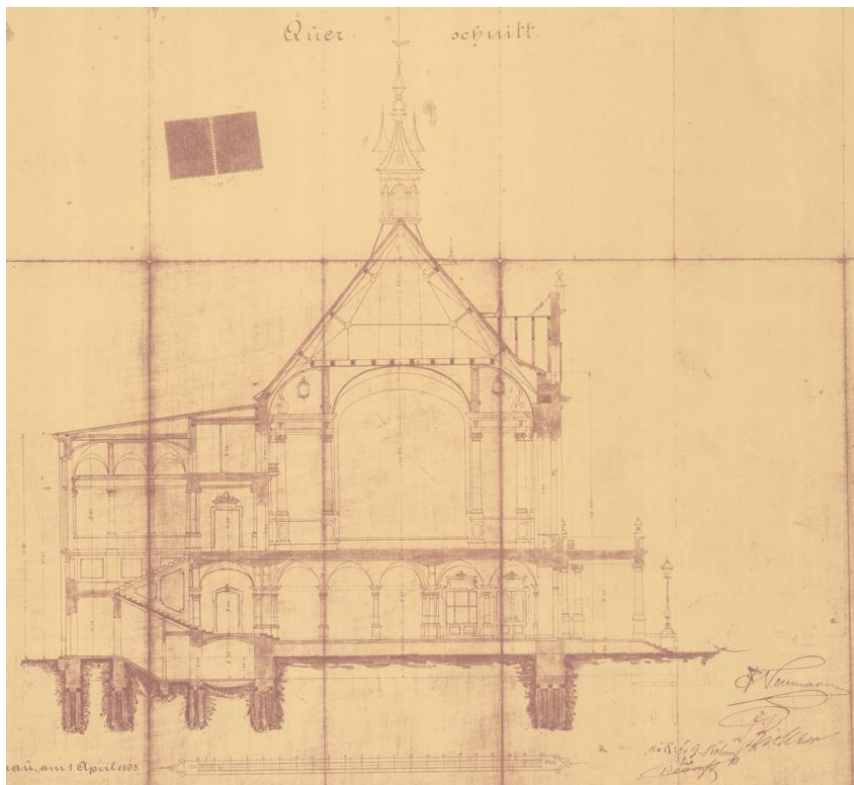


Fig. 3: Original technical documentation of the German House [9]

And as we can see, Serlio's constructions according to types a) and c) were probably used (Fig. 4).

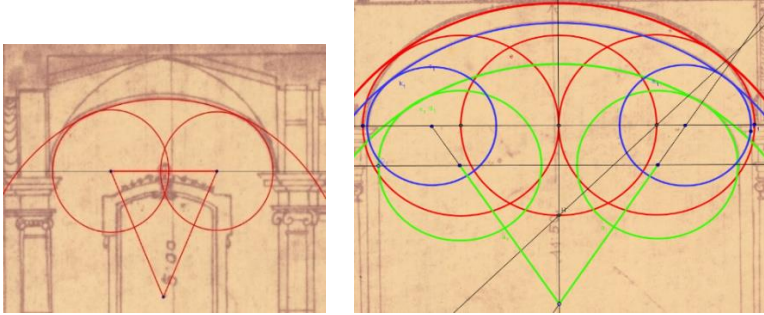


Fig. 4: Detail of the technical documentation [9] supplemented by the construction of part of the oval. Left: construction according to type a) of the Serlio's construction. Right: construction of type c) in red to draw the contour arc, other constructions of type a)

If the teacher does not have the original building documentation directly available, he or she can use project-based learning and students can find individual architectural elements on their own in the field. These are usually different types of facade decoration, arches over windows or doors of buildings. The student takes a photograph and then tries to find the oval using an approximation. For example, at Ostrava Architecture we can see that the oval is also a popular design element used to decorate buildings. It appears in individual elements on the building of the Kindergarten in Dvořákova Street, which was originally the villa of Judr. Karel Richter. It is a neo-baroque villa from 1896, designed by architect Felix Neumann, when villa construction was already regulated in Ostrava and the nearby original cemetery was converted into a park for capacity reasons. Since the building was reconstructed with sensitivity, the valuable facade, richly articulated with historicizing elements and even fragments of the original stucco decoration in the interior space, has been preserved.[6][7] Most probably Serlio's construction of type a) was used in the creation of the window above the entrance (Fig. 5).



Fig. 5: Detail of a window on the building of the kindergarten in Dvořákova Street, Ostrava

Another example is located near the kindergarten and is a building on Milíčova Street, which originally served as a tenement villa for the architect Paul Hawlik (1908), who designed it and embodied the Nordic inspiration based on asymmetrical vertical composition unusual in Ostrava at that time. He thus managed to combine Neo-Romanticism and Anglophilia with the receding Vegetable Art Nouveau.[6][7]



Fig. 6: Building and its detail on Milíčova Street, Ostrava

## 4 Conclusion

At the beginning of the geometry lecture, when students sketch plane shapes and curves, an oval was included in the assignment. The result was that the vast majority of students sketched a "running oval" i.e. a plane symmetrical curve which is bounded by two segments and two circular arcs, other answers included a sketch of an ellipse and only in one case an oval in the shape of an "egg" was sketched. Subsequently, the construction of ovals and their application to practical demonstrations and reconstruction of buildings was incorporated into the lesson, during which students consolidated and deepened their knowledge of the properties of the circle. As the incorporation took place after the teaching of conics, students already had an awareness of the properties of ellipses. One student response was that an oval could be an approximation of an ellipse, which they based on their knowledge of ellipses using occluding circles. They are also aware of the realization of the basic properties of a circle given by three points on it. From the technical practice, they mostly mentioned bridge structures, the use of circular arches by supra-orbital arches, etc.

Therefore, we recommend that also in connection with the setting of teaching standards for knowledge usable in practical applications, that, for example, the basic properties of ovals be added to the part of teaching about conics.

## References

- [1] J. Bakala and K. Jiřík, *Dějiny Ostravy*. Ostrava: Sfinga, 1993.
- [2] P. Broulík, *Fajront! Když Ostravsko zavalili lidé z Haliče. Jsme jejich potomky?* Patriot. 2023
- [3] H. Brunn, *Ueber Ovale und Eiflächen*. Mnichov: Akademische Buchdruckerei von R. Straub, 1887.
- [4] Z. Grúňová, M. Holešová, *Ellipse and Oval in Baroque Sacral Architecture in Slovakia*. *Civil and Environmental Engineering*. 2017;13(1): 30-41.
- [5] S. Sebastiano, *Il Primo Libro [- Secondo] D'architettura*. In Vinetia: per Cornelio de Nicolini da Sabbio a instantia de Marchio Sessa, 1551.
- [6] J. Vybíral, V. Šlapeta, N. Goryczková, M. Strakoš, *Slavné vily Moravskoslezského kraje*. Praha: Foibos, 2008.
- [7] P. Šopák, *Tvořit město: (Opava a Moravská Ostrava 1850-1950: architektura a urbanismus)*. Opava: Slezské zemské muzeum, 2017.
- [8] *Plan über die Umgestaltung der M. Ostrauer Schiesstattlocalitäten.*, 1867. Lokace uložení 1019/1733, Statutární město Ostrava, Archiv města Ostravy
- [9] *Plan für den Neubau "Deutsches Haus" auf der Parcellen No. 155/2 in M. Ostrau, Bahnhofstrasse dem Vereine "Deutsches Haus" gehörig.* 1893. Lokace uložení 1019/1749, Statutární město Ostrava, Archiv města Ostravy

# Osobnosti slovenskej matematiky – inšpirácia a životné vzory pre budúce generácie

## Prominent personalities of Slovak Mathematics - idols for future generations

Ján Gunčaga<sup>1</sup>, Štefan Tkačík<sup>2</sup>

<sup>1</sup>*Univerzita Komenského v Bratislave, Pedagogická fakulta  
Račianska 59, 813 34 Bratislava, Slovenská republika  
email: guncaga@fedu.uniba.sk*

<sup>2</sup>*Katolícka Univerzita v Ružomberku, Pedagogická fakulta  
Hrabovská 1, 034 01 Ružomberok, Slovenská republika  
email: stefan.tkacik@ku.sk*

**Abstract.** In the frame of the KEGA project No. 004KU-4/2022 "Personalities of Slovak Mathematics II" we continue the successful edition „Personalities of Slovak Mathematics “. The project is aimed at capturing the life and work of important personalities of Slovak mathematics in the 20th century in their own words. Within the paper we want to present the processed materials about doc. RNDr. Daniela Velichová, CSc. She is an important personality in the field of geometry and geometric modelling. She is also involved in computer graphics, e-learning in teaching mathematical disciplines. Her example can serve as an inspiration for young and prospective scientists, and it shows that even mathematics can be an interesting and wonderful discipline accessible to the young people.

*Keywords:* mathematics education, personalities of Slovak Mathematics, Daniela Velichová, the ideas of personalities, publications about personalities

*Kľúčové slová:* vyučovanie matematiky, osobnosti slovenskej matematiky, Daniela Velichová, myšlienky osobností, publikácie o osobnostiach

## 1 Ciele a základné informácie o projekte

Cieľom prebiehajúceho projektu KEGA „Osobnosti slovenskej matematiky II - životné vzory pre budúce generácie“ je zmapovanie osobností slovenskej matematiky – matematikov a matematičiek, ktorí zasvätili svoj život tejto krásnej, a bohužiaľ, v súčasnej dobe tak neobľúbenej a nepreferovanej vede.

Na základe oslovenia všetkých relevantných pracovísk, kde sa na Slovensku matematika vyučuje na vysokých školách, vznikla databáza významných slovenských matematikov. Ide o otvorenú databázu, kde postupne pribúdajú ďalšie osobnosti, podmienkou je, aby svoj životný príbeh vyrozprávali svojimi vlastnými slovami. Následne spracujeme ich životné príbehy, tiež názory na kardinálne otázky súčasnosti (napr. ich vzťah k matematike, k spôsobu

vyučovania matematiky, k smerovaniu súčasnej matematiky, ...) a ich výsledkov v oblasti matematiky, s dôrazom na ich odkazy mladej generácií.

Čiastkovými cieľmi je vydanie publikácií o živote a diele osobností slovenskej matematiky, vytvorenie webovej stránky poskytujúcej informácie o týchto osobnostiach, propagácia výsledkov a šírenie svedectiev osobností.

Prostredníctvom projektu chceme sprístupniť materiál nielen pre učiteľov matematiky, ale aj pre zachovanie nášho kultúrneho dedičstva a v neposlednom rade chceme žiakom a študentom základných i stredných škôl priblížiť, že aj na Slovensku žijú a pracujú svetoví matematici. Domnievame sa, že tak by sme mohli v nich vzbudiť záujem a motiváciu pre matematiku pomocou osobnostných vzorov a odkazu významných osobností slovenskej matematiky.

Projekt prebiehal v 2 častiach, ten prvý začal v roku 2018 a trval do roku 2021. Súčasný projekt prebieha v rokoch 2022 – 2024. Na jeho riešení sa podieľajú Pedagogická fakulta Katolíckej univerzity v Ružomberku, Vysoká škola Dubnický technologický inštitút v Dubnici nad Váhom, Prírodovedecká fakulta Univerzity Pavla Jozefa Šafárika v Košiciach, Pedagogická fakulta Univerzity Komenského v Bratislave.

## 2 Vytvorenie databázy a edície publikácií o osobnostiach slovenskej matematiky

Za účelom vytvorenia databázy o významných slovenských matematikoch sme oslovili predstaviteľov stavovských organizácií:

- Matematický ústav Slovenskej akadémie vied,
- Jednota slovenských matematikov a fyzikov,
- Slovenská matematická spoločnosť.
- Vysokoškolské pracoviská, kde sa vyučovala matematika (učiteľská alebo vedecká).

Každé pracovisko navrhlo 10 žijúcich významných osobností a na základe spoločného prieskumu a odporúčania vznikla databáza, z ktorej postupne oslovujeme jednotlivé osobnosti.

Riešitelia prvého projektu PdF KU, FPV UKF, VŠ DTI a PdF KU iniciovali vznik Edície Osobnosti slovenskej matematiky. V rámci nej sa dohodla štruktúra publikácií, vzhľad a forma a základné otázky pre jednotlivé osobnosti. Najprv sa prostredníctvom Slovenskej národnej knižnice v Martine získali rešerše domácej a zahraničnej publikačnej činnosti 25 významných osobností. Následne sa komunikovalo s autorským zväzom LITA (p. Berglová), aby pri uverejňovaní neboli dotknuté autorské práva. Významným krokom bolo vytvorenie Vedeckej rady edície Osobnosti slovenskej matematiky. Nakoniec sa schválila predbežná štruktúra publikácií a jednotlivé otázky, ktoré boli v publikáciách položené:

- oficiálny životopis osobnosti,
- životopis a dôležité medzníky v živote prerozprávané danou osobnosťou,

- otázky a odpovede, ktoré dopĺňajú významné udalosti v živote danej osobnosti,
- otázky týkajúce sa aktuálnych otázok postavenia matematiky, jej vyučovania, systému vzdelávania,
- publikačná činnosť,
- obrazová príloha.

### 3 Vydané publikácie o matematických školách a osobnostiach

V rámci tohto aj predošlého projektu už boli publikované (porovnaj s [1] až [7]):

1. Mikulášska matematická škola
2. Košická matematická škola 1. diel - Seminár z teórie množín a topológie
3. Osobnosti slovenskej matematiky Roman Frič (1. diel)
4. Osobnosti slovenskej matematiky Milan Hejný (2. diel)
5. Osobnosti slovenskej matematiky Lev Bukovský (3. diel)
6. Osobnosti slovenskej matematiky Anatolij Dvurečenskij (4. diel)
7. Osobnosti slovenskej matematiky Stanislav Jendroľ (5. diel)
8. Osobnosti slovenskej matematiky Ondrej Šedivý (6. diel)
9. Osobnosti slovenskej matematiky Daniela Velichová (7. diel)

V nasledujúcej časti príspevku sa budeme venovať osobnosti Daniely Velichovej (pozri [7]). V tlači sú pripravené ďalšie 2 diely o Kataríne Cechlárovej a Jánovi Čižmárovi.

### 4 Osobnosť Daniely Velichovej

Jej profesijný rast predznamenal jej neskoršiu prácu v akademickom prostredí:

- 1969 – 1974 Prírodovedecká fakulta Univerzity Komenského v Bratislave, špecializácia Matematika a Deskriptívna geometria
- 1981 Matematicko-fyzikálna fakulta Univerzity Komenského v Bratislave, štátna rigorózná skúška, titul RNDr., Diplomová práca Zväzy v geometrii, vedúci doc. RNDr. Milan Hejný, CSc. (Milan Hejný (2. diel))
- 1992 Matematicko-fyzikálna fakulta Univerzity Komenského v Bratislave, dizertácia v odbore geometria - topológia a počítačová grafi-ka, titul CSc., Dizertačná práca Kreatívna geometria – modelovanie útvarov trojrozmerného priestoru, školitelia doc. RNDr. Ján Čižmár, CSc., prof. RNDr. Václav Medek,
- 1999 Fakulta elektrotechniky a informatiky Slovenskej technickej univerzity v Bratislave, habilitácia – komisia pre Aplikovanú matematiku, titul doc. Habilitačná práca Modelovanie masívov
- 2012 Strojnícka fakulta Slovenskej technickej univerzity v Bratislave, mimoriadna profesorka v odbore Aplikovaná matematika

Pracovne pôsobila:

- 1975 – 1976 Stavebná fakulta Slovenskej technickej univerzity v Bratislave externá asistentka na Katedre matematiky a deskriptívnej geometrie

1982 – 2022 Strojnícka fakulta Slovenskej technickej univerzity v Bratislave, odborná asistentka, docentka, mim. prof. na Katedre matematiky

2011– 2021 Strojnícka fakulta Slovenskej technickej univerzity v Bratislave, vedúca Ústavu matematiky a fyziky

S jej pracovným pôsobením úzko súvisí aj jej vedecká a publikačná činnosť zameraná na oblasti:

*Diferenciálna geometria kriviek, plôch a masívov* (MDT: 514.1, MSC: 53A04-A07)

- modelovanie nehomogénnych buniek masívov (MDT: 514.18, MSC: 68U07)
- modelovanie diferencovateľných variet pomocou Minkowského množinových operácií,

*Geometrické modelovanie s podporou počítačov* (MDT: 514.1, MSC: 65D17)

- počítačová geometria (MDT: 514.1, MSC: 65Y25)
- interpolačné útvary (MDT: 514.182, MSC: 65D05, 65D010)
- simulácie (MDT: 514, MSC: 68U20)

*Deskriptívna geometria* (MDT: 514.182.1-7, MSC: 51N05)

- premietacie metódy (MDT: 514.182.1-7)
- algoritmy vizualizácie viacrozmerných priestorov (MSC: 51N10 - 25)

*Pedagogika/didaktika matematiky na technických univerzitách*

- e-learning (MSC:97 U50)
- tvorba elektronických učebných textov (MSC:97 U20)

Docentka Daniela Velichová má aj bohatú činnosť v rôznych organizáciách:

- Členka riadiaceho výboru európskej spoločnosti pre vzdelávanie inžinierov SEFI Mathematics Special Interest Group - SEFI MWG
- Členka výboru European Women in Mathematics EWM, národná koordinátorka pre SR
- Ambasádorka ICM – medzinárodného výboru pre ženy v matematike pri Medzinárodnej matematickej únii IMU
- Predsedníčka Slovenskej Spoločnosti pre Geometriu a Grafiku - SSGG
- Členka výboru Medzinárodnej Spoločnosti pre Geometriu a Grafiku - ISGG
- Čestná členka Polskiego Towarzystwa Geometrii i Grafiki Inżynierskiej - PTGiGI
- Členka Jednoty slovenských matematikov a fyzikov - JSMF, resp. Slovenskej matematickej spoločnosti SMS

Cenné sú aj jej myšlienky o učiteľoch matematiky a o jej vyučovaní:

„Jediným východiskom je navrátiť učiteľom spoločenské uznanie, ktoré im právom patrí, a obnoviť vážnosť postavenia učiteľov v hierarchii spoločenského rebríčka reflektujúcu ich zodpovednosť za formovanie mladej generácie. Zástupcovia štátnej moci by mali akklamatívne prejaviť učiteľom patričný rešpekt



a oceniť ich nezastupiteľnú úlohu, ktorú zohrávajú zodpovednou prácou pri formovaní budúcnosti celej spoločnosti a jej hodnôt. Spoločnosť, ktorá si neváži prácu učiteľov, je nevyhnutne odsúdená na neúspech. Kvalitné vzdelanie učiteľov je zárukou rozvoja vzdelanosti a prosperity, napredovania spoločnosti, udržateľného rastu a zachovania dedičstva našich predkov. Nezáujem o učiteľské povolanie, nedostatok učiteľov, najmä matematiky a prírodovedných predmetov, ktorý začína naša spoločnosť intenzívne pociťovať, je dôsledkom narastajúcej náročnosti tejto zodpovednej práce v dôsledku významných spoločenských zmien. Tieto sú vo veľkej miere spôsobené paradigmou 21. storočia, ktorou je digitalizácia všetkých procesov spoločenského diania, zasahujúca až do základov kognitívnych procesov pri utváraní poznatkov a svetonázoru jednotlivcov, spoločností, resp. ľudského vedomia všeobecne. Kvalita vzdelávania, či kvalita prípravy budúcich učiteľov, a to nielen učiteľov matematiky, sú takmer vždy predmetom a témou celospoločenskej diskusie; ale skutočná zodpovednosť stále ostáva na pleciach spoločnosťou systematicky nedoceňovaných a sústavne kritizovaných učiteľiek a učiteľov, skutočných nositeľov, strojcov a realizátorov toľko glorifikovaného kvalitného vzdelávania. Ale kto si trúfa s istotou povedať, čo máme považovať za kvalitné vzdelávanie? A je vôbec možné pokúsiť sa o jeho zabezpečenie bez náležitej podpory, uznania a celospoločenského rešpektu?“

## 5 Záver

V súčasnosti sa pripravuje publikácia o profesorky Kataríne Cechlárovej a profesorovi Jánovi Čižmárovi. Predpokladáme pokračovať v Edícii Osobnosti slovenskej matematiky aj v nasledujúcom roku. Máme záujem spracovať ďalšie semináre a konferencie v rámci košickej matematickej školy. Zameriame sa na konferencie

- Konferencia (Cycles and Colourings),
- Konferencia košických matematikov v Herľanoch.

Riešiteľský kolektív je otvorený ďalším nápadom, ako sú vývoj, vzdelávanie a výchova matematických talentov vrátane matematickej spoločnosti.

Z uvedených dôvodov predpokladáme spoluprácu aj so Slovenskou spoločnosťou pre geometriu a grafiku.

## Podakovanie

Tento článok vznikol za podpory grantu KEGA č. 004KU-4/2022 „Osobnosti slovenskej matematiky II - životné vzory pre budúce generácie“

## Literatúra

- [1] Štefan Tkačik (ed.): Osobnosti slovenskej matematiky Roman Frič Roman Frič, Ružomberok: Verbum, 2020

- 
- [2] Lucia Csachová, Ján Gunčaga, Edita Partová, Katarína Žilková (ed.): Osobnosti slovenskej matematiky, Milan Hejný, Ružomberok: Verbum 2021
  - [3] Tomáš Lengyelfalussy, Štefan Tkačik (ed.): Osobnosti slovenskej matematiky Lev Bukovský, Ružomberok: Verbum, 2021
  - [4] Mária Jurečková (ed.): Osobnosti slovenskej matematiky Anatolij Dvurečenskij, Ružomberok: Verbum, 2021
  - [5] Štefan Tkačik (ed.): Osobnosti slovenskej matematiky Stanislav Jendroľ, Ružomberok: Verbum, 2021
  - [6] Jozef Fulier, Dušan Vallo (ed.): Osobnosti slovenskej matematiky Ondrej Šedivý, Nitra: Univerzita Konštantína Filozofa, 2021
  - [7] Ján Gunčaga, Lilla Koreňová, Věra Ferdiánová (ed.): Osobnosti slovenskej matematiky Daniela Velichová, Ružomberok: Verbum, 2023

# On the use of Bézier bicubic surface for shape reconstruction

Marta Hlavová

*Faculty of Mechanical Engineering, CTU in Prague  
Karlovo nám. 13, 121 35 Prague 2, Czech Republic  
email: marta.hlavova@fs.cvut.cz*

**Abstract.** How to exactly interpolate quadrilateral grid of points? In this article, some possibilities of using a Bézier bicubic patch for interpolation surface modelling are presented.

*Keywords:* CAD model, interpolation, Bézier bicubic surface, continuity, patching, accuracy

## 1 Introduction

A Bézier surface [1] is a type of mathematical representation used in computer graphics and computer-aided design (CAD) to describe freeform curved surfaces. It is an extension of the concept of Bézier curves, which are widely used for defining smooth and precise curves in two-dimensional space. The great advantage of Bézier surfaces is a possibility of patching that allows to describe a much more complex shape without increasing the surface degree (in both directions). The main topic of this article is to use Bézier bicubic surfaces to interpolate the same set of definition points in different ways and compare the accuracy of the interpolation CAD models. In this article, the grid of definition points was selected from a set of points obtained by means of real tactile measurement of CTU freeform standard Pharaoh [2] on coordinate measuring machine (CMM), fig. 1 left. The measured area (47 mm × 30 mm) with 58622 measured points and the grid of selected 8 × 8 definition points is shown in fig. 1 right. Maximum distance between two adjacent definition points is 11.0553 mm. From the same set of measured points, the test set of 24719 points was chosen to compare the accuracy of the interpolation CAD models.

This paper is organized as follows. In section 2, some key properties of Bézier bicubic surface are mentioned and the basic assignment of the task is outlined. An example of the simplest use of a such surface for this kind of shape reconstruction is given in subsection 2.1. Subsection 2.2. contains several examples of solving a more difficult variant of the assignment, subsection 2.3. compares all solutions in terms of accuracy. Section 3 concludes the paper.

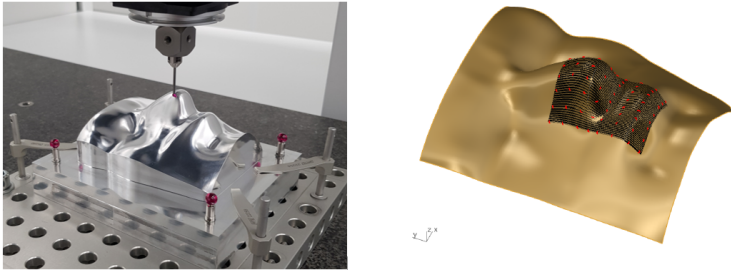


Fig. 1: CTU freeform standard Pharaoh (left), CAD model of its functional freeform surface (right) with all measured points (black) and the grid of definition points (red).

## 2 Interpolation and Bézier bicubic surface

A Bézier bicubic surface  $\mathbf{P}(u, v)$  is defined by a grid of control points  $\mathbf{V}_{i,j}$  (where  $i = 0, 1, 2, 3$  and  $j = 0, 1, 2, 3$ ), arranged in a  $4 \times 4$  matrix

$$\mathbf{M} = \begin{pmatrix} \mathbf{V}_{0,0} & \mathbf{V}_{0,1} & \mathbf{V}_{0,2} & \mathbf{V}_{0,3} \\ \mathbf{V}_{1,0} & \mathbf{V}_{1,1} & \mathbf{V}_{1,2} & \mathbf{V}_{1,3} \\ \mathbf{V}_{2,0} & \mathbf{V}_{2,1} & \mathbf{V}_{2,2} & \mathbf{V}_{2,3} \\ \mathbf{V}_{3,0} & \mathbf{V}_{3,1} & \mathbf{V}_{3,2} & \mathbf{V}_{3,3} \end{pmatrix}.$$

Vector equation of such surface is given by

$$\mathbf{P}(u, v) = \mathbf{B}(u) \cdot \mathbf{M} \cdot \mathbf{B}^T(v), \quad (u, v) \in [0, 1]^2,$$

where  $\mathbf{B}(w) = (B_{0,3}(w), B_{1,3}(w), B_{2,3}(w), B_{3,3}(w))$ ,  $w \in \{u, v\}$  and  $B_{k,3}(w) = \binom{3}{k} (1-w)^{3-k} w^k$ ,  $k = 0, 1, 2, 3$  are Bernstein polynomials.

The mesh of these 16 control points determines the shape of the surface and allows to create a CAD model of a smooth,  $C^2$  continuous, and curved surface. Although it is an approximation surface, the Bézier surface can be used for interpolation, because it interpolates the four control corner points  $\mathbf{V}_{0,0}$ ,  $\mathbf{V}_{0,3}$ ,  $\mathbf{V}_{3,0}$  and  $\mathbf{V}_{3,3}$  and four boundary Bézier cubic curves given by boundary control polygons.

### 2.1 The basic task and Example 1

Suppose, we have a quadrilateral grid of definition points  $\mathbf{Q}_{i,j}$ ,  $i \in \{0, 1, \dots, m\}$ ,  $j \in \{0, 1, \dots, n\}$  for the surface to pass through and we need to find the solution how to simply interpolate these points using Bézier bicubic surfaces.

Thanks to the fact, that Bézier bicubic surfaces allow  $C^2$  continuous patching, the simplest solution is a uniform clamped bicubic B-spline surface, which is just composed of  $C^2$  joined Bézier bicubic patches. The corner points of each Bézier patch are the definition points and the remaining 12 control points (of each patch) are calculated according to the  $C^2$  condition of continuity. In fig. 2 (left), the grid of definition points (red), control points of each Bézier patch (black) and boundary curves of each Bézier patch (blue) are shown. Visual evaluation of this CAD model accuracy is depicted in fig. 2 (right). The distances of the 24719 test points from surface were processed using the Rhinoceros tools.

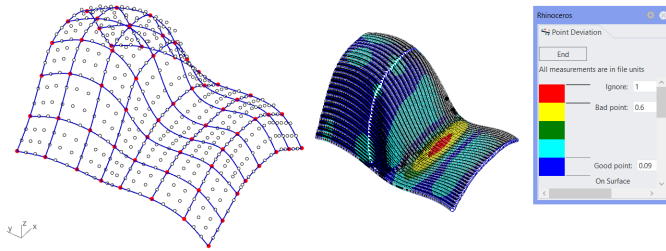


Fig. 2:  $C^2$  continuously joined Bézier patches (Example 1).

## 2.2 The task modification

However, the result of the tactile measurement on the CMM does not have to be only the coordinates of the measured point, but also information about the normal vector of the measured surface (at the given point) [3]. This insight will certainly lead to an improvement in the shape of the fitted surface, but due to the requirement to use the Bézier bicubic surface, it will be necessary to reduce the demands on the continuity of the joined patches. The  $C^1$  continuous patching is possible in the case of a Hermite bicubic surface with zero twist vectors at corner points, also known as Ferguson 12 vector surface [4]. This kind of surface can be easily redefined as Bézier bicubic patch, because each triplet of corner neighboring control points with this corner point have to form a parallelogram. To meet the normal vector requirement at all definition (i.e. corner) points, this parallelogram must lie in the tangent plane of the patch. Consequently, there are countless possibilities to place the remaining 12 control points of each Bézier patch in "their" tangent planes to form parallelograms of four. In the following, three examples of the specific location of these points will be presented and the accuracy of the resulting CAD model will be evaluated.

### 2.2.1 Example 2

For interior  $\mathbf{Q}_{i,j}$  ( $i \in \{1, 2, \dots, m-1\}, j \in \{1, 2, \dots, n-1\}$ ) definition points, the missing boundary Bézier control points (for each Bézier patch) are obtained by orthogonal projection of points

$$\mathbf{Q}_{i,j} \pm \frac{1}{6} \overrightarrow{\mathbf{Q}_{i-1,j} \mathbf{Q}_{i+1,j}}, \quad \mathbf{Q}_{i,j} \pm \frac{1}{6} \overrightarrow{\mathbf{Q}_{i,j-1} \mathbf{Q}_{i,j+1}}$$

into the tangent plane at definition point  $\mathbf{Q}_{i,j}$ . In each Bézier patch, the quartet of interior remaining control points is then added from the parallelogram condition. In fig. 3, all definition points with control points of each Bézier patch and visualization of  $C^1$  continuity are shown.

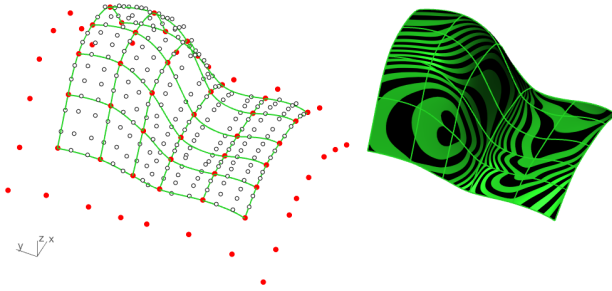


Fig. 3:  $C^1$  continuously joined Bézier patches (Example 2).

### 2.2.2 Example 3

Using the same notation as in Example 2, the missing boundary Bézier control points (for each Bézier patch) are obtained by orthogonal projection of points

$$\mathbf{Q}_{i,j} \pm \frac{1}{5} \overrightarrow{\mathbf{Q}_{i-1,j} \mathbf{Q}_{i+1,j}} \quad \text{and} \quad \mathbf{Q}_{i,j} \pm \frac{1}{5} \overrightarrow{\mathbf{Q}_{i,j-1} \mathbf{Q}_{i,j+1}}$$

into the tangent plane at point  $\mathbf{Q}_{i,j}$ , remaining inner control points are computed via parallelogram condition. This CAD model is just a variation of previous Example 2, but from fig. 4 it is clearly seen that increasing the distance between the boundary control point and corner point in the tangent plane has a favorable effect on the accuracy of the surface.

### 2.2.3 Example 4

In the last example, the missing boundary Bézier control points are given by orthogonal projection of points

$$\mathbf{Q}_{i,j} + \frac{b_i}{3c_i(a_i + b_i)}, \quad \mathbf{Q}_{i,j} - \frac{a_i}{3c_i(a_i + b_i)},$$

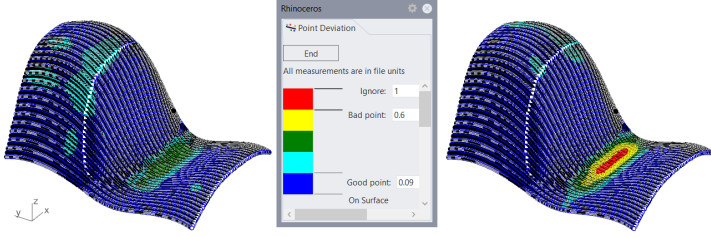


Fig. 4: Visual comparison of accuracy, Example 3 (left) and Example 2 (right).

$$\begin{aligned}
 (c_i = \|\overrightarrow{\mathbf{Q}_{i-1,j}\mathbf{Q}_{i+1,j}}\|, a_i = \|\overrightarrow{\mathbf{Q}_{i-1,j}\mathbf{Q}_{i,j}}\|, b_i = \|\overrightarrow{\mathbf{Q}_{i,j}\mathbf{Q}_{i+1,j}}\|) \\
 \mathbf{Q}_{i,j} + \frac{b_j}{3c_j(a_j + b_j)}, \mathbf{Q}_{i,j} - \frac{a_j}{3c_j(a_j + b_j)}, \\
 (c_j = \|\overrightarrow{\mathbf{Q}_{i,j-1}\mathbf{Q}_{i,j+1}}\|, a_j = \|\overrightarrow{\mathbf{Q}_{i,j-1}\mathbf{Q}_{i,j}}\|, b_j = \|\overrightarrow{\mathbf{Q}_{i,j}\mathbf{Q}_{i,j+1}}\|)
 \end{aligned}$$

into the tangent plane of point  $\mathbf{Q}_{i,j}$ . Thanks to the proportional distribution of the boundary control points created in this way, the patches will not be connected with parametric  $C^1$  continuity, but only with geometric continuity  $G^1$ , fig. 5.

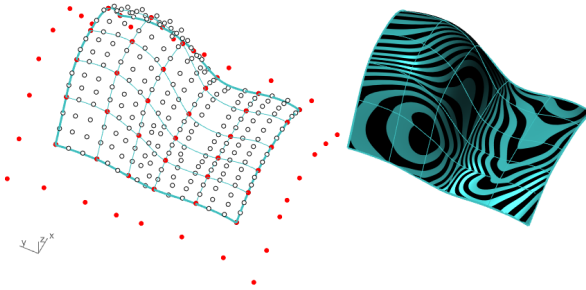


Fig. 5:  $G^1$  continuously joined Bézier patches (Example 4).

### 2.3 Accuracy evaluation

The accuracy of each CAD model exemplified was evaluated using the set of 24719 test points selected independently on the set of definition points from the set of 58622 measured points. In table 1, all important values obtained by Rhinoceros tool were collected. From this table it can be seen

CAD model	average distance	standard deviation	max. distance
Ex. 1 ( $C^2$ )	0.1199	0.1129	0.6500
Ex. 2 ( $C^1$ )	0.0612	0.1029	0.6346
Ex. 3 ( $C^1$ )	0.0606	0.0639	0.4216
Ex. 4 ( $G^1$ )	0.0603	0.1078	0.6833

Table 1: Statistical evaluation of accuracy, all values in mm

that the use of normal vectors leads to a decrease in average distance compared to Example 1 and the maximum distance of test points from CAD model is the smallest in the case of Example 3. These two values, together with the largest distance between two interpolated points (11.0553 mm), is very significant for comparing the accuracy of the given model.

### 3 Conclusion

Some possibilities of using the Bézier bicubic patch for shape reconstruction via interpolation are described and demonstrated on specific assignments in the paper. It is clear, that the idea of preserving the normal surface vectors to make the most accurate CAD model of surface leads to many solutions. In our case, the proposed result models consist of only  $C^1$  resp.  $G^1$  joined Bézier bicubic patches, but this degree of continuity is for CAD models and its further processing quite sufficient. A significant advantage of this approach is the modifiability of Hermite/Bézier patch control point locations, which will be addressed in future work.

### Acknowledgements

This work was supported by the Student Grant Competition of the Czech Technical University in Prague, grant Applications of mathematical-geometric modelling in mechanical engineering SGS21/148/OHK2/3T/12.

### References

- [1] L. Piegl, W. Tiller: *The NURBS Book*, Monographs in Visual Communications. Springer, Berlin, 1997
- [2] I. Linkeová, M. Hlavová: *CTU freeform standard Pharaoh* Proceedings of the Czech-Slovak Conference on Geometry and Graphics, SCHK, Bratislava, 2022
- [3] M. Hlavová, I. Linkeová: *Construction of interpolation B-spline curve for technical application* Proceedings of the Czech-Slovak Conference on Geometry and Graphics, SCHK, Bratislava, 2022
- [4] I. Linkeová: *Konvexní obal Fergusonova plátu* Proceedings of Symposium on Computer Geometry, STU, Bratislava, 2006



# The most famous illusions of Adalbert Ames Jr.

Marie Koktavá, Miroslava Tkadlecová

*Dept. of Mathematics, Faculty of Forestry and Wood Technology, MENDELU  
Zemědělská 3, 613 00 Brno, Czech Republic  
email: marie.koktava@mendelu.cz, miroslava.tkadlecova@mendelu.cz*

**Abstract.** Last year, as usual, we participated in the Czech European Researchers' Night at MENDELU. Since the theme was "With all the senses", as geometers we focused on vision. We created two of Adalbert Ames Jr.'s most famous illusions, namely the Ames Room and the Ames Window. In this paper we will describe how these illusions work and how we recreated them.

*Keywords:* Ames window, Ames room, illusion, perception.

## 1 Introduction

Adalbert Ames, Jr. (1880 – 1955) was an American ophthalmologist and perceptual psychologist.

As an ophthalmologist, he is credited with diagnosis of aniseikonia, a malformation of the eyes in which the right and left retinal images are so distinctively varied in size that they cannot readily be fused by the brain.

He is more widely remembered as a perceptual psychologist and the creator of a series of visual illusions, most of them summed up in the Ames Demonstrations in Perception [2]. There is about 22 laboratory demonstrations, probably the most famous are Ames window and Ames room.

## 2 Ames window

The shape of the Ames window is an isosceles trapezoid created as anamorphosis of the rectangular window with 6 openings. It is usually mounted on a vertical shaft that rotates, driven by a small electric motor.

The rotating trapezoid should be viewed from a short distance monocularly, or binocularly from a long distance. Most of the observers would not see the window as rotating, but oscillating back and forth. The perception of the illusion is better when the center of the trapezoid is at eye-level height, illumination of the object and the surrounded scene is uniform and the viewer can focus only on the rotating window.

It was believed that the only reason of this illusion lies in the fact that we are living in the environment where most of the objects as houses, rooms, furniture, windows are rectangular, but we usually see them as trapezoids. When looking on the Ames window, our brain suppose it is rectangle. This hypothesis was mostly declined by Harvard study among Zulus [3]. Two groups of children were formed, one from the city and the

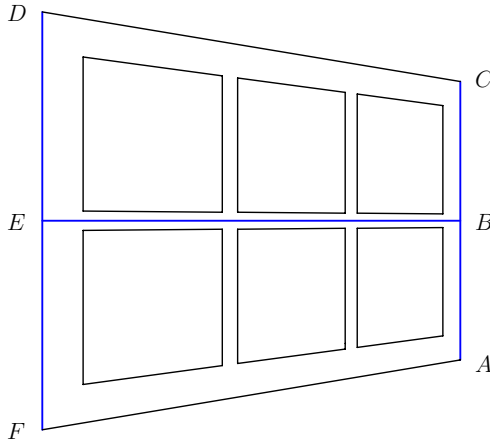


Fig. 1: Ames window.

other one from the villages, where they were living in round huts. There was expected difference of perceiving the illusion when looking with two eyes from 10ft distance, but nearly no difference when looking with one eye from 20ft distance.

Experiments with perceiving the illusion among small babies [5] confirmed that the ability of perceiving the illusion is connected to the depth perception.

To make the illusion even more interesting, various objects can be attached on the trapezoid and rotate with it. For example, a tube can be suspended through one of the openings, or a cube can be attached to side edge of the trapezoid. The attached object looks rotating while the window looks oscillating, which is quite confusing for the viewer.

It is possible to find templates for making the Ames window on the internet. These templates are usually not drawn in perspective correctly. Therefore when creating model, we started by drawing the window in perspective projection. Our first model was made from paper and cardboard. It was clear at first glance that it was not ideal. After gluing the layers together, the window bowed. In addition, we later discovered that it did not have the ideal proportions to create a strong optical illusion. Despite these flaws, the illusion worked.

We always supposed that not every trapezoidal window gives illusion of the same strength. Later on, we came upon the experiment [4], where the authors looked for the best dimensions of the trapezoidal window. They

selected nine various trapezoids of various parameters. These parameters were ratios of the lengths of the segments marked on the Fig. 1. The parametres and the presence or absence of shadows are given in next tabular.

	1	2	3	4	5	6	7	8	9
$\frac{ DF }{ AC }$	1	1	1,07	1,07	1,07	1,15	1,15	1,5	1,5
$\frac{ BE }{ AC }$	1	1,5	2,25	1,5	1	2,25	1	1,5	1
shadows	0	0	0	1	1	1	1	1	1

They asked observers to report changes in the direction of rotation and investigated how different shape of the window affect the illusory effect. Results of observation are given in Fig. 2.

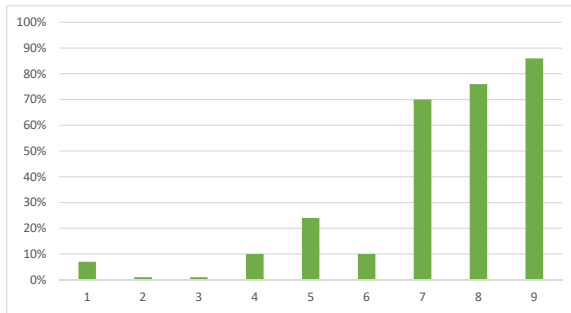


Fig. 2: Results of experiment.

Conclusions of the experiment:

- The bigger the  $\frac{|DF|}{|AC|}$  ratio, the stronger the illusory perception.
- The longer the horizontal length of the window, the weaker the illusory perception.
- The application of shadows increases the illusory effect.

We followed these results when making the second attempt to create the Ames window from the board. You can see our final plan for Ames window on Fig. 3.

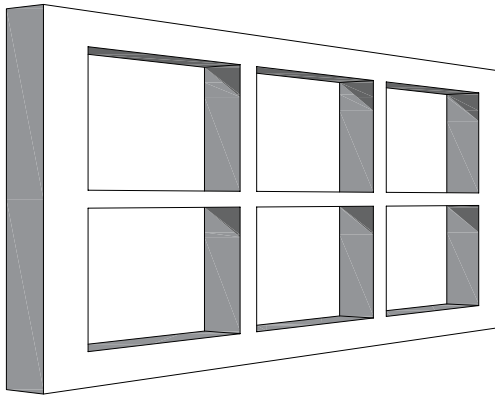


Fig. 3: Our Ames window.

### 3 Ames room

The Ames room is somehow deformed room, but when viewed from a proper point with one eye, it looks like ordinary orthogonal room. That is one part of the illusion. The viewing point is usually placed in one of the walls as a peephole and it has to be the center of projection which was used to project some parts of ordinary shaped room (or whole room) to get the deformed one.

When looking for the Ames room on internet for the first time, we came across many templates which used such construction that the floor and ceiling were surfaces of higher degree (not developable). That was not solution for us, because we wanted to create the room from boards. Therefore we gave up trying to make our work easier and started again from scratch with modeling the room. We wanted to get such distorted room, that would be easy to construct. Such a shape is in Fig. 4. Walls, floor and ceiling are planar and two side walls are parallel.

We found out later that this shape is probably the most common, when creating the Ames room and the construction is similar to the one Ames used. The difference is in the shape of original room. Ames used a cube and he projected most of it to get the resulting deformation.

There are infinitely many possibilities how the Ames room can be shaped and Ames was aware of that. He first created two such rooms in laboratory size and later one of them in full size (roughly corresponded twelve-foot cube). There is a detailed construction of that room in [2]

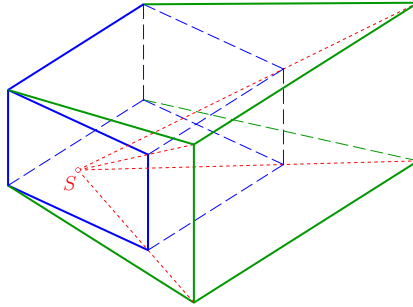


Fig. 4: Projection of the orthogonal room.

To make the illusion more believable, it is good to have windows in there and furnish the room. It is necessary to think about the location of these objects in advance, because their position in the room clearly determines their deformation as well (moving of the furniture is not possible later on).



Fig. 5: Our model of the Ames room viewed from the peephole.

The other part of the illusion lies in the fact that we can put in the corners (facing the viewing point) two objects of the same size, but one of them will look smaller. We used paper dolls, which can be switched the places. When viewed through the peephole, the one in the more distant corner will always look smaller (Fig. 5).

The illusion does not work when viewed with both eyes or from another point of view (Fig. 6).



Fig. 6: Model of the Ames room from other then viewing point.

## 4 Conclusion

Ames did not propose only these illusions. The room we call by his name, Ames called monocular room and also proposed and constructed less known binocular room. We advise the reader to see [2] for the details of other illusions Ames created.

## References

- [1] R. Behrens: *The Life and Unusual Ideas of Adelbert Ames, Jr.*, Faculty Publications. 5., University of Northern Iowa, The MIT Press, 1987
- [2] W. Ittelson: *The Ames Demonstration in Perception*, Princeton, Princeton University Press, 1952
- [3] G. Allport, T. Pettigrew: *Cultural influence on the perception of movement: the trapezoidal illusion among Zulus*, *The Journal of Abnormal and Social Psychology*, 55(1), 104–113, 1957
- [4] T. Papatomas, M. Karakatsani, S. Silverstein, N. Baker, M. de Heer: *Experiments and Computational Models for the Ames Window Illusion*, F1000Posters, presented at European Conference of Visual Perception 2013
- [5] S. Oross 3rd, E. Francis, D. Mauk, R. Fox: *The Ames window illusion: perception of illusory motion by human infants*, *The Journal of Experimental Psychology: Human Perception and Performance*, 13(4), 609-613, 1987

# Sú „prírodné fraktály“ naozaj fraktály?

## Are „natural fractals“ really fractals?

Alexej Kolcun

University of Ostrava, Faculty of Science, University of Ostrava  
30. dubna 22, 710 00 Ostrava, Czech Republic  
alexej.kolcun@osu.cz

**Abstract.** The work is focused on the applicability of the Box Counted Method for determining the fractal dimension of natural formations that show self-similarity features. The questionable moments of this approach are pointed out.

*Keywords:* Fractals, fractal dimension, Box Counted Method, Koch curve

*Kľúčové slová:* Fraktály, fraktálna dimenzia metóda BCM, Kochova krivka

### 1 Základné definície a vzťahy

Mandelbrotova kniha [1] a v nej zavedený pojem fraktálu má dodnes veľký ohlas (napr. [5]). Google dnes nachádza pre pojem „fraktálna množina“ viac ako 44 000 000 odkazov a pre pojem „fraktálna dimenzia“ takmer 20 000 000 odkazov. Záujem o túto metódu vyjadrenia geometrie je motivovaný tým, že v prírode často nachádzame objekty so zložitou štruktúrou, ktorá pri prechode na podrobnejšie zobrazenie má tendenciu sa opakovať, napr. [1], [2], [3].

V článku chceme ukázať určitú spornosť používaných konštrukcií. Obmedzíme sa na analýzu samopodobných štruktúr, ktoré sú tvorené iteračne lineárne lomenou čiarou, kde v nasledujúcej iterácii každú jej úsečku nahradíme adekvátne škálovanou replikou generátora (Lindenmeyerovské systémy).

1. *Kochova krivka* **K**, kde generátorom pre úsečku  $AB=$  je lineárne lomená čiara  $ACDEB$ , s dĺžkami úsečiek

$$|AC| = |CD| = |DE| = |EB| = \frac{|AB|}{3}$$

a uhlami medzi úsečkami

$$\alpha(AC, CD) = \alpha(DE, EB) = 120^\circ, \alpha(CD, DE) = 60^\circ$$

2. *racionálny variant Kochovej krivky* **V1**, (napr. v [4] pod názvom *Vicsek growth model*). Generátorom pre  $AB=$  je ortogonálna lineárne lomená čiara  $ACDEFB$ , kde

$$AC \perp CD, CD \perp DE, DE \perp EF, EF \perp FB$$

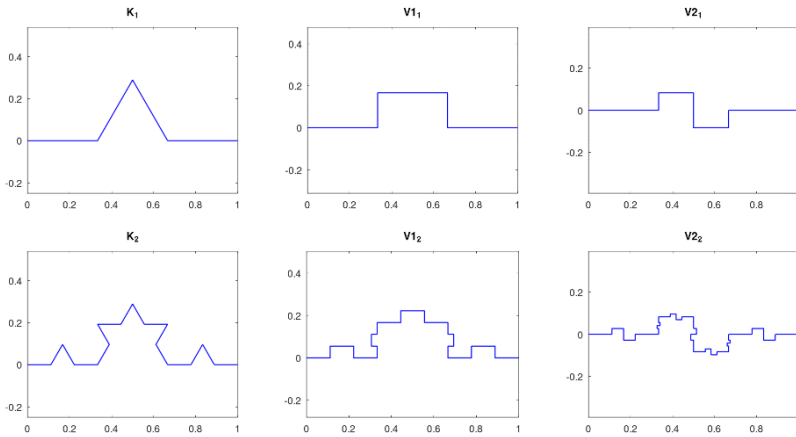
a dĺžky úsečiek sú

$$|AC| = |DE| = |FB| = \frac{|AB|}{3}, |CD| = |EF| = \frac{|AB|}{6},$$

3. *racionálny variant Kochovej krivky* **V2**, s generátorom  $ACDEFGHB$ , kde  $AC \perp CD, CD \perp DE, DE \perp EF, EF \perp FG, FG \perp GH, GH \perp HB$

a dĺžky úsečiek sú

$$|AC| = |HB| = \frac{|AB|}{3}, |DE| = |EF| = |FG| = \frac{|AB|}{6}, |CD| = |GH| = \frac{|AB|}{12}.$$



Obr. 1: Prvá a druhá iterácia použitých štruktúr  $\mathbf{K}$ ,  $\mathbf{V1}$  a  $\mathbf{V2}$

Fraktálnou dimenziou nazývame hodnotu

$$D = \lim_{r \rightarrow 0} \frac{\log N_r}{\log \frac{1}{r}}, \quad (1)$$

kde  $r$  je dĺžka jednotkového elementu a  $N_r$  je počet jednotiek, pokrývajúcich analyzovaný objekt. Je jednoduché sa presvedčiť, že vyššie uvedené štruktúry majú fraktálnu dimenziu

$$D_{\mathbf{K}} = D_{\mathbf{V1}} = D_{\mathbf{V2}} = \frac{\log 4}{\log 3} \doteq 1,2619. \quad (2)$$

Pre odhad hodnoty fraktálnej dimenzie sa spravidla používa metóda zvaná Box Counting (BCM). V našom prípade to znamená, že

1. skonštruujeme  $k$ -tu iteráciu objektu,  $\mathbf{F}_k \subset [0,1] \times [0,1]$ ,
2.  $\mathbf{F}_k$  preškálujeme a rasterizujeme v celočíselnej rastrovej mriežke

$$\mathbf{F}_{k,n} \subset \{1,2, \dots, n\} \times \{1,2, \dots, n\},$$

3. fraktálnu dimenziu odhadneme z hodnôt

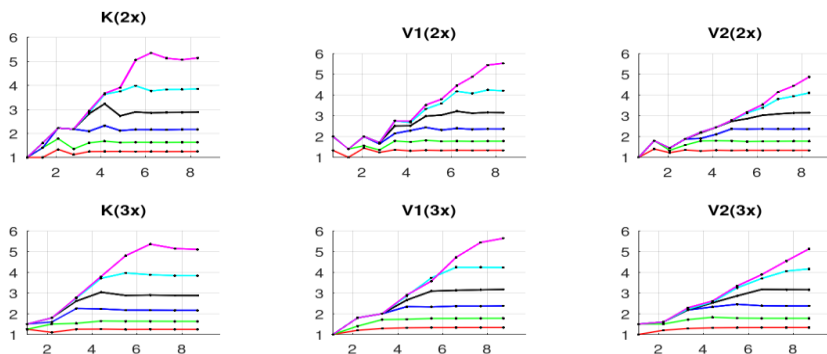
$$D_{\mathbf{F}_{k,n}} = \frac{\log N_{k,n}}{\log n} \quad (3)$$

kde  $N_{k,n}$  je počet pixelov reprezentujúcich  $\mathbf{F}_{k,n}$  a  $n$  definuje jemnosť rastrovej mriežky.

## 2 BCM pre rôzne scenáre zjemnenia rasterizačnej siete

Snaha o určenie fraktálnej dimenzie reálnych objektov naráža na to, že v reálnych situáciách vždy máme len konečný počet analyzovaných rastrových obrazov rôznych rozlíšení. Preto vo vysoko zjemnenej rastrovej mriežke, keď je veľkosť pixelu podstatne menšia ako najmenší detail analyzovaného objektu, vzťah (3) zjavne konverguje k  $D = 1$ . Je to dôsledok Shannonovho vzorkovacieho teorému. V tomto kontexte je analýza fraktálnej dimenzie založená na analýze podvzorkových obrázkov.





Obr. 2: „Dĺžka“ rastrového obrazu krivky pre rôzny počet iterácií a rôzne scénare zjemnenia rastrovej mriežky pre štruktúry **K**, **V1** a **V2**

Na Obr. 2 vidíme rôzne modifikácie dĺžky  $L_{F_{k,n}} = \frac{N_{k,n}}{n}$ . Iteráciám  $k = 1, \dots, 6$  (tj. jemnosti reprezentácie jednotlivých fraktálov) odpovedajú postupne farby R,G,B,K,C,M. Rôznym scénarom zjemňovania diskkrétnej mriežky odpovedajú kódy

(2x) – tj. zdvojnásobovanie diskkrétnej mriežky:

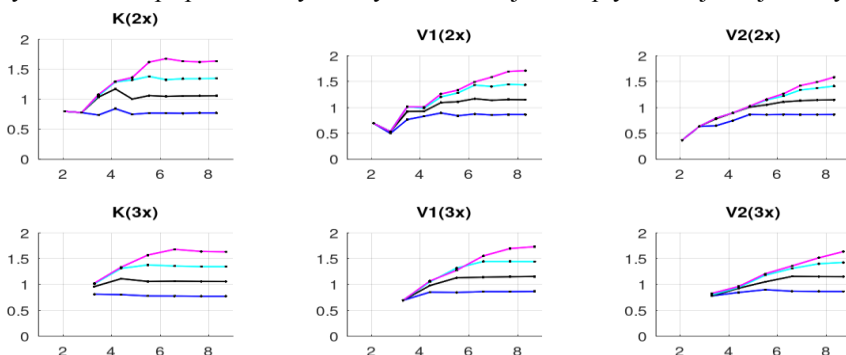
$$n \in \{3, 5, 9, 17, 33, 65, 129, 257, 513, 1025, 2049, 4097\}$$

(3x) – tj. strojnásobenie diskkrétnej mriežky:

$$n \in \{4, 10, 28, 82, 244, 730, 2188, 6562\}$$

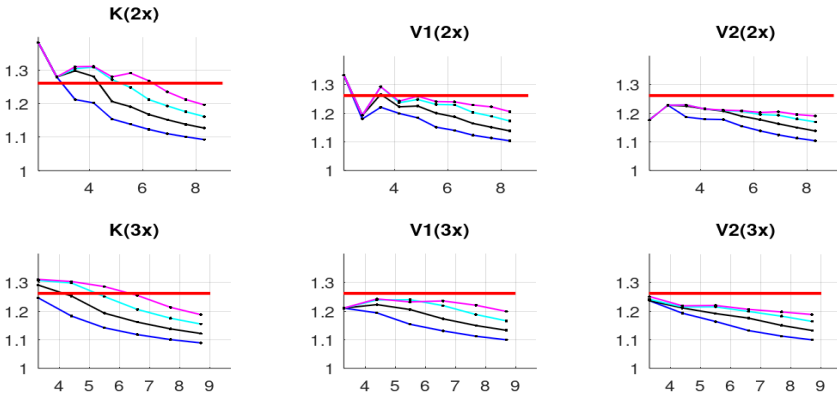
Na horizontálnej osi je logaritmická škála hodnoty  $n$ . Vidíme, že s narastajúcou hodnotou  $n$  každá z kriviek postupne prechádza “z exponenciály na priamku”. Vidíme taktiež, že strojnásobenie rastrovej mriežky je vzhľadom na konštrukciu použitých fraktálov prirodzenejšia ako zdvojnásobenie, čo sa prejavuje menším zaťažením diskretizačnou chybou (grafy vykazujú hladší priebeh).

Exponenciálnosť ľavých častí grafov je viac patrnejšia z Obr. 3, kde obe osi sú v logaritmickej škále ( $x = \log n$ ,  $y = \log N_{k,n} - \log n$ ). Vzhľadom na vzťah (3) by v ideálnom prípade všetky krivky mali v ľavej časti splyvať do jednej úsečky.



Obr. 3: Odhad fraktálnej dimenzie pre  $k = 3, \dots, 6$  a  $n_{(2x)} \geq 9$ ,  $n_{(3x)} \geq 28$ .

Názornejšie vyjadrenie odhadov fraktálnej dimenzie (3) je na Obr. 4, kde červená čiara reprezentuje skutočnú hodnotu (2) fraktálnej dimenzie.



Obr. 4: Odhad fraktálnej dimenzie pre  $k = 3, \dots, 6$  a  $n_{(2x)} \geq 9, n_{(3x)} \geq 28$ .

### 3 Záver

Výsledky ukazujú, že BCM metóda odhadu fraktálnej dimenzie je veľmi citlivá na scenár diskretizácie použitej rastrovej mriežky. Jej použitie sa zdá byť veľmi problematické pre fraktály, v ktorých sa vyskytuje zložitejšia štruktúra prvkov generátora (rôzne veľké elementy generátora).

Naviac, i pre najjednoduchší prípad (Kochova krivka) je nutný vysoký stupeň iterácie ( $k = 5, k = 6$ ), ktorý môže byť v praxi ťažko dosiahnuteľný.

### Pod'akovanie

Tento článok vznikol s inštitucionálnou podporou rozvoja KIP PŕF Ostravskej univerzity

### Literatúra

- [1] B. B. Mandelbrot, *The Fractal Geometry of Nature*, W. H. Freeman, New York 1982.
- [2] K. Falconer, *Fractal Geometry, Mathematical Foundations and Applications*, J. Wiley 2003.
- [3] *Thinking in Patterns* (M.M. Novak ed.), World Scientific 2004.
- [4] S. Buczkowski, S. Kyriacos, F. Nekka, L. Cartilier, *The Modified Box-Counting Method: Analysis of Some Characteristic Parameters*, Pattern Recognition Vol. 31, No. 4 (1998), pp. 411-418.
- [5] Jiaxin Wu et al., *An effective method to compute the box-counting dimension based on the mathematical definition and intervals*, Results in Engineering 6(2020).

# Triangulation of implicit surfaces with singularities

Kristína Korecová, Pavel Chalmovianský

*Department of algebra and geometry*

*Faculty of Mathematics, Physics and Informatics Comenius University*

*Mlynská dolina, 842 48 Bratislava, Slovak Republic*

*email: korecovak@gmail.com, pavel.chalmoviansky@fmph.uniba.sk*

**Abstract.** The paper covers a marching triangle approach for triangulating an implicitly defined surface in  $\mathbb{E}^3$ . The surface is allowed to have singularities which are given or can be computed. The singularities are of ADE type or non-isolated regular curves. Local approximations around singularities are extended over the regular part of the surface. Comparisons with SingSurf using quantitative criteria as well as using visualized examples are provided.

*Keywords:* triangulation, marching triangles, singularities

## 1 Introduction

During the processing of surfaces (e.g. modeling), they are often given in an implicit way. The approximation and visualization of such surfaces is one of the key items in a long list of procedures with them. We also propose a method of visualizing for certain isolated and non-isolated singularities on a surface as well as marching triangle type of approach for approximation of a regular part of an implicitly defined surface. Since the determining the position and type of isolated singularities is a difficult task on its own, we suppose such data are given for the surface in a suitable way. The non-isolated singularities, which are spatial regular curves can be often computed (traced) as intersection of induced surfaces.

An implicitly defined surface (IDS)  $Z(F) = \{\mathbf{x} \in \mathbb{R}^3 : F(\mathbf{x}) = 0\}$  is a zero set of a suitable function  $F: \mathbb{R}^3 \rightarrow \mathbb{R}$ . We often work with polynomial  $F$ , hence arbitrary order differentiability of  $F$  is guaranteed.

Typically, the set  $Z(F)$  can be locally parameterized by a regular surface in a suitable neighborhood of almost each of its points. However, singular points given by an additional condition  $\nabla F = \mathbf{0}$  might not have this property. Among them, we distinguish between simple isolated singularities (having a regular ring neighborhood and ADE structure) and non-isolated singularities along regular curves laying on the surface.

Visualization of IDS has already been done by several approaches for several decades – Marching cubes [4], Marching Triangles [1, 5], raytracing (developing rapidly with hardware acceleration), volumetric methods (used in many scanning techniques in medicine), particle based images and others.

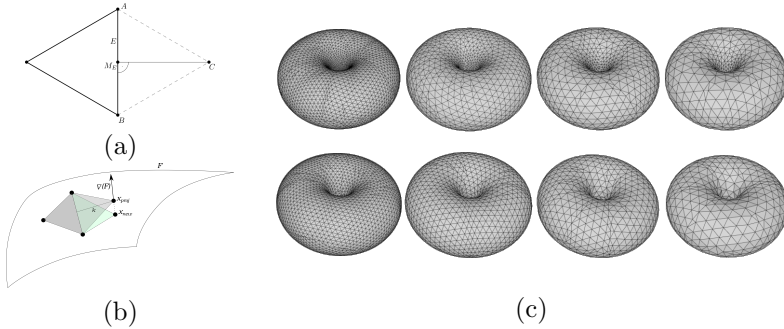


Fig. 1: Steps and results of Marching Triangles algorithm (a) estimation of the new triangle vertex (b) projecting the new vertex to a surface and forming a new approximation triangle, (c) results of the MT of torus using several starting lengths of the edge of the triangle with adaptive approach (top row) and uniform approach (lower row).

## 2 Triangulation

A triangulation approximating the surface can be obtained in several ways. Marching Triangles (MT) algorithm is briefly introduced for regular surfaces.

In general, finding a first point of a triangulation is a difficult task due to the fact that it deals with its existence. Suppose we are given such a point and it is a regular one. Using a triangle in its tangent plane, we might obtain the first triangle of the triangulation using a projection of this tangent triangle onto the given IDS. The edges of the projected triangle form a starting boundary of the triangulated region.

Continuing from such a triangle, one adds another neighboring triangle at a time along the boundary of the triangulated region so that a final triangulation is obtained (see Fig. 1). A boundary has to be updated and maintained when a new triangle is added. Such a boundary can have several connected components that appear or are enclosed. It is a technically complex problem.

The approach of the determining of the new triangles can be modified using several additional properties of the surface  $Z(F)$ . Often, various functions of curvature of the approximated surface (principal, Gaussian, mean, see Fig. 2) are taken into account. They are important local and after integration also global characterization of a surface. In the proposed approach, the lengths of the triangle edges are computed adaptively according to curvedness (see [2]) resulting in the triangulation shown in Fig. 1 (c), top row.

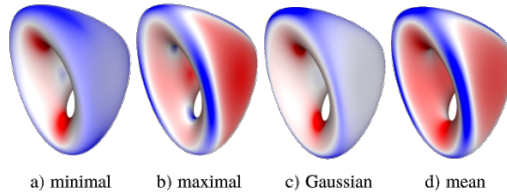


Fig. 2: Various types of curvature measured on a surface. Blue represents high values, white corresponds to middle values, red means low values (by the authors of [6]).

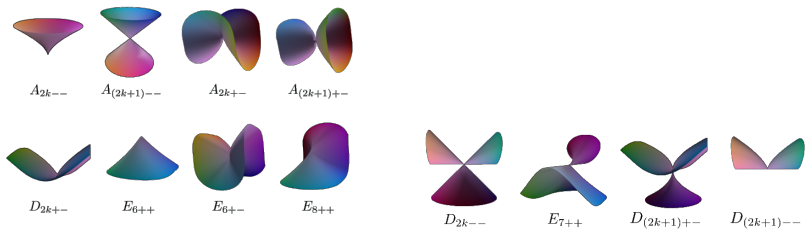


Fig. 3: Local behavior of ADE singularities.

### 3 Singularities

Isolated singular points on a surface can have a complicated and numerically unstable structure. Hence, only ADE singularities are considered (see Fig. 3). Although there are infinitely many ADE singularities, they can be classified into several groups locally given up to a smooth change of coordinates by the equations

$$\begin{aligned}
 A_{n\pm\pm} : f(x, y, z) &= x^{n+1} \pm y^2 \pm z^2, n \geq 1 \\
 D_{n\pm\pm} : f(x, y, z) &= yx^2 \pm y^{n-1} \pm z^2, n \geq 4 \\
 E_{6\pm\pm} : f(x, y, z) &= x^3 \pm y^4 \pm z^2 \\
 E_{7\pm\pm} : f(x, y, z) &= x^3 \pm xy^3 \pm z^2 \\
 E_{8\pm\pm} : f(x, y, z) &= x^3 \pm y^5 \pm z^2
 \end{aligned}$$

Singularities come into play in many circumstances. One of them considers finite subgroups of  $SO(3)$  corresponding to the isometries of regular or semi-regular polyhedra (see Fig. 4). Certain types of non-isolated singularities (curves in this case) are considered as well.

Considering their shape, there have been created only few mesh pat-

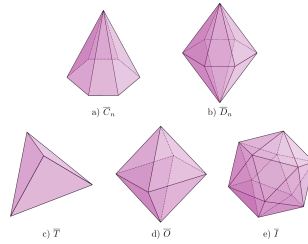


Fig. 4: Isometries of some polyhedra form ADE singularities.

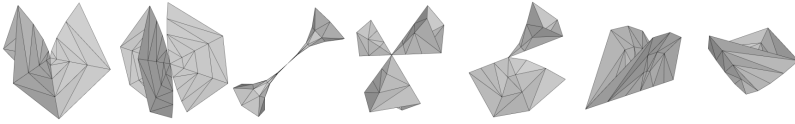


Fig. 5: Local meshes for the ADE singularities.

terns for their approximation (see Fig. 5). Using the symmetry and geometrical characteristics of the canonical isolated singularities, a set of parameters is determined for each type of singularity for the enhancement of a local approximation which is computed (see Fig. 6). One still has to take into account numerical limitations of such triangulations.

## 4 Results of the algorithm and their evaluation

The computed triangulations are compared using several criteria of quality (see Fig. 9).

- $k_1$  – the mean ratio of the length of the sides of the triangle.
- $k_2$  – a discrete approximation of the Hausdorff distance of the original surface and its approximation.
- $k_3$  – the mean distance of the gravity center and its perpendicular projection for each triangle.
- $k_4$  – the mean distance of the neighbor vertices from a vertex and the standard deviation of the distance from the mean.

Main comparison was between adaptive and non-adaptive approaches to the SingSurf program [5].

Visual comparisons of the results in several setups follow.

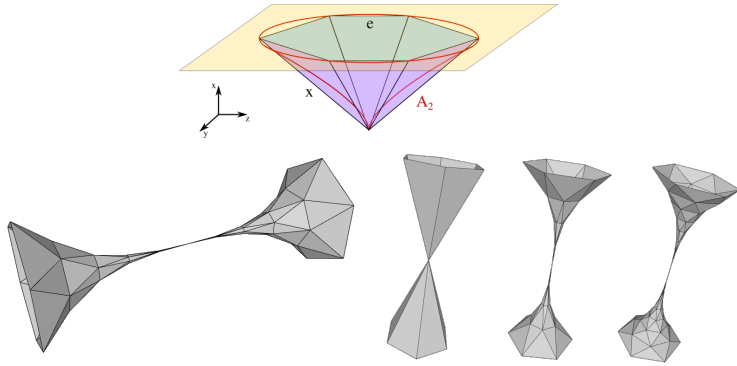


Fig. 6: Local approximation of singularities based on local parameters.

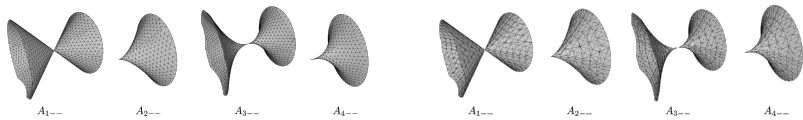


Fig. 7: Visual comparison of the approximation with Marching Triangles approach (left) and Marching Cubes (right) approach.

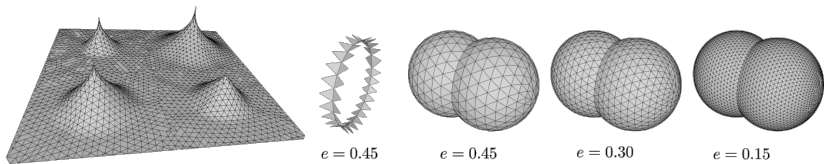


Fig. 8: Example of the surface with isolated singularities (left) and non-isolated singularities (right) constructed using CSG operations.

$A_{n--}$ singularities					$D_n$ singularities					$E_n$ singularities							
type		$k_1$	$k_2$	$k_3$	$k_4$	type		$k_1$	$k_2$	$k_3$	$k_4$	type		$k_1$	$k_2$	$k_3$	$k_4$
$A_{1--}$	SingSurf	0.113	0.015	0.001	0.052	$D_{4--}$	SingSurf	0.091	0.017	0.002	0.052	$E_{6++}$	SingSurf	0.006	0.043	0.003	0.069
	Uniform	0.834	0.007	0.001	0.010		Uniform	0.761	0.023	0.002	0.013		Uniform	0.831	0.013	0.002	0.017
	Adaptive	0.760	0.011	0.002	0.017		Adaptive	0.686	0.025	0.002	0.020		Adaptive	0.738	0.021	0.002	0.030
$A_{2--}$	SingSurf	0.072	0.008	0.001	0.051	$D_{4+}$	SingSurf	0.094	0.028	0.003	0.078	$E_{6+-}$	SingSurf	0.011	0.040	0.003	0.077
	Uniform	0.793	0.008	0.001	0.010		Uniform	0.650	0.032	0.003	0.027		Uniform	0.842	0.014	0.002	0.017
	Adaptive	0.729	0.008	0.001	0.017		Adaptive	0.713	0.028	0.003	0.040		Adaptive	0.721	0.034	0.002	0.034
$A_{3--}$	SingSurf	0.049	0.012	0.001	0.048	$D_{5--}$	SingSurf	0.001	0.032	0.006	0.076	$E_{7+-}$	SingSurf	0.198	0.024	0.004	0.110
	Uniform	0.651	0.008	0.001	0.011		Uniform	0.763	0.059	0.005	0.026		Uniform	0.797	0.027	0.004	0.027
	Adaptive	0.599	0.008	0.001	0.018		Adaptive	0.685	0.061	0.006	0.040		Adaptive	0.673	0.028	0.004	0.048
$A_{4--}$	SingSurf	0.325	0.020	0.001	0.045	$D_{5+-}$	SingSurf	0.132	0.029	0.003	0.076	$E_{8+-}$	SingSurf	0.260	0.045	0.004	0.100
	Uniform	0.309	0.008	0.001	0.014		Uniform	0.747	0.030	0.003	0.027		Uniform	0.803	0.028	0.004	0.032
	Adaptive	0.365	0.008	0.001	0.020		Adaptive	0.670	0.027	0.003	0.038		Adaptive	0.703	0.022	0.004	0.056

Fig. 9: Comparison of the computed triangulations with singularities using the criteria  $k_1$ - $k_4$ .

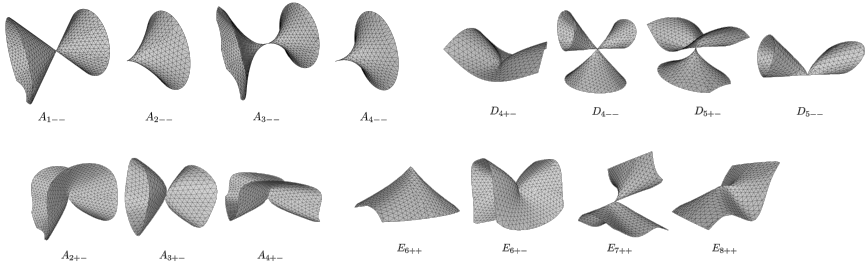


Fig. 10: Uniform triangulations of ADE singularities.

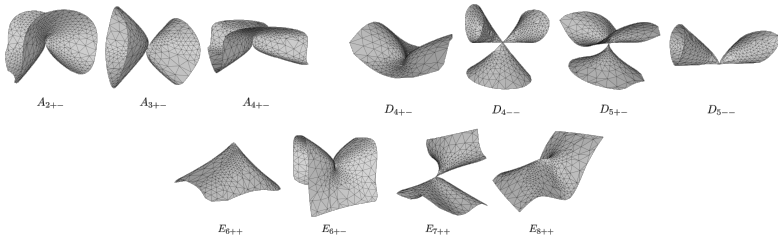


Fig. 11: Adaptive triangulations of ADE singularities.



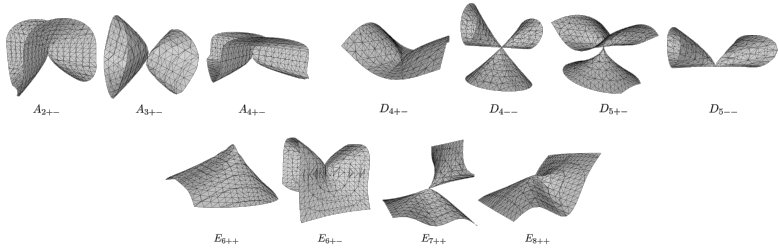


Fig. 12: SingSurf triangulations of ADE singularities is significantly less quality in term of triangle distribution.

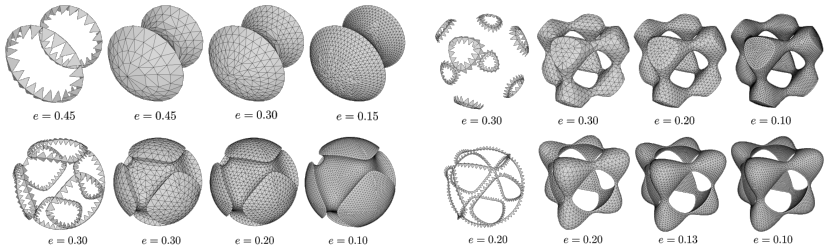


Fig. 13: Uniform triangulations with singular curves and various length of the triangle edge.

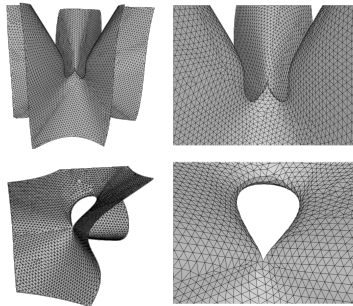


Fig. 14: A more complex uniform triangulations with ADE singularities.

## 5 Conclusion and future work

There are much detail on algorithms and examples written in the diploma thesis of the first author upon which is this paper based (see [3]).

Further progress of this topic is focused on the computation of the position and type of singularities on a surface. The determination of the singularities is particularly difficult via numerical methods for isolated singularities. Other qualitative methods have to be taken into account.

The non-isolated singularities (curves) may themselves contain singular points. Their determination is another challenge though such case are even rarer.

## Acknowledgement

The second author is supported by VEGA 1/0596/21.

## References

- [1] Samir Akkouche and Eric Galin. “Adaptive implicit surface polygonization using marching triangles”. In: *Computer Graphics Forum*. Vol. 20. 2. Wiley Online Library, 2001, pp. 67–80.
- [2] Jan J Koenderink and Andrea J Van Doorn. “Surface shape and curvature scales”. In: *Image and vision computing 10.8* (1992), pp. 557–564.
- [3] Korecova Kristina. “Triangulation of implicitly defined surfaces”. MA thesis. Faculty of Mathematics, Physics and Informatics Comenius University, 2023.
- [4] William E. Lorensen and Harvey E. Cline. “Marching cubes: A high resolution 3D surface construction algorithm.” In: *SIGGRAPH*. Ed. by Maureen C. Stone. ACM, 1987, pp. 163–169. ISBN: 0-89791-227-6.
- [5] Richard Morris. “A Client-Server System for the Visualisation of Algebraic Surfaces on the Web”. In: *Algebra, Geometry and Software Systems*. Ed. by Michael Joswig and Nobuki Takayama. Berlin, Heidelberg: Springer Berlin Heidelberg, 2003, pp. 239–253. ISBN: 978-3-662-05148-1.
- [6] Tiago Novello et al. “Exploring differential geometry in neural implicit”. In: *Computers & Graphics 108* (2022), pp. 49–60. ISSN: 0097-8493. DOI: <https://doi.org/10.1016/j.cag.2022.09.003>. URL: <https://www.sciencedirect.com/science/article/pii/S0097849322001649>.

# Parametrizace vybraných šroubových ploch a jejich zobrazení v programu Maple

## The parametrization of selected screw surfaces and their display in Maple program

Alice Králová

*Ústav matematiky LDF Mendelovy univerzity v Brně  
Zemědělská 3, 613 00 Brno, Česká republika  
email: alice.kralova@mendelu.cz*

**Abstract.** This paper describes the derivation of parametric equations of selected screw surfaces. This allows us to create graphical representations of these surfaces in the Maple graphic program.

*Keywords:* Helix, screw surface, parametrization, Maple.

*Klíčová slova:* Šroubovice, šroubová plocha, parametrizace, Maple.

### 1 Úvod

Tento příspěvek předkládá odvození parametrických rovnic u vybraných šroubových ploch, pomocí nichž jsou vytvořeny vizualizace těchto ploch v programu Maple, případně v programu GeoGebra. Protože nejobtížnější je nalezení parametrizací pro šroubový torzus a Archimédovu serpentinu, bude se příspěvek věnovat právě těmto dvěma plochám.

### 2 Šroubovice

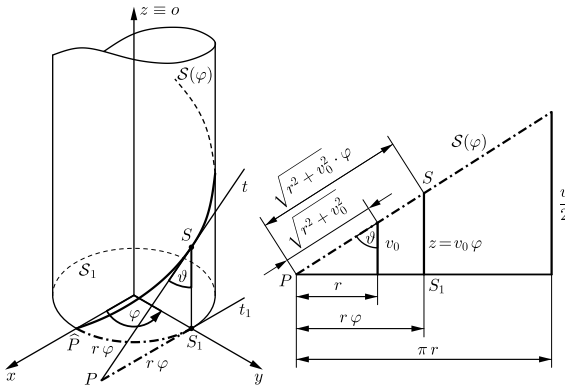
Výchozím objektem pro nalezení parametrizací šroubových ploch je jeden závit pravotočivé šroubovice s parametrickými rovnicemi

$$\mathcal{S}(\varphi) = (r \cos \varphi, r \sin \varphi, v_0 \varphi), \quad \varphi \in \langle 0; 2\pi \rangle,$$

které vyjadřují, že šroubový pohyb bodu je v základní situaci složením rovnoměrného rotačního pohybu bodu po kružnici o poloměru  $r$  se středem  $[0, 0]$  v půdorysně  $\pi = (x, y)$  a rovnoměrným posunem tohoto bodu ve směru osy  $z$ . Šroubovice je křivka navinutá na rotační válcovou plochu, kterou po rozvinutí do roviny vidíme jako přímkou. Jeden závit šroubovice daný otočením o úhel  $2\pi$  a posunutím o *výšku závitu*  $v$  je po rozvinutí přeponou pravoúhlého trojúhelníka s odvěsnami  $2\pi r$  a  $v$ . Otočení bodu o úhel 1 radián přísluší oblouk kružnice o délce  $r$  a posunutí o *redukovanou výšku závitu*  $v_0$ . Při otočení o obecný úhel  $\varphi$  má oblouk kružnice délku  $r\varphi$  a posunutí je dáno hodnotou  $z$ . Je tedy

$$\frac{v_0}{r} = \frac{v}{2\pi r} = \frac{z}{r\varphi} \Rightarrow v_0 = \frac{v}{2\pi} \wedge z = v_0 \varphi.$$

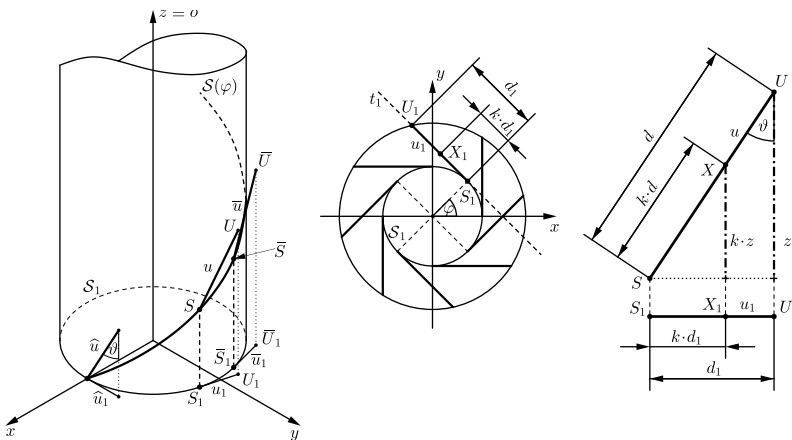
Dvě základní skupiny šroubových ploch jsou dány tím, zda se šroubuje přímkou nebo kružnicí. Jejich poloha pak určuje konkrétní typ *přímkové* resp. *cyklické* šroubové plochy.



Obr. 1: Vlastnosti šroubovice

### 3 Kosoúhlá otevřená přímková šroubová plocha

Plocha vzniká šroubovým pohybem přímky, která je s osou  $o \equiv z$  šroubového pohybu mimoběžná a svírá s ní obecný úhel  $\vartheta \in (0, \pi) \setminus \{\frac{\pi}{2}\}$ . Bod přímky umístěný nejbližše k ose vytváří při pohybu *hrdelní* šroubovici  $\mathcal{S}$ . Budeme parametrizovat plochu  $\mathcal{P}$ , jež vzniká šroubováním úsečky dané délkou  $d$  s krajním bodem na hrdelní šroubovici  $\mathcal{S}$  určené hodnotami  $r$  a  $v_0$ .



Obr. 2: Vytvoření kosoúhlé otevřené přímkové šroubové plochy

Tvořící úsečka  $u = SU$ ,  $|SU| = d$ , je přeponou pravoúhlého trojúhelníka a se směrem osy  $z$  svírá úhel  $\vartheta$ . Kolmým průmětem do půdorysny  $\pi$

je úsečka  $S_1U_1$  o délce  $d_1$  ležící na tečně kružnice  $\mathcal{S}_1$ , která je kolmým průmětem šroubovice  $\mathcal{S}$  do  $\pi$ . Z toho plyne, že  $z = d \cos \vartheta$  a  $d_1 = d \sin \vartheta$ .

Poloha obecného bodu  $X$  na úsečce  $u$  je dána součinem  $k \cdot d$  pro parametr  $k \in \langle 0; 1 \rangle$ . Promítnutím do půdorysny je  $|S_1X_1| = k \cdot d_1 = k d \sin \vartheta$ . Průmětem šroubovice  $\mathcal{S}$  do půdorysny je kružnice  $\mathcal{S}_1 = (r \cos \varphi, r \sin \varphi)$ , takže tečný vektor o délce  $r$  má vyjádření  $\mathcal{S}'_1 = (-r \sin \varphi, r \cos \varphi)$ .

Pomocí jednotkového tečného vektoru  $\vec{i} = (-\sin \varphi, \cos \varphi)$  lze parametrizovat bod  $X_1 \in \pi$  pro  $k \in \langle 0; 1 \rangle$  vztahem

$$X_1 = S_1 + k d \sin \vartheta \cdot \vec{i} = (r \cos \varphi - k d \sin \vartheta \sin \varphi, r \sin \varphi + k d \sin \vartheta \cos \varphi).$$

Rozdíl  $z$ -ových souřadnic bodů  $X$  a  $S$  je roven  $kz = k d \cos \vartheta$ , z čehož  $z$ -ovou souřadnici bodu  $X$  určíme jako  $v_0 \varphi + k d \cos \vartheta$ .

Tím jsme pro  $k \in \langle 0; 1 \rangle$  a  $\varphi \in \langle 0; 2\pi \rangle$  našli parametrizaci kosouhlé otevřené přímkové šroubové plochy ve tvaru

$$\mathcal{P} = (r \cos \varphi - k d \sin \vartheta \sin \varphi, r \sin \varphi + k d \sin \vartheta \cos \varphi, v_0 \varphi + k d \cos \vartheta).$$

### 3.1 Rozvinutelná přímková šroubová plocha

Pokud hodnota úhlu  $\vartheta$ , který svírá tvořící úsečka s osou  $o \equiv z$  šroubovice není libovolná, ale tato úsečka je vůči hrdelní šroubovici tečná, získáme *rozvinutelnou* přímkovou šroubovou plochu neboli *šroubový torzus*.

Tečný vektor ke šroubovici má tvar  $\mathcal{S}' = (-r \sin \varphi, r \cos \varphi, v_0)$ , jednotkový vektor osy  $z$  je  $\vec{j} = (0, 0, 1)$ , pokud tyto vektory svírají úhel menší než  $\frac{\pi}{2}$ , jedná se o hledaný úhel  $\vartheta$ . Pro odchylku vektorů platí

$$\cos \vartheta = \frac{\mathcal{S}' \cdot \vec{j}}{\|\mathcal{S}'\| \cdot \|\vec{j}\|} = \frac{v_0}{\sqrt{r^2 + v_0^2}}, \quad \sin \vartheta = +\sqrt{1 - \cos^2 \vartheta} = \frac{r}{\sqrt{r^2 + v_0^2}}.$$

Tytéž vztahy vidíme na obr. 1 po rozvinutí šroubovice do roviny. Jejich dosazením do parametrizace plochy  $\mathcal{P}$  získáme vyjádření rozvinutelné šroubové plochy

$$\mathcal{R} = \left( r \cos \varphi - \frac{k d r}{\sqrt{r^2 + v_0^2}} \sin \varphi, r \sin \varphi + \frac{k d r}{\sqrt{r^2 + v_0^2}} \cos \varphi, v_0 \varphi + \frac{k d v_0}{\sqrt{r^2 + v_0^2}} \right).$$

Standardně se zobrazuje část rozvinutelné šroubové plochy, která je omezena hrdelní šroubovicí  $\mathcal{S}$  a křivkou  $\mathcal{E}$  v půdorysně  $\pi$ . Tedy  $z = 0$  neboli  $\varphi + \frac{k d}{\sqrt{r^2 + v_0^2}} = 0$ . Požadujeme, aby tvořící úsečka plochy, jež je omezena

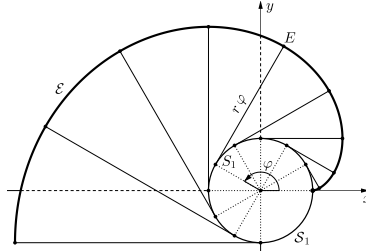
krajním bodem  $S$  šroubovice  $\mathcal{S}$  ležícím v obecné výšce  $v_0 \varphi$ , měla druhý krajní bod v bodě  $P \in \pi$ . To znamená, že délka této úsečky je rovna hodnotě  $d = \sqrt{r^2 + v_0^2} \cdot \varphi$ , což opět vidíme v obr. 1. Poloha bodu  $P$  tedy odpovídá hodnotě parametru  $k = -1$ . Dosazením do parametrizace plochy  $\mathcal{R}$  obdržíme vyjádření křivky  $\mathcal{E} = (r \cos \varphi + r \varphi \sin \varphi, r \sin \varphi - r \varphi \cos \varphi, 0)$ .

Tato křivka je *evolventou* kružnice  $\mathcal{S}_1 \in \pi$ , do níž se kolmo promítá hrdelní šroubovice  $\mathcal{S}$ . Názorně si lze evolventu kružnice představit jako dráhu koncového bodu natažené nitě, kterou odvíjíme z cívky. Obecný bod  $E$  evolventy  $\mathcal{E}$  leží na tečně ke kružnici ve vzdálenosti  $r \varphi$  od dotykového bodu  $S_1$  s kružnicí. Vektor  $\overrightarrow{S_1E}$  má opačný směr vzhledem k jednotkovému vektoru  $\vec{i} = (-\sin \varphi, \cos \varphi)$ , takže pro evolventu kružnice platí

$E = S_1 - r \varphi \cdot \vec{i} \Rightarrow \mathcal{E} = (r \cos \varphi + r \varphi \sin \varphi, r \sin \varphi - r \varphi \cos \varphi)$ ,  
 což se shoduje s předchozím výsledkem.

Pro zobrazení části rozvinutelné šroubové plochy mezi hrdeční šroubovicí  $\mathcal{S}$  a evolventou  $\mathcal{E}$  je třeba do parametrizace  $\mathcal{R}$  plochy dosadit odvozenou délku  $d = \varphi \sqrt{r^2 + v_0^2}$  tvořící úsečky plochy, přičemž rozsah parametru  $k$  je dán intervalem  $\langle -1; 0 \rangle$ .

$$\widehat{\mathcal{R}} = (r \cos \varphi - k r \varphi \sin \varphi, r \sin \varphi + k r \varphi \cos \varphi, (k + 1) v_0 \varphi)$$



Obr. 3: Evolventa kružnice

### 3.2 Vizualizace šroubového torzu

Rozvinutelnou šroubovou plochu zobrazíme v programu Maple pomocí následující animace, kterou bychom mohli přizpůsobit i programu GeoGebra.

```
> restart;with(plots):
> b1:=color=blue:b2:=color=red:b3:=color=violet:t1:=thickness=3:
  st:=style=patchngrid:
> r:=5:v0:=6:
> ST:=[r*cos(p)-k*r*p*sin(p),r*sin(p)+k*r*p*cos(p),(k+1)*v0*p],k=-1..0,
  p=0..pos,st:
> S:=[r*cos(p),r*sin(p),v0*p],p=0..pos,b1,t1:
> E:=[r*cos(p)+r*p*sin(p),r*sin(p)-r*p*cos(p),0],p=0..pos,b2,t1:
> u:=[r*cos(pos)-k*r*pos*sin(pos),r*sin(pos)+k*r*pos*cos(pos),
  (k+1)*v0*pos],k=-1..0,b3,t1:
> A1:=animate(plot3d,[ST],pos=0..4*Pi,frames=240):
> A2:=animate(spacecurve,[S],pos=0..4*Pi,frames=240):
> A3:=animate(spacecurve,[E],pos=0..4*Pi,frames=240):
> A4:=animate(spacecurve,[u],pos=0..4*Pi,frames=240,trace=24):
> display({A1,A2,A3,A4},scaling=constrained);
```

## 4 Archimédova serpentina

Jedná se o cyklickou šroubovou plochu, která je určena podmínkou, že šroubovaná kružnice  $k$  o poloměru  $R$  leží v každé poloze v rovině  $\rho$  kolmé k tečně šroubovice. Střed  $O$  kružnice  $k$  je přitom bodem šroubovice. Archimédova serpentina je zároveň *obalovou plochou* šroubojící se kulové plochy  $\mathcal{K}$  o téžže poloměru  $R$ .

Těčný vektor šroubovice je normálovým vektorem roviny  $\rho$ , takže rovina  $\rho$  má rovnici  $-x r \sin \varphi + y r \cos \varphi + z v_0 + d = 0$ , přičemž hodnotu  $d$  dopočítáme dosazením souřadnic bodu šroubovice. Je tedy

$$-r^2 \cos \varphi \sin \varphi + r^2 \sin \varphi \cos \varphi + v_0^2 \varphi + d = 0 \Rightarrow d = -v_0^2 \varphi$$

Rovnice roviny  $\rho : x r \sin \varphi - y r \cos \varphi - z v_0 + v_0^2 \varphi = 0$ .

Kulovou plochu  $\mathcal{K}$  budeme parametrizovat pomocí úhlů  $\alpha$  a  $\beta$ , kde  $\alpha$  je odchylka průmětu  $OK_1 \in \pi$  průvodiče  $OK$ ,  $|OK| = R$ , od kladného směru osy  $x$  a  $\beta$  je odchylka průvodiče  $OK$  od kladného směru osy  $z$ . Prozatím uvažujme, že  $O[0, 0, 0]$ . Pro souřadnice bodu  $K \in \mathcal{K}$  platí vztahy

$$x = |OK_1| \cos \alpha \wedge y = |OK_1| \sin \alpha \wedge |OK_1| = R \sin \beta \wedge z = R \cos \beta$$

Tím získáme vyjádření kulové plochy

$$\mathcal{K} = (R \cos \alpha \sin \beta, R \sin \alpha \sin \beta, R \cos \beta), \alpha \in \langle 0; 2\pi \rangle, \beta \in \langle 0; \pi \rangle.$$

Protože střed  $O$  kulové plochy leží na šroubovici  $\mathcal{S}$ , parametrizace se změní na  $\mathcal{K} = (r \cos \varphi + R \cos \alpha \sin \beta, r \sin \varphi + R \sin \alpha \sin \beta, v_0 \varphi + R \cos \beta)$ . Dosazením vztahů pro kulovou plochu  $\mathcal{K}$  do rovnice roviny  $\rho$  a následnou úpravou získáme vyjádření kružnice  $k$ .

$$r \sin \varphi (r \cos \varphi + R \cos \alpha \sin \beta) - r \cos \varphi (r \sin \varphi + R \sin \alpha \sin \beta) - v_0 (v_0 \varphi + R \cos \beta) + v_0^2 \varphi = 0$$

$$r R \cos \alpha \sin \beta \sin \varphi - r R \sin \alpha \sin \beta \cos \varphi - v_0 R \cos \beta = 0$$

$$r \sin \beta (\sin \varphi \cos \alpha - \cos \varphi \sin \alpha) - v_0 \cos \beta = 0$$

$$r \sin \beta \sin(\varphi - \alpha) - v_0 \cos \beta = 0$$

Dále rovnici umocníme na druhou a vyjádříme funkce  $\sin^2 \beta$  a  $\cos^2 \beta$ .

$$r^2 \sin^2 \beta \sin^2(\varphi - \alpha) = v_0^2 \cos^2 \beta \Rightarrow r^2 (1 - \cos^2 \beta) \sin^2(\varphi - \alpha) = v_0^2 \cos^2 \beta$$

$$\cos^2 \beta (v_0^2 + r^2 \sin^2(\varphi - \alpha)) = r^2 \sin^2(\varphi - \alpha)$$

$$\cos^2 \beta = \frac{r^2 \sin^2(\varphi - \alpha)}{v_0^2 + r^2 \sin^2(\varphi - \alpha)} \Rightarrow \sin^2 \beta = 1 - \cos^2 \beta = \frac{v_0^2}{v_0^2 + r^2 \sin^2(\varphi - \alpha)}$$

Protože  $\beta \in \langle 0; \pi \rangle$ , je  $\sin \beta \geq 0$ , a tedy  $\sin \beta = \frac{v_0}{\sqrt{v_0^2 + r^2 \sin^2(\varphi - \alpha)}}$ .

Funkce  $\cos \beta$  nabývá kladných i záporných hodnot a její znaménko je dáno znaménkem funkce  $\sin(\varphi - \alpha)$ . Vyjádříme  $\cos \beta = \frac{r \sin(\varphi - \alpha)}{\sqrt{v_0^2 + r^2 \sin^2(\varphi - \alpha)}}$ .

Dosazením těchto výrazů získáme vyjádření kružnice  $k$  na šroubové ploše, a tím i parametrizaci Archimédovy serpentiny.

$$\mathcal{A} = \left( r \cos \varphi + \frac{R v_0 \cos \alpha}{\sqrt{v_0^2 + r^2 \sin^2(\varphi - \alpha)}}, r \sin \varphi + \frac{R v_0 \sin \alpha}{\sqrt{v_0^2 + r^2 \sin^2(\varphi - \alpha)}}, v_0 \varphi + \frac{r R \sin(\varphi - \alpha)}{\sqrt{v_0^2 + r^2 \sin^2(\varphi - \alpha)}} \right)$$

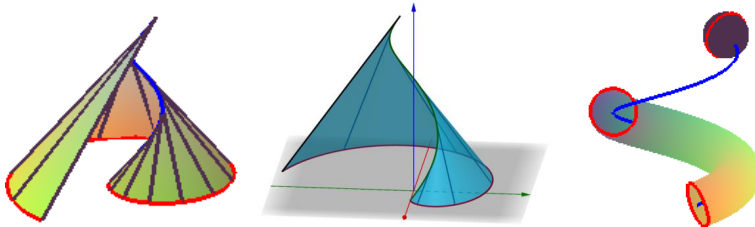
## 4.1 Vizualizace Archimédovy serpentiny

```
> restart;with(plots):
> b1:=color=red:b2:=color=blue:b3:=color=violet:t1:=thickness=3:
  st:=style=patchngrid:
> r:=8:R:=3:v0:=2.5:
> AS:=[ [r*cos(p)+R*v0*cos(a)/sqrt(v0^2+r^2*(sin(p-a))^2),
  r*sin(p)+R*v0*sin(a)/sqrt(v0^2+r^2*(sin(p-a))^2),
  v0*p+r*R*sin(p-a)/sqrt(v0^2+r^2*(sin(p-a))^2) ] ],
  p=0..pos,a=0..2*Pi,st,grid=[100,100]:
> S:=[ [r*cos(p),r*sin(p),v0*p] ],p=0..4*Pi-pos,b2,t1:
> K:=[ [r*cos(4*Pi-pos)+R*cos(a)*sin(b),r*sin(4*Pi-pos)+R*sin(a)*sin(b),
  v0*(4*Pi-pos)+R*cos(b) ] ],a=0..2*Pi,b=0..Pi,st,b3:
```

```

> k_1:={[r*cos(pos)+R*v0*cos(a)/sqrt(v0^2+r^2*(sin(pos-a))^2),
r*sin(pos)+R*v0*sin(a)/sqrt(v0^2+r^2*(sin(pos-a))^2),
v0*pos+r*R*sin(pos-a)/sqrt(v0^2+r^2*(sin(pos-a))^2)]},a=0..2*Pi,t1,b1:
> k_2:={[r*cos(4*Pi-pos)+R*v0*cos(a)/sqrt(v0^2+r^2*(sin(4*Pi-pos-a))^2),
r*sin(4*Pi-pos)+R*v0*sin(a)/sqrt(v0^2+r^2*(sin(4*Pi-pos-a))^2),
v0*(4*Pi-pos)+r*R*sin(4*Pi-pos-a)/sqrt(v0^2+r^2*(sin(4*Pi-pos-a))^2)]},
a=0..2*Pi,t1,b1:
> l:=spacecurve([r+R*v0*cos(a)/sqrt(v0^2+r^2*(sin(a))^2),
R*v0*sin(a)/sqrt(v0^2+r^2*(sin(a))^2),
-r*R*sin(a)/sqrt(v0^2+r^2*(sin(a))^2)],a=0..2*Pi,t1,b1):
> A1:=animate(plot3d,[AS],pos=0..4*Pi,frames=80):
> A2:=animate(spacecurve,[S],pos=0..4*Pi,frames=80):
> A3:=animate(plot3d,[K],pos=0..4*Pi,frames=80):
> A4:=animate(spacecurve,[k_1],pos=0..4*Pi,frames=80):
> A5:=animate(spacecurve,[k_2],pos=0..4*Pi,frames=80):
> display({A1,A2,A3,A4,A5,l},scaling=constrained);

```



Obr. 4: Animace šroubového torzu a Archimédovy serpentiny v Maplu

## 5 Závěr

Ačkoliv je práce v GeoGebře výrazně jednodušší než v Maplu, podstatným omezením je, že při parametrizaci ploch v GeoGebře je nutné obě proměnné ohraničit číselnými hodnotami a nelze vykreslit plochu, v níž je jeden parametr funkcionálně závislý na druhém parametru. Přestože se při vizualizaci výše uvedených ploch tento problém nevyskytl, je třeba mít toto omezení na paměti a v případě nutnosti použít Maple.

Závěrem lze říci, že vhodné zobrazení určité plochy technické praxe může být náhradou fyzického modelu této plochy.

## Literatura

- [1] F. Machala: *Plochy technické praxe*, Rektorát Univerzity Palackého v Olomouci, Olomouc, 1986



# Parametric CAD model of axial blood pumps components

Ivana Linkeová, Jaroslav Cibulka

*Czech Technical University in Prague, Faculty of Mechanical Engineering  
Karlovo nám. 13, 121 35 Prague 2, Czech Republic  
email: ivana.linkeova@fs.cvut.cz*

**Abstract.** The paper presents the development of a fully parametric CAD model of axial blood pumps components in Grasshopper, a graphical algorithm editor integrated in Rhinoceros. Since scientific papers report very little (if any) geometric information about the pumps, a special reverse engineering process was used to develop the parametric CAD model.

*Keywords:* parametric CAD model, axial blood pump, helicoidal blade, Rhinoceros, Grasshopper.

## 1 Introduction

Parametric CAD (Computer Aided Design) modelling represents a high-performance tool for designing virtual 3D geometries of engineering components and assemblies. An appropriately chosen system of input parameters allows defining mutual relationships and dimensional properties of the modelled geometric shapes. This paper presents the development of underlying geometry for CFD (Computation Fluid Dynamics) analysis of hemolytic properties of blood pumps in a form of a fully parametric CAD model. The CAD model is created in Rhinoceros, which is intended for direct modelling. Parameterisation of the CAD model is provided by Grasshopper, a graphical algorithm editor integrated in Rhinoceros.

Blood pumps are implantable mechanical rotary support systems providing artificial assistance for patients with heart failure. The optimisation of the rotary blood pumps design with respect to the hemolytic properties of the device such as avoidance of thrombogenicity and red blood cell damage represents a highly challenging problem [1]. To investigate the hemolytic properties of blood pumps, CFD mathematical models of blood flow are developed and various blood pump geometries are analysed, [2, 3, 4, 5]. In [5], the hemolytic properties of axial blood pump shown in fig. 1 (left) are analysed while the impeller and diffuser designs are varied. In this paper, the development of parametric CAD model of the diffuser inspired by geometry given in [5], see fig. 1 (right), is described.

## 2 Set of parameters for diffuser modelling

The diffuser drawn in fig. 1 (right) consists of cylindrical hub with flat and hemisphere caps and helicoidal blades. Unlike [5], where the geometry of the diffuser blades is varied by only two values of inlet angle (25° and 45°)

and two values of chord length (9 mm and 14 mm), the set of parameters proposed here allows full control over the geometry, see table 1.

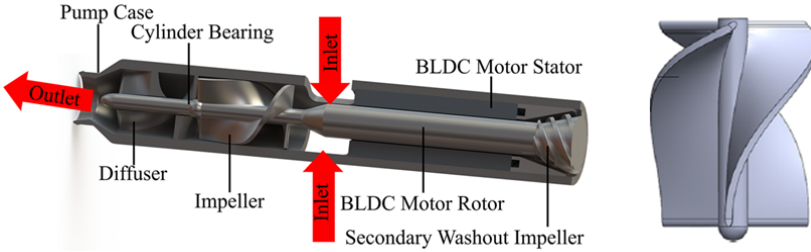


Fig. 1: Axial blood pump design (left), CAD model of diffuser (right) [5]

CAD model	Parameter	Description
	$r_1$	Hub radius
	$r_2$	Tip radius
	$t$	Blade thickness
	$b$	Tip shape
	$n$	Blades number
	$w$	Wrap angle
	$h$	Height
	$p$	Helix shape

Table 1: Set of parameters

### Set of parameters

- $r_1$  – hub radius in mm.
- $r_2$  – tip radius in mm.
- $t$  – thickness of the blade in mm.
- $b$  – tip shape parameter allowing to design convex ( $b > 0$ ), straight ( $b = 0$ ) or concave ( $b < 0$ ) shaping of the blade tip, see fig. 2. The profile of blade tip is modelled as a Bézier cubic curve given by four control points  $V_0, V_1, V_2$  and  $V_3$ . Parameter  $b$  determines the orientation of  $\vec{V_0V_1}$  and  $\vec{V_2V_3}$  vectors.

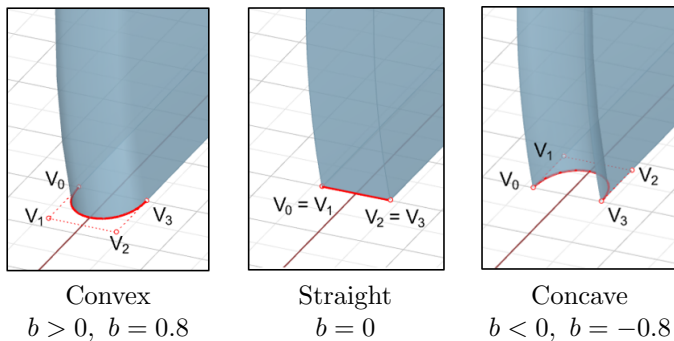


Fig. 2: The influence of tip shape parameter  $b$

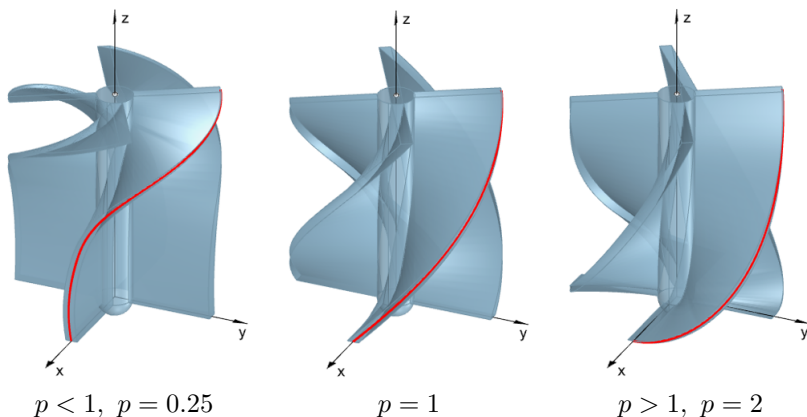


Fig. 3: The influence of helix shape parameter  $p$

- $n$  – number of blades.
- $w$  – wrap angle of the helicoidal blade in degrees.
- $h$  – height of the diffuser hub in mm.
- $p$  – helix shape parameter allowing to control disproportionality between the translation along the axis of screw motion ( $z$ -axis) and angle of rotation about the axis of screw motion, see fig. 3.

Parametric equations of the directing helix are given by

$$\begin{aligned}
 x(v) &= r_2 \cos(v) \\
 y(v) &= r_2 \sin(v) \\
 z(v) &= h \left( \frac{v}{w} \right)^p, \quad v \in [0, w], \quad p > 0.
 \end{aligned} \tag{1}$$

Consequently, the cross-section of the gap between the blades changes, see fig. 3, where the helix (1) is drawn in red. The decreasing ( $b < 1$ ) or increasing ( $b > 1$ ) cross-section of the gap between the blades is used for the flow regulation. For  $b = 1$ , the translation is directly proportional to the rotation and the cross-section of the gap between the blades is constant.

Note that the blade tip is straight, i.e.  $b = 0$  for all the three examples in fig. 3.

The variability of the diffuser CAD model created by suitable parameter settings is almost infinite. Four different CAD models similar to the ones analysed in [5] are shown in table 2 together with the parameter values.

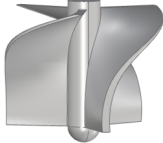



Diffuser I	Diffuser II	Diffuser III	Diffuser IV
			
$r_1 = 1.25 \text{ mm}$	$r_1 = 1.25 \text{ mm}$	$r_1 = 1.25 \text{ mm}$	$r_1 = 1.25 \text{ mm}$
$r_2 = 6.00 \text{ mm}$	$r_2 = 6.00 \text{ mm}$	$r_2 = 7.00 \text{ mm}$	$r_2 = 7.00 \text{ mm}$
$t = 0.6 \text{ mm}$	$t = 0.6 \text{ mm}$	$t = 0.6 \text{ mm}$	$t = 0.6 \text{ mm}$
$b = 0$	$b = 0$	$b = 0.8$	$b = 0.8$
$n = 3$	$n = 3$	$n = 3$	$n = 3$
$w = 100^\circ$	$w = 67^\circ$	$w = 150^\circ$	$w = 120^\circ$
$h = 9 \text{ mm}$	$h = 9 \text{ mm}$	$h = 15 \text{ mm}$	$h = 15 \text{ mm}$
$p = 0.31 \text{ mm}$	$p = 0.25$	$p = 0.33 \text{ mm}$	$p = 0.40 \text{ mm}$

Table 2: Examples of diffuser geometries

### 3 Diffuser modelling in Grasshopper

Grasshopper as a graphical programming environment is implemented in Rhinoceros. Individual components are placed onto a canvas and connected with subsequent components. The preview of the Grasshopper project of the diffuser parametric CAD model is shown in fig. 4. To keep the clarity of the picture, the connecting wires are hidden.



## 4 Conclusion

The paper presents the development of a parametric CAD model of a diffuser for axial blood pumps. Fully parametric geometry is modelled in Grasshopper integrated in Rhinoceros. The Grasshopper project has the following sections: definition of a set of parameters through which it is possible to control the geometry of the diffuser, modelling the hub as a cylinder of revolution with flat and hemispheric caps, modelling the blade profile as a normal section of the blade helicoidal surface, and modelling the blade helicoidal surface by helical motion of the blade profile.

## Acknowledgements

This work was supported by the Student Grant Competition of the Czech Technical University in Prague, grant Applications of mathematical-geometric modelling in mechanical engineering SGS21/148/OHK2/3T/12.

## References

- [1] Arvand, A., Hormes, M. and Reul, H.: A Validated Computational Fluid Dynamics Model to Estimate Hemolysis in a Rotary Blood Pump. *Artificial organs*. <https://doi.org/10.1111/j.1525-1594.2005.29089.x>
- [2] Blum, C., Groß-Hardt, S., Steinseifer, U. et al.: An Accelerated Thrombosis Model for Computational Fluid Dynamics Simulations in Rotary Blood Pumps. *Cardiovasc Eng Tech* 13, 638–649 (2022). <https://doi.org/10.1007/s13239-021-00606-y>
- [3] Dai W-F, Wu P, Liu G-M.: A two-phase flow approach for modeling blood stasis and estimating the thrombosis potential of a ventricular assist device. *The International Journal of Artificial Organs*. 2021;44(7):471-480. <https://doi.org/10.1177/0391398820975405>
- [4] D. Carswell, D. McBride, T.N. Croft, A.K. Slone, M. Cross, G. Foster: A CFD model for the prediction of haemolysis in micro axial left ventricular assist devices. *Applied Mathematical Modelling* 37 (2013) 4199–4207, <http://dx.doi.org/10.1016/j.apm.2012.09.020>
- [5] Smith, P.A., Wang, Y., Bieritz, S.A. et al.: Design Method Using Statistical Models for Miniature Left Ventricular Assist Device Hydraulics. *Annals of Biomedical Engineering* 47 (2018): 126 - 137. <https://doi.org/10.1007/s10439-018-02140-w>

# Subdivision and conchoids

Marcel Makovník

*Katedra algebry a geometrie, Fakulta matematiky, fyziky a informatiky,  
Univerzita Komenského v Bratislave*

*Mlynská Dolina, 84248 Bratislava, Slovenská republika*

*email: marcel.makovnik@fmph.uniba.sk*

**Abstract.** We discuss the refinement of a planar polyline using conchoids. For each segment of the polyline, we construct a conchoid, which interpolates its endpoints. This is achieved by choosing a feasible coordinate system, scaled by the input global parameter. Then, we choose new points from the interpolating conchoid, symmetrically to the horizontal axis. Afterwards, we transform the new pair of points to the original coordinate system. The refined polyline is obtained in the "corner-cutting" fashion, i. e. by joining the subsequent pairs of new points. The process of refinement may be applied repeatedly to achieve the desired level of detail. The proposed refinement scheme is approximating and non-linear. We provide several examples that demonstrate the behaviour of the refinement. Also, we inspect on the influence of the value of the global parameter. For the specific value, we obtain the well-known Chaikin's algorithm.

*Keywords:* Subdivision, conchoids, curve fitting.

## 1 Introduction

Subdivision curve is generated by iterative refinement of the input polyline. If the points of the refined polyline are obtained as linear combinations of the original ones, we refer to such schemes as linear and non-linear otherwise. Convergence and continuity of linear subdivision schemes is well studied [2]. For the case of non-linear schemes (see e. g. [4, 5, 7]), the idea of proximity to a certain linear scheme is used, see [3] and [6]. In our contribution, we describe a subdivision scheme in a plane which utilizes a local interpolation by conchoids.

## 2 Preliminaries

### 2.1 Conchoids

In our work, we utilize a conchoid of de Sluze  $\mathcal{C}$ , which is a cubic curve given implicitly by

$$\mathcal{C} : (x - 1)(x^2 + y^2) - ax^2 = 0. \quad (1)$$

Depending on the value of the parameter  $a \in \mathbb{R}$ , various families of curves may be generated (classified by the type of the singularity at the point  $(0, 0)^\top$ ). For  $a \neq 0$ , the conchoid  $\mathcal{C}$  has an asymptote  $x = 1$ , see Fig. 1.

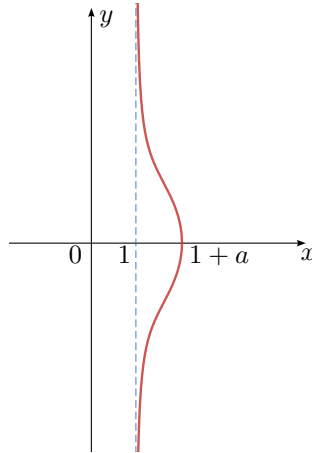


Fig. 1: Conchoid of de Sluze (red) given by the parameter  $a$  and its asymptote  $x = 1$  (blue).

## 2.2 Subdivision step

Consider an input polyline, given by a sequence of points  $V_0, V_1, \dots, V_n \in \mathbb{R}^2$ . For each segment  $V_i V_{i+1}$  of the input polyline we assign a pair of new points  $P_i$  and  $Q_i$  in corner cutting fashion, similarly as in Chaikin's algorithm [1]. After one step of subdivision we obtain a new sequence of points  $P_0, Q_0, P_1, Q_1, \dots, P_{n-1}, Q_{n-1} \in \mathbb{R}^2$ . Hence the refined polyline has  $2n$  points after one iteration.

## 3 Computation of newly inserted points

In this section, we describe the computation of the coordinates of the new points  $P_i, Q_i$  assigned to the segment  $V_i V_{i+1}$ . These are precomputed in the coordinate system  $\langle O_i, \mathbf{m}_i, \mathbf{n}_i \rangle$ , given by

$$\begin{aligned} \mathbf{n}_i &= V_i - V_{i+1} =: (x_{\mathbf{n}_i}, y_{\mathbf{n}_i})^\top, \\ \mathbf{m}_i &= (-y_{\mathbf{n}_i}, x_{\mathbf{n}_i})^\top, \\ O_i &= E_i - w\mathbf{m}_i, \end{aligned} \quad (2)$$

where

$$E_i = \frac{1}{2}V_i + \frac{1}{2}V_{i+1} \quad (3)$$

and  $w \in \mathbb{R}$ ,  $w \neq 0$  is a global parameter.

For clarity, coordinates of a point in the system  $\langle O_i, \mathbf{m}_i, \mathbf{n}_i \rangle$  are distinguished by a bar, e. g. for the point  $V_i$  we use the notation  $\bar{V}_i = (x_{\bar{V}_i}, y_{\bar{V}_i})$ .



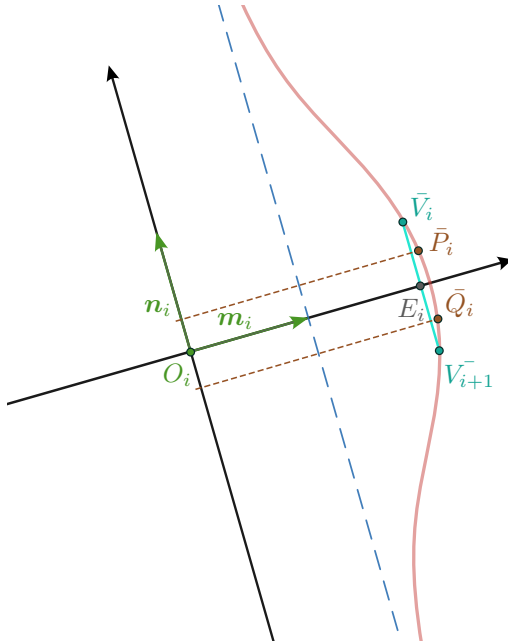


Fig. 2: Fitting of the conchoid in the coordinate system  $\langle O_i, \mathbf{m}_i, \mathbf{n}_i \rangle$ .

Now, we fit the conchoid  $\mathcal{C} : (x - 1)(x^2 + y^2) - ax^2 = 0$ , so it passes through the points  $\bar{V}_i, \bar{V}_{i+1}$ , see Fig. 2. By plugging the  $x$ -coordinate of  $\bar{V}_i$  we easily obtain the parameter  $a$  as

$$a = \frac{(x_{\bar{V}_i} - 1)(x_{\bar{V}_i}^2 + y_{\bar{V}_i}^2)}{x_{\bar{V}_i}^2}. \tag{4}$$

Then, we set the  $y$ -coordinates of the new points  $\bar{P}_i = (x_{\bar{P}_i}, y_{\bar{P}_i})^\top$  and  $\bar{Q}_i = (x_{\bar{Q}_i}, y_{\bar{Q}_i})^\top$  as

$$y_{\bar{P}_i} := \frac{y_{\bar{V}_i}}{2} \quad y_{\bar{Q}_i} := \frac{y_{\bar{V}_{i+1}}}{2}. \tag{5}$$

Subsequently, the coordinate  $x_{\bar{P}_i}$  is obtained as follows:

1. Plug the value  $y_{\bar{P}_i}$  into the equation of the conchoid  $\mathcal{C}$ .
2. Compute the roots of the resulting cubic polynomial (in variable  $x$ ) using Bézier clipping on the interval

$$[\min(1 + a, 1), \max(1 + a, 1)]. \tag{6}$$

3. Set  $x_{\bar{P}_i}$  as the root, whose value is the closest to  $x_{\bar{V}_i}$ .

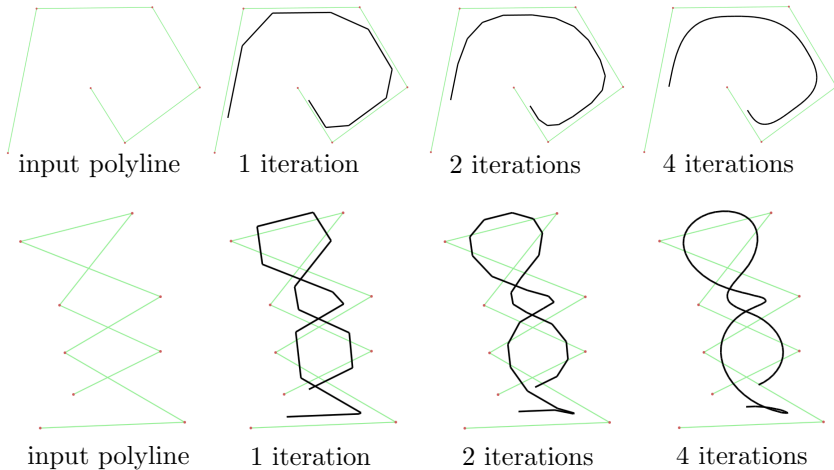


Fig. 3: Refinement with respect to increasing number of iterations. Top row depicts subdivision of the simple polyline with  $w = 1.5$ . Bottom row depicts subdivision of the polyline with self intersections with  $w = 0.75$ .

The value  $x_{\bar{Q}_i}$  is computed analogously.

After these computations, the points  $\bar{P}_i$  and  $\bar{Q}_i$  are transformed back to the original system, and these are the new points  $P_i$  and  $Q_i$ . After repeating the process for all segments  $V_i V_{i+1}$ ,  $i = 0, \dots, n - 1$  we obtain the refined polyline. The process of refinement may be repeated iteratively to reach the desired level of detail.

## 4 Results

We demonstrate performance of the proposed method on various examples and provide several observations.

In the top row of Fig. 3, we see the refinement of the simple non-intersecting polyline with the value of the global parameter  $w = 1.5$ . In general, the points of the polyline after one subdivision step do not lie on the original polyline. After several steps of subdivision we obtain visually smooth curve, which respects the shape of the input polyline. In the bottom row, we refine the polyline with several self intersections and  $w = 0.75$ . Since the proposed scheme does not interpolate the endpoints of the input polyline, some of the self-intersections disappear and new may be introduced with increasing number of subdivision steps.

In the case of the input polygon in Fig. 4 we focus on the impact of the global parameter  $w$ . The polyline after 10 subdivision step is enclosed, which is ensured by adding two more control points  $V_{n+1} = V_0$ ,  $V_{n+2} = V_1$ .

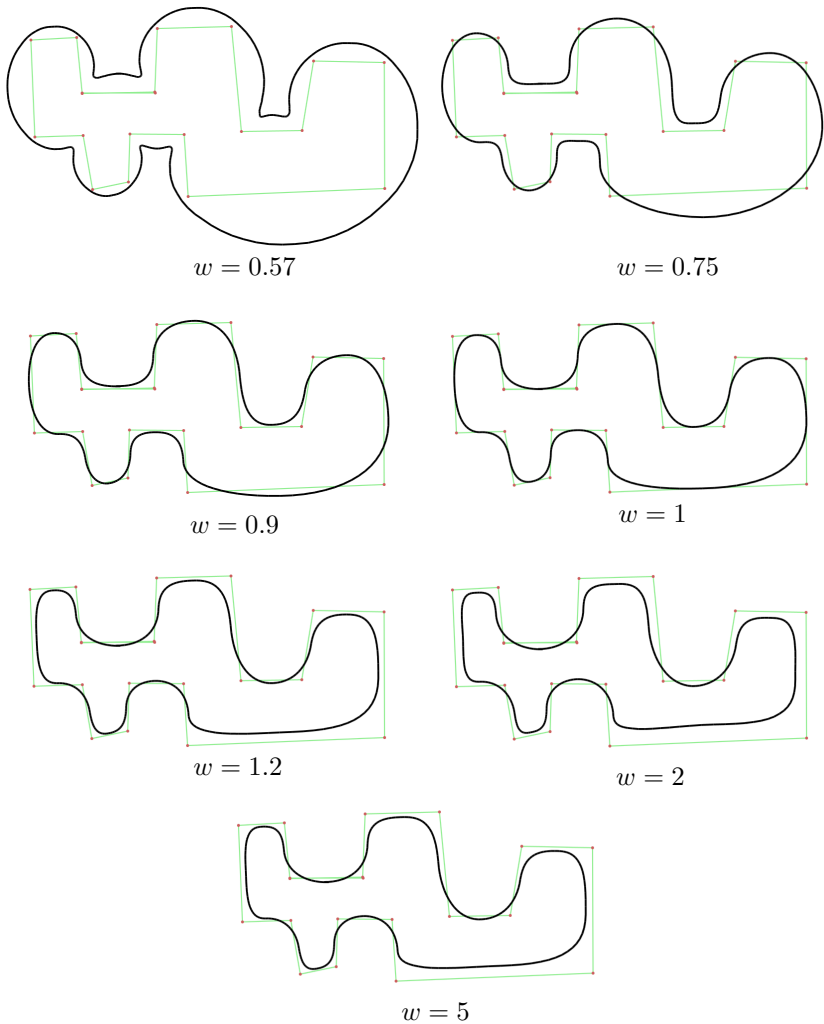


Fig. 4: Refinement of the control polygon (green) after 10 iterations with respect to different values of the global parameter  $w$ . Note, that for  $w = 1$  we obtain the same result as produced by Chaikin's algorithm.

For the value  $w = 1$  our method is identical to Chaikin's algorithm, since each fitted conchoid is a line. If  $w < 1$ , we see, that decreasing of this value causes expansion of the refined curve. For the sufficiently small value ( $w = 0.57$  in Fig. 4) the resulting curve even encapsulates the input control polygon. In the case  $w > 1$ , the increasing values cause shrinking of the curve. Note, that for  $w > 1$  the resulting curve lies in the convex hull of the control polygon.

## 5 Conclusion

In this paper, we introduced a subdivision scheme utilizing local conchoid interpolation. The proposed scheme is non-linear and approximating. Our method provides the adjustable the global parameter which affects the shape of the output curve. Moreover, our approach contains Chaikin's algorithm as a special case. In future, we plan to provide the proof of convergence and inspect on the order of continuity w. r. t. the global parameter. Also, we need to describe and prove properties of the curve, mainly the convex hull property. The rescaling of the global parameter would provide more intuitive handling of the resulting curve and find its applications in e. g. graphic design for shrinking and expanding polygons.

## References

- [1] G. M. Chaikin: *An algorithm for high-speed curve generation*, Computer graphics and image processing. Elsevier, 1974
- [2] N. Dyn, J. A. Gregory, D. Levin: *Analysis of uniform binary subdivision schemes for curve design*, Constructive Approximation. Springer, 1991
- [3] J. Wallner, N. Dyn: *Convergence and  $C1$  analysis of subdivision schemes on manifolds by proximity*, Computer Aided Geometric Design. Elsevier, 2005
- [4] N. Dyn: *Three families of nonlinear subdivision schemes*, Studies in Computational Mathematics. Elsevier, 2006
- [5] S. Schaefer, E. Vouga, R. Goldman: *Nonlinear subdivision through nonlinear averaging*, Computer Aided Geometric Design. Elsevier, 2008
- [6] P. Grohs: *A general proximity analysis of nonlinear subdivision schemes*, SIAM Journal on Mathematical Analysis. SIAM, 2010
- [7] X. Yang: *Point-normal subdivision curves and surfaces*, Computer Aided Geometric Design. Elsevier, 2023

# The Kárteszi points of a triangle, via three reflections theorem and geometric algebra

To memory of my professor and doctor father,  
Ferenc Kárteszi (1907-1989)

Emil Molnár

*Department of Algebra and Geometry, Institute of Mathematics,  
Budapest University of Technology and Economics, Hungary  
email: emolnar@math.bme.hu*

**Abstract.** Professor Ferenc Kárteszi was a charismatic personality of the Hungarian mathematics education and science (descriptive, projective and finite geometries). He made presentation trips also in Slovakia. A brief information is presented, how to start with a school task dealing with triangle configurations, which could be extended from the elementary Euclidean case to more general ones, as hyperbolic plane, "absolute plane" by János Bolyai (just 200 years ago), then Minkowski and Galilei (isotropic) plane. Comments on prof. Ferenc Kárteszi are included in connection to his presented didactical credo.

*Keywords:* configuration of triangles, Kárteszi point, three reflections theorem, geometric algebra

Let us recall a **well-known school task**: *In the (Euclidean  $E^2$ ) plane of a triangle  $ABC$  we draw regular triangles outward on sides of  $ABC$ , say  $ABC^+$ ,  $BCA^+$ ,  $CAB^+$ , respectively. Prove that the segments  $AA^+$ ,  $BB^+$ ,  $CC^+$  intersect each other in a point  $K$ , that is the isogonal point of  $ABC$  and the distance sum  $AK + BK + CK$  is minimal for  $K$  among all points of the plane.*

Professor Kárteszi noticed that instead of regular triangles we can draw isosceles ones with all equal base angles, and the above  $K$  (called *Kárteszi point*) exists also in the Bolyai–Lobachevsky hyperbolic plane  $H^2$  (in the sphere  $S^2$  as well, (see also Kálmán, 1989 and Sect. 2), the orthocentre, barycentre are specific cases. There is a **more general extremum problem** of a similar kind (Yaglom, 1968, problem **83**, with modified notation):

*In the plane ( $E^2$ ) of a given triangle  $ABC$  find a point  $K$  such that the quantity  $\alpha KA + \beta KB + \gamma KC$ , where  $\alpha, \beta, \gamma$  are given positive numbers, has the smallest possible value.*

This problem leads to a more general triangle configuration and to an analogous extremal point  $K$ . Moreover, **as a new result of this paper**, an extension onto "absolute plane" ( $S^2$ ,  $E^2$ ,  $H^2$ ,  $M^2$  Minkowski plane,  $G^2$  Galilei (or isotropic) plane) can be formulated and solved by three reflections theorem (see e.g. Molnár, 1978 and Sect. 4, Weiss, 2018), and geometric (Grassmann–Clifford type) algebra (Perwass et al., 2004 and Sect. 3). Open problems arise as well.

By this we want to follow **F. Kárteszi's didactical credo** (see also his wonderful book (Kárteszi, 1976) of great international success):

*Start with a natural, elementary, visually well understandable task! Then follow the manipulations, tools, new mathematical concepts, the technical machinery; then the solution, occasional theory, further applications, extensions, ....*

The full publication with title *On the Kárteszi point of a triangle via three reflections theorem and geometric algebra* is to appear in the monograph volume of The 9<sup>th</sup> International Scientific Colloquium Mathematics and Children, founded by Margita Pavleković, Osijek, Croatia, 19-20 May 2023.

## References

- [1] Kálmán, A. (1989, 2002). Elements of Non-Euclidean Geometries (Nemeuklideszi geometriák elemei, in Hungarian). Nemzeti Tankönyvkiadó.
- [2] Kárteszi, F. (1976). Introduction to Finite Geometries. *Disquisitiones Mathematicae Hungaricae* 7. Feltrinelli (1978. in Italian), Nauka (1980. in Russian), North-Holland (2014).
- [3] Molnár, E. (1978). Kegelschnitte auf der metrischen Ebene. *Acta Mathematica Academiae Scientiarum Hungaricae*, 31, 317-343.
- [4] Perwass, C. B. U. and Hildenbrand, D. (2004). Aspects of Geometric Algebra in Euclidean, Projective and Conformal Space. An Introductory Tutorial.
- [5] Weiss, G. (2018). The Three Reflections Theorem Revisited. *KoG* 22-2018, 41-48.
- [6] Yaglom, I. M. (1968). *Geometric Transformations II*. 21. Random House (translated from Russian by Allen Shields).

# Impact of surface continuity on 3D model

Jakub Müller, Ivana Linkeová

*Department of Technical Mathematics, Faculty of Mechanical Engineering,  
CTU in Prague*

*Karlovo náměstí 13 Praha 2 – Nové Město 121 35, Czech Republic  
email: jakub.muller@fs.cvut.cz, ivana.linkeova@fs.cvut.cz*

**Abstract.** In an engineering environment, continuity is one of the important concepts. Not only does it have a significant impact on the aesthetic aspect of products, which is an essential parameter for commercial success, but it is equally a very crucial parameter from a technological point of view. The continuity of the geometry of 3D CAD models determines how smooth the transition between two adjacent surfaces of the model is.

$C^2$  continuity, i.e. continuity up to the second derivative, has become the standard for the vast majority of CAD software today. This work focuses on increasing the degree of contiguous surfaces to  $C^3$  continuity using CAD software Rhinoceros 7 to improve the quality of the model for CNC processing.

*Keywords:* Bézier curve, CAD model, surface continuity,  $C^3$  continuity, CNC processing.

## 1 Introduction

CNC (computer numerical control) machining became one of the most reliable ways for developing highly sophisticated models and products while staying consistent in quality and quantity beside other means of production.

The process begins with the preparation of a quality model that becomes core for a CAM (computer-aided manufacturing) code for CNC processing. While CAM code is prepared, processed and a prototype is made for acquisition of data for further analysis, the prototype may appear insufficient in spaces, where different surfaces meet, as these places provide a challenge for a correct toolpath and an optimisation is needed. Usual way to fix such issues is via changing the parameters of process to reach optimal conditions for best outcome.

For complicated geometries this optimization might be insufficient and other solution is needed. One of the possibilities is to focus on the 3D model that lies on the very beginning of the process.

## 2 Impact of surface continuity on 3D model

As proved by experimental measurements [1], [2], the  $C^3$  continuity of surfaces is most suitable option for a smooth CNC toolpath on highly sophisticated surfaces of 3D models. With  $C^2$  continuity being standard for the CAD software nowadays, easily obtained from software itself,  $C^3$  continuity has to be obtained through other means. Following theory of Bézier curves [3], [4], decomposition of curve is used in reversed pace to build up control polygons between examined surfaces. Polygons are then used to define Bézier surface interconnecting aforementioned surfaces achieving  $C^3$  continuity not only on cylindrical surfaces joined along a plane curve, as is investigated in [1], [2], but also on freeform surfaces joined along a spatial curve.

### 2.1 Continuity of Bézier curve

Suppose quartic Bézier curve  $\mathbf{C}(u)$ ,  $u \in [0, 1]$  is given by control points  $\mathbf{V}_0, \mathbf{V}_1, \mathbf{V}_2, \mathbf{V}_3, \mathbf{V}_4$  with known positions and derive the rules for construction of unknown control points  $\mathbf{W}_0, \mathbf{W}_1, \mathbf{W}_2, \mathbf{W}_3, \mathbf{W}_4$  of quartic Bézier curve  $\mathbf{K}(v)$ ,  $v \in [0, 1]$  connected with  $C^K$ ,  $K = 0, 1, 2, 3$  continuity at the common point  $\mathbf{C}(1)$ . Vector equation of Bézier curve  $\mathbf{C}(u)$  and its first three derivatives is given by

$$\mathbf{C}^{(K)}(u) = \sum_{i=0}^4 N_{i,4}^{(K)}(u) \mathbf{V}_i, \quad K = 0, 1, 2, 3. \quad (1)$$

Thus, it is useful to calculate function values of Bernstein polynomials of 4-th degree and their first three derivatives at  $u = 0$  and  $u = 1$ , see tab. 2.1 where the simplified notation  $N(u)$  is used instead of  $N_{i,4}(u)$ .

With respect to the values in tab. 2.1, the continuity conditions

$$\mathbf{C}^{(i)}(1) = \mathbf{K}^{(i)}(0), \quad i = 1, \dots, K. \quad (2)$$

expressed as positions of unknown control points  $\mathbf{W}_i$ , see fig. 1.

$i$	$N(u)$	$N(0)$	$N(1)$	$N'(0)$	$N'(1)$	$N''(0)$	$N''(1)$	$N'''(0)$	$N'''(1)$
0	$(1-u)^4$	1	0	-4	0	12	0	-24	0
1	$4u(1-u)^3$	0	0	4	0	-24	0	72	-24
2	$6u^2(1-u)^2$	0	0	0	0	12	12	-72	72
3	$4u^3(1-u)$	0	0	0	-4	0	-24	24	-72
4	$u^4$	0	1	0	4	0	12	0	24

Table 1: Bernstein polynomials of 4-th degree and their derivatives for  $u = 0, 1$



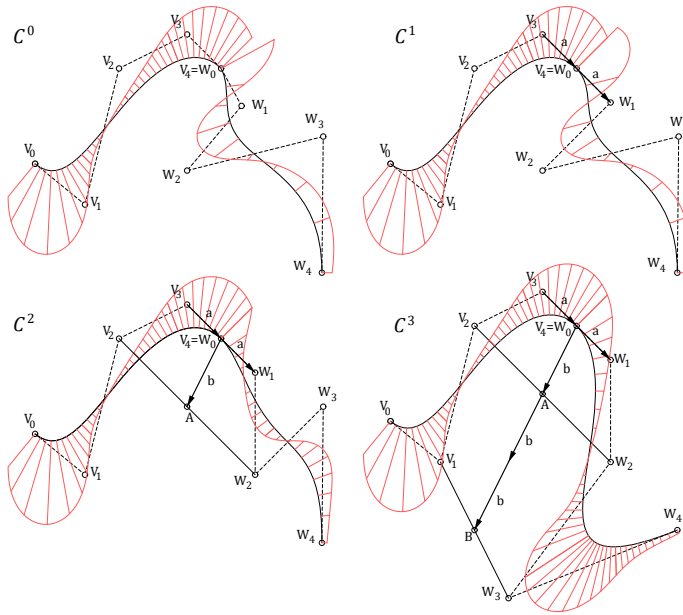


Fig. 1: Constructive conditions of  $C^0$ ,  $C^1$ ,  $C^2$  and  $C^3$  continuity of two quartic Bézier curves

- $C^0$ : Unknown position of  $\mathbf{W}_0$  is given by

$$\mathbf{W}_0 = \mathbf{V}_4, \quad (3)$$

i.e. the curves have a common endpoint. The positions of all other control points have no influence on  $C^0$  continuity.

- $C^1$ : Considering condition (3), unknown position of  $\mathbf{W}_1$  is given by

$$\mathbf{W}_1 = 2\mathbf{V}_4 - \mathbf{V}_3, \quad (4)$$

i.e. the common point of the curves lies at the centre of straight line segment with endpoints  $\mathbf{V}_3$  and  $\mathbf{W}_1$ . In other words, the vectors given by the adjacent legs of control polygons are identical, designated by  $\mathbf{a}$  in fig. 1. Positions of all other control points have no influence on  $C^1$  continuity.

Note that vector  $\mathbf{a}$  represents  $1/p$  of tangent vector at end points of Bézier curve of  $p$ -th degree.

- $C^2$ : Considering conditions (3) and (4), unknown point  $\mathbf{W}_2$  is given by

$$\mathbf{W}_2 = \mathbf{V}_2 + 4(\mathbf{V}_4 - \mathbf{V}_3). \quad (5)$$

Thus, point  $\mathbf{W}_2$  can be determined by  $\mathbf{W}_2 = \mathbf{V}_2 + 4\mathbf{a}$ . Or, designating  $\mathbf{b}$  the vector given by sum of vectors

$$\mathbf{b} = \mathbf{V}_3\mathbf{V}_2 + \mathbf{V}_3\mathbf{V}_4, \quad (6)$$

point  $\mathbf{A}$  lying at the centre of straight line segment with endpoints  $\mathbf{V}_2$  and  $\mathbf{W}_2$  is given by

$$\mathbf{A} = \mathbf{V}_4 + \mathbf{b}. \quad (7)$$

Note that vector  $\mathbf{b}$  represents  $1/(p(1-p))$  of second derivative vector at end point of Bézier curve of  $p$ -th degree.

- $C^3$ : Considering conditions (3), (4) and (5), unknown point  $\mathbf{W}_2$  is given by

$$\mathbf{W}_3 = -\mathbf{V}_1 + 6\mathbf{V}_2 + 8\mathbf{V}_4 - 12\mathbf{V}_3. \quad (8)$$

To construct point  $\mathbf{W}_3$ , modify condition (8) into the form

$$\frac{\mathbf{W}_3 + \mathbf{V}_1}{2} = \mathbf{V}_4 + 3\mathbf{b}. \quad (9)$$

The left side of (9) represents the centre  $\mathbf{B}$  of straight line segment with end points at  $\mathbf{W}_3$  and  $\mathbf{V}_1$ .

## 2.2 Study artefact

For the purpose of testing the effect of continuity on CNC processing, four identical sets of two cubic-quartic Bézier surfaces were prepared. The quartic Bézier curve were oriented into the space, where connection of surfaces was intended to be constructed.

Following the conditions for  $C^0$  and  $C^1$  continuities, interconnecting surfaces were prepared. For the  $C^2$  and  $C^3$  continuity, reversed decomposition was used. Fig. 2 shows the reversed decomposition in case of  $C^3$  continuity. Result is smooth  $C^3$  connection between initial Bézier curves done via four quartic Bézier curves as shown on fig. 3.

The process was then repeated for each of the quartic curves, until a grid of control points was achieved for connecting with Bézier surfaces. Fig. 4 shows final form of the artefact with increasing degree of continuity between surfaces from left to right. Place of connection between initial surfaces and interconnecting surfaces is shown with black curves.

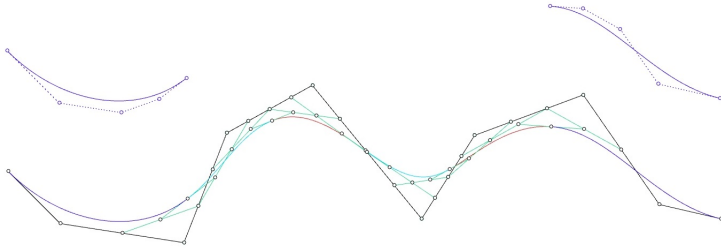


Fig. 2: Construction of  $C^3$  continuity between Bézier curves

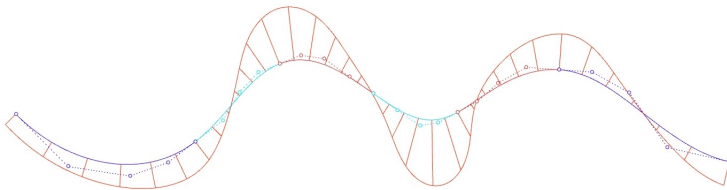


Fig. 3: Graph of curvature on the constructed chain of curves

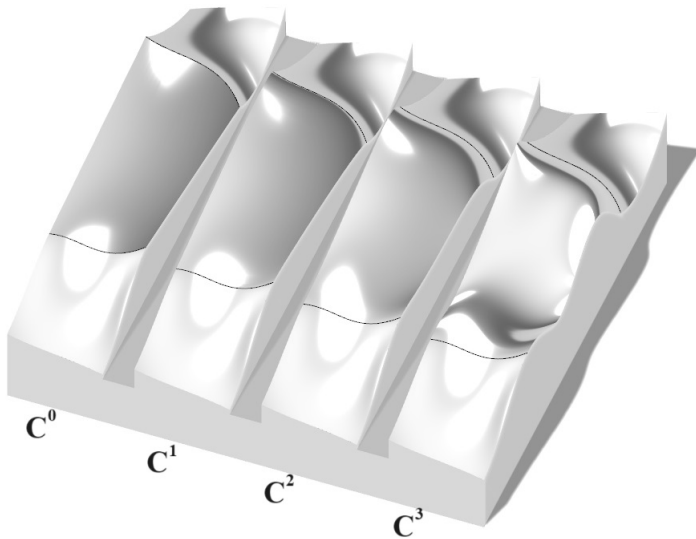


Fig. 4: Final model of the artefact

### 3 Conclusion

Using the knowledge of Bézier curves, an artefact was designed and constructed for further studies of impact of surface continuity on CNC machining. Ranging from  $C^0$  to  $C^3$  continuities, the artefact will be used to examine machined surfaces mainly aiming on quality and efectivity of CNC machining process.

### Acknowledgements

This work was supported by the Student Grant Competition of the Czech Technical University in Prague, grant Applications of mathematical-geometric modelling in mechanical engineering SGS21/148/OHK2/3T/12.

### References

- [1] D. Kučera: *Influence of CAD model geometry on quality and efficiency of machining on CNC machine tools*, Master Thesis. CTU FME. Department of Technical Mathematics.
- [2] D. Kučera, I. Linkeová, M. Stejskal: *The influence of CAD model continuity on accuracy and productivity of CNC machining*, Int J Adv Manuf Technol 124, 1115–1128 (2023). <https://doi.org/10.1007/s00170-022-10422-w>
- [3] I. Linkeová: *Základy počítačového modelování křivek a ploch*, 3rd ed., CTU FME, Prague, 2008.
- [4] G. Farin: *Curves and Surfaces for Computer Aided Geometric Design*, 3rd ed., Academic Press, Boston, 1992.

# Variations on Frégier's Theorem

Boris Odehnal

*University of Applied Arts Vienna  
Oskar-Kokoschka-Platz 2  
email: boris.odehnal@uni-ak.ac.at*

**Abstract.** We show that Frégier's theorem allows for some generalizations within the framework of projective geometry. This also contains the notion of non-Euclidean versions of Frégier's theorem and Frégier conics. Two different generalizations of Frégier's theorem shall be considered: (1) The involution of right angles is replaced with an arbitrary involution induced by some polarity. (2) The envelopes of chords of a conic whose endpoints are assigned in a projective mapping (not involutive) are conics.

*Keywords:* Frégier's theorem, Frégier conic, involution, polarity, projective mapping, pencil of conics.

## 1 Introduction

Let  $c$  be a conic and assume that  $P$  is a point on  $c$ . Then, let  $(g, g')$  be a pair of lines through  $P$  such that  $g$  and  $g'$  are orthogonal (in the Euclidean sense). Further, let  $Q = c \cap g \setminus \{P\}$  and  $Q' = c \cap g' \setminus \{P\}$ . Now, Frégier's theorem states (cf. [1, 2]):

*The chords  $[Q, Q']$  pass through a single point  $F$  (the Frégier point of  $P$  with respect to<sup>1</sup>  $c$ ) independent of the choice of  $g$ .*

Generalizations to non-Euclidean Frégier conics have been studied in [4]. Quadratic transformations based on Frégier's constructions are defined and investigated in [5, 6] along with higher dimensional analogues. The fact that the ordinary Euclidean Frégier conics are the only conic shaped generalized offsets to conics is shown in [3]. Especially in the latter article, the right angle which is a substantial ingredient for Frégier's theorem was replaced with an arbitrary fixed angle  $\phi$ . It turned out that the thus defined chords  $[Q, Q']$  envelop conics (the generalized Frégier conics)  $c_\phi$  assigned to the point  $P$  and w.r.t.  $c$ . If the angle  $\phi$  traces the open interval  $]0, \frac{\pi}{2}[$ , then the generalized Frégier conics  $c_\phi$  trace a pencil of conics of the third kind (to which  $c$  also belongs, see [3]) and the ordinary Frégier point is the only real point of a singular conic in the Frégier pencil.

In the following, we generalize Frégier's theorem by replacing fixed angles at first by an involutive mapping induced by some polarity in Sec. 2. There are six different types of such Frégier constructions depending on whether the polarity is elliptic or hyperbolic, and then, since a hyperbolic polarity is always that of a conic  $d$ , we have to distinguish between the five different types of pencils spanned by  $c$  and  $d$ . For special assumptions on the polarity, this yields the non-Euclidean notion (cf. [4]) of Frégier conics

<sup>1</sup>We shall write w.r.t. short hand for *with respect to*.

as by-catch. This immediately raises the question: What happens if we look at the chords of a conic  $c$  whose endpoints are assigned in an arbitrary projective mapping acting on  $c$ ? This will be described in Sec. 3.

## 2 Polarities instead of the right angle

The right angles appearing in Frégier’s construction as well as the constant angles in the Frégier variant described in [3] induce special projective mappings on the underlying regular conic  $c$  with the polarity  $\gamma$ . Now, we may assume that in the pencil around the pivot point  $P \in c$  an arbitrary involution is acting. The involution shall be induced by an arbitrary polarity  $\delta$  which assigns to each line  $g \ni P$  a unique line  $g' \ni P$  by

$$g' = [\delta^*(g), P],$$

where  $\delta^*$  is the adjoint mapping of the polarity  $\delta$ . The lines  $g$  and  $g'$  intersect  $c$  in  $P$  and each in a further point  $Q \in g$  and  $Q' \in g'$ . Now, we can state and prove:

**Theorem 2.1.** *Let  $c$  be a regular conic, let  $P$  be a point on  $c$ , and let further  $\delta$  be a regular polarity (different from that w.r.t.  $c$ ). Now, consider the projective and involutive mapping  $\alpha$  in the pencil of lines around  $P$  that sends each line  $g$  to the line  $g' = [P, \delta^*(g)]$ . If now  $Q$  and  $Q'$  are defined as above, then the chords  $[Q, Q']$  pass through a single point  $F$  (the generalized Frégier point of  $P$  w.r.t.  $c$ ).*

*Proof.* The generalized Frégier point  $F$  is simply the center of the involution  $\alpha$  lifted to the conic  $c$  (see [2]). □

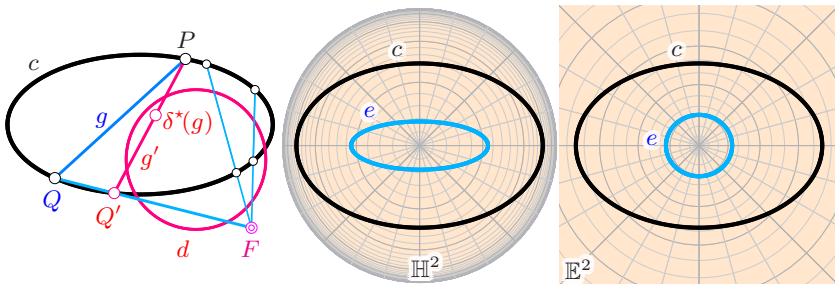


Fig. 1: Left: A Frégier point  $F$  defined by means of a generic involution induced by a polarity w.r.t. a conic  $d$ . Center and right: Frégier conics  $e$  of a conic  $c$  in a hyperbolic and an elliptic plane.

The polarity  $\delta$  may either be that of a conic  $d$  with real points (hyperbolic polarity) or that of an empty conic (elliptic polarity). The case of the

elliptic polarity causes no special cases since there no real self-conjugate points w.r.t.  $\delta$ . In the case of the polarity w.r.t. a real conic  $d$ , we have to distinguish between five cases, according to the type of pencil spanned by  $c$  and  $d$ . We are able to show:

**Theorem 2.2.** *The construction of the generalized Frégier conic from Thm. 2.1 does not depend on the type of pencil spanned by  $c$  and  $d$ .*

*Proof.* We just lay down what is necessary in order to give a synthetic proof. First, it means no restriction to assume that  $c$  is given by  $x_0x_2 - x_1^2 = 0$ . The polarity  $\delta$  shall be that of a conic  $d$  that spans a pencil of 1., ..., 5. kind with  $c$ . Therefore, we can assume that the equations of the conics  $d$  in the pencil of type are given by  $d = c + \lambda s_i$  (we identify the conic with its equation), where  $s_i$  is the equation of a singular conic in the pencil of the  $i$ -th kind and can be chosen as:  $s_1 : x_1(px_0 - (1+p)x_1 + x_2)$ ,  $s_2 : x_2(x_2 - x_0)$ ,  $s_3 : x_1^2 = 0$ ,  $s_4 : x_2(x_1 - x_2) = 0$ , and  $s_5 : x_2^2 = 0$ . In any case, the pivot point  $P$  can be given by  $1 : t : t^2$  (with  $t \neq 0, 1, \infty$ ). In  $s_1$ ,  $p \neq 0, 1, \infty$  guarantees that  $c$  and  $s_1$  really span a pencil of the 1. kind. Further,  $Q = 1 : u : u^2$  (with  $u \neq p, t, 0, 1, \infty$ ). For a special but proper choice of  $\mu$ , we obtain a regular conic  $d$  in the pencil, and thus, a polarity  $\delta$ . Then,  $g = [P, Q]$  and we are able to compute the pole  $\delta^*(g)$  of  $g$  w.r.t. all conics in the pencil (variable  $\lambda \neq 0$ ). Finally,  $g' = [P, \delta^*(g)]$  and  $Q' = g' \cap c \setminus \{P\}$ . Then, we can show that  $[Q, Q']$  passes through a point  $F$  (independent of  $Q$ , *i.e.*, the parameter  $u$ ). For variable pivot point  $P$  (*i.e.*, variable  $t$ ), the points  $F$  trace a conic, the generalized Frégier conic  $e$  of  $c$  w.r.t.  $\delta$ . It can be shown that  $e$  passes through the base points of the pencil only if they are at least of multiplicity two by intersecting  $e$  and  $c$ .  $\square$

Fig. 2 shows a generalized Frégier conic  $e$  (red) of a conic  $c$  (blue) w.r.t. to the polarity  $\delta$  of a regular conic  $d$  (magenta) which, together with  $c$ , spans a pencil of the first, second, third, fourth, or fifth kind.

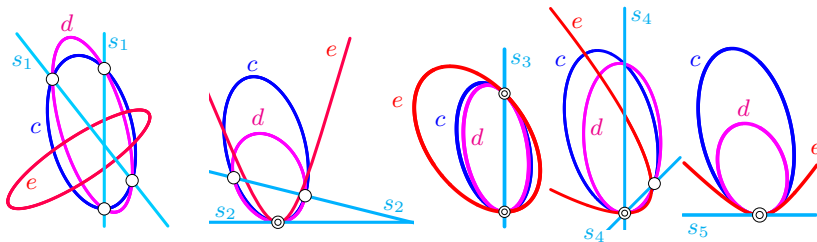


Fig. 2: The generalized Frégier conics  $e$  according to Thm. 2.1 pass through base points of the pencil  $\lambda c + \mu d$  only if these are at least two-fold.

### 2.1 Non-Euclidean versions

We assume that the polarity w.r.t. to  $c$  and the polarity  $\delta$  have a common polar triangle, *i.e.*, the corresponding bilinear forms can be diagonalized simultaneously. Thus, we can assume that  $c$  is given by  $x_1^2/a^2 + x_2^2/b^2 = x_0^2$  (with  $a, b \neq 0$  and  $a \neq b$ ). The case  $b^2 < 0$  needs a separate discussion. In the hyperbolic case,  $\delta$ 's self-conjugate points can be given by  $\omega : x_1^2 + x_2^2 = x_0^2$ . The conic  $\omega$  can be viewed as the absolute conic of hyperbolic geometry. Therefore, for any point  $P = 1 + t^2 : a(1 - t^2) : 2bt$  (with  $t \in \mathbb{R} \cup \{\infty\}$ ), the Frégier point

$$F_h = (a^2b^2 - a^2 - b^2)(1+t^2) : a(a^2b^2 + a^2 - b^2)(t^2 - 1) : -2bt(a^2b^2 - a^2 + b^2)$$

in the sense of hyperbolic geometry traces the *hyperbolic Frégier conic*

$$x_0^2 = \frac{(a^2b^2 - a^2 - b^2)^2}{a^2(a^2b^2 + a^2 - b^2)^2}x_1^2 + \frac{(a^2b^2 - a^2 - b^2)^2}{b^2(a^2b^2 - a^2 + b^2)^2}x_2^2.$$

The hyperbolic Frégier conic is regular if, and only if,  $(a^2b^2 - a^2 + b^2)(a^2b^2 + a^2 - b^2)(a^2b^2 - a^2 - b^2) \neq 0$ . This leads to a three-branched variety of singular hyperbolic Frégier conics which are studied in detail in [4].

The conic  $\omega : x_0^2 + x_1^2 + x_2^2 = 0$  is empty (over the real numbers) and can serve as the absolute conic of elliptic geometry. Then, the point  $P = 1 + t^2 : a(1 - t^2) : 2bt$  on the conic  $c : x_1^2/a^2 + x_2^2/b^2 = x_0^2$  defines the *elliptic Frégier point*

$$F_e = (a^2b^2 + a^2 + b^2)(1+t^2) : a(a^2b^2 - a^2 + b^2)(t^2 - 1) : -2bt(a^2b^2 + a^2 - b^2)$$

which traces the *elliptic Frégier conic*

$$x_0^2 = \frac{(a^2b^2 + a^2 + b^2)^2}{a^2(a^2b^2 - a^2 + b^2)^2}x_1^2 + \frac{(a^2b^2 + a^2 + b^2)^2}{b^2(a^2b^2 + a^2 - b^2)^2}x_2^2.$$

The elliptic Frégier conic is regular if, and only if,  $(a^2b^2 - a^2 + b^2)(a^2b^2 + a^2 - b^2) \neq 0$ . (The factor  $a^2b^2 + a^2 + b^2$  cannot vanish under the above made assumptions.) However, in elliptic geometry, the singular Frégier conics of a given conic can only be arranged in two groups (for details see [4]). Fig. 1 shows the generalized Frégier conic (in the sense of Thm. 2.1) for a hyperbolic (center) and an elliptic polarity (right). The curves  $e$  can be viewed as the Frégier conics of the conic  $c$  in the hyperbolic and elliptic plane.

### 2.2 Euclidean and pseudo-Euclidean Frégier conics

A singular polarity, *i.e.*, an involutive mapping on a straight line  $l$  can also be the basis of the Frégier construction. If  $l$  is chosen as the line at infinity, then the involutive mapping  $\alpha : l \rightarrow l$  can either be hyperbolic



or elliptic. In the first case, we can consider this Frégier construction as the *pseudo-Euclidean* version, while in the second case,  $\alpha$  acting on  $l$  can serve as the absolute polarity of Euclidean geometry which leads to the well-known *Euclidean* version.

### 3 Arbitrary (non-involutive) projective mappings

In what follows, we shall replace the involutive projective mapping  $\alpha$  acting on  $c$  with an arbitrary projective mapping  $\beta : c \rightarrow c$ . Such a mapping is uniquely defined by prescribing three pairs of assigned points, *i.e.*, three by two points  $A, A', B, B', C, C' \in c$  with  $A' = \alpha(A)$ ,  $B' = \alpha(B)$ , and  $C' = \alpha(C)$ . We can show the following result:

**Theorem 3.1.** *The chords  $[X, \alpha(X)]$  of  $c$  joining each point with its projective image envelop a conic  $f$  which spans with  $c$  a pencil of conics of the third kind if  $\alpha$  is elliptic or hyperbolic. In the case of a parabolic projectivity  $\alpha$ , the conics  $c$  and  $f$  span a pencil of the fifth kind, *i.e.*, they hyperosculate each other.*

*Proof.* It means no loss of generality to assume that  $c$  is given by the homogeneous equation  $x_0x_2 - x_1^2 = 0$ . Further, we can assume that  $A = 1 : 0 : 0$ ,  $B = 1 : 1 : 1$ ,  $C = 0 : 0 : 1$  and  $A' = 1 : u : u^2$ ,  $B' = 1 : v : v^2$ ,  $C' = 1 : w : w^2$  (with  $u, v, w \neq 0, 1, \infty$ ,  $u \neq v \neq w \neq u$ ). Then, the axis  $a$  of the projectivity  $\alpha$  (which contains the points  $[A, B'] \cap [A', B]$ ,  $[A, C'] \cap [A', C]$ ,  $[B, C'] \cap [B', C]$ ) has the homogeneous coordinates  $a = u\bar{u} : w\bar{w} - \bar{u} : -\bar{w}$ , where  $\bar{u} = v - w$ ,  $\bar{v} = w - u$ ,  $\bar{w} = u - v$ . Hence, a point  $X = 1 : t : t^2$  (with  $t \neq u, v, w, 0, 1, \infty$ ) is mapped to

$$X' = (t\bar{w} + \bar{u})^2 : (t\bar{w} + \bar{u})(tw\bar{w} + u\bar{u}) : (tw\bar{w} + u\bar{u})^2.$$

The chords  $s = [X, X']$  with homogeneous coordinates

$$s = t(tw\bar{w} + u\bar{u}) : -t^2\bar{w} - t(w\bar{w} + \bar{u}) - u\bar{u} : t\bar{w} + \bar{u}$$

envelop the conic

$$e : \mathbf{x}^T \begin{pmatrix} u^2\bar{u}^2 & u\bar{u}(w\bar{w} - \bar{u}) & -\bar{u}\bar{w}(\bar{v} + w) \\ u\bar{u}(w\bar{w} - \bar{u}) & \bar{w}^2((u + \bar{w})^2 + 4u - 4\bar{w} + 4) & -\bar{w}(w\bar{w} - \bar{u}) \\ -\bar{u}\bar{w}(\bar{v} + w) & -\bar{w}(w\bar{w} - \bar{u}) & \bar{w}^2 \end{pmatrix} \mathbf{x} = 0,$$

The conics  $c$  and  $e$  span a pencil of the third kind with the repeated line  $a$  as a singular conic in the pencil. The common points of  $a$  and  $c$  are the fixed points of  $\alpha$ . The projectivity  $\alpha$  is parabolic if, and only if,  $a$  is tangent to  $c$ , and then,  $c$  and  $e$  hyperosculate each other, *i.e.*, they span a pencil of the fifth kind. □

Figure 3 shows the three possible cases: an elliptic projectivity (left), a hyperbolic projectivity (in the middle), and a parabolic projectivity where  $p_\alpha$  touches  $c$  and  $e$  (which are hyperosculating at the common point).

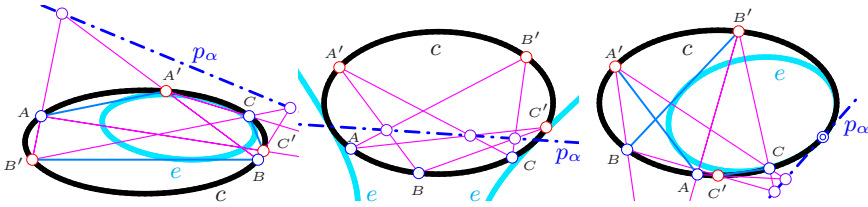


Fig. 3: The chords of  $c$  envelop a conic  $e$  provided that the endpoints are assigned in a projective mapping  $\alpha$ . If  $\alpha$  is elliptic or hyperbolic, the pencil spanned by  $c$  and  $e$  is of the third kind. A pencil of the fifth kind is obtained if  $\alpha$  is parabolic.

## 4 Conclusion

We have shown two variations of Frégier's theorem. Both can be formulated in terms of projective geometry. The mathematical approach towards these generalizations are formulated in terms of polynomial equations and rational parametrizations. At no instant, extensions or assumptions on characteristic of underlying fields are necessary which makes the computations possible within the framework of finite fields. Hence, these results are universal in the sense of [7].

## References

- [1] M. FRÉGIER: *Théorèmes nouveaux sur les lignes et surfaces du second ordre*. Annales de Mathématiques pures et appliquées, tome 6 (1815-1816), 229–241.
- [2] G. GLAESER, H. STACHEL, B. ODEHNAL: *The Universe of Conics*. From the ancient Greeks to 21<sup>st</sup> century developments. Springer-Spektrum, Springer-Verlag, Heidelberg, 2016.
- [3] B. ODEHNAL: *Pencils of Frégier conics*. KoG **26/26** (2022), 33–43.
- [4] H.-P. SCHRÖCKER: *Singular Frégier Conics in Non-Euclidean Geometry*. J. Geom. Graphics, **21/2** (2017), 201–208.
- [5] G. WEISS: *Frégier points revisited*. In: *Proceedings of the Czech-Slovak Conference on Geometry and Graphics 2018*, 277–286.
- [6] G. WEISS, P. PECH: *A quadratic mapping related to Frégier's theorem and some generalisations*. J. Geom. Graphics **25/1** (2021), 127–137.
- [7] N.J. WILDBERGER: *Divine Proportions: Rational Trigonometry to Universal Geometry*. Wild Egg, Sydney, 2005.

# Printing as a supporting tool teaching mathematics through discovery

Bronislaw Pabich

*XX Liceum Ogólnokształcące w Krakowie  
Wyższa Szkoła Nauk Oświatowych Warszawa, Polska  
email: bronek.pabich@gmail.com*

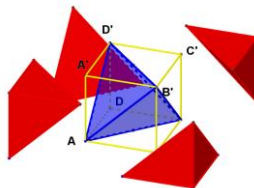
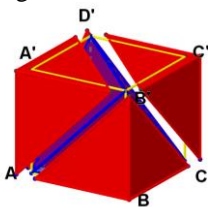
**Abstract.** Nowadays, many of us know what 3D printing, its design and other technical details are all about. However, **it is worth considering how 3D printing can help teach geometry**, especially spatial geometry, and even make it easier for students to discover algebraic patterns of abbreviated multiplication.

In my presentation, I will show some of models, the purpose of which is to better assimilate concepts such as the duality of polyhedrons, stellations, quick determination of the volume of selected solids, the search for geometric relationships between them and the development of students' spatial imagination by preparing numerous puzzles and 3D puzzles.

Key words: *Printing 3D, software SketchUp, GeoGebra, teaching math,*

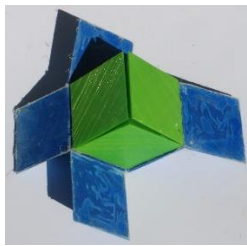
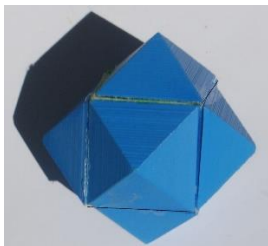
## 3D models allow you to:

1. Discover the formula for the volume of a 3D solid – for example the volume of a regular tetrahedron. - just put the tetrahedron in the cube.

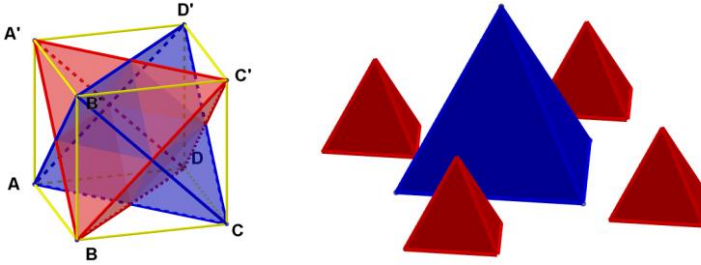


$$V_{tetrahedron} = a^3 - 4 \cdot \frac{1}{3} \cdot \frac{1}{2} \cdot a^2 \cdot a = a^3 - \frac{2}{2} \cdot a^3 = \frac{1}{3} \cdot a^3$$

2. Visualize dynamically that the rhombicuboctahedron has a volume twice as large as the cube from which it was created

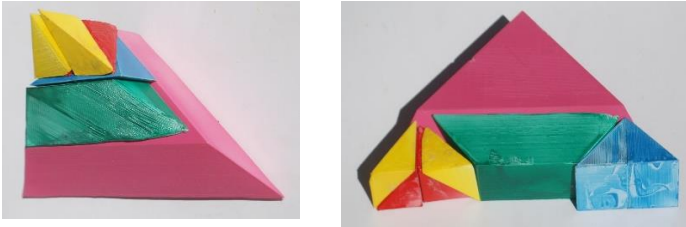


3. Discover a new problem - the volume of the Stella Octangula is equal to  $\frac{1}{2}$  the volume of the cube in which we placed it, so we should construct a second stela from the remaining elements. Can we do this? This is known as Hilbert's Third Problem. Perhaps after such an experience, Hilbert posed his Third Problem at the 1900 Conference.



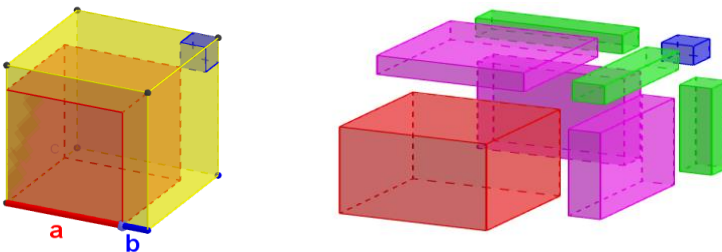
$$V_{stella} = V_{blue\ tetra} + 4 \cdot V_{red\ tetra} = \frac{1}{3} \cdot a^3 + 4 \cdot \frac{1}{8} \cdot \frac{1}{3} a^3 = \frac{1}{3} a^3 + \frac{1}{6} a^3 = \frac{1}{2} a^3$$

4. Dynamic visualization of what is difficult to show on a sheet of paper - Hill's tetrahedron - this is one of the few pyramids that can be cut so as to obtain a prism with the same volume.



Not every pyramid can be cut into elements that can be used to assemble a prism. Hill discovered six such pyramids. Here is a printout of one of them and a prism created from it

5. Discovering elements of algebra - abbreviated multiplication formula: sum cube. Transforming one polyhedron into another - a truncated octahedron can be cut so as to create a cube of the same volume in two ways.

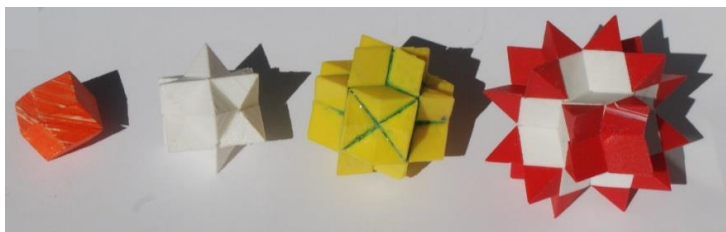


$$(a + b)^3 = a^3 + b^3 + 3a^2b + 3b^2a$$

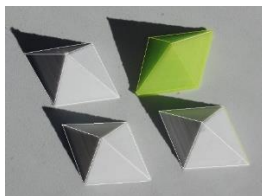
6. Show that rhombic dodecahedrons can fill 3D space



7. Show three Dormann stellations of a rhombic dodecahedron and see that they are all made of the same pentahedrons.

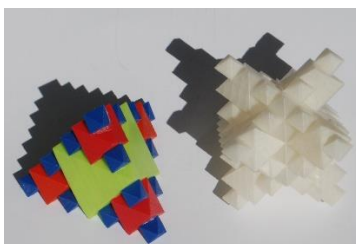


Rhombic dodecahedron and its first, second and third stellation,



From these pentahedrons you can build a rhombic dodecahedron and any of its stellations.

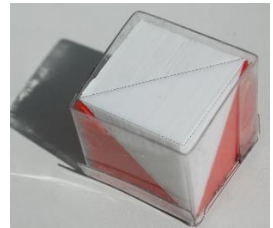
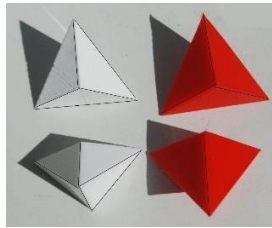
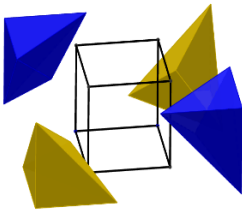
8. Illustrate spatial fractals, for example built on a regular octahedron.



9. Visualize how the Klein bottle is composed of two Mobius strips.

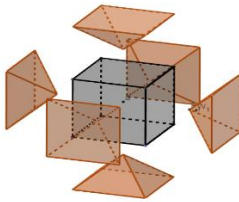


10. Developing spatial imagination by solving appropriate puzzles – for example dividing a cube into 4 congruent polyhedra

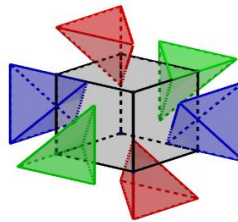


11. Dividing a cube into 6 congruent polyhedra (two ways).

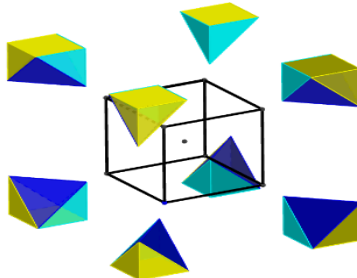
First way:



Second way:



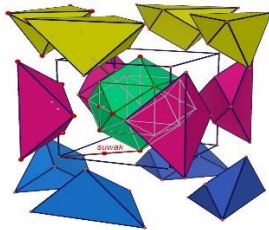
12. Dividing a cube into 4 congruent polyhedral



13. Dividing a cube into 12 congruent polyhedral



14. Dividing a cube into 16 congruent polyhedral (idea of autor – 1995)



The rhombic dodecahedron also consists of these pentahedrons

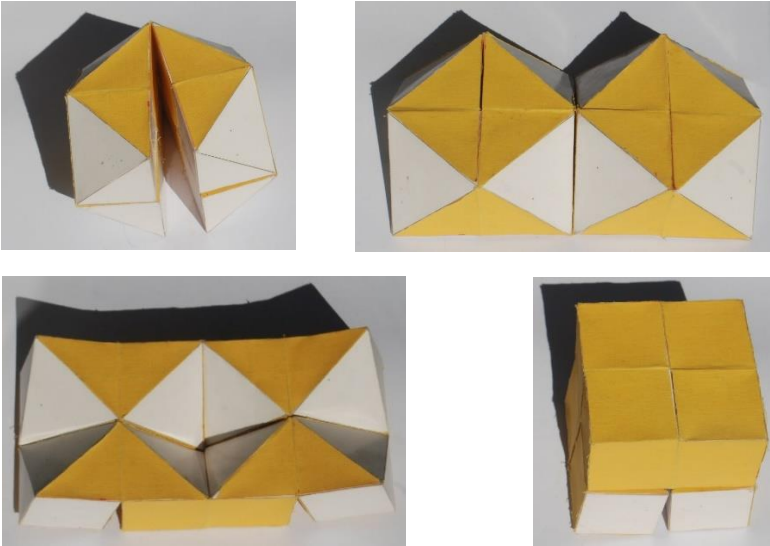
15. Dividing a cube into 24 congruent polyhedra (idea of Tadeusz Dorociński - polish architect in Deutschland).



16. Decomposition of the stella octangula into four congruent parts



17. Transformation of a cube into a cubeoctahedron and an octahedron in 4 steps (idea of Bronek Pabich)



18. Find a solid so that it can be moved through the holes: circle, triangle and square.



## References

- [1] <http://www.math-comp-educ.pl>



# The family of uniform polyhedra

**Bronislaw Pabich**

*XX Liceum Ogólnokształcące Kraków  
Wyższa Szkoła Nauk Pedagogicznych Warszawa, Polska  
email: bronek.pabich@gmail.com*

**Abstract.** Few mathematicians in geometry deal with uniform polyhedra. Many of my friends, serious mathematicians find these polyhedrons difficult to create and do not see their use in other fields of knowledge. Hence, little interest in this issue. However, these polyhedrons are so captivating and beautiful, they require so much hard thought on how to create cardboard models or 3D prints of them.

They were mostly created in the 20th century. They are somewhat analogous to what Archimedean polyhedra are to Platonic polyhedra, with the difference that we now allow faces to be non-convex polygons. There are 54 of them in total, but the last ones were discovered in the 1970s and are very difficult.

In my presentation, on the example of one of the uniform polyhedra, I will show the principle of their construction and I will show the ones whose models I made with my students.

*Keywords:* Printing 3D, software SketchUp, GeoGebra, uniform polyhedra.

## 1 Introduction

Uniform Polyhedra is a family of semi-regular polyhedra whose corners are congruent and whose faces are regular convex or concave polygons.

The UP include 5 Platonic solids, 13 Archimedean solids, two families of regular prisms and regular antiprisms and 54 non-convex polyhedra

## 2 Main part of paper

Historically, the first uniform polyhedron was created by Johannes Kepler in the 17th century. Kepler called it the eared or spiky polyhedron (Fig. 1).

In the 19th century, Badoureau discovered 37 non-convex homogeneous polyhedra. In the 20th century, polyhedrons of this kind were studied by H.S.M. Coxeter, J.C.P. Miller, H.C. Higgins, J. Lesavre, R. Mercier, and J. Skiling.

Each of them discovered dozens of them.

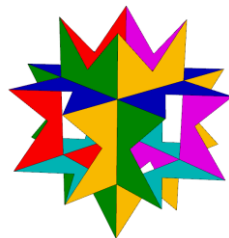


Fig. 1

Coxeter in 1954 found that there are 75 polyhedra in which only 2 faces can share one edge, which was proved by the Russian mathematician S. P. Sopov in 1970.

John Skilling in 1975 confirmed this proof using computer algorithms. My students have been making Uniform Polyhedra models from cardboard in the math circle (Fig. 2). This was a difficult task, because it was necessary to find meshes of segments of such a polyhedron. In the era of computers and printers, it is worth designing UNIFORM POLYHEDRA on such printers. There are even more problems with this.



Fig. 2

In the last two years, my students have started printing uniform polyhedra. The hardest part was designing them in SketchUp. They had to demonstrate good spatial imagination and knowledge of spatial geometry. They managed to print a set of polyhedra with tetrahedral and cubic octahedral symmetry (Fig. 3).

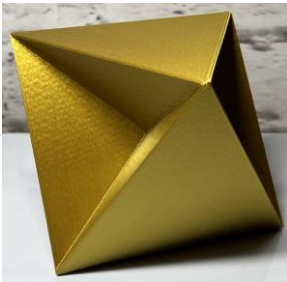


Fig. 3:  
Tetrahemihexahedron

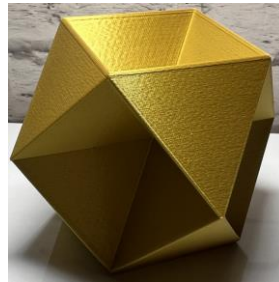


Fig. 4 :  
Octahemioctahedron

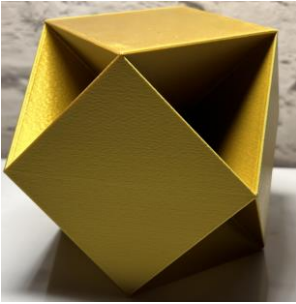


Fig. 5:  
Cubohemioctahedron

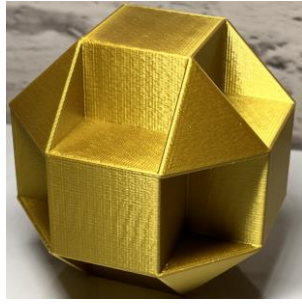


Fig. 6:  
Cubocuboctahedron

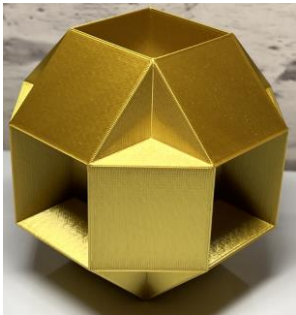


Fig. 7:  
Small rhombihexahedron

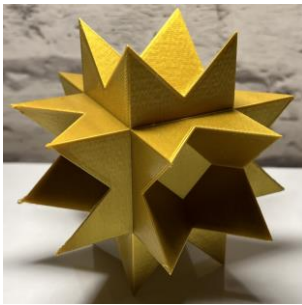


Fig. 8:  
Stellated truncated hexahedron



Fig. 9:  
Great rhombi hexahedron



Fig. 10:  
Great cubicub octahedron



Fig. 11:  
Rhombi cuboctahedron



Fig. 12:  
Cubocta truncated cuboctahedron

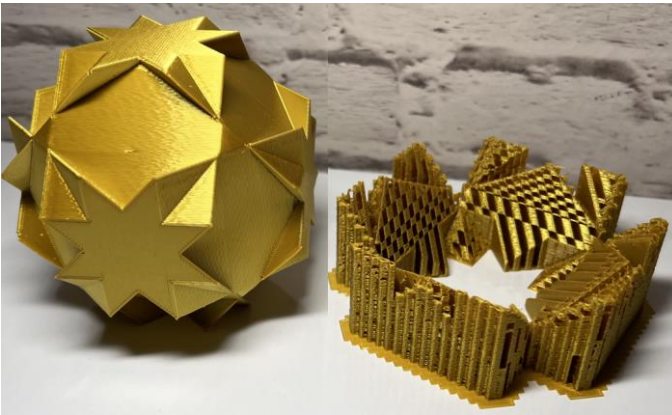


Fig. 13:  
Great truncated cuboctahedron

They also printed several polyhedra of dodecahedral symmetry (Fig. 14).



Fig. 14

### 3 How to create uniform polyhedral

The drawings below illustrate the steps to create *Rhombi cubocthedron*, an example of Uniform Polyhedra

We rotate the upper square face by  $45^\circ$  and from the intersection of sides with sides of this upper face we will get the vertices regular octagon.

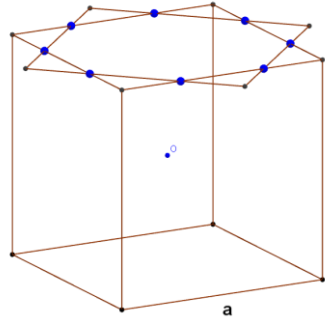


Fig. 15

We connect the obtained points with segments to create lattice on the top face of the cube.

We mark its intersection points of these segments.

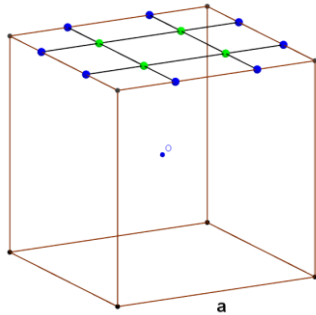


Fig. 16

We draw grid points on the remaining ones walls.

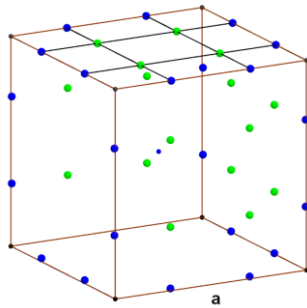


Fig. 17

Let's create an equilateral triangle and two squares with sides of length  $a$ .

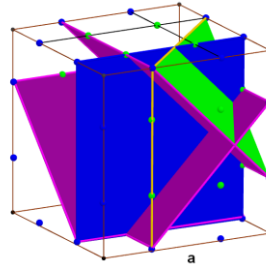


Fig. 18

We create copies of the triangular wall for all possible ways.

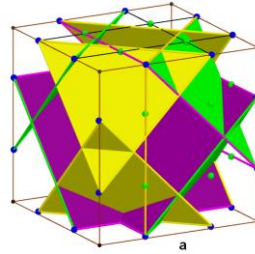


Fig. 19

Similarly to the triangle, we now create 6 copies of a vertical square (blue).  
**Rhombi cuboctahedron** is ready.

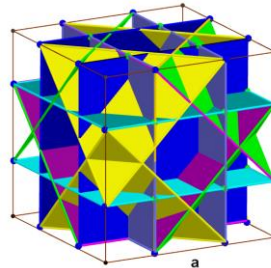


Fig. 20

## 4 Conclusion

The introduction of 3D printers to Polish schools has resulted in significant progress in the use of computer technologies. However, printers are not always used for teaching purposes. This lecture shows how to properly direct the use of 3D printers for teaching purposes in mathematics, especially geometry.

## References

- [1] Cundy Rolett „Mathematics Models”
- [2] Wenninger “Models of Polyhedra”
- [3] B Pabich “Stereometry 3D with Cabri 3D”
- [4] <http://www.math-comp-educ.pl>

# Priamkové plochy – tlačené 3D modely vytvorené v prostredí Rhinoceros

## Ruled surfaces – printed 3D models created in Rhinoceros environment

Tatiana Rückschlossová

*Department of mathematics and descriptive geometry, Faculty of Civil Engineering,  
Slovak University of Technology in Bratislava  
Radlinského 11, 810 05 Bratislava, Slovak Republic  
email: tatiana.ruckschlossova@stuba.sk*

**Abstract.** Ruled surfaces are often used in construction and architecture for their mathematical simplicity and adaptability. They are efficient in terms of usable material and construction. They provide the opportunity to create unique architectural elements that are aesthetic and modern. Students of architecture are familiar not only with this group of surfaces within the course Descriptive geometry II. We suitably supplemented the teaching process with groups of printed 3D models. We represented the modeling of lines lying on these surfaces using the "pipe" tool in the Rhinoceros environment in combination with the graphical editor Grasshopper.

*Keywords:* ruled surface, Rhinoceros, Grasshopper, 3D printed model

*Kľúčové slová:* priamková plocha, Rhinoceros, Grasshopper, 3D tlačený model

### 1 Využitie priamkových plôch v architektúre

Priamkové plochy sú v stavebníctve a architektúre často využívané pre ich širokú variabilitu. Sú efektívne z hľadiska materiálu a pevnosti, či stability konštrukcie. Je možné ich jednoducho priemyselne vyrábať postupmi ako liatie alebo presné frézovanie. Ľahko sa s nimi pracuje pri návrhoch a modelovaní. Poskytujú možnosť vytvárať jedinečné architektonické prvky, ktoré sú čisté, estetické a moderné. Jedným zo svetových architektov, ktorý sa nimi inšpiroval pri viacerých svojich návrhoch je napr. Santiago Calatrava (Obr.1, [5]).

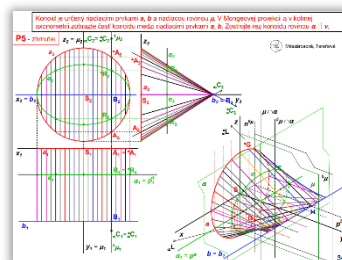
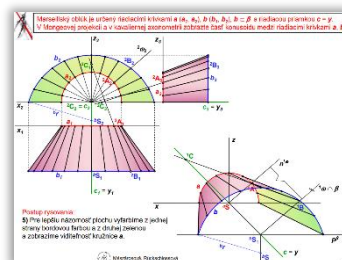
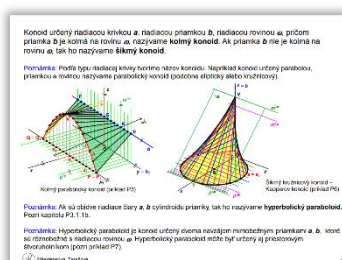
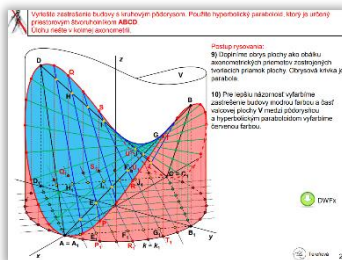
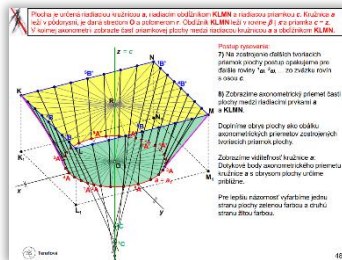
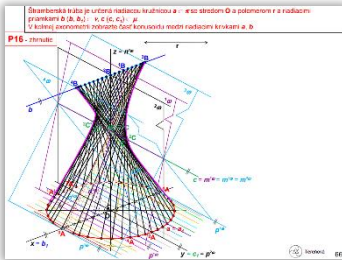


Obr. 1: vľavo - Žel. stanica Reggio Emilia AV, Mediopadana, Taliansko, vpravo - Vinárstvo Bodegas Ysios, Laguardia, Španielsko



## 2 Priamkové plochy – výučbové a študijné materiály

V rámci predmetu Deskriptívna geometria sa študenti na FAD a na SvF STU učia o rôznych typoch geometrických plôch. Z nich najčastejšie aplikované v praxi sú práve priamkové plochy. Študenti sú oboznámení s ich klasifikáciou a princípom generovania. Naučia sa ich tiež zobrazovať v Mongeovej projekcii prepojenej s axonometriou (kolmou aj šikmou).

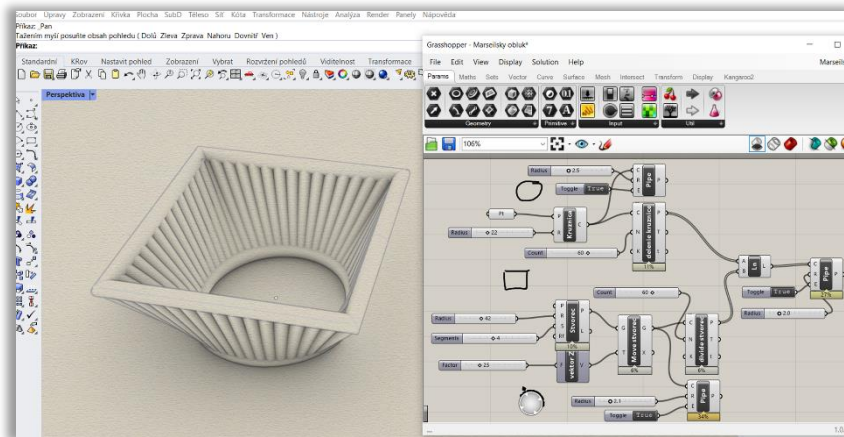


Obr. 2: Ukážka snímok zo študijných materiálov [2]

Veľmi efektívnym nástrojom pre výučbu sú študijné materiály prístupné online vo forme PowerPoint prezentácií [1], [2], (Obr.2). Sú doplnené počítačovými modelmi (\*.dwx) a umožňujú pohľad na objekty pri spojitom otáčaní.



V nich sú študentom prezentované okrem teoretických znalostí aj konkrétne príklady realizovaných diel v oblasti architektúry a dizajnu, kde boli aplikované rôzne typy plôch, medzi inými aj priamkové. Tieto príklady slúžia ako inšpirácia a učebný nástroj, ktorý ukazuje, ako môžu byť geometrické princípy aplikované v reálnom svete. Vyučovaci proces sme vhodne doplnili skupinou tlačných 3D modelov.

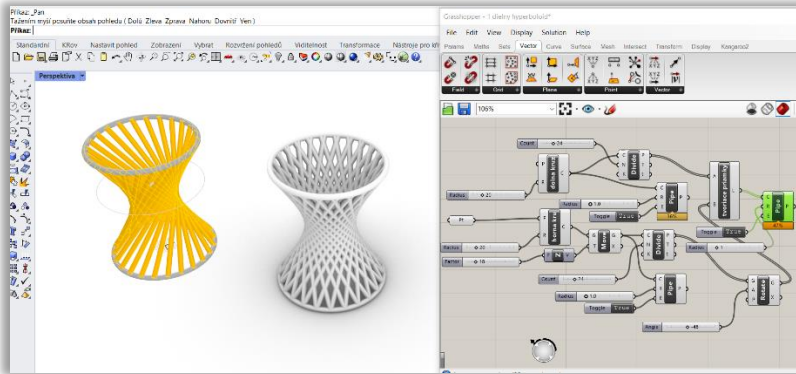


Obr. 3: Modelovanie konusoidu: Montpeliersky oblúk

### 3 Modelovanie v Rhinocerose s nadstavbou Grasshopper

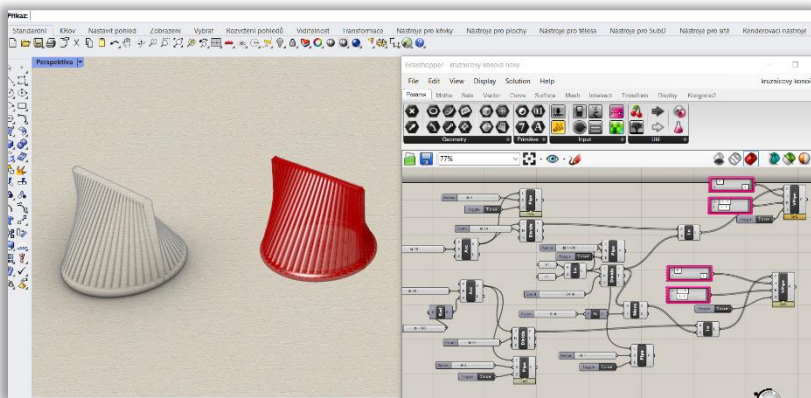
V nadväznosti na predchádzajúce skúsenosti pri tvorbe takýchto modelov [3], naďalej testujeme možnosti ich vytvárania pomocou rôznych vhodných softvérov. Pre tvorbu digitálnych modelov priamkových plôch sme využili softvér Rhinoceros, ktorý poskytuje široké spektrum nástrojov pre 3D modelovanie a ktoré môžu byť prispôbené rôznym potrebám a odvetviam.

So zámerom zvýrazniť priamky na príslušných plochách sme efektívne využili nadstavbu Grasshopper, ktorá je integrovaná do softvéru Rhinoceros ako vizuálny programovací nástroj [6]. Namiesto tradičného písania kódu umožňuje vytvárať parametrické modely a generatívne dizajny pomocou grafického rozhrania. Deje sa tak pomocou spájania a usporiadania rozličných komponentov, ktoré reprezentujú rôzne akcie a operácie.



Obr. 4: Modelovanie 1-dielneho hyperboloidu

Grasshopper umožňuje vytvárať parametrické modely, kde môžeme interaktívne meniť hodnoty parametrov a vidieť, ako sa správa výsledný model. Tento prístup sa ukázal veľmi užitočný pre rýchle experimentovanie s rôznymi variantami modelu.



Obr. 5: Modelovanie kružnicového konoidu

Pri tvorbe našich modelov sme na reprezentáciu priamok využili komponent pipe (potrubie), kde sme mohli meniť priemery rúrok a ich výplň (Obr. 3, 4, 5). Pomocou komponentu divide (delenie) generujúcich elementov sme mohli upravovať počet „priamok“ (rúrok). Taktiež sme mohli meniť napríklad veľkosť generujúcich elementov, či ich pohyb v danom smere v priestore (komponenty: scale, move, vector).



Obr. 6: Ukážky tlačných 3D modelov priamkových plôch

## 4 Záver

Vytlačené 3D modely, ktoré si študenti môžu prakticky ohmatať, veľmi vhodne dopĺňajú výučbu tematického celku Priamkové nerozvinuteľné plochy. Takýto spôsob 3D tlače priamkových modelov pomocou tlačne „množiny priamok“, ktoré sú rozlíšiteľné aj na dotyk, je tiež veľmi vhodný napríklad pre zrakovopostihnutých študentov. Fotky týchto modelov, a tiež modelov rôznych iných typov geometrických plôch sa dajú pozrieť v galérii na stránke [4]. Na Obr. 6 je ukážka niekoľkých modelov spolu s názvom zodpovedajúcej plochy, ktorú reprezentujú.

## Literatúra

- [1] K. Mészárosová, T. Rückschlossová, Z. Tereňová: *Deskriptívna geometria II. Prvá časť – Rotačné a skrutkové plochy*, Vydavateľstvo STU v Bratislave, 2014, ISBN 978-80-227-4275-7. Dostupné na internete: <http://www.math.sk/skriptaDG2/1/>
- [2] K. Mészárosová, T. Rückschlossová, Z. Tereňová: *Deskriptívna geometria II. Druhá časť – Priamkové, translačné, klinové a kanálové plochy*, STU v Bratislave, 2018, ISBN 978-80-227-4767-7. Dostupné na internete: <http://www.math.sk/skriptaDG2/2/>
- [3] T. Rückschlossová: *Surfaces of technical practice - creating of printed 3D models*, Proceedings of the Czech-Slovak Conference on Geometry and Graphics 2022. Plzeň: Vydavateľský servis, 2022, s. 147--154. ISBN 978-80-86843-79-7.
- [4] <https://www.math.sk/~galeria/3d-tlacene-modely/>
- [5] [https://calatrava.com/projects.html?project\\_type=buildings](https://calatrava.com/projects.html?project_type=buildings)
- [6] <https://www.grasshopper3d.com/>

# Selected geometric constructions and proofs

JakubŘada

*Mathematical Institute, Faculty of Mathematics and Physics,  
Charles University*

*Ke Karlovu 2027/3, 121 16 Praha 2, Czech Republic  
email: rada@karlin.mff.cuni.cz*

**Abstract.** There is a trend in many countries to replace geometric synthetic proofs with other proofs. We present some geometric proofs and constructions that can replace other types of proofs. The paper will be focused on one of the many geometrical proofs of Pappus-Pascal's theorem and the construction of an osculating circle of an ellipse.

**Keywords:** Pappus-Pascal's theorem, Osculating circle, Geometric construction.

## 1 Introduction

The methods of synthetic geometry are powerful, and using them can make some proofs simpler than using analytical methods. Historically, but also nowadays, a lot of proofs of geometric constructions are based on analytical calculations. But for many analytical proofs it is possible to find a synthetic geometric proof, which in addition develops logical thinking [9], [14]. There are even a few authors who sometimes primarily use geometric proofs that are based only on figures. For example Bogomolny [3] in his book uses some proofs based on figures, and Akopyar [1] in his book proofed a geometric statement only with one figure.

In many countries geometry in secondary schools has almost disappeared from the curriculum and has been replaced by calculus, and the same efforts have been made in the Czech Republic [10].

This article describes the most common proof of Pappus-Pascal's theorem which uses homogenous coordinates. In addition, we present two another geometrical proofs of the Pappus-Pascal's theorem. One uses a perspective point of view, and the other uses projectivities.

We will focus not only on proofs of this famous theorem but also on some geometric constructions, especially the construction of the osculating circle of an ellipse. This article is inspired by the book *The Universe of Conics: From the ancient Greeks to 21st-century developments* [5].

## 2 Pappus-Pascal's theorem

*Pappus-Pascal's theorem* is one of the fundamental theorems of projective geometry. The theorem was originally stated by *Pappus of Alexandria* in the 4th century in *Pappus's Collection, book VII*. [7] as *Pappus's hexagon theorem*. In the 17th century, the French philosopher and mathematician Blaise Pascal generalized this theorem to the case where points  $A$  to  $F$  lie on a conic. Pascal formulated his *Pascal's theorem* in 1639 when he was

16 years old and published it as a broadside titled *Essay pour les coniques* [2]. Later, the theorem was generalized into Pappus-Pascal's theorem.

**Theorem 1** (Pappus's hexagon theorem). *Let  $A, B, C$  be three points on one line and  $D, E, F$  be three points on another line. If  $\overline{AE}$  intersect  $\overline{BD}$  at  $X$ ,  $\overline{AF}$  intersect  $\overline{CD}$  at  $Y$ , and  $\overline{BF}$  intersect  $\overline{CE}$  at  $Z$ , then the three points  $X, Y, Z$  are collinear.*

**Theorem 2** (Pascal's theorem). *Let the points  $A, B, C, D, E, F$  be given. Moreover suppose that the three intersections  $X = (\overline{AE} \times \overline{BD})$ ,  $Y = (\overline{AF} \times \overline{CD})$ ,  $Z = (\overline{BF} \times \overline{CE})$  exist. The three points  $X, Y, Z$  are collinear if and only if the point  $A, B, C, D, E, F$  lie on the same conic.*

**Theorem 3** (Pappus-Pascal's theorem). *Let  $A, B, C$  and  $D, E, F$  be two non-simultaneous systems. Moreover, suppose that the points  $X = (\overline{AE} \times \overline{BD})$ ,  $Y = (\overline{AF} \times \overline{CD})$ ,  $Z = (\overline{BF} \times \overline{CE})$  exist. Then  $X, Y, Z$  are collinear.*

Pappus's hexagon theorem is stated for lines, Pascal's theorem is stated on a conic and Pappus-Pascal's theorem generalizes the statement for two non-simultaneous systems. Let us start with the most common proof of Pappus's hexagon theorem which is based on homogeneous coordinates [8].

*Proof of the Theorem 1.* Without loss of generality, let us choose homogeneous coordinates such that:

$$A = (0, 1, 0), \quad D = (0, 0, 1), \quad X = (1, 1, 1), \quad O = (1, 0, 0),$$

where  $O$  is intersection of lines  $\overline{ABC}$  and  $\overline{DEF}$ . We have

$$\overline{OA} \cup \overline{DX} = B = (1, 1, 0), \quad \overline{AX} \cup \overline{OD} = E = (1, 0, 1).$$

Assuming that  $A \neq C$  and  $D \neq F$  we get

$$C = (1, s, 0), \quad F = (1, 0, t),$$

where  $s, t \in \mathbb{R}$ . Then the remaining points are

$$\overline{AF} \cup \overline{CD} = Y = (1, s, t), \quad \overline{BF} \cup \overline{CE} = Z = (1 - st, s - st, t - st).$$

Points  $X, Y, Z$  are collinear because  $Y = Z + (s \ t) X$ . The situation is illustrated in Fig. 1. □

Let us introduce the first geometric proof in this paper which is based on a perspective view.

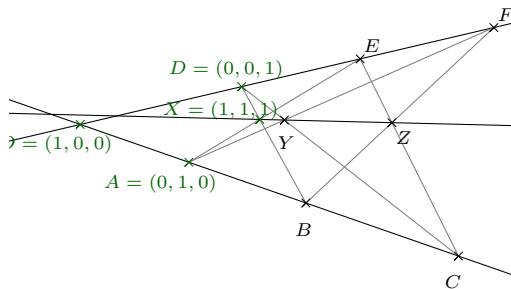


Fig. 1: Proof of the Pappus's hexagon theorem based on homogeneous coordinates.

*Proof of the Theorem 1.* Let the lines between the collinear points  $ABC$  and  $DEF$  be parallel. In Euclidean space or a perspective, parallel lines intersect at a line at infinity. Parallel lines in a ground plane  $\pi(x, y)$  intersect at a point on the horizon line  $h$ . In this case, the parallel lines  $\overline{AE}$  and  $\overline{BF}$  intersect at point  $X$ , the parallel lines  $\overline{AD}$  and  $\overline{CF}$  intersect at point  $Y$ , and the parallel lines  $\overline{BD}$  and  $\overline{EC}$  intersect at point  $Z$ . All three intersection points  $X, Y, Z$  lie on the horizon  $h$  (Fig. 2b) or at the line at infinity  $l_\infty$  (Fig. 2a).

□

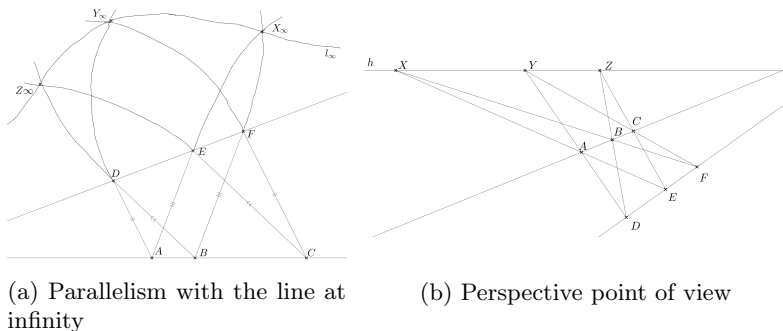


Fig. 2: Proof of the Pappus's hexagon theorem based on parallelism/perspective

There are several proofs of the Theorem 2. We will present one which uses collinearity, projectivity and Steiner's definition. For clarity, we recall here this definition.

**Definition 1** (Steiner's definition). *Let two pencils of lines at two points  $H, H'$  and a projective but not perspective mapping  $\pi$  from  $H$  to  $H'$  be given. For any line  $a$  in pencil  $H$  we have  $\pi(a) = a'$  in pencil  $H'$ . The intersection points of corresponding lines ( $a \cap a'$ ) form a non-degenerate projective conic section.*

**Theorem 4.** *In the projective plane, any projectivity between two different ranges  $h$  and  $h'$  of points can be created as the product of at most two perspectivities between ranges.*

*A projectivity is a perspectivity if, and only if, the point  $h \cap h'$  is mapped onto itself.*

Using *Definition 1* and *Theorem 4*, we can prove the Pappus-Pascal's theorem on the conic.

*Proof of the Theorem 2.* We prove the two implication separately.

1. There are 6 points on the conic  $c = \{A, B, C, D, E, F\}$ . According to Steiner's definition 1, we put  $H = A$  and  $H' = C\check{c}$ . The projectivity  $\alpha$  from the pencil  $H$  to the pencil  $H'$  generates conic  $c$ . The straight line  $h = \overline{DE}$  is a perspective from the pencil  $H$ , and the straight line  $h' = \overline{EF}$  is a perspective from the pencil  $H'$ . According to the Theorem 4,  $h$  and  $h'$  are linked with a projectivity  $\beta$ , which is perspective, because  $\alpha(E) = E$ . The projectivity  $\beta$  sends  $X = \overline{HB} \cap h$  to  $Z = \overline{BH'} \cap h'$  because  $\alpha(\overline{HB}) = \overline{BH'}$  [ $\alpha(\overline{AB}) = \overline{BC}$ ]. Since  $\beta$  is perspective on  $X$  and  $Z = \beta(X)$  is collinear with  $Y$ , which is the center of perspective  $\beta$ . Let  $D' = \overline{H'D} \cap h'$  and  $F' = \overline{HF} \cap h$ . Using  $\alpha(\overline{HD}) = \overline{H'D}$ , we obtain  $D = \beta(D')$  and  $\beta(D') = D$ . Similarly, it follows from  $\alpha(\overline{HF}) = \overline{H'F}$  that  $F = \beta(F')$  and  $\beta(F') = F$ . Therefore, the center of perspective is the point  $Y$ , found as  $Y = \overline{DD'} \cap \overline{FF'}$  (Fig. 3).
2. Every conic is uniquely given by 5 points  $A, B, C, D, E$ . We need to prove that the point  $F$  lies on the same conic  $c$ . The chain  $\beta$  of perspectivities from pencil  $H$  to the line  $h$  and further to the line  $h'$  with the center in  $Y$  and then through the line  $h'$  to the pencil  $H'$  is a projectivity because it is a finite chain of perspectivities. Then  $\beta$  is well-defined and  $\overline{HB} \rightarrow \overline{BH'}$ ,  $\overline{HD} \rightarrow \overline{DH'}$  and  $\overline{EB} \rightarrow \overline{EH'}$  for  $X, Y, Z$  are collinear. Therefore, the chain  $\beta$  is a factorization of the projectivity  $\alpha$  and therefore  $\overline{HF} \rightarrow \overline{F'H'}$ . Therefore, points  $A, B, C, D, E, F$  lie on the same conic  $c$ .

It is also worth mentioning that according to Steiner's definition 1, it does not matter which point is labelled as  $H$  and  $H'$ .  $\square$

There exist another geometric proofs of Pappus-Pascal's theorem. For example [12] shows a proof based on double-ratios and a proof via ori-



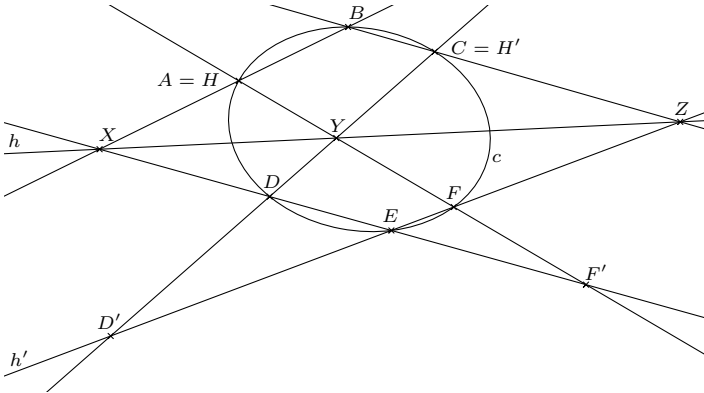


Fig. 3: Geometric proof of collinearity of points  $X, Y, Z$  based on projectivities

ented triangle area, [4] uses Tarski’s geometry in proofs and [13] nicely reinterprets the proof of Pappus-Pascal’s Theorem using determinants.

Geometry is suitable not only for proofs but also for constructions. It is known from differential geometry that an osculating circle exists at any point of an ellipse. The center of that osculating circle can be computed by curvature. In descriptive geometry, osculating circles are drawn only at the vertices of an ellipse. Usually no general construction of an osculating circle is given. The following section describes the geometric construction of the center of the osculating circle.

### 3 Osculating circle of an ellipse

Description of osculating circles is often based on differential geometry:

*“The osculating circle of a curve  $c$  at a given point  $P$  is the circle  $k$  that has the same tangent as  $c$  at point  $P$  as well as the same curvature. Just as the tangent line is the line best approximating a curve at a point  $P$ , the osculating circle is the best circle that approximates the curve at  $P$ .” ([6], pp. 111).*

The set of all centers of the osculating circles forms an evolute (Fig. 4), where the cusps<sup>1</sup> are the centers of the osculating circles at the vertices of the ellipse. There are many constructions of osculating circles at vertices of the ellipse. In descriptive geometry, an ellipse is often drawn according to the plotted osculating circles. Let us begin with the construction of an osculating circle at any point of the ellipse.

<sup>1</sup>Cusp is a point of a curve, where the moving point must reverse direction. It is a type of singular point of a curve.

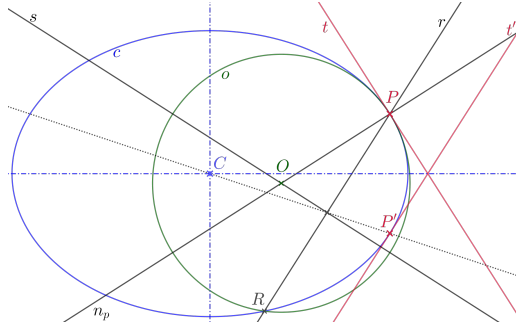
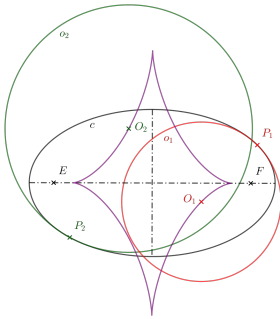


Fig. 4: Evolute of an ellipse    Fig. 5: Construction of an osculating circle

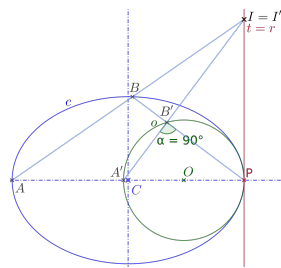
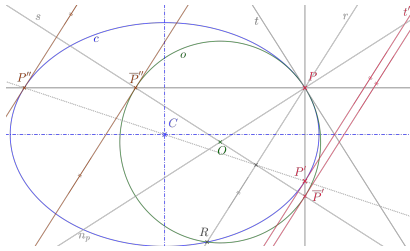


Fig. 6: The Osculating circle  $o$  as collinear image of  $c$     Fig. 7: Hyperosculating circle

Let  $c$  be a given ellipse,  $C$  a center and  $a, b$  the axes of this ellipse. Moreover, let  $P$  be an arbitrary point of the ellipse  $c$  which is not equal to some of it's vertices. We construct tangent  $t$  to the conic  $c$  at the point  $P$  (see Fig. 5). We continues as follows:

1. We find a point  $P'$  and a tangent  $t'$  axisymmetric along one of the axis of the ellipse (WLOG  $a$ ).
2. We draw a straight line  $r$  parallel to the tangent line  $t'$  through the point  $P$
3. The straight line  $r$  intersects conic  $c$  at points  $P$  and  $R$ . (Point  $R$  also lies on the osculating circle)
4. We find a line  $n_P$  normal to the tangent  $t$  at the point  $P$  (line  $n_P$  is perpendicular to the line  $t$  at the point  $P$ ).
5. We draw a line  $s$  perpendicular to the line  $r$  at a point of intersection of lines  $CP'$  and  $r$ .
6. Then the lines  $s$  and  $n_P$  intersect at the center  $O$  of osculating circle  $o$  of the ellipse  $c$  at the point  $P$ .

The correctness of this construction could be verified using differential calculus. In this paper we prefer a verification using projective geometry.

Firstly, we need to show that the center  $O$  of the osculating circle  $o$  lies on the normal line  $n_p$ . This follows from the basic knowledge of differential geometry.

Secondly, the osculating circle  $o$  and the ellipse  $c$  osculate each other at the common point  $P$ , because there exists perspective collineation with the center at  $P$  and the axis  $t$ . This follows from the fact that the straight line  $r$  of an elation passes through the point  $P$ . Finally, we need to prove that the tangents of the ellipse  $c$  parallel to the straight line  $r$  are mapped to parallel tangents of the circle  $o$ . Elation is a special case of axial affinity, where the direction of the affinity is parallel to the axis of the elation. Therefore, we can conclude from Fig. 6 that tangents of the ellipse  $c$  parallel to straight line  $r$  are mapped to parallel tangents of the circle  $o$ . Therefore, we can say that  $o$  is the osculating circle of the ellipse  $c$  at point the  $P$ .

Now, we will address a previously omitted case of the osculating circle in the vertices. In the Fig. 7, there is the given ellipse  $c$  and the searched circle  $o$ . The tangential line  $t$  through the vertex  $P$  is identical to the line  $r$  from the previous construction. Therefore, an invariant point on the tangential line  $t$  has to exist. For this reason, a collinearity centered at the invariant point maps the ellipse  $c$  to the circle  $o$ .

## 4 Conclusion

In this article, we have demonstrated the power of geometry. We showed two proofs of the Pappus-Pascal's theorem different from the proof using homogeneous coordinates. Our proofs are based on a perspectivity and a projectivity. In the second part of this article, we showed the construction of an osculating circle of an ellipse including geometric clarification instead of using the standart method of computation via curvature. Another example of how to replace arithmetic calculation by geometric constructions is given in article [11], where the author finds roots of a quadratic equation graphically.

## Acknowledgements

The work was supported by the grant SVV No. 260701.

## References

- [1] A. V. Akopyan. *Geometry in figures*. Createspace, 2017.
- [2] N. L. Biggs. Tp kirkman, mathematician. *Bulletin of the London Mathematical Society*, 13(2):97–120, 1981.
- [3] A. Bogomolny and N. Taleb. *Cut the knot: Probability riddles*. Wolfram Media Champaign, IL, 2020.

- [4] G. Braun and J. Narboux. A synthetic proof of pappus' theorem in tarski's geometry. *Journal of Automated Reasoning*, 58:209–230, 2017.
- [5] G. Glaeser, H. Stachel, and B. Odehnal. *The Universe of Conics: From the ancient Greeks to 21st century developments*. Springer, 2016.
- [6] A. Gray. Osculating circles to plane curves. *Modern differential geometry of curves and surfaces with mathematica*, 2nd edn. CRC Press, Boca Raton, pages 111–115, 1997.
- [7] A. Jones. *Pappus of Alexandria Book 7 of the Collection: Part 1. Introduction, Text, and Translation and Part 2. Commentary Index, And Figures*, volume 8. Springer Science & Business Media, 2013.
- [8] Mathcam. Proof of Pappus's theorem, 2013.
- [9] J. Molnár. *Rozvíjení prostorové představivosti (nejen) ve stereometrii*. Univerzita Palackého v Olomouci, 2009.
- [10] V. Moravcová. *Výuka deskriptivní geometrie v našich zemích*. PhD thesis, Univerzita Karlova, Matematicko-fyzikální fakulta, 2016.
- [11] J. Řada. Řešení kvadratické rovnice graficky, 6.2. 2022.
- [12] J. Richter-Gebert. *Perspectives on projective geometry: A guided tour through real and complex geometry*. Springer Science Business Media, 2011.
- [13] A. Roscoe. Pappus' theorem and 7 proofs. *Mathematics REU*, 8, 2021.
- [14] M. K Tomić, B. Aberšek, and I. Pesek. Geogebra as a spatial skills training tool among science, technology engineering and mathematics students. *Computer Applications in Engineering Education*, 27(6):1506–1517, 2019.

# Application of Euler path

Šárka Voráčová

*Dept. of Applied mathematics, Fac. of Transportation Sciences, CTU in Prague  
Konviktská 20, 110 00 Prague, Czech Republic  
email: sarka.voracova@cvut.cz*

**Abstract.** Graph theory is a valuable mathematical modelling tool with a wide variety of geometric connections. It deserves more attention in all types of education. Starting with Euler paths, graph colouring, and Hamilton icosian game pupils can learn the terms and methods important for future programming. This concept can be very useful in real-life applications, such as how to solve transportation problems. In the contribution, the Hamiltonian paths and Eulerian cycles are presented together with their connection to the vehicle routing problems

*Keywords:* Euler path, Chinese postman problem

## 1 Introduction

Graphs can be used to model a wide variety of real-world problems, including social networks, transportation, and communication networks.

Graphs are highly visual, making it easy to communicate complex data and relationships clearly and concisely. This makes them useful for presentations, reports, and data analysis. It gives the perfect comprehensible tool that helps in all phases of mathematical modeling:

- Understanding of the problem.
- Simplification and structuring of the problem.
- Mathematization of the real problem.
- Math work using the right tools and skills.
- Analysis of the results.
- Validation of the results in the environment.

## 2 Graph theory in education

Authors such as [1, 2] consider the use of graph theory as a conceptual tool in the construction of models; problem-solving enables the acquisition and development of skills such as intuition, exploration, discovery, and the design of hypotheses, which contribute to the development of logical thinking, spatial vision, and abstract reasoning in students.

Many problems related to the graph theory could be applied in everyday situations and non-academic contexts, providing a practical application of the mathematical concepts worked on in the classroom. The classic application is in maps and plans, where vertices represent places and edges present roads. This is a very helpful metaphor used to think about graphs (Fig. 1).

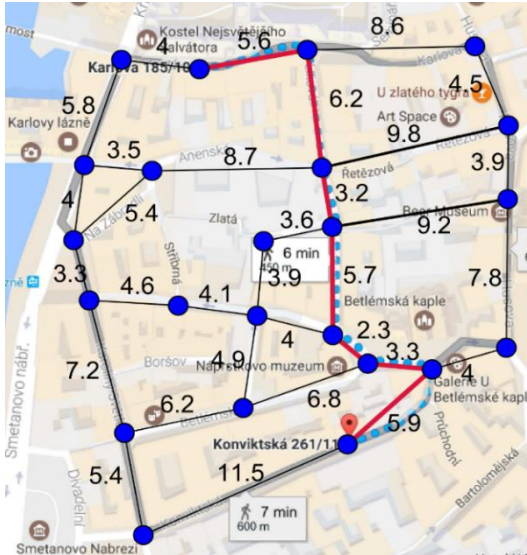


Fig. 1: The Shortest path in GeoGebra

Educational games and puzzles (Fig. 2) could offer introduction to the formulation and solution of the Traveling Salesmen Problem (TSP) and other routing problems because only a relatively small number of routes are feasible, thereby reducing the real situation to a manageable size for beginning students [2].

Further processing includes translating notations (natural language description, drawing, list, matrix) and systematic traversing. The point is to make pupils understand a few key points which will make their approach systematic and which will enable them reinvent the algorithm if needed [3].

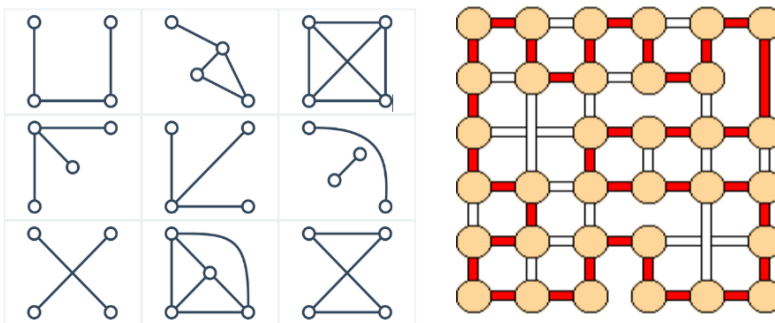


Fig. 2: Left – Graph isomorphism, learning website umimeto.org, Right – Friedman, E: Hamiltonian game

Excellence of the graph theory topic in education on all types of schools is given by following features:

- The transition from pure mathematics to the applied mathematics that has meaning to students.
- The use and the role of digital tools in the teaching of mathematical modelling.
- Geometric representation and application in purely geometric problems, such as tessellation colouring and classification of polyhedral.

### 3 Eulerian Path

The most famous problem of Graph theory is the Eulerian path traversing each edge of the graph exactly once. Eulerian paths and cycles are sometimes used as puzzles for small children but historically they played a remarkable role. The year 1736, when Euler solved the problem of seven bridges of Königsberg, is taken to mark the birth of graph theory.

Leonard Euler (1707–1783) proved that a necessary condition for the existence of Eulerian circuits is that all vertices in the graph have an even degree and stated without proof that connected graphs with all vertices of even degree have an Eulerian circuit [6].

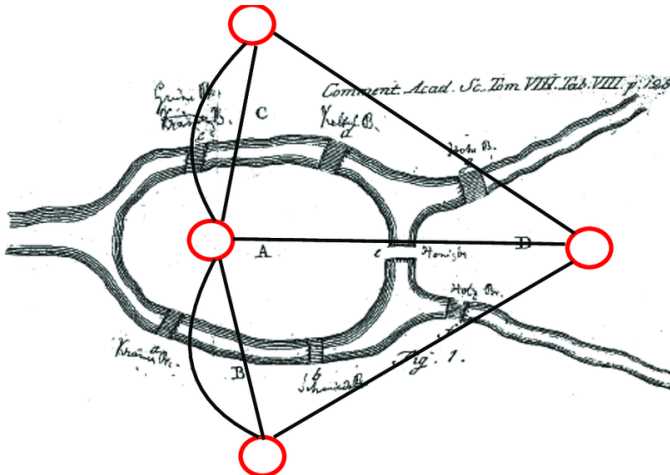


Fig. 3: The problem of the 7 bridges of Königsberg (L. Euler to L.G. Ehler, March 9th, 1736) and modern representation of graphs.

Euler felt this problem was trivial, stating in a 1736 letter to Carl Leonhard Gottlieb Ehler, mayor of Danzig (now Gdansk in Poland, 120 km west of Königsberg), who asked him for a solution to the problem [9, 11].

*Thus, you see, most noble Sir, how this type of solution bears little relationship to mathematics....*

*...In the meantime, most noble Sir, you have assigned this question to the geometry of position, but I am ignorant as to what this new discipline involves, and as to which types of problem Leibniz expected to see expressed in this way*

...

Nevertheless, after ten days L. Euler wrote a letter to G. Marinoni, an astronomer in the court of Emperor Leopold I: [9]

*This question is so banal, but seemed to me worthy of attention in that geometry, nor algebra, nor even the art of counting was sufficient to solve it. In view of this, it occurred to me to wonder whether it belonged to the geometry of position [Geometrian Situs], which Leibniz had once so much longed for...*

In the same year, Euler wrote up his solution in his celebrated paper in the *Commentarii Academiae Scientiarum Imperialis Petropolitanae* under the title “Solutio problematis ad geometriam situs pertinentis”[6] together with a diagram of the Königsberg bridges (background in Fig. 4). Let us note that Euler didn’t draw the standard schematic graph with red vertices and straight edges in Fig. 4; graphs of this kind didn’t make their first appearance until the second half of the nineteenth century.

It is not hard to invent some strategy for finding an Euler circuit (a closed walk that covers every edge once) on the small graph. Some naive algorithms are useful for real applications, for example, Fleury’s algorithm is implemented in the Python graph library Network X [15]. Fleury’s method is simple: at each step, it chooses the next edge in the path to be one whose deletion would not disconnect the graph, unless there is no such edge, in which case it picks the remaining edge left at the current vertex. Due to the bridge-finding algorithm, Fleury’s path has quadratic complexity in the number of edges, i.e.  $O(|E|^2)$ .

Construction of the Eulerian path is an important part of heuristic algorithms of NP-hard problems, such as variations on the Traveling Salesman Problem (TSP) or Chinese Postmen Problem (CPP) [3, 10].

## 4 The Chinese postman problem

The Traveling Salesman and Routing Problems are integral parts of bachelor and master programs related to Operations Research/Management Science. This is due to their relevance in both practical applications and research. The Routing Problems lead to many other related areas of Operation Research, including integer programming, approximation algorithms, Lagrangean relaxation, and various heuristic approaches (such as greedy and k-opt).

For students, it is essential to gain a deep understanding of the problems’ inherent complexity [13]. The combinatorial complexity of these problems demands a practical and comprehensible visualization for teaching purposes. Without any digital tools, only very small instances can be analysed in the classroom. These are typically too small to give students the right impression of their computational complexity [3].



The Chinese postman problem or Routing Problem is to find the shortest closed path that visits every edge of a graph at least once. When the graph has an Eulerian circuit, that circuit is an optimal solution. Otherwise, the optimization problem is to find the smallest number of graph edges to duplicate so that the resulting multigraph (graph with multiple parallel edges) does have an Eulerian circuit. The exact algorithm for an undirected graph consists of three parts:

- Find all nodes with odd degree
- Add edges to the graph such that all nodes of odd degree are made even. Added edges must be duplicates from the original graph.
- Given a starting point, find the Eulerian tour over the augmented dataset.

As we can conclude from the above-mentioned method, the CPP can be solved in polynomial time [3], but in real applications, we hardly get the basic CPP. In contrast to the solutions for basic Chinese Postman Problem, some variants are NP-complete or NP-hard.

## 5 Conclusion

The objective of proposing a problem based on a game was to bring mathematics closer to students' hobbies, which helped to attract their attention, as observed during the development of the problem's resolution in class.

Educational targets combine both the practical usability of graphs and theoretical knowledge. These two shall strengthen each other synergistically. This enhances students' lives, providing them with tools to solve problems and making them understand the usefulness of mathematical modeling at the same time. On a higher level, students should be aware of some metaknowledge and heuristics. Influenced by all the examples in graph theory, students learned to work systematically with presentable structure, virtually whenever it is possible.

The Chinese postman problem and the Traveling Salesman Problem are perhaps the most studied discrete optimization problems. Their popularity is because they are easy to formulate, difficult to solve, and have a large number of applications with several variations and generalizations. The strategy for solving the real application is sometimes analogous to the one used in the classroom. Once the students are familiar with the basics of mathematical modeling and graph approach, they can implement their own algorithm on real data.

## References

- [1] Blum, W.; Leiss (2007), D. How do Students and Teachers Deal with Modelling Problems? In *Mathematical Modelling: Education, Engineering and Economics*; UK, 2007; pp. 222–231.
- [2] Cordero, A.; Jordan, C.; Murillo-Arcila, M.; Sanabria-Codesal, E. (2022) A Game for Learning How to Model in Graph Theory. *Mathematics*, 10.
- [3] Edmonds, J.; Johnson, E.L. (1973), "Matching Euler tours and the Chinese postman problem", *Mathematical Programming*, 5, 88–124

- [4] Eglese, R.W. and Li, L.Y.O. (1992), “*Efficient Routing for Winter Gritting*”, *Journal of Operational Research Society* 43, 1031–1034
- [5] Eiselt, H.A., Gendreau, M. and Laporte, G. (1995), “Arc Routing Problems, Part I: The Chinese Postman Problem”, *Operations Research* 43(2), 231–242
- [6] Euler, L.(1735), *Solutio problematis ad geometriam situs pertinentis*” In *Commentarii academiae scientiarum Petropolitanae* 8, 1741, pp. 128–140 available on <http://eulerarchive.maa.org/docs/originals/E053.pdf>, english translation in J. R. Newman, J.R (1956), *The World of Mathematics*, Vol 1, Simon and Schuster, New York
- [7] Guan, M. (1984), "On the windy postman problem", *Discrete Applied Mathematics*, 9 (1): 41–46, doi:10.1016/0166-218X(84)90089-1.
- [8] Hollis, W. (2023). *The Mathematics of Mazes*. *Mathematics Today*. 59.
- [9] Hopkins, B., R. J. Wilson, R. J. The Truth about Königsberg, In: *The college Mathematics Journal*, Vol 35, No 3, p 198–207. 2004.
- [10] Christofides, N. (1986) *Graph Theory. An Algorithmic Approach*; Academic Press Inc.: Cambridge, MA, USA.
- [11] Kleinert, A. (2015), *Leonhardi Euleri Opera Omnia: Editing the works and correspondence of Leonhard Euler*. *Prace Komisji Historii Nauki PAU*. IVX. 13–35. 10.4467/23921749PKHN\_PAU.16.002.5258
- [12] Lenstra, J.K.; Rinnooy Kan, A.H.G. (1981), "Complexity of vehicle routing and scheduling problems", *Networks*, 11 (2): 221–227, doi:10.1002/net.3230110211
- [13] Lessner, D. (2011).: “Graph Theory at Czech Grammar Schools”, In *WDS'11 Proceedings of Contributed Papers, Part I*, 78–84, Matfyzpress
- [14] Masoud, O. (2007):"Efficient routing of snow removal vehicles" (2007). *Graduate Theses, Dissertations, and Problem Reports*. 4325. <https://researchrepository.wvu.edu/etd/4325>
- [15] *NetworkX Notebooks. Euler’s Algorithm – NetworkX Notebooks*. <https://networkx.org/nx-guides/content/algorithms/euler/euler.html>

# Note on computation of symmetries of algebraic objects

Jan Vršek, Miroslav Lávička

*Department of Mathematics & NTIS, Faculty of Applied Sciences  
University of West Bohemia, Univerzitní 8, 301 00 Plzeň, Czech Republic  
email: vrsekjan@kma.zcu.cz, lavicka@kma.zcu.cz*

**Abstract.** Many algorithms designed to compute symmetries often have a common unifying pattern that greatly simplifies the symmetry identification process by treating it as an alternative problem. In the following article, we present this technique in more detail and refer to several recent papers where this idea has been used effectively.

*Keywords:* Algebraic curves and surfaces, symmetries, groups.

## 1 Introduction

Symmetry detection is a classical challenge that finds applications in various domains, including geometry, computer graphics, computer vision, geometric modelling, and pattern recognition. This research field has witnessed a significant surge in interest, exemplified by a growing body of literature on the subject.

Mathematicians primarily focus on uncovering the global, exact symmetries of objects that are described implicitly or through rational parametrizations. Conversely, the task of identifying symmetries in objects represented discretely as point sets is a vital concern within the realm of computer science. Remarkably, the numerous algorithms designed to compute symmetries often share a unifying pattern that greatly simplifies the symmetry identification process by treating it as an alternative problem. In the following text, we discuss this technique in more detail.

## 2 Symmetries of algebraic objects

Roughly speaking, *algebraic object* is an object which can be given by a collection of polynomial equations. Among typical representatives occurring in applied geometry we can include, for instance, the following particular examples:

1. algebraic curves and surfaces – these are the solutions of polynomial equations (e.g. the unit circle  $x^2 + y^2 - 1 = 0$ ),
2. rationally parametrized curves and surfaces – curves and surfaces in parametric form given by rational functions (e.g. the unit circle  $[2t/(1+t^2), (1-t^2)/(1+t^2)]$ ),
3. finite sets of points,
4. algebraic vector fields – vector fields whose coordinate representations are given by rational functions.

In order to define a notion of a symmetry of an object we need to specify a group of its admissible transformations first. We always consider a object contained in some ambient space together with its group of automorphisms, i.e., we have the pairs  $(X, \mathcal{G})$ , where  $X$  is a space and  $\mathcal{G}$  the group of automorphisms  $X \rightarrow X$ . The typical examples are the projective space with the group of projective transformations  $(\mathbb{P}^n, \mathbb{P}GL_{n+1})$ , the Euclidean space with its isometries  $(\mathbb{E}^n, \mathcal{E}_n)$ , the sphere with the Möbius transformations  $(S^2, \text{Mob})$ , etc.

For  $\phi \in \mathcal{G}$  and  $Y \subset X$  we write  $\phi(Y) = \{\phi(y) \mid y \in Y\}$ . The group  $\mathcal{G}_Y = \{\phi \in \mathcal{G} \mid \phi(Y) = Y\}$  will be called the group of *symmetries* of  $Y$ .

Recall that a group  $\mathcal{G}$  is *algebraic* if it is at the same time an algebraic variety and two maps given by  $(\phi_1, \phi_2) \mapsto \phi_1\phi_2$  and  $\phi \mapsto \phi^{-1}$  are regular maps, see [8] for more details.

**Proposition 1.** *If both  $Y \subset X$  and  $\mathcal{G}$  are algebraic then so is  $\mathcal{G}_Y$ .*

The above observation has two immediate consequences. First, a possible group of symmetries of an algebraic objective must be restricted. For example, an algebraic object  $Y \subset \mathbb{E}^2$  cannot have a frieze group or a wallpaper group as its group of symmetries. This is obvious as these groups have infinitely many connected components, which is impossible for an algebraic group. And second,  $\mathcal{G}_Y$  can be given by a collection of polynomial equations and thus it may be directly found.

**Example 2.** *Consider the ellipse  $Y = Z(x^2 + 2y^2 - 1) \subset \mathbb{E}^2$  in the Euclidean plane, i.e.,  $(X, \mathcal{G}) = (\mathbb{E}^2, \mathcal{E}_2)$ . Any isometry  $\phi \in \mathcal{E}_2$  can be given as*

$$\phi \in \mathcal{E}_2 : \phi(x, y) = \begin{pmatrix} a_1 & a_2 \\ \mp a_2 & \pm a_1 \end{pmatrix} \begin{pmatrix} x \\ y \end{pmatrix} + \begin{pmatrix} b_1 \\ b_2 \end{pmatrix}, \tag{1}$$

where  $a_i, b_i \in \mathbb{R}$  and  $a_1^2 + a_2^2 = 1$ .  $\phi^{-1}$  and thus  $\phi$  as well is a symmetry of  $Y$  if and only if  $f \circ \phi = \lambda f$  for some nonzero  $\lambda$ . Using (1) this can be rewritten as

$$\begin{aligned} b_1^2 + 2b_2^2 + \lambda - 1 &= 0, & -2a_1a_2 &= 0, \\ 2a_2b_1 \pm 4a_1b_2 &= 0, & a_1^2 + 2a_2^2 - \lambda &= 0, \\ 2a_1^2 + a_2^2 - 2\lambda &= 0, & a_1^2 + a_2^2 - 1 &= 0, \\ 2a_1b_1 \mp 4a_2b_2 &= 0, \end{aligned}$$

which is a system of polynomial equations with unknowns  $a_1, a_2, b_1, b_2$ . This system has exactly four solutions which yield the four obvious symmetries of the original ellipse:

$$\phi(x, y) = \begin{pmatrix} \pm 1 & 0 \\ 0 & \pm 1 \end{pmatrix} \begin{pmatrix} x \\ y \end{pmatrix} \quad \text{and} \quad \phi(x, y) = \begin{pmatrix} \pm 1 & 0 \\ 0 & \mp 1 \end{pmatrix} \begin{pmatrix} x \\ y \end{pmatrix}. \tag{2}$$

Finally, any geometric construction in  $(X, \mathcal{G})$  is said to be  $\mathcal{G}$ -invariant if it commutes with any element of  $\mathcal{G}$ . For example, the construction of a convex hull is  $\mathcal{E}_n$ -invariant because it does not matter whether we first apply an isometry to a set and then compute the convex hull or vice versa.

**Lemma 3.** *Let  $\Sigma$  be a  $\mathcal{G}$ -invariant construction. Then for all admissible  $X$  it holds*

$$\mathcal{G}_X \subset \mathcal{G}_{\Sigma(X)}, \tag{3}$$

*i.e.,  $\mathcal{G}$ -invariant constructions preserve the symmetries of the set w.r.t. the group  $\mathcal{G}$ .*

*Proof.* Let  $Y = \Sigma(X)$  and let  $\phi \in \mathcal{G}_X$  then

$$\phi(Y) = \phi(\Sigma(X)) = \Sigma(\phi(X)) = \Sigma(X) = Y.$$

□

### 3 Application examples

**Symmetries of planar curves.** By a planar curve we understand a set defined by a single polynomial equation  $f(x, y) = 0$ , where  $f$  is a real polynomial in  $x$  and  $y$ . Consider the Laplace operator  $\Delta f = \frac{\partial^2 f}{\partial x^2} + \frac{\partial^2 f}{\partial y^2}$ . Replacing the curve  $f = 0$  by  $\Delta f = 0$  is  $\mathcal{E}_2$ -invariant construction, which means that all the symmetries of  $f = 0$  are the symmetries of  $\Delta f = 0$  as well. The resulting chain of Laplace operators terminates in so called harmonic curve whose symmetries are easy to compute. For more details see [1]. This approach was also used for implicit surfaces in [2].

**Projective equivalences of rational curves.** Projective equivalences of rational curves were studied in [4], where the computation of projective equivalences was replaced by the computation of Möbius transformations of a finite subset in one-dimensional projective space. This may be seen as a generalization of the  $\mathcal{G}$ -invariant constructions, where the domain and the target space of the construction are not the same. This approach also allowed to compute affine equivalences between implicit curves or projective equivalences between rational ruled surfaces.

**Symmetries of point clouds.** The approach used in [5, 7] decomposes the point cloud into simpler shapes whose symmetries can be found more easily. The decomposition is based on the discrete Laplace operator, which analogously to continuous case is  $\mathcal{E}_n$ -invariant. In 2D situation the problem is closely related to the so called trigonometric curves and their symmetries – see [6]. Note that this approach can be used for the computation of approximate symmetries as well.

**Symmetries of vector fields.** An algebraic planar vector field is a field  $V(x, y) = (v_1(x, y), v_2(x, y))$ , where  $v_i$  are real polynomials. Its symmetries can be found among the symmetries of a suitable finite subset of  $\mathbb{E}^2$ , which in addition is a collection of the roots of the univariate complex polynomial

$$\sigma_V(z) = \operatorname{res}_w \left( v_1 \left( \frac{z+w}{2}, \frac{z-w}{2i} \right), v_2 \left( \frac{z+w}{2}, \frac{z-w}{2i} \right) \right).$$

This is true as the map  $V \mapsto \sigma_V$  is  $\mathcal{E}_2$ -invariant construction. Since the symmetries of roots of the univariate polynomial can be found without knowledge of the roots, this significantly simplifies the problem, see [3].

## 4 Conclusion

In this short note we discussed a unifying pattern identified in several algorithms devoted to computation of symmetries of algebraic objects. The method was presented on particular examples with a number of references to recent papers where the idea has been thoroughly studied and then efficiently applied.

## Acknowledgments

The authors were supported by the grant 21-08009K *Generalized Symmetries and Equivalences of Geometric Data* of the Czech Science Foundation.

## References

- [1] J.G. Alcázar, M. Lávička, J. Vršek: *Symmetries and similarities of planar algebraic curves using harmonic polynomials*, Computational and Applied Mathematics, Vol. 357, pp. 302–318, 2019
- [2] J.G. Alcázar, M. Lávička, J. Vršek: *Computing symmetries of implicit algebraic surfaces*, Computer Aided Geometric Design, Vol. 104, July 2023
- [3] J.G. Alcázar, M. Lávička, J. Vršek: *Symmetries of planar algebraic vector fields*, Computer Aided Geometric Design, submitted
- [4] M. Bizzarri, M. Lávička, J. Vršek: *Computing projective equivalences of special algebraic varieties*, Journal of Computational and Applied Mathematics. Vol. 367, March 2020
- [5] M. Bizzarri, M. Lávička, J. Vršek: *Approximate symmetries of perturbed planar discrete curves*, Computer Aided Geometric Design, Vol. 96, June 2022
- [6] M. Bizzarri, M. Lávička, J. Vršek: *Symmetries of discrete curves and point clouds via trigonometric interpolation*, Journal of Computational and Applied Mathematics, Vol. 408, July 2022
- [7] M. Bizzarri, M. Lávička, J. Vršek: *Symmetries of point clouds in 3D via decomposition method*, Computer Aided Geometric Design, submitted
- [8] I.R. Shafarevich: *Basic Algebraic Geometry 1: Varieties in Projective Space*, Springer Science & Business Media, 2013.

# 3D-versions of theorems related to Miquel's Theorem

Gunter Weiss

*Universities of Technology Dresden (Germany) and Vienna (Austria)*

*email: weissgunter@gmx.at*

**Abstract.** The elementary geometric Miquel theorem concerns a triangle  $ABC$  and points  $R, S, T$  on its sides, and it states that the circles  $OART$ ,  $OBR S$ ,  $OCST$  have a common point  $M$ , the Miquel point to these givens. To a given point  $M$  there exists a one-parameter set of point triplets  $R, S, T$ . Choosing  $R, S, T$  in special ways one receives the so-called “*Beermat theorem*”, the *Brocard theorems*, and the *Simson-Wallace theorem* as special cases of Miquel's theorem. Remaining within Euclidean geometry we deal with 3D modifications of these theorems. It turns out that, while the Miquel theorem can be generalized to  $n$ -simplices, 3D versions of the Brocard theorems need some modifications. The 3D Steiner-Simson-Wallace theorem based on Miquel's theorem is different from the standard generalization (see e.g. [4]), but it connects properties of the 2D case with Brocard's modifications.

*Keywords:* Brocard points, Miquel's theorem, three-circle-theorem

## 1 Introduction

In 1838 Auguste Miquel (\* ~1816, † 1851) published a theorem (c.f. [3] and [6]), which later on is called after him and got the meaning of an important axiom in circle geometries, (see e.g. [1]). The elementary geometric version of Miquel's theorem concerns a triangle  $\Delta ABC$  and points  $R, S, T$  on its sides, and it states that the circles  $OART$ ,  $OBR S$ ,  $OCST$  have a common point  $M$ , the “Miquel point” to these givens, see Fig.1.

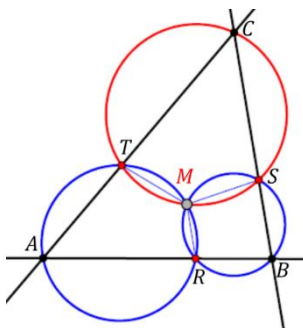


Fig. 1: Elementary geometric version of Miquel's theorem.

For  $M$  there exists a two-parametric set of possibilities, such that there is a one-parameter set of triplets  $R, S, T$  to a given point  $M$ . The consequences of this fact will be treated in Chapter 2.

Obviously, when choosing  $R, S, T$  dependent (e.g. collinear) resp. at a special position (e.g. infinitesimally close to the vertices  $A, B, C$ ), the corresponding Miquel point  $M$  will get special meanings and connect Miquel's theorem to e.g. that of Steiner and Simson-Wallace resp. to Brocard's theorems. It shows that even the well-known "beer mat theorem" resp. it's dual, namely the "three circle theorem", is a relative of Miquel's theorem. We dedicate Chapter 3 to these 2-dimensional cases, even though the topic is rather well-known. Finally, in Chapter 4, we generalize these theorems to the Euclidean 3-space.

## 2 "Miquel stars"

To an arbitrarily chosen point  $M$  we construct the feet  $R, S, T$  on the sides of  $\Delta ABC$ . Therewith, as the lines  $RM, SM, TM$  are parallel to the altitudes of  $\Delta ABC$ , they include angles  $\angle RMT = \pi - \alpha, \angle RMS = \pi - \beta, \angle SMT = \pi - \gamma$ , see Fig.2. Choosing another point  $R' \in AB$  leads to Miquel circles  $OAR'TM, OBR'M$ , which intersect  $BC$  in  $S'$  and  $CA$  in  $T'$ , see Fig.2.

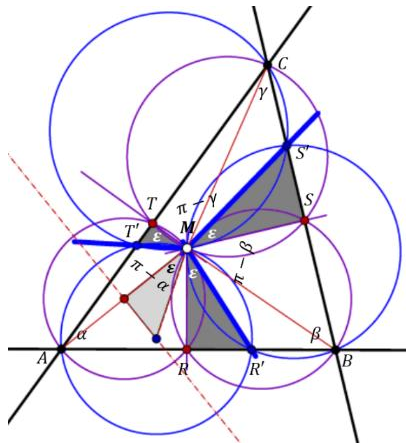


Fig. 2: The triplets  $(R, S, T), (R', S', T')$  belonging to a fixed Miquel point  $M$  define congruent „Miquel stars“.

For quadrangles inscribed in these circles opposite angles must sum up to  $\pi$ , and therefore  $\angle RMR' = \angle SMS' = \angle TMT'$ . In the following we call the triplet of half-lines  $(MR', MS', MT')$  a "Miquel star" to point  $M$ . Therewith we can state



**Theorem 1:** If  $R'$  runs through  $AB$ , then the Miquel star rotates about  $M$ . The Miquel stars to different Miquel points are congruent.

Furthermore, we can state:

If  $R'$  runs through  $AB$ , the sides of  $\Delta R'S'T'$  envelop three parabolas with common focus  $M$ . Their common cords form a complete quadrangle consisting of the incenter  $I$  and the excenters of  $\Delta R''S''T''$ , see Fig. 3. ( $R'', S'', T''$  are the images of reflections of  $M$  at sides of  $\Delta ABC$ , and  $\Delta R''S''T''$  consists of the directrix lines of the above mentioned parabolas.)

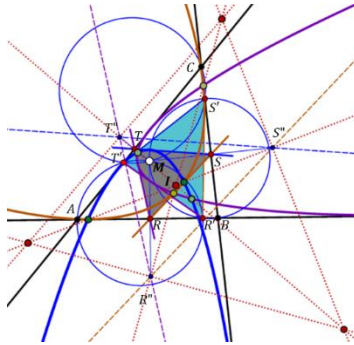


Fig. 3: The sides of  $\Delta R'S'T'$  envelop three parabolas with common focus  $M$ . Their common cords form a complete quadrangle.

### 3 Miquel's theorem and its relatives

When we choose  $R, S, T$  infinitely close to  $A, B, C$ , - there are two possibilities for that, due to the two orientations of  $\Delta ABC$  -, the Miquel circles will touch the sides of  $\Delta ABC$  at its vertices and become "Brocard circles", see Fig. 4. The Miquel points are then called "first" and "second Brocard point"  $B_1, B_2$ , see e.g. [2]. For these points the Miquel stars pass through all three vertices of  $\Delta ABC$ , Fig. 5.

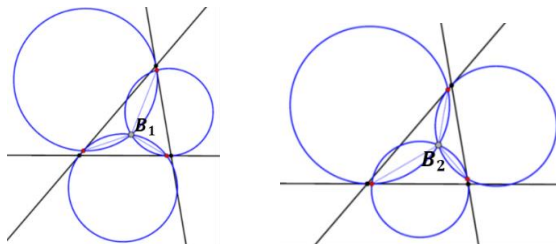


Fig. 4: Brocard circles and Brocard points of a triangle.

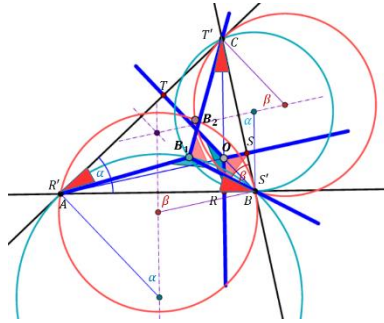


Fig. 5: Miquel-stars through the three vertices of a triangle.

As a second special case we mention collinearly chosen points  $R, S, T$ . In other words,  $R, S, T$  fulfil the “Menelaos condition”. Now the triangle  $\Delta RST$  is degenerated and the, in general, three parabolas (/Fig. 3) coincide in a single one with the Miquel point  $M$  as focus, see Fig. 6. J. Steiner interprets line  $RS$  as the fourth line of a quadrilateral and states that the four circumcircles of its four partial triangles intersect in one point, namely the focus of the single parabola  $p$  touching all four lines. In the sense of Miquel all Miquel triangles  $\Delta R'S'T'$  must be degenerated and  $M$  is a point of the circumcircle of  $\Delta ABC$ . The pedal points of  $M$  at the sides of  $\Delta ABC$  are therefore collinear with the vertex tangent of parabola  $p$ , which means that the theorem of Simson-Wallace becomes an obvious consequence.

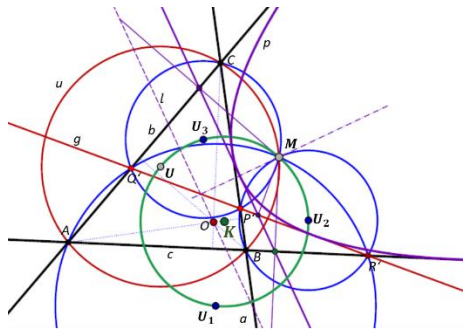


Fig. 6: Collinearly chosen points  $R, S, T$  lead to the theorems of Steiner and Simson-Wallace.

If  $R, S, T$  fulfill the “Ceva condition”, (i.e.  $RC, SA,$  and  $TB$  meet at a point  $P$ ), what is somehow dual to the former case, we get another remarkable case. Hereby a mapping of  $P$  to the Miquel point  $M$  is induced, which is algebraic of 5<sup>th</sup> degree.

### 4 3D-generalisations of Miquel's theorem.

We start with generalizing the classical theorem of Miquel: Six points  $P, Q, R, S, T, V$  on the edges of a tetrahedron  $\Sigma = ABCD$  define Miquel points  $M_i^2$  within the four face planes of  $\Sigma$ , as well as four “Miquel spheres”, which intersect in a Miquel point  $M^3$ , see Fig. 7. A proof for that can be found e.g. in [5, p.360]. There is a 6-parametric set of octahedra  $P, Q, R, S, T, V$ , while there is only a 3-parametric set of possibilities for  $M^3$ , each chosen point  $M^3$  is reached by a 3-parameter set of  $P, Q, R, S, T, V$ . For example, if  $P, Q, R, S, T, V$  are chosen as pedal points of  $M^3$  on the edges of  $ABCD$ , then  $M_i^2$  are the pedal points of  $M^3$  in the faces of  $\Sigma$  and give rise to a “Miquel-star” with half-lines parallel to the (in general skew) altitudes of  $\Sigma$ . Ther Miquel spheres are then the Thales spheres over the diameters  $[M^3A], \dots, [M^3D]$ .

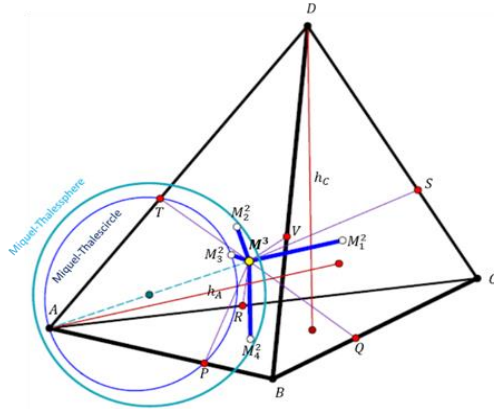


Fig. 7: Miquel point  $M^3$  and Miquel-star of a tetrahedron.

Therewith, based on Thales-hyperspheres, one can conjecture:

*Given an  $n$ -simplex  $\Sigma$  and on each of its edges a point  $M_i^1$ , then the  $n+1$  hyperspheres through vertices and neighboring points  $M_i^1$  have a common point  $M^n$ , the “Miquel point” to these givens.*

Obviously holds

**Theorem 2:** If  $M_i^1$  are chosen as the midpoints of the edges of an  $n$ -simplex  $\Sigma$ , then the Miquel point  $M^n$  becomes the circumcenter of  $\Sigma$ .

We add a Möbius-geometric interpretation: The  $nD$ -version of the theorem of Miquel is a proposition concerning configurations and incidences in Möbius hypersphere spaces. For example, for  $\dim\Pi = 1, 2,$  and  $3$  these configurations are  $(3_4, 4_3), (6_4, 8_3),$  and  $(8_8, 16_4)$ .

To look for a 3D-version of the theorems of Brocard we can choose the 6-tuplet  $P, Q, R, S, T, V$  in limit positions such that the Miquel spheres become “Brocard spheres” passing through a vertex and touching the opposite face in another vertex. This is only possible for the three vertices of a face of  $\Sigma$ , see Fig. 8. The possible limit positions of  $P, Q, R, S, T, V$  for a 3D-version of the theorems of Brocard, when related to Miquel’s theorem. The 4<sup>th</sup> Miquel sphere then becomes the circumsphere of  $\Sigma$ , and, indeed, the four spheres have a common point  $M^3 =: B_j$ , see Fig. 9.

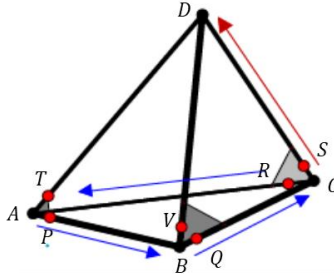


Fig. 8: Sketch of the possible limit positions of  $P, Q, R, S, T, V$  for a 3D-version of the theorems of Brocard, if related to Miquel’s theorem.

**Theorem 3:** The circumsphere of the tetrahedron  $\Sigma$  contains 8 outer Brocard points, which stem from triplets of Brocard spheres. To each face  $\Delta_j$  of  $\Sigma$  there are two triplets of Brocard spheres. The 2<sup>nd</sup> intersections of these triplets are the Brocard points  $B_i^2 = M_j^2, (i = 1, 2; j = 1, \dots, 4)$  to this face triangle  $\Delta_j$ .

Adding the faces of  $\Sigma$  as Möbius spheres through the absolute point of the Möbius space, we get the  $(8_8, 16_4)$ -configuration of Möbius spheres. Finally, the “Brocard-Miquel limit case” can also be seen as “Steiner-Wallace-Simson case”, as the sextuplet  $(P, Q, R, S, T, V)$  coincide with the three vertices of a face  $\Delta_j$ , and therefore is coplanar.

Independent of a Miquel-related interpretation we can consider the 12 Brocard spheres to a tetrahedron  $\Sigma$ , and especially their midpoints, see Fig. 9. While in the 2D-case the 6 midpoints of Brocard circles form two congruent triangles, which are similar to the start triangle  $\Delta ABC$ , there seems to be nothing known about the 3D-case. One might expect that the 12 points can be ordered as vertices of a pair of octahedra, but also three tetrahedra could be possible. For a regular tetrahedron  $\Sigma$  there are only 6 Brocard spheres. Their radii are equal to that of the circumsphere  $\Sigma$ , namely  $r = \sqrt{6}/4$ ; (the edge length of  $\Sigma$  is 1). Their centers form a regular octahedron with edge length 1. Pairs of Brocard spheres have planes of intersections through the circumcentre  $Z$  of  $\Sigma$ . All Brocard spheres touch spheres concentric with  $Z$  and radii  $r_{1,2} = \sqrt{2}(2 \pm \sqrt{3})/4$ .

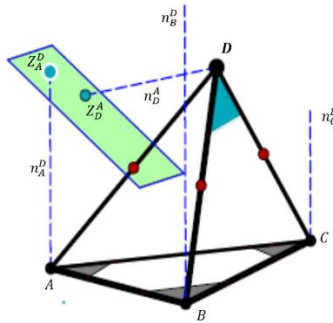


Fig. 9: A symbolic depiction of some centres of Brocard spheres to a tetrahedron.

We get another special case of 3D-Miquel's theorem case, when choosing a coplanar sextuplet  $(P, Q, R, S, T, V) \in \varepsilon$ . Therewith we get a "3D-Desargues figure"  $\Sigma \cup \varepsilon$ , see Fig. 10. In generalising the theorems of Steiner and Wallace-Simson for quadrilaterals and triangles we get

**Theorem 4:** The Miquel point  $M^3$  to coplanar chosen points  $P, Q, R, S, T, V \in \varepsilon$  belongs to the circumsphere of the tetrahedron  $\Sigma$ . In the sense of Steiner,  $M^3$  is the intersection point of the 5 circumspheres of the partial tetrahedra of  $\Sigma \in \varepsilon$ .

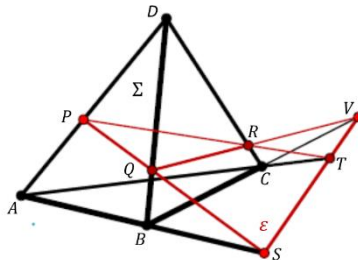


Fig. 10: Coplanar points  $P, Q, R, S, T, V$  result in a Miquel point  $M^3$  belonging to 5 circumspheres of partial tetrahedra.

Note that this generalization is different from the one due to P. Pech (see [4]). The pedal points of  $M^3$  are not coplanar! There is still an open question, whether the three-parametric set of sextuplets  $(P', \dots, V')$  consists of spheres and planes only.

### 5 Conclusion

The attempts to generalize important elementary geometric statements at least to the three-dimensional Euclidean space can perhaps open up research on

generalizations to higher dimensions and to some Cayley-Klein geometries, too. But, as mentioned in Chapter 4, there are still many open questions already in the classical Euclidean 3-space. For example, in this paper, we refrain from dealing with the “three congruent circles theorem” and its reverse, the “beer-mat-theorem”, which also are relatives of Miquel’s theorem. A first attempt for a 3D-version of these theorems could be based on *equifaced* tetrahedra  $\Sigma$ . Such a tetrahedron has no Euler line and thus generalizes the equilateral triangle.

We know that the topic treated in this paper is not mainstream science, but it might make curious about “Advanced Elementary Geometry” and this could perhaps justify its treatment.

## References

- [1] Benz, W.: *Vorlesungen über Geometrie der Algebren*. Springer Berlin 1973, ISBN 978-3-642-88671-3
- [2] Kimberling, C., *Encyclopedia of Triangle Centers*, Part 1, <https://faculty.evansville.edu/ck6/encyclopedia/etc.html> .
- [3] Miquel, A.: *Théorèmes sur les intersections des cercles et des sphères*, Journal de mathématiques pures et appliquées, Paris (Journal de Liouville), Vol. 3, 1838, S. 517–522,
- [4] P. Pech: *Generalization of Simson–Wallace theorem: planar and spatial formulation*, JGG 2023
- [5] H. Schumann: *Elementare Tetraedergeometrie, eine Einführung in die Raumgeometrie*. Franzbecker Taschenbuch 2018, ISBN-13: 978-3881205207
- [6] [https://de.wikipedia.org/wiki/Auguste Miquel – Wikipedia](https://de.wikipedia.org/wiki/Auguste_Miquel)

# Calculating on a parabola

Michal Zamboj

*Charles University, Faculty of Education  
M. Rettigová 4, Praha 1, Czech Republic  
email: michal.zamboj@pedf.cuni.cz*

**Abstract.** K. G. Ch. von Staudt described simple geometric constructions of arithmetic operations in his *Beiträge zur Geometrie der Lage*. We discuss a special case of a parabola in particular. Elementary and derived constructions of addition and multiplication are presented synthetically and analytically, and straightforward algebraic observations are interconnected with the deeper geometric properties of a parabola. We focus on constructions of arithmetic, geometric, and harmonic mean. Von Staudt's constructions are also discussed in relation to the Matiyasevich–Stechkin parabola and Möbius' parabolic nomogram.

*Keywords:* geometric algebra, von Staudt's constructions, nomogram, parabola

## 1 Introduction

Transferring arithmetic problems into geometry can lead to unexpectedly strong mathematical connections. In this paper, we discuss a representation of (extended) real numbers and operations with them on a parabola. The use of graphical tables or diagrams for solving equations is well described in nomography (for further reading, see [1],[7]). For an example, see a simple multiplication abacue in Fig. 1 from d'Ocagne's comprehensive work [4].

An interesting result on a graph of a parabola was described by Matiyasevich and Stechkin (see [2]). Lines connecting integer values on both sides of a parabola (for  $x \leq -2$  and  $x \geq 2$ ) intersect the  $y$ -axis in the composed numbers, and consequently, it creates a sieve of prime numbers. A parabolic abacue was also studied much earlier by Möbius (Figure 2, [3]). We will join the idea of a geometric calculator on a parabola with von Staudt's constructions on conics in projective geometry ([6, pp. 166–176],[9, pp. 20–23]).

## 2 Operations on a parabola

The following lines demonstrate a special case of von Staudt's constructions of addition and multiplication. Let us have a parabola

$$y = x^2 \tag{1}$$

in the Cartesian coordinate system. We will denote the points on the parabola by their  $x$ -coordinates (e.g.,  $2[2, 4], A[a, a^2] \dots$ ). In other words, we map the real  $x$ -axis to a parabola in the stereographic projection from the improper point of the parabola.

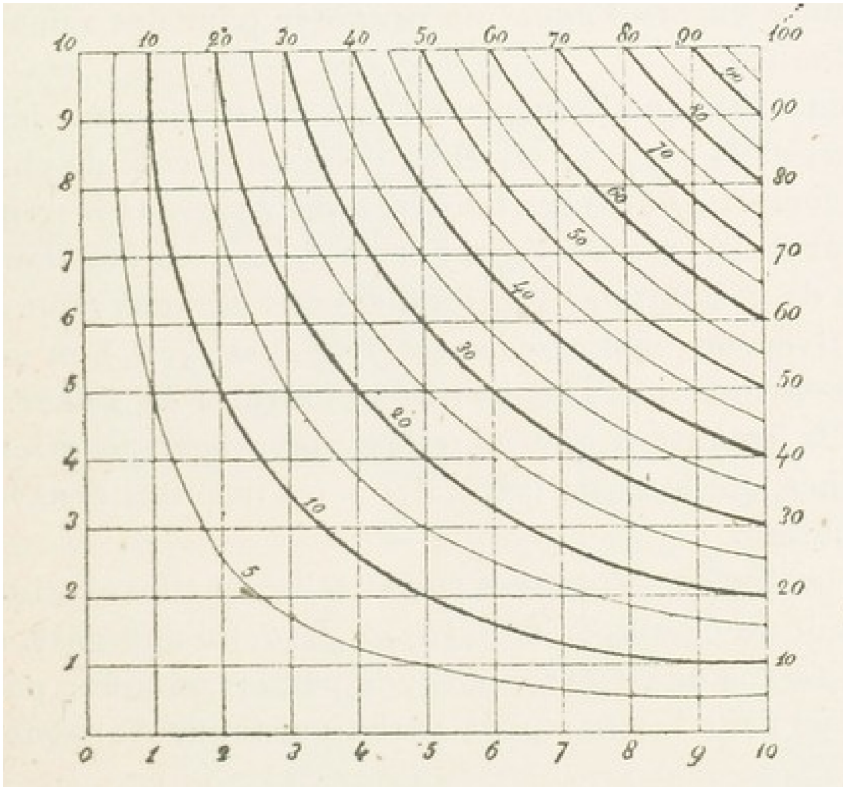


Fig. 1: A multiplication table by d'Ocagne. Assume, for example, the lines  $x = 5, y = 2$ . Their intersection lies on the hyperbola  $xy = 10$ .

Source: gallica.bnf.fr / Bibliothèque nationale de France

## 2.1 Addition and an arithmetic mean

Let us have two points  $A$  and  $B$  on the parabola (Figure 3, left). From von Staudt's construction, the sum  $A + B$  will be created by joining  $\overline{AB}$ . Then, join the intersection of  $\overline{AB}$  with the tangent in the improper point  $\infty$  and the point  $0$  (the parallel with  $\overline{AB}$  through  $0$ ). The intersection of the parabola with the parallel is the point  $A + B$ . We may find the coordinates of  $(A + B)$  to verify if such construction is correct. The equation of the line  $\overline{AB}$  is

$$y = (a + b)x - ab. \quad (2)$$

Then, the parallel through  $0$  is

$$y = (a + b)x. \quad (3)$$



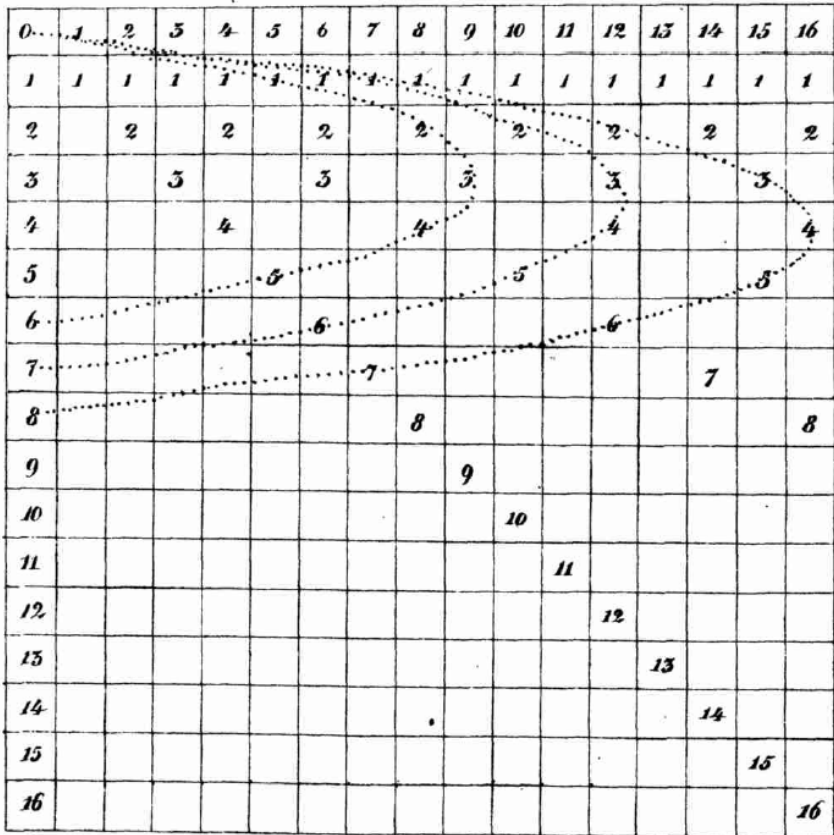


Fig. 2: Möbius' graphical multiplication on a parabola  
 Source: gallica.bnf.fr / Bibliothèque nationale de France

The intersection with the parabola (Equation 1) after the substitution into (Equation 3) has the coordinates  $x = a + b, y = (a + b)^2$ .

A straightforward consequence of the previous construction is that each secant of the parabola parallel to  $\overline{AB}$  intersects the parabola in the points with the same sum  $A + B$  (Figure 3, right). In other words, the direction of the line through  $A, B$  is the value of their sum.

Next, let us find the arithmetic mean of two values. The arithmetic mean of  $A$  and  $B$  is  $\frac{A+B}{2}$ . Since  $A+B = \frac{A+B}{2} + \frac{A+B}{2}$ , the line intersecting the parabola in a double point  $\frac{A+B}{2}$  is its tangent in the direction  $A + B$ .

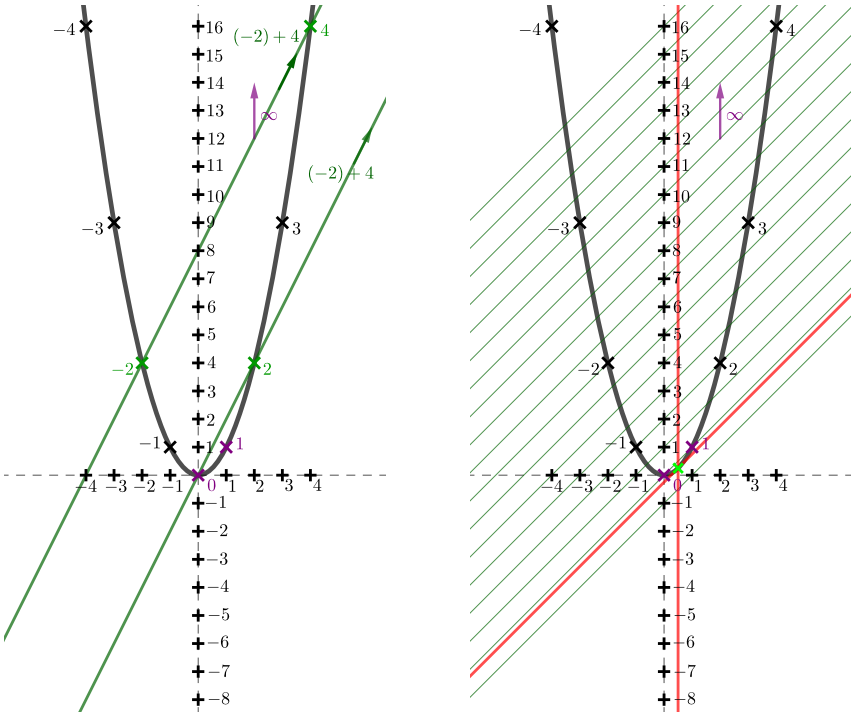


Fig. 3: (left) A construction of the sum of  $-2$  and  $4$ . (right) The intersections of a parabola with each of the parallel lines have the same sum. The point of tangency is the arithmetic mean.

Considering the  $x$ -coordinates of points and their arithmetic mean, we can further observe a well-known property of a parabola that midpoints of chords of a parabola with the same sum lie on a line parallel with its axis. This line intersects the parabola in the tangent point of the tangent in the direction of the chords.

### 2.2 Multiplication and a geometric mean

We will follow with a construction of a product. Again, let us have  $A, B$  on the parabola (Figure 4, left), and we will construct the product  $A \cdot B$  according to von Staudt's constructions. First, find the intersection of  $A, B$  with the parabola's axis. Next, construct a line through the intersection and  $1$ . The second point in which it intersects the parabola is  $A \cdot B$ . To verify the construction, recall the equation of  $\overline{AB}$  (Equation 2). The axis of the parabola is the  $y$ -axis of the coordinate system. Hence the intersection of  $\overline{AB}$  and  $y$  has coordinates  $x = 0, y = -a \cdot b$ . Now,

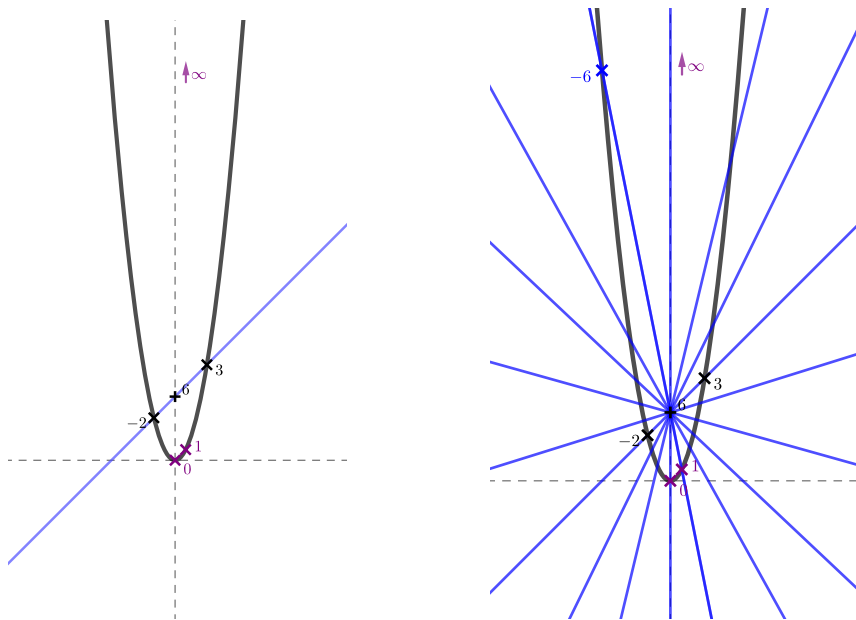


Fig. 4: (left) A construction of the product of  $-2$  and  $3$ . (right) The intersections of a parabola with each of the lines in the bundle have the same product.

observe that this holds for any choice of  $A, B$  (even zero and infinity). Therefore, each secant of a parabola through the point  $[0, -a \cdot b]$  intersects the parabola in the points with the product  $a \cdot b$  of their  $x$ -coordinates (Figure 4, right). And so, it also holds for the points  $1[1, 1]$  and  $A \cdot B[a \cdot b, (a \cdot b)^2]$ .

Observe that points on the  $y$ -axis are for integers without  $-1, 0, 1$  composed numbers, and so they create a sieve of prime numbers (the Matiyasevich-Stechkin property) (see also in [5, pp. 181–183], [8]).

Further on, let us find the geometric mean of two points (Figure 5, left). First, assume  $A$  and  $B$  such that  $A \cdot B \geq 0$ . In such cases, the intersection of  $\overline{AB}$  with the  $y$ -axis lies in the negative direction. We are looking for the value  $\sqrt{A \cdot B}$ . See that  $\pm\sqrt{A \cdot B} \cdot \pm\sqrt{A \cdot B} = A \cdot B$ , and so (similarly to the arithmetic mean), one tangent through  $[0, -a \cdot b]$  touches the parabola in the double point  $\sqrt{A \cdot B}$  and the second tangent in  $-\sqrt{A \cdot B}$ . Observe that for  $A \cdot B < 0$ , the intersection with the  $y$ -axis is an inner point of the parabola, so it has no real tangents.<sup>1</sup>

<sup>1</sup>However, the extension for imaginary elements is possible.

### 2.3 Harmonic mean

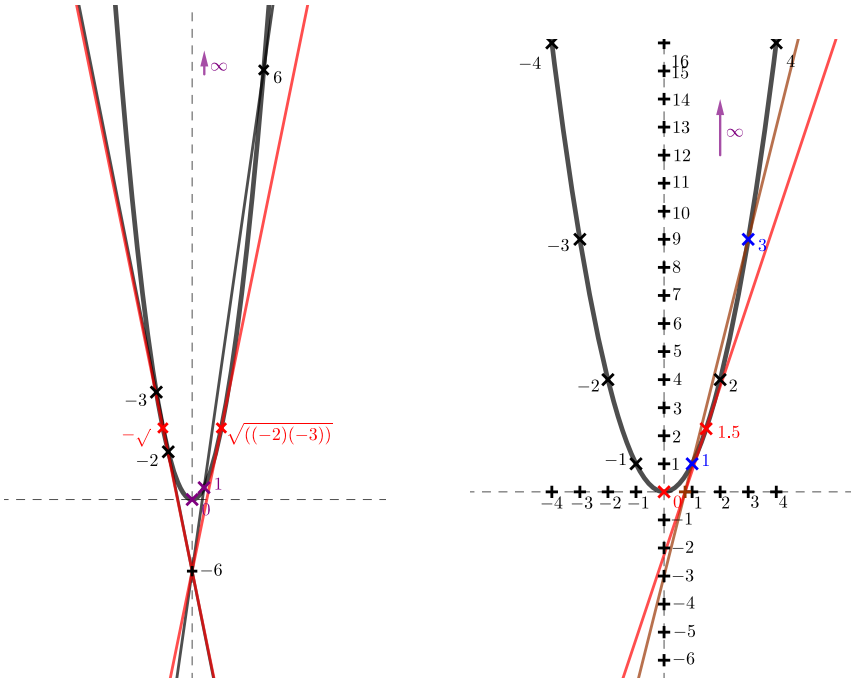


Fig. 5: (left) A construction of the geometric mean of  $-2$  and  $-3$ .  
 (right) A construction of the harmonic mean of  $1$  and  $3$ .

At last, we will explore the harmonic mean of two points on the parabola (Figure 5, right). Let us find the intersection of the line  $\overline{AB}$  with the  $x$ -axis (the tangent of the parabola through  $0$ ). Substituting  $y = 0$  into (Equation 2), we have  $[\frac{a+b}{a \cdot b}, 0]$ . One tangent to the parabola through this point is  $x$ -axis, and the second tangent has the equation

$$\frac{a + b}{a \cdot b}x - \frac{1}{2}y = 0. \tag{4}$$

The tangent point of the second tangent on the parabola has the coordinates  $[\frac{2a \cdot b}{a+b}, (\frac{2a \cdot b}{a+b})^2]$ , and so it represents the harmonic mean of  $A$  and  $B$ . To finalize the extent of our observations, notice that points  $0, A, \frac{2A \cdot B}{A+B}, B$  create a harmonic quadruple. This could be verified on the  $x$ -coordinates of these points. Counting the cross-ratio, we have

$$\left( A, B; \frac{2A \cdot B}{A + B}, 0 \right) = \frac{A - \frac{2A \cdot B}{A+B}}{B - \frac{2A \cdot B}{A+B}} \cdot \frac{B - 0}{A - 0} = -1.$$

### 3 Conclusion

Representing real numbers on a parabola, we have shown geometric constructions leading to elementary arithmetic operations. Moreover, the arithmetic operations via these constructions works well on the extended real numbers, supplementing the improper point of the parabola as  $\infty$ . Similar constructions can be carried out in projective geometry in more general settings. We can choose arbitrary regular conic and also the coordinate system  $(0, 1, \infty)$ . In the end, let us revisit Möbius' multiplication on the table with parabolas from this point of view (Figure 6). See that his choice of the point 0 is always in the top left corner of the table. The point  $\infty$  is in the horizontal direction of the axis of the parabola. The choice of 1 in the first row is the choice of the parabola. In this setting, the line through 2 and 3 intersects the line  $0\infty$  in the point 6. Compared to our choice  $y = x^2$  where  $0\infty$  is the  $y$ -axis, Möbius chose  $0\infty$  as the top row of the table. Otherwise, all the constructions work in the same manner.

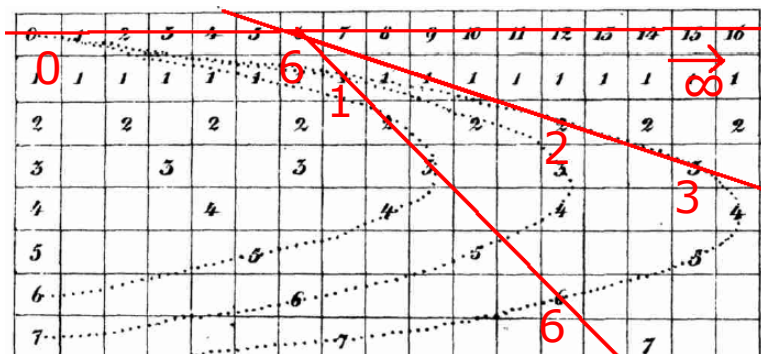


Fig. 6: Reconstruction of Figure 2. The system  $(0, 1, \infty)$  and multiplication construction of  $2 \cdot 3$  and  $1 \cdot 6$  is highlighted.

### References

- [1] H. A. Evesham: *The History and Development of Nomography*. Do-cent Press, 2010.
- [2] J. Matiyasevich: *First encounter with nomograms* (russian). *Kvant*, 2(5), 25, 1971, p. 4.
- [3] A. F. Möbius: *Geometrische Eigenschaften einer Factorentafel*. *Journal für die reine und angewandte Mathematik*, Issue 22, 1841, pp. 276–284.
- [4] M. d’Ocagne: *Traité de nomographie*. Paris, Gauthier-Villars, 1899.

- 
- [5] J. Richter-Gebert: *Perspectives on Projective Geometry*. Springer-Verlag Berlin Heidelberg, 2011.
  - [6] K. G. Ch. von Staudt: *Beiträge zur Geometrie der Lage*. Nuremberg, Fr. Korn, 1856
  - [7] D. Tournes: *Calculating with hyperbolas and parabolas*. É. Barbin (ed.). *Let History into the Mathematics Classroom*, Springer, pp.101-114, 2018.
  - [8] M. Zamboj: *Parabola a jej podobnostvá*. Dva dny s didaktikou matematiky 2018, Prague, Czech Republic, pp. 73-77.
  - [9] M. Zamboj: *Synthetic Projective Geometry*. Dissertation thesis, Charles University, 2019.

## List of Participants

BEGANOVÁ	Juliana	Stavebná fakulta, STU v Bratislave
BOSÁKOVÁ	Adriana	FMFI, UK, Bratislava
BRAJERČÍK	Ján	Fakulta human. a príř. vied, PU, Prešov
CIBULKA	Jaroslav	Fakulta strojnř, ČVUT v Praze
DAS	Manaswita	FMFI, UK, Bratislava
ČAVARGA	Martin	FMFI, UK, Bratislava
ČEČÁKOVÁ	Stanislava	Fakulta architektury ČVUT v Praze
FERDIÁNOVÁ	Viera	Přřirodovědecká fakulta, Ostravská univerzita
FERKO	Andrej	FMFI, UK, Bratislava
GUNČAGA	Ján	Pedagogická fakulta UK v Bratislave
HLAVOVÁ	Marta	Fakulta strojnř, ČVUT v Praze
HOLEŠOVÁ	Michaela	Stavebná fakulta Žilinskej univerzity v Žiline
CHALMOVIANSKÝ	Pavel	FMFI, UK, Bratislava
CHODOROVÁ	Marie	PřřF, Univerzita Palackého v Olomouci
KOKTAVÁ	Marie	Mendelova univerzita v Brně
KOLÁŘOVÁ	Dana	Fakulta architektury ČVUT v Praze
KOLCUN	Alexej	Přřirodovědecká fakulta, Ostravská univerzita
KOREŇOVÁ	Božena	Kremnica
KRÁLOVÁ	Alice	LDF, Mendelova univerzita v Brně
KRUPKA	Demeter	Lepage Reasearch Institute, Prešov
KUŠAR	Domen	Fakulteta za arhitekturo, Ljubljana
LÁVIČKA	Miroslav	Fakulta aplikovaných věd, ZČU v Plzni
LINKEOVÁ	Ivana	Fakulta strojnř, ČVUT v Praze
MAKOVNÍK	Marcel	FMFI, UK, Bratislava
MOLNÁR	Emil	Budapesti Muszaki és Gazdaságtudományi Egyetem
MRÓGALA	Jan	PřřF, Ostravská univerzita
MÜLLER	Jakub	Fakulta strojnř, ČVUT v Praze
ODEHNAL	Boris	University of Applied Arts Vienna
PABICH	Bronisław	Wyższa Szkoła Nauk Pedagogicznych, Wieliczka
PEŠKA	Patrik	PřřF, Univerzita Palackého v Olomouci
RIČHTÁRIKOVÁ	Daniela	Strojnická fakulta, STU v Bratislave
RÜCKSCHLOSSOVÁ	Tatiana	Stavebná fakulta, STU v Bratislave
ŘADA	Jakub	Matematicko-fyzikální fakulta UK, Praha
SZARKA	Ján	Bratislava
SZARKOVÁ	Dagmar	SSGG, Bratislava
ŠÍR	Zbyněk	Matematicko-fyzikální fakulta UK, Praha
TKAČIK	Štefan	PF, Katolícka univerzita v Ružomberku

TKADLECOVÁ	Miroslava	Mendelova univerzita v Brně
VAJSÁBLOVÁ	Margita	Stavebná fakulta, STU v Bratislave
VELICH	Ilja	Geometer emeritus, Bratislava
VELICHOVÁ	Daniela	Strojnícka fakulta, STU v Bratislave
VÍTKOVÁ	Lenka	PřF, Univerzita Palackého v Olomouci
VORÁČOVÁ	Šárka	Fakulta dopravní, ČVUT v Praze
VRŠEK	Jan	Fakulta aplikovaných věd, ZČU v Plzni
WEISS	Gunter	TU Dresden & TU Wien
ZAMBOJ	Michal	PF, Univerzita Karlova, Praha



Proceedings of the  
9<sup>TH</sup> SLOVAK-CZECH CONFERENCE  
ON GEOMETRY AND GRAPHICS 2023

Editors:

Miroslav Lávička, Dagmar Szarková, Daniela Velichová

Published by

Vydavatelský servis  
Republikánská 28, Plzeň



First Edition

Plzeň 2023

ISBN 978-80-86843-82-7 (CD-ROM)

ISBN 978-80-86843-81-0 (online)